

Novel Cryptophycin Analogues and Conjugates for Tumor Targeted Therapy

Dissertation

Zur Erlangung des akademischen Grades

Doctor rerum naturalium (Dr. ret. nat.)

Eduard Figueras Agustí

Organic and Bioorganic Chemistry

Department of Chemistry

Bielefeld University

2019

The work herein described was mainly carried out at Bielefeld University at the Department of Chemistry from September 2015 to December 2018 under the supervision of Prof. Dr. Norbert Sewald.

1. Referee: Prof. Dr. Norbert Sewald
Organic and Bioorganic Chemistry, Department of Chemistry
Bielefeld University
2. Referee: Prof. Dr. Ines Neundorf
Faculty of Mathematics and Natural Sciences, Institute of Biochemistry
University of Cologne

I was taught that the way of progress was neither swift nor easy

Marie Skłodowska-Curie

**Als de Casa,
que m'ho han ensenyat tot**

Acknowledgments

With this thesis, an important and exciting stage of my life comes to an end. During these three years and a half I have met amazing people and I have grown as a person and as a scientist. To all the people that have contributed to make this time more special, I would like to give my most sincere and deep acknowledgment. None of this would have been possible without your help.

I would like to thank Prof. Dr. Norbert Sewald the opportunity to work on his multicultural and multidisciplinary nice research group. I am thankful that I was chosen for this exciting and challenging project, for all the advices during the thesis, and the good moments in all the conferences.

To the group who has received me with open arms and willingness to always help me, I thank all the former and current member of the OC3. Special mention needs to be done to Marco Wißbrock, Anke Nieß, Iris Dopheide, Carmela Michalek, and Dr. Marcel Frese for their help and effective solution of any kind of daily problem. I also want to thank the people which I spent more time. To Isabell Kemker for all the help and the German/Spanish lessons. To Hendrik Groß and Christian Schnepel for all the good and funny conversations, the trip to USA and the proofreading of the thesis. To Pia Neubauer, I am happy that we started the PhD at the same time, and we could share the office and spent time together. To Nils Janson, because although we make jokes of each other and I push you a lot, I am happy that you are somehow related to the cryptophycins.

The Magicbullet started like a project but with the time it became something more special, the network meetings have been a great experience to learn and to meet all the members every half year and is one of the things that I will miss the most. From all the members, one person has shared the same way to the obtention of the PhD, the same project, the same laboratory, and the same office. To Adina Borbély, we have had our ups and downs, but I am very happy that we have got to meet and shared the trail of the PhD. I also want to thank the members which I shared more moments, Sabine, André, Paula, and Lucia.

The secondments in Milan were a great experience and I want to thank all the people who have made that possible. I would like to acknowledge Prof. Dr. Cesare Gennari and all the members of his group for hosting me, in special I want to thank Arianna Pina for all the help in the laboratory and the infinite moments of fun skiing, playing beach volley,

and many more. I also want to thank Dr. Christian Steinkühler and the people of Italfarmaco for the short and intense secondment.

In terms of collaborations, I want to thank Mohamed Ismail for the molecular docking studies of chapter 3. Prof. Dr. Dario Neri and Samuele Cazzamalli are greatly acknowledged for the cryptophycin-acetazolamide project that constitutes the chapter 4. I also want to thank Prof. Dr. Karsten Niehaus, Marco Giampà and Judith Kampa for the MALDI imaging studies.

The collaboration project with Exiris has been the most challenging one and we have worked it out as a good team. For this reason, I want to thank, once again, Dr. Christian Steinkühler and Dr. Paola Gallinari for your support and help. Ana Martins, your incorporation after one year of magicbullet has been one of the best things that happened to the project. I want to thank your dedication, the great amount of experiments that you have performed for the project, and the friendly moments in the network meetings.

This work has been possible with the bachelor thesis of Arne, Lea, and Mazlum and the master internships of Falk, Hannes, Moritz, and Nicolai which are warmly acknowledged.

Thomas Schachtsiek and Clara Belu, it was a pleasure to help two talented students like you during the master thesis. I wanted to thank your dedication to the project and to bring a positive atmosphere to the laboratory. I hope you enjoyed this time like I did, and I wish you all the best for the future.

Finalment, vull donar les gràcies a la gent de casa, família i amics, per estar sempre al meu costat i rebre el vostre suport incondicional. Aquesta tesi va per vosaltres!

Abbreviations

ADC	Antibody-drug conjugate
Boc	<i>tert</i> -butyloxycarbonyl
CA	Carbonic anhydrase
CAIX	Carbonic anhydrase IX
CAL	Fluorobenzosulfonamide
CDR	Complementary determining region
CuAAC	Copper(I)-catalyzed alkyne-azide cycloaddition
DAR	Drug-to-antibody ratio
DAVLBH	Desacetylvinblastin hydrazide
DM1	Mertansine
DNA	Deoxyribonucleic acid
DOTA	1,4,7,10-Tetraazacyclododecane-1,4,7,10-tetraacetic acid
DUPA	2-[3-(1,3-dicarboxy propyl)ureido]pentanedioic acid
EGFR	Epidermal growth factor receptor
EMA	European Medicines Agency
EPR	Enhanced permeability and retention
FDA	Food and Drug Administration
FR	Folate receptor
GDP	Guanosine diphosphate
GSH	Glutathione
GTP	Guanosine triphosphate
HER	Human epidermal growth factor receptor
Igs	Immunoglobulins
mAb	Monoclonal antibody
MDR	Multi-drug resistant
MED	Minimum effective dose
MTD	Maximum tolerated dose
MT1-MMP	Membrane type 1 matrix metalloproteinase
PCa	Prostate cancer
P-gp	P-glycoprotein
PSMA	Prostate-specific membrane antigen

SAR	Structure-activity relationship
SMDC	Small molecule-drug conjugate
SPR	Surface plasmon resonance
SST	Somatostatin
SSTR	Somatostatin receptor
WHO	World Health Organization

List of Amino acids

Name	Three letter code	One letter code
Alanine	Ala	A
Arginine	Arg	R
Asparagine	Asn	N
Aspartic acid	Asp	D
Citrulline	Cit	
Cysteine	Cys	C
Glutamine	Gln	Q
Glutamic acid	Glu	E
Glycine	Gly	G
Histidine	His	H
Isoleucine	Ile	I
Leucine	Leu	L
Lysine	Lys	K
Methionine	Met	M
Sarcosine	Sar	
Phenylalanine	Phe	F
Proline	Pro	P
Serine	Ser	S
Threonine	Thr	T
Tryptophan	Trp	W
Tyrosine	Tyr	Y
Valine	Val	V

D-amino acids are described by D-Xaa in the three letter code and with the small letter in the one letter code.

Table of contents

Abstract.....	15
Chapter 1 - General introduction.....	17
1.1 Cancer and chemotherapy	19
1.2 Targeted therapy.....	22
1.2.1 Antibody-Drug Conjugates (ADCs).....	24
1.2.2 Small Molecule-Drug Conjugates (SMDCs).....	29
1.2.2.1 SMDCs targeting the folate receptor (FR)	30
1.2.2.2 SMDCs targeting the Prostate-Specific Membrane Antigen (PSMA) ...	32
1.2.2.3 SMDCs targeting Carbonic Anhydrase IX (CAIX)	33
1.2.2.4 SMDCs targeting Somatostatin Receptors (SSTRs)	35
1.2.3 The linker.....	37
1.2.4 The payload	39
1.3 Cryptophycin	41
1.3.1 Biological mode of action	43
1.3.2 Structure-activity relationship (SAR) studies.....	45
1.3.2.1 Unit A	45
1.3.2.2 Unit B	46
1.3.2.3 Unit C	47
1.3.2.4 Unit D	48
1.3.3 Conjugates containing cryptophycin as payload	49
1.4 References	53
Chapter 2 - Objectives	61
Chapter 3 – Novel analogues of cryptophycin modified in the unit B.....	65
Chapter 4 – Cryptophycin conjugate targeting carbonic anhydrase IX.....	73
Chapter 5 – Cryptophycin conjugates targeting the somatostatin receptor 2	81

Chapter 6 – Summary	93
Chapter 7 - Appendix	101
7.1 – Appendix I: supporting information of chapter 3	103
7.2 – Appendix II: supporting information of chapter 4.....	145
7.3 – Appendix III: supporting information of chapter 5	157

Abstract

The cure of cancer represents an ultimate challenge for scientists from different fields. Cancer complexity and diversity hamper the discovery of a broadly applicable treatment, and consequently, cancer represents the second cause of premature death worldwide. Despite the continuous approval of new drugs, the cancer burden keeps increasing due to different factors and leaves a vast number of patients helpless. Conventional chemotherapy still represents the backbone of cancer medical care. However, these agents are not able to selectively accumulate at the disease site which limits their efficacy and cause severe side effects. In the last years, targeted therapy has appeared as an innovative approach to overcome the drawbacks shown by traditional chemotherapeutics. In this approach, a cytotoxic agent is directed to the tumor site through the covalent conjugation to homing devices (e.g. antibodies, small molecules).

Cryptophycins are cyclic depsipeptides with natural origin that present high cytotoxicity against several cell lines. Although cryptophycins cannot be used as stand-alone agent due to their side effects, they hold great potential as cytotoxic agent for tumor targeted therapy. Therefore, the discovery of new cryptophycins that can be conjugated to homing devices and their vectorization could be translated in a significant therapeutic activity.

In the first part (chapter 3), the discovery of new cryptophycin analogues that retain the high cytotoxicity of the parent compound and present a functional group that can be used for conjugation to a delivery vehicle was described. Moreover, the usage of molecular dynamics to predict the biological activity of new analogues was explored.

The second part (chapters 4 and 5), describes the usage of cryptophycin-55 glycinate as payload in small molecule-drug conjugates (SMDCs). In chapter 4, the payload was conjugated to a ligand capable to target the carbonic anhydrase IX, a transmembrane enzyme that is widely overexpressed in tumors. The cytotoxic activity of the resulting conjugate was studied *in vitro*, and the therapeutic activity was investigated in mice. In chapter 5, the payload was further explored by coupling it to a cyclic peptide targeting the somatostatin receptor 2, a marker which is commonly overexpressed in neuroendocrine tumors. The cytotoxicity of the conjugates was evaluated in a cell-based assay. In this case, further investigations in their targeting properties and stability were performed. Finally, the antitumor activity of the lead compound was investigated *in vivo*.

Chapter 1 - General introduction

1.1 Cancer and chemotherapy

Despite the continuous development of new and more efficient treatments, cancer remains the second cause of premature death worldwide.^[1] According to a report from the World Health Organization (WHO), this disease caused approximately 8 million fatalities in 2012 and this number is expected to increase up to 9.6 million in 2018.^[2] The prediction for the next decades is not better with a continuous increase of cases and deaths. The main reasons of this unceasing escalation are the steady population growth, ageing, and the increase of risk factors (e.g. tobacco use, unhealthy diet, lack of physical activity).

Cancer cannot be understood as one single disease but as a complex group of diseases which have in common the abnormal cell division without control that can invade nearby tissues and, if not treated, lead to the death of the host.^[3] The high diversity between cancer types is the reason that incidence and mortality are not directly related (Figure 1). While lung and prostate cancer are prevalent in men, mortality of lung cancer is circa three times higher. A similar situation is found in women: albeit breast cancer is three times more incident than colorectum, the mortality differs in less than two-fold.

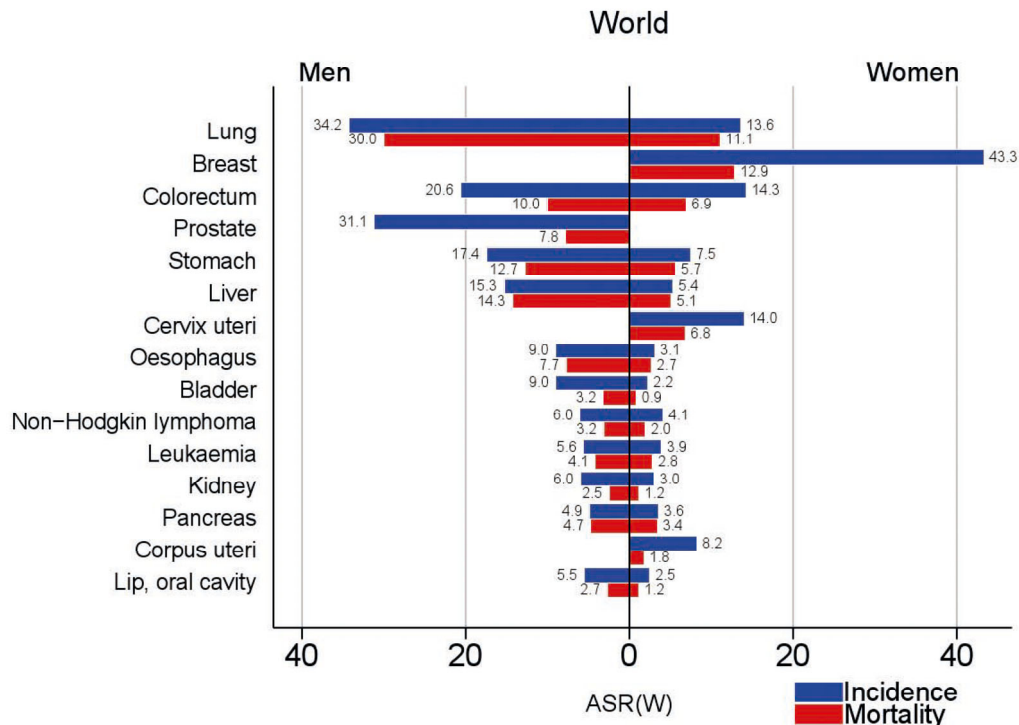


Figure 1. Estimated age-standardized (World) cancer incidence and mortality rates (ASR) per 100 000, by majors sites, in both genders, 2012.^[1]

The heterogeneity of cancer makes treatment even more challenging. However, in all cases regular care is based on the surgical removal of the tumor, when this is possible, radiotherapy, and chemotherapy. Conventional chemotherapy consists in the administration of small cytotoxic agents that aim cell death by affecting fundamental cellular processes such as cell division.^[4] This strategy was first coined by the Nobel laureate Paul Ehrlich in the early 1900s and reached a substantial milestone in 1949 with the first chemotherapeutic to receive Food and Drug Administration (FDA) approval. More than half century later the concept is still valid, and many new treatments have appeared. The classical categorization of chemotherapeutics is based on their mechanism of action and can be subdivided in different groups (Figure 2).^[5]

- **DNA alkylating agents**^[6] were the earliest drugs to be developed, being mechlorethamine the first chemotherapeutic agent to be approved for cancer treatment. Its activity relies in the presence of highly electrophilic groups which can be attacked by the N7-position of guanine bases and crosslink the DNA strands blocking their replication. The high reactivity of mechlorethamine prevents oral administration and for this reason, derivatives such as chlorambucil (FDA approved in 1957) and cyclophosphamide (1959) were developed.
- Although their mode of action relies in the formation of metal adducts with DNA instead of the previously described alkylation of DNA, platinum complexes can be also included in this group. The serendipitously discovery of cisplatin, approved in 1978, was of high relevance and opened the research field of platinum complexes such as carboplatin (1989) and oxaliplatin (2002).^[7] Nowadays, they play an essential role in the treatment and there is a high interest on discovering new analogues.^[8]
- **Antimetabolites** were the next compounds to be developed. This class of compounds is able to mimic essential cellular molecules and interferes with the DNA by competing with the natural substrate.^[6] Methotrexate (1953) and 5-fluorouracil (1962) are the most important examples of antimetabolites. The first one was inspired in the observation that folic acid plays an essential role in tumor growth and thus, folate antagonists could have antitumor properties. The second one, is the result of adding a fluorine in the C5-position of the essential nucleobase uracil.
- **Antibiotics** with antitumor activity were first identified on a program related to the second world war and they can show different mechanisms of action. Dactinomycin

(1964) is one compound from this class.^[9] The anthracyclines were also first classified in this group but are better regarded as topoisomerase inhibitors.^[10]

- **Topoisomerase inhibitors** block the changes in DNA structure by interfering with the topoisomerase enzyme (I and II) which catalyzes unravelling of DNA double strand for replication. Topoisomerase enzyme I initiates the cleavage of one DNA strand while topoisomerase enzyme II cleaves both DNA strands.^[11] Camptothecin and their analogues act as topoisomerase I inhibitors while the anthracyclines such as doxorubicin (1974) are topoisomerase II inhibitors.
- **Mitosis inhibitors** include *vinca* alkaloids and taxanes.^[12,13] Microtubules are an essential part of the cytoskeleton, which plays a substantial role in cell division. By interfering with their dynamics, the cell is no longer able to divide and initiates apoptosis. *Vinca* alkaloids such as vinblastine (1965) prevent the polymerization of tubulin into microtubules. On the other hand, taxanes like paclitaxel (1992) present a different mode of action. They stabilize microtubule and block their disassembly impeding the formation of free tubulin.

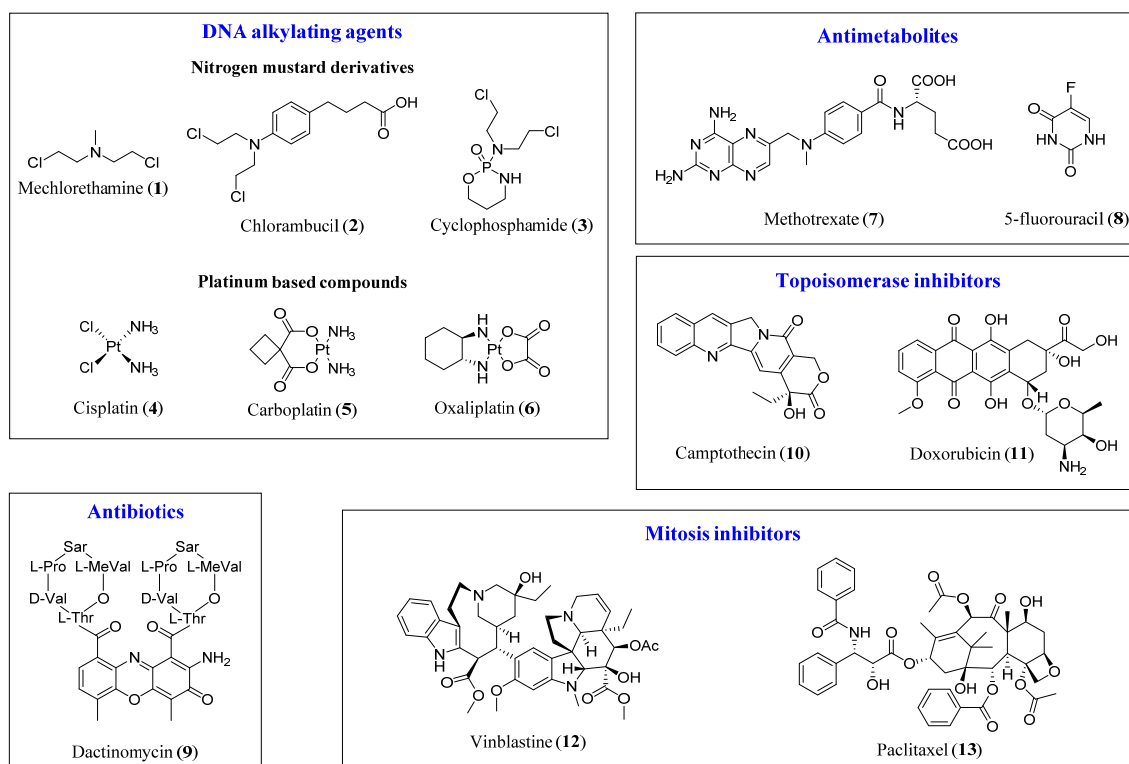


Figure 2. Structures of traditional chemotherapeutic agents classified by their mode of action.

Chemotherapeutics, administered as single agent or in combination with radiotherapy and surgery, have certainly contributed to decline the cancer mortality rate. Nevertheless, complete and durable cure remains the exception rather than the rule. The main reason for the lack of efficacy, especially in metastatic cancer, is that anticancer drugs lack tumor preference and affect healthy tissues.^[14] As a consequence, chemotherapeutics display a narrow therapeutic window, which can be described as the dosage range of a drug that can treat the disease effectively without displaying harsh side effects. In order to have efficacy, anticancer drugs are administered near the maximum tolerated dose (MTD) which results in severe side effects (e.g. bone marrow suppression, nausea, hair loss).^[15]

In another early vision from Paul Ehrlich, the idea of a “magic bullet” was conceived. An agent that could specifically attack the disease without harming the rest of the tissues would constitute an ideal drug that he named *Zauberkegel*, the magic bullet. This early vision was fulfilled more than 20 years ago with the discovery (1996) and later FDA approval of imatinib (2001), a tyrosine kinase inhibitor. Since then, targeted therapy has emerged as a promising approach to overcome the limitations observed by traditional chemotherapeutics and enhance their effectivity.

1.2 Targeted therapy

In the last years, research on cancer therapy has experienced a shift from discovery of cytotoxic agents to targeted therapy.^[16] The better understanding of the mechanism of cancer and its hallmarks have provided knowledge to develop efficient targeting systems.^[17,18] For example, the observation that tyrosine kinases have an abnormal function in most of cancers prompted the development of multiple tyrosine kinase inhibitors.^[16] Another approach is based on the conjugation of cytotoxic agents to carriers that will selectively deliver the compound to the disease site. The targeting can be mediated by two different mechanisms: passive or active.^[19]

Passive targeting is based in the enhanced permeability and retention (EPR) effect.^[20] Due to the lack of effective lymphatic drainage and other disorders in tumors, large molecules (e.g. liposomes, nanoparticles) are directed towards the tumor tissue in a bigger extent than to the healthy one. Successful examples of passive targeting can be found in

the liposomal formulation of doxorubicin (Caelyx™)^[21] or the albumin-bound paclitaxel (Abraxane™).^[22]

On the other hand, the overexpression of different receptors in tumors can be used for active targeting. In this approach, a targeting molecule (e.g. antibody, peptide, peptidomimetic) is covalently attached to a cytotoxic agent. The conjugation is done through a linker that allows good plasma stability and efficient drug release at the tumor site due to the higher presence of certain enzymes or physiological conditions. Once the payload is released from the conjugate, it recovers its original potency and induces apoptosis of the tumor cells (Figure 3).^[23–25]

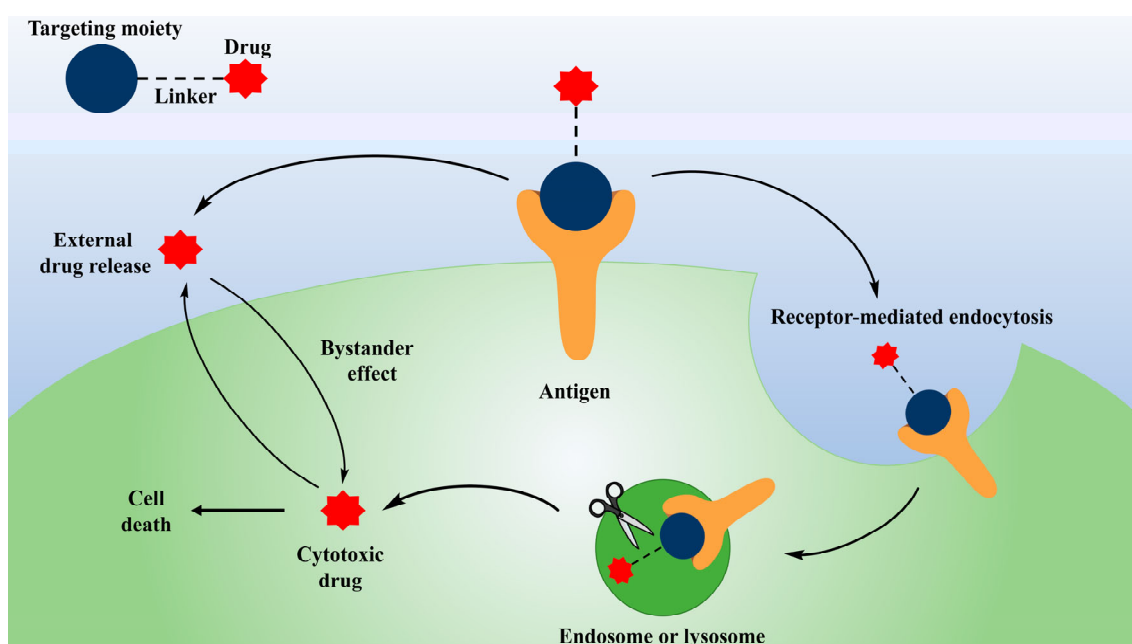


Figure 3. Mechanism of action in active tumor targeting approach.

Two main approaches are used to increase the therapeutic window of this class of compounds. The first one, consists in the discovery of new homing devices which recognize a specific antigen with exquisite selectivity and thus, increases the MTD of the conjugate. On the other hand, the research of new cytotoxic agents with increased potency contributes to reduce the minimum effective dose (MED). An ideal system would combine both techniques to enhance the therapeutic window as much as possible to have better chances of success.

Active targeting represents the cornerstone of current research in targeted therapy. Hundreds of products are currently in clinical trials and many more are in the research pipeline of the most important pharmaceutical companies worldwide.^[26]

The next sections will be exclusively focused on active targeting using antibodies or small molecules as targeting moieties, different type of linkers and payloads.

1.2.1 Antibody-Drug Conjugates (ADCs)

Antibodies, also called immunoglobulins (Igs), are large Y-shaped proteins consisting of four polypeptides, two identical light chains and two identical heavy chains, which are connected via disulfide bridges. Their production by the plasma cells enables the immune system to neutralize pathogens that could harm our body (e.g. bacteria, viruses) as they are able to recognize antigens with excellent specificity. These characteristics promoted the development of antibodies targeting certain antigens which are overexpressed in cancer cells.

The first antibodies were produced by vaccinating mice with a target antigen that stimulated the production of specific antibodies in the sera. Nevertheless, this procedure led to a mixture of antibodies, some of them being nonspecific, in poor yields. Seeking for a better methodology, Köhler and Milstein developed in 1975 the hybridoma technology, which was later awarded with the Nobel prize in physiology or medicine in 1984.^[27] In this technique, antibody-producing B cells from the spleen of a mice are isolated and fused with tumor cells resulting in hybridoma cells. These hybridoma cells can be then cultured *in vitro* to produce large amounts of the same monoclonal antibody (mAb) which can be used to treat different diseases. In cancer treatment, they can trigger an immune system response and are able to induce cancer cell death through different mechanisms.^[28]

However, after the first clinical trials in 1980, several drawbacks were observed. The murine origin of the mAbs produced an immune response resulting in a rapid clearance from the circulation. Modifications of the mAb through recombinant DNA technology resulted in the production of “chimeric” antibodies, in which some sequences of the mouse antibody were replaced by naturally occurring sequences in human antibodies

(Figure 4). The specific binding of the antibody was retained but chimeric antibodies contained a significant number of murine residues. Further development made possible the production of “humanized” antibodies, where only the indispensable complementary determining regions (CDRs) responsible for antigen recognition were from mouse origin. The continuous advancement of antibody engineering with the introduction of phage display technology, recently awarded with the Nobel prize in chemistry 2018 to George Smith and Sir Gregory Winter, and the usage of transgenic mice led the obtention of human antibodies. These products showed reduced or null immune response and the circulatory half-life was prolonged up to three weeks, an enormous extension when compared to murine antibodies (typically two to three days).

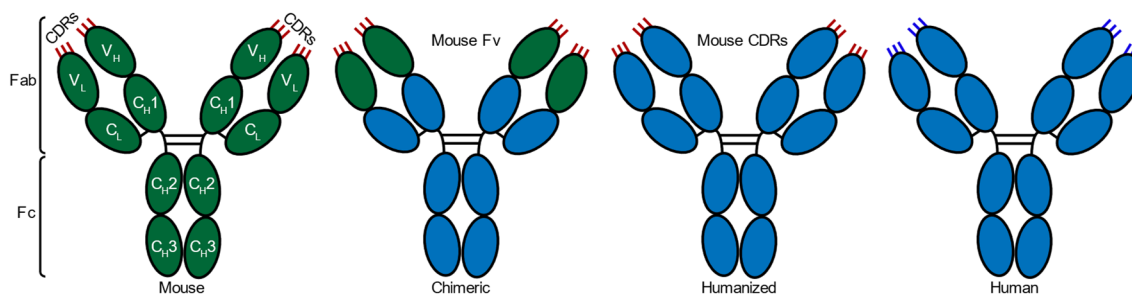


Figure 4. Representation of mouse, chimeric, humanized and human antibodies. Mouse fragments are represented in green and red while human fragments are represented in blue. The antibody subdomains are shown: fragment antigen binding (Fab), fragment crystallizable region (Fc), fragment variable domain (F_v), heavy-chain variable (V_H), heavy-chain constant (C_H), light-chain variable (V_L), light-chain constant (C_L) and complementary determining regions (CDRs).

All the efforts in the field were compensated with the FDA approval of the first antibody for the treatment of cancer, rituximab (1997) a chimeric antibody for the treatment of non-Hodgkin’s lymphoma. This accomplishment was successively followed by alemtuzumab (2001) and ofatumumab (2009). Despite the undeniable step forward of cancer treatment using antibodies, the therapeutic activity in solid tumors was modest at best and the treatment had to be combined with chemotherapeutic agents. Moreover, only two cell-surface receptors (HER2 and EGFR) were successfully targeted to treat solid tumors.

With the need to improve the therapeutic window of many cytotoxic agents and the clear evidences that antibodies could selectively recognize certain antigens from cancer cells, it appeared the idea to arm antibodies with payloads to create antibody-drug conjugates (ADCs).^[29] The mechanism of action of ADCs is based on Figure 3, a mAb recognizes

and binds an antigen that is overexpressed on the cancer cell surface. Then, the fused ADC-antigen undergoes internalization via receptor-mediated endocytosis. Through this route, the complex ends up in endosomes, which are responsible for two crucial steps. On the one hand, the antigen is recycled and transported back to the cell surface. On the other hand, it transports the ADC to the lysosome. In this compartment, the ADC undergoes different degradation pathways to release the cytotoxic agent in its unimpaired potent form. The complexity of ADCs arises the necessity of a multiparameter optimization from the three components (antibody, linker, and cytotoxic agent) in order to increase the possibilities of clinical success.^[30]

The first generation of ADCs was devoted to provide tumor selectivity of traditional chemotherapeutics.^[31] The best example from this class of compounds is an ADC that resulted from the conjugation of doxorubicin to the chimeric antibody BR96, which targets the Lewis-Y antigen. This conjugate was the only one from its class that reached phase II human clinical trial, but the limited antitumor activity in metastatic breast cancer and the observed toxicity in the gastrointestinal tract halted its development.^[32] The early clinical failure from the first ADCs lowered the initial enthusiasm that was generated in this challenging research area. However, deep analysis of the mistakes that were made established the basis for the development of efficient ADCs.^[33]

- First, the usage of a chimeric antibody resulted in a considerable immunogenic response, an important aspect to be considered in the next generation of conjugates that could be solved adopting humanized or human immunoglobulins as targeting devices.
- Second, the acid-labile hydrazone linker that was chosen to connect the antibody to the drug was unstable under physiological conditions showing a slow release of the drug which resulted in a lower therapeutic index and systematic toxicity. The design of new linkers should find a balance between good plasma stability and efficient intracellular drug release.^[34]
- Third, traditional cytotoxic agents were lacking potency to produce antitumor activity due to distinct uptake mechanisms. Based on different experiments, it was predicted that drugs with picomolar activity are required, which opened a new field of research of more potent payloads.

- Finally, the drug-to-antibody ratio (DAR) affects the potency and pharmacological properties. In general terms, higher DAR leads to increased *in vitro* potency but to unfavorable biodistribution and pharmacokinetics.^[35] Although it has been recently reported that a higher DAR can be beneficial when the hydrophobicity is reduced,^[36] the first generation of ADCs suffered from an overloaded antibody.

With all the previous considerations in mind, a second generation of ADCs was generated. As a result, four conjugates have received FDA approval (Figure 5).

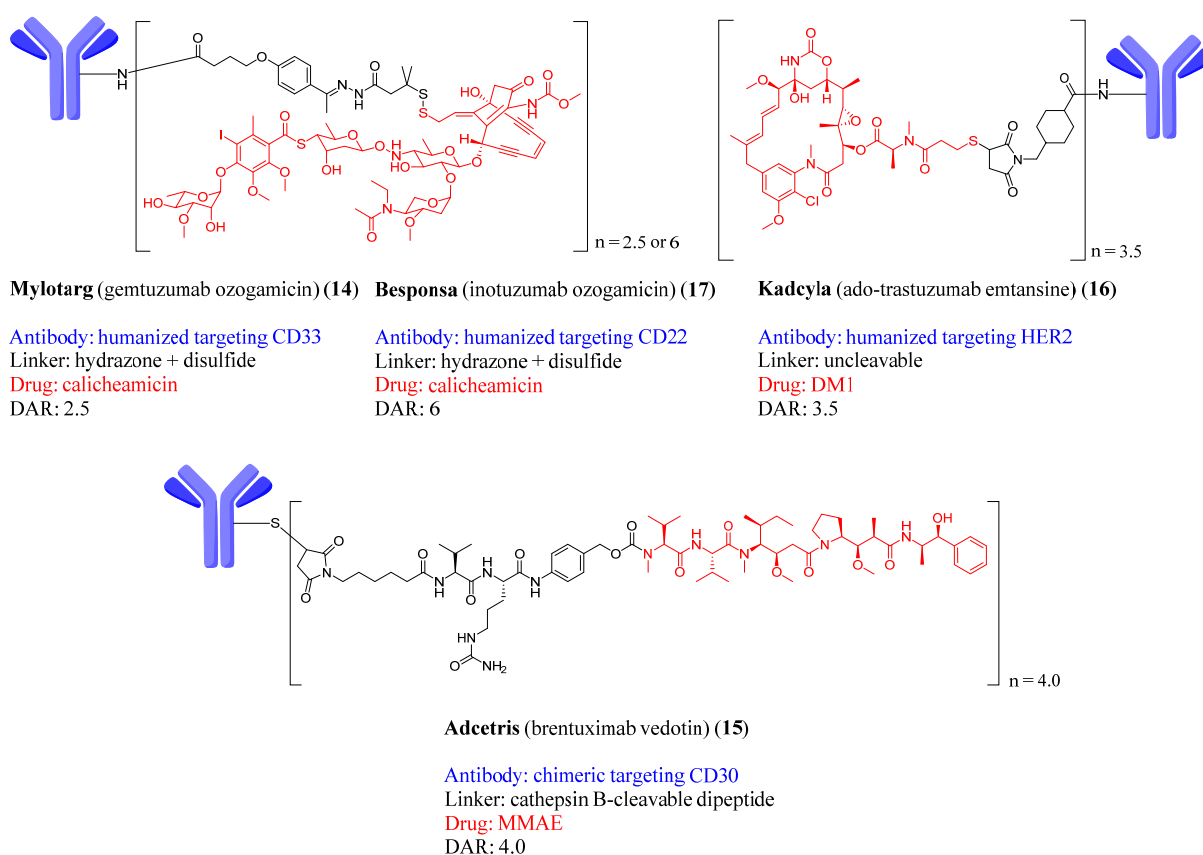


Figure 5. Molecular structures of the currently FDA approved ADCs.

Mylotarg™ (14, Figure 5) was the first ADC to receive FDA approval in 2000 for the treatment of acute myeloid leukemia.^[37] Due to its accelerated approval, a postmarketing clinical trial was done with an unexpected outcome. It was not possible to confirm a therapeutic benefit in the treatment group and, moreover, a slight increased treatment-related mortality was observed. As consequence, the drug was withdrawn from the market in 2010. However, subsequent trials with lower doses and fractioned regimens resulted in the long-awaited reapproval in 2017.^[38] More than ten years after the first ADC approval, Adcetris™ (15, Figure 5) was approved in 2011 for the treatment of relapsed Hodgkin

lymphoma and systematic anaplastic large cell lymphoma.^[39] Only two years later, in 2013, Kadcyla™ (**16**, Figure 5) was approved for treating HER2 positive breast cancer.^[40] Besponsa™ (**17**, Figure 5) is the most recent example of success in this field with its approval in 2017 for the treatment of acute lymphoblastic leukemia.^[41]

The success of the first ADCs raised the interest in this area of research and many companies introduced them in their pipelines.^[42] As a result, about 60 products are currently in different stages of clinical trials and many more are in the preclinical phase.^[43] However, this technology is far from being optimal and presents several drawbacks to take into account.^[44]

- Due to its large size, antibodies present a poor penetration in solid tumors and the long circulatory half-life can produce side effects due to premature payload release.
- Although the usage of human antibodies has dramatically reduced the immunogenicity, an immune response can still be triggered upon long treatments and, as a result, the efficacy gets compromised.
- The products obtained using traditional thiol-maleimide strategy are heterogeneous mixtures of compounds with different DAR. The properties of them varies drastically and the purification to obtain a homogenous product is challenging. The site-specific conjugation has appeared as a new approach to overcome this problem but the technology is still under development.^[45,46]
- Finally, the large-scale production of ADCs is challenging, as it requires simultaneously the usage of sterile conditions and safety precautions due to the high cytotoxicity. As a result, this class of compounds presents high cost-of-goods which limit their development and increase the costs of the treatment.

Moreover, the mechanism of action is not yet fully understood. A special mention regarding the requirement of internalization for anticancer efficacy needs to be done. While it was generally accepted that active targeted therapy activity relies on the efficient internalization of the construct, it has been recently proven that non-internalizing compounds can display potent and selective antitumoral activity.^[47-52] In this case, upon binding of the antibody to the desired antigen, the drug is released in the tumor microenvironment and the drug effects its cytotoxicity by the so-called bystander effect.

With all these limitations, there is a strong motivation to explore alternative homing devices which may be easier to produce and can reach diseased cells more efficiently.

1.2.2 Small Molecule-Drug Conjugates (SMDCs)

Small molecules (e.g. peptides, peptidomimetics) have emerged as a promising alternative to antibodies as homing devices.^[53–57] Their smaller size renders a better extravasation and penetration in the tumor. Moreover, the conjugation chemistry used to produce small molecule-drug conjugates (SMDCs) leads to defined molecular structures that can be easily purified and characterized. This characteristic also allows a hit-to-lead optimization and dramatically reduces the production costs when compared to ADCs. Another advantage of SMDCs is their lack of immunogenicity.

The biggest difference between ADCs and SMDCs is their pharmacokinetics. While ADCs remain in circulation up to one week, SMDCs are readily cleared through the kidneys and usually display half-life shorter than one day. Although ADCs can display activity via EPR effect, the rapid pharmacokinetics of SMDCs allows higher payload concentration in the tumor tissue and reduce the side effects to other organs (Figure 6).^[58] Nevertheless, due to its faster pharmacokinetic profile, SMDCs may require more frequent dosing.

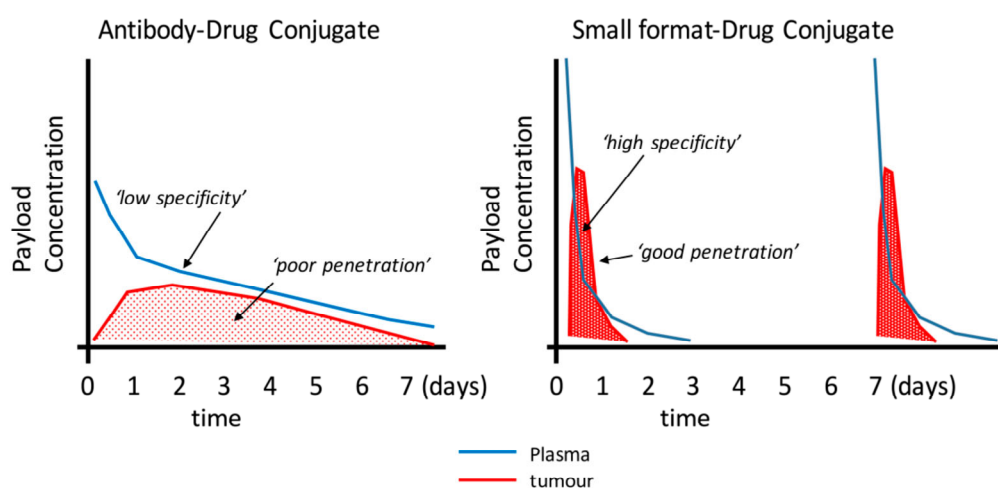


Figure 6. Schematic illustration of the potential mechanistic and pharmacokinetic differences between an ADC and a SMDC.^[58]

Despite all the advantages of small molecules as targeting moieties compared to antibodies, their clinical application has not been proven yet. One may attribute that to several reasons. On the one hand, peptides usually suffer from short plasma half-life as a result of their fast clearance and poor stability against proteases. However, the progress in the field has minimized the problem using different methods such as cyclization, *N*-methylation or the introduction of D-amino acids.^[59] On the other hand, while antibodies can be virtually generated against any antigen, peptide targeting remains limited to a small number of targets. Among the antigens that have been successfully targeted with small molecules, the Folate Receptor (FR), the Prostate-Specific Membrane Antigen (PSMA), the Somatostatin Receptors (SSTRs) and Carbonic Anhydrase IX (CAIX) have received most of the attention and will be described in the following sections. More recently, other receptors (e.g. the biotin receptor, bombesin receptor, Eph receptor) have gained attention as they can be potentially targeted with small molecules. In this direction, Bicycle Therapeutics have made excellent progress discovering bicyclic peptides targeting different receptors using phage display techniques. The compound named BT1718, a bicyclic peptide targeting the membrane type 1 matrix metalloproteinase (MT1-MMP) conjugated to DM1, is their lead molecule and is currently being evaluated in a phase I/IIa clinical trial. Moreover, with the growing interest in this field, the development of phage display techniques, and the increasing knowledge in the design of ligand-targeted cancer therapeutics, it is expected that many receptors can be targeted in the future using small molecules.^[60,61]

1.2.2.1 SMDCs targeting the folate receptor (FR)

Larger amounts of vitamins are required to sustain the fast-growing rate of cancer cells. To fulfill their needs, certain tumors overexpress vitamin receptors and this expression level increases in advanced stage of the disease. Among them, the folate receptor (FR) has received most of the attention and several compounds primarily developed by Endocyte have entered clinical trials. Folic acid, also known as folate or vitamin B₉, has shown optimal properties as targeting moiety for the folate receptor. Its high binding affinity ($K_d = 1-10$ nM) and easy functionalization allowed the construction of conjugates for diagnosis and therapeutic purposes.^[62,63]

The first compounds using folate as targeting moiety were devoted to imaging purposes. Etarfolatide (**16**, Figure 7) was one of the first products of its class that reached clinical trials. The molecule consists in the conjugation of folate to an imaging agent based on technetium-99m which has been used in different clinical stages to identify FR positive patients.^[64,65] Folate-fluorescein, better known as EC17 (**17**, Figure 7), was also developed for diagnosis purposes and has been used for intraoperative tumor removal.^[66] With the successful identification of FR positive tumors using several imaging conjugates, different SMDCs employing folate as targeting moiety have been reported.^[67]

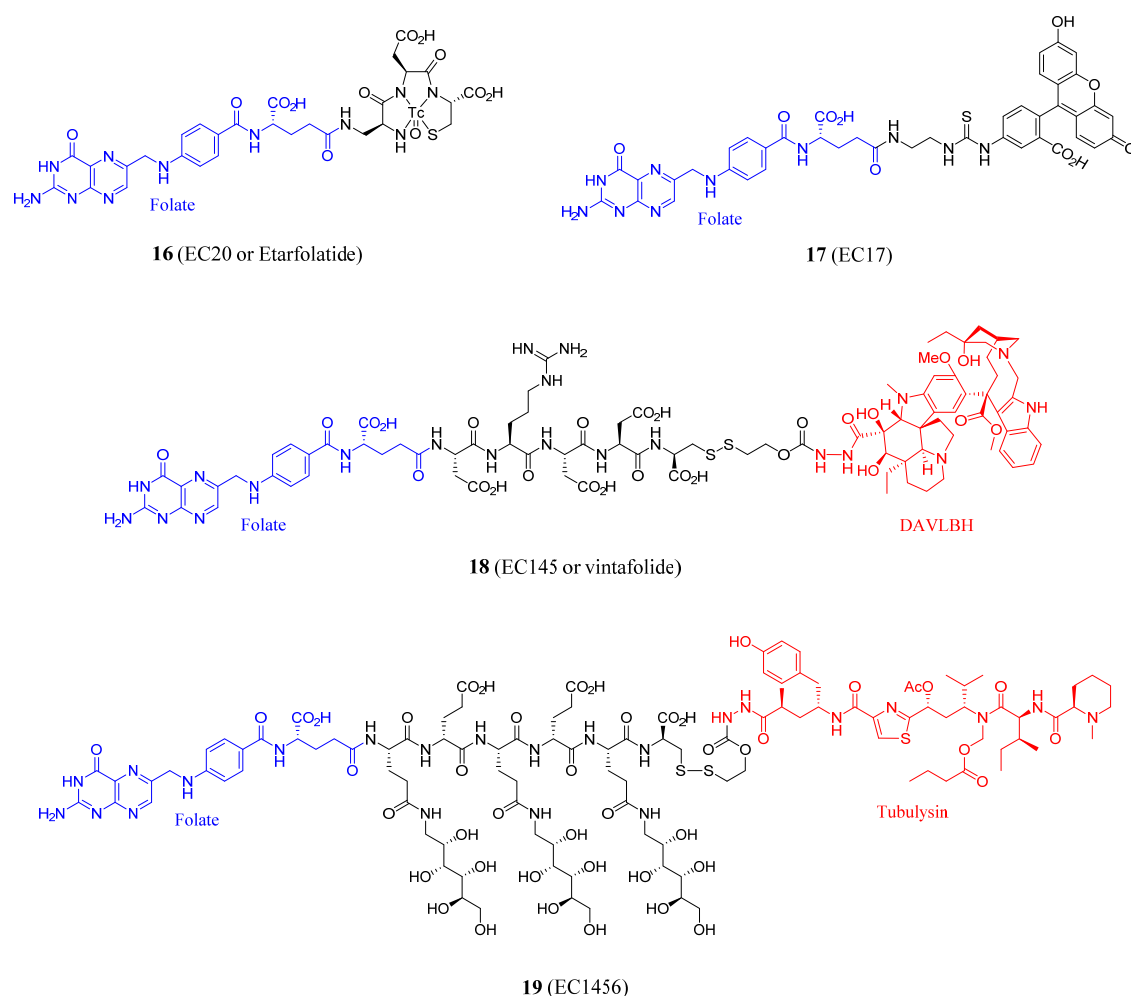


Figure 7. Molecular structures of folate conjugates for imaging or therapeutic purposes.

The most studied SMDC using folic acid as delivery vehicle is vintafolide (**18**, Figure 7), a conjugate containing desacetylvinblastin hydrazide (DAVLBH) as drug.^[68,69] First developed by Endocyte and later licensed to Merck in an operation worth up to \$1 billion, it reached phase III clinical trials for platinum-resistant ovarian cancer. However, the

results of the clinical trials, reported shortly after the European Medicines Agency (EMA) had recommended the drug approval, halted its development. With the recent setback of vintafolide, the efforts of Endocyte are now focused on novel conjugates bearing different payloads such as tubulysin (**19**, Figure 7), currently in clinical trials phase I, or pyrrolobenzodiazepines.^[70,71]

1.2.2.2 SMDCs targeting the Prostate-Specific Membrane Antigen (PSMA)

Prostate cancer (PCa) represents the second most prevalent cancer among men worldwide. The prostate-specific membrane antigen (PSMA) is a specific marker used for the diagnosis of PCa because its concentration is elevated in case of prostate disorders. Moreover, this glycoprotein is overexpressed in the cell surface of prostate cancer cells and represents an interesting dartboard to be targeted.^[72] Interestingly, the expression levels are further enhanced with cancer aggressiveness and metastasis. The 2-[3-(1,3-dicarboxypropyl)ureido]pentanedioic acid (DUPA) motif and several derivatives have high binding affinity to PSMA and can be used for targeting purposes. Like in the folate receptor field, most of the advances and clinical trials have been reported by Endocyte. More recently, Heidelberg Pharma has also entered in this research area developing ADCs and SMDCs targeting PSMA.

One of the first compounds to be developed used the metastable nuclear technetium-99m for the diagnosis of PSMA positive tumors (**20**, Figure 8).^[73] More recently, the conjugation of a DUPA analogue to the cytotoxic agent tubulysin led to EC1169 (**21**, Figure 8), which showed good *in vivo* activity in mice and has been tested in clinical trial phase I although no results have been reported so far.^[74] The most promising PSMA targeting compound, Lu-PSMA-617 (**22**, Figure 8) was developed by Endocyte and is currently in clinical trial phase III. The therapeutic activity of this compound relies on the β -particle radiation emitted by Lutetium-177 which causes cell death. Due to the well defined range of action of these particles (1 mm), only cancer cells expressing PSMA are affected and side effects to other tissues are reduced.^[75] Moreover, the efficacy of this compound has been enhanced with the incorporation of several albumin-binding motifs (**23**, Figure 8) to increase the circulatory half-life, although only preclinical data is available.^[76,77]

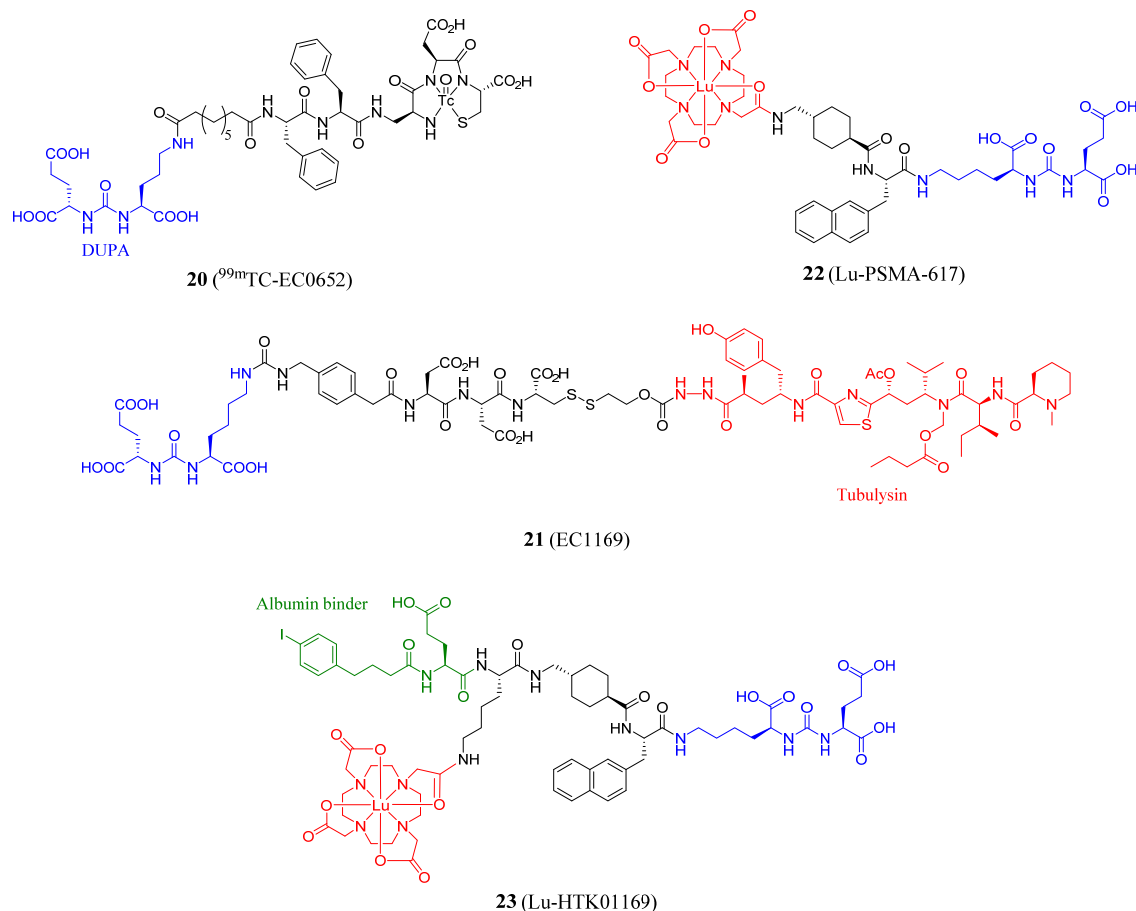


Figure 8. Molecular structures of conjugates targeting the PSMA receptor.

1.2.2.3 SMDCs targeting Carbonic Anhydrase IX (CAIX)

The fast metabolism of tumors to sustain the uncontrolled proliferation of cancer cells leads to acidic microenvironment and hypoxic regions.^[55] Carbonic anhydrases (CAs) are transmembrane zinc metalloenzymes responsible to catalyze the reversible hydration of carbon dioxide to hydrogen carbonate and proton ($\text{CO}_2 + \text{H}_2\text{O} \leftrightarrow \text{HCO}_3^- + \text{H}^+$).^[78] Their most important function is to maintain the acid-base balance and to transport carbon dioxide out of the tissues. As a consequence, two from the fifteen known isoforms of carbonic anhydrase, CA9 and CA12, are overexpressed in many tumors. Carbonic anhydrase IX (CAIX) is the most strongly overexpressed gene in response to hypoxia in cancer cells and is a marker for unfavorable prognosis.^[79] Moreover, its expression in healthy tissues is limited to low levels in the gastro-intestinal tract making it an exquisite marker for targeted therapy.

In the last years, several advances have been made by Neri and co-workers from Philogen, and more recently Endocyte has entered this field as well. A first and prominent milestone was the discovery that an acetazolamide derivative can efficiently target CAIX.^[80] This moiety was used to create SMDCs using duocarmycin derivatives or mertansine (DM1) as cytotoxic agents and produced a significant tumor growth delay in nude mice. More interestingly, the acetazolamide moiety has been labeled with technetium-99m for diagnosis purposes and the obtained compound (**24**, Figure 9) is currently entering clinical trials phase I.^[81]

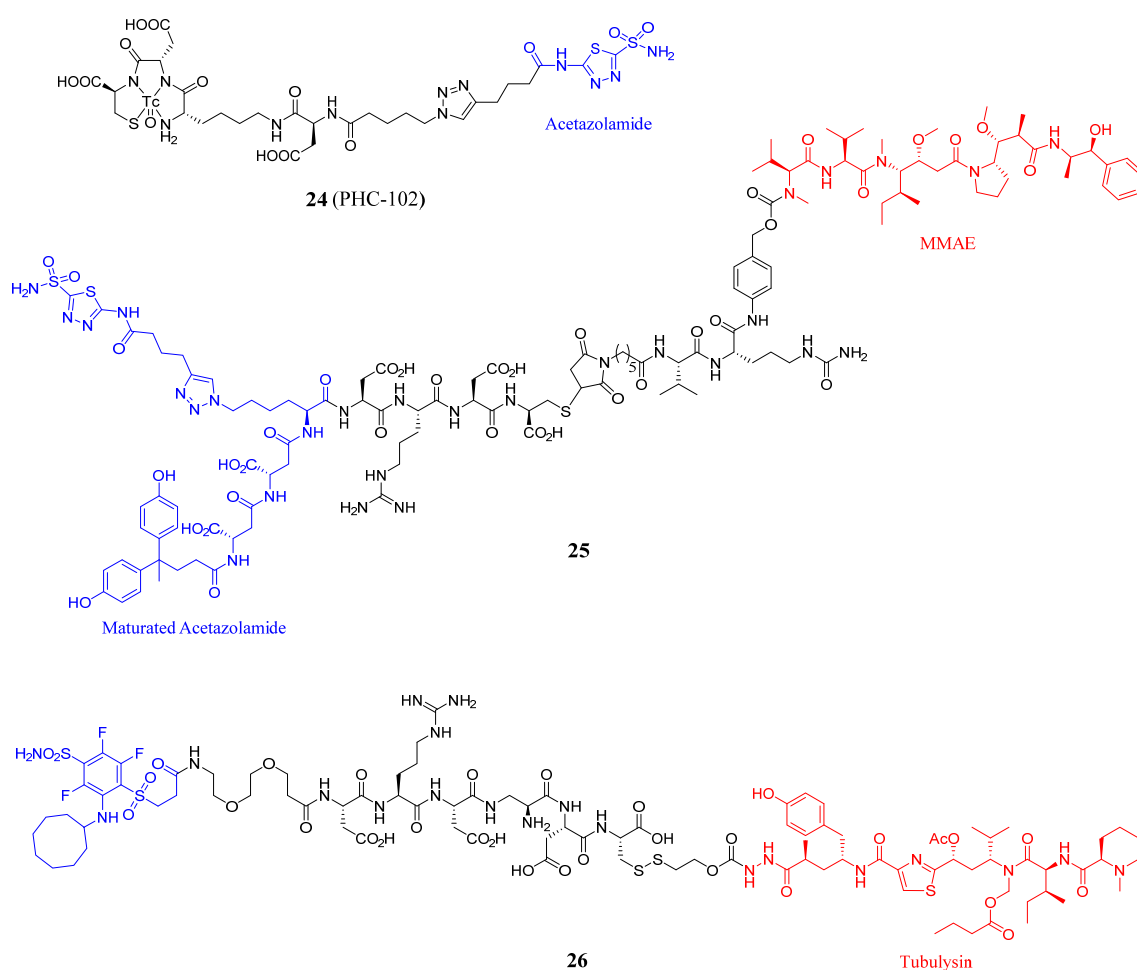


Figure 9. Molecular structures of conjugates targeting the CAIX enzyme.

With the basis established, the conjugates were further improved by studying different payloads and optimizing the linker to be used in order to obtain an efficient release of the cytotoxic agent and avoid side effects.^[82,83] Further improvements of the targeting properties were achieved using different methods. The usage of a bivalent acetazolamide moiety clearly increased the therapeutic activity of previously reported conjugates.^[84]

Alternatively, dual-display DNA-encoded chemical libraries can identify new fragments to increase the binding affinity due to chelate effect. Using this technique, a new fragment was discovered and the resulting bidentate ligand displayed an improved binding affinity.^[85] Employing the matured acetazolamide moiety and the best linker-drug combination from previous publications, a SMDC (**25**, Figure 9) was prepared.^[86] Conjugate **25** showed remarkable tumor growth delay and was able to challenge the therapeutic efficacy of an ADC targeting the same antigen and employing an equal linker-drug moiety. Moreover, the compound showed better biodistribution at early time points and when combined with interleukin-2 it was able to eradicate cancer in all studied nude and immunocompetent mice.^[87]

More recently, the fluorobenzosulfonamide (CAL) moiety targeting CAIX has been used to develop a conjugate using tubulysin as cytotoxic agent (**26**, Figure 9).^[88,89] The compound exhibited the characteristic non-internalizing properties of CAIX targeting conjugates and showed a remarkable tumor growth delay in nude mice.

1.2.2.4 SMDCs targeting Somatostatin Receptors (SSTRs)

The somatostatin receptors (SSTRs) are a superfamily of G protein-coupled receptors which can be subdivided in five subfamilies, SSTR1-SSTR5. The native somatostatin (SST) peptide hormone is responsible for the regulation of the neuroendocrine system by interacting with the SSTRs. Among other functions, somatostatin is responsible to suppress the growth hormone and the insulin secretion.^[90]

Many neuroendocrine tumors overexpress the SSTRs, mainly SSTR2, which could be potentially targeted with SST (Figure 10). Unfortunately, somatostatin, which is presented in two active forms, sst-14 and sst-28, cannot be used due to its short half-life *in vivo* (2-3 min). However, peptide development allowed the identification of octreotide (**28**, Figure 10), an octapeptide analogue of somatostatin. The incorporation of D-amino acids and the downsizing of the peptide dramatically increased the half-life (2 h). Moreover, while SST presents high affinity for the five SSTRs subtypes, octreotide shows specificity for SSTR2. For all these reasons, octreotide is used to treat acromegaly and tumors producing growth hormone and is the third top-selling non-insulin peptide.^[91]

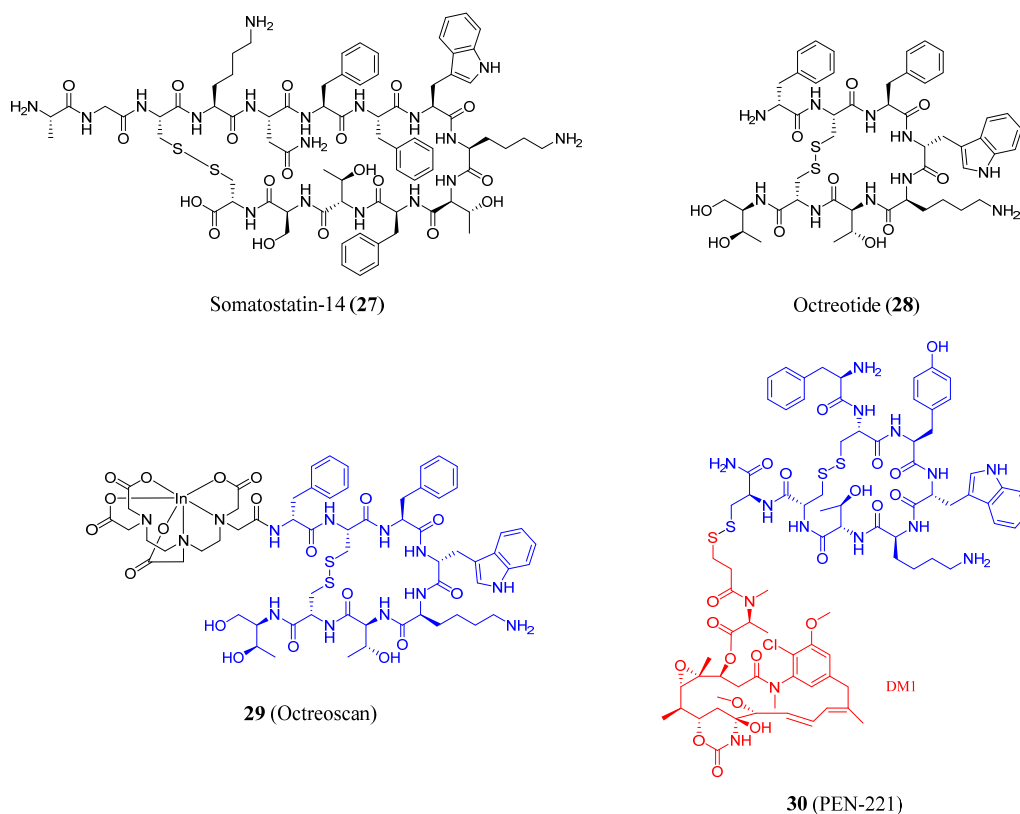


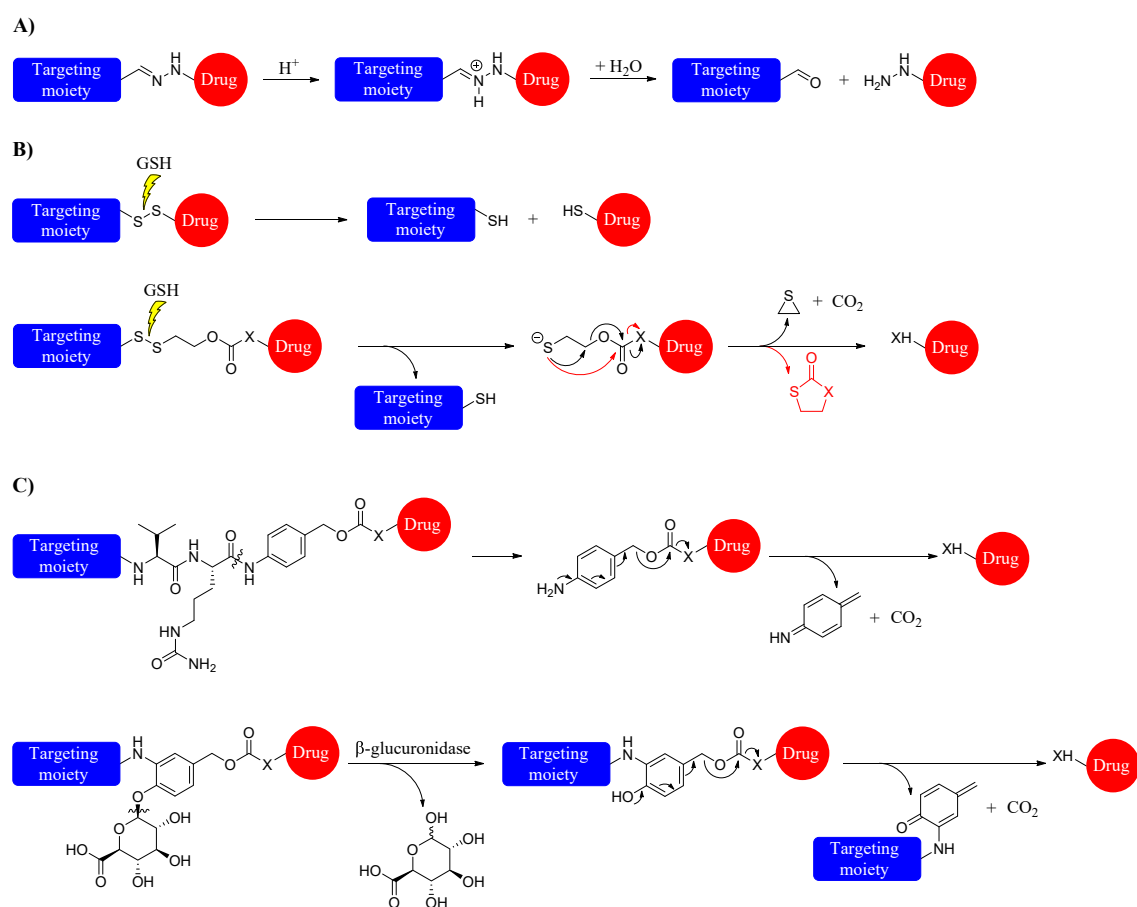
Figure 10. Molecular structures of somatostatin-14, octreotide, octreoscan, and PEN-221.

Octreotide conjugates have been largely studied for the diagnosis and therapy of neuroendocrine tumors. The most successful example is octreoscan, an indium-111 radiolabeled octreotide, clinically used for more than 20 years to detect pancreatic neuroendocrine tumors (29, Figure 10). More recently, a gallium-68 conjugate showed higher sensitivity and resolution to image neuroendocrine tumors compared to octreoscan and received FDA approval in 2016. This compound, also named ^{68}Ga -DOTATATE, consists of Tyr³-octreotate, a closely related analogue of octreotide containing a carboxylic acid at the C-terminus (octreotate) and a tyrosine in the third position of the sequence. The DOTA chelator at the N-terminus allows the complexation of gallium-68. The same compound but containing the radiotherapeutic lutetium-177 is approved for the treatment of SSTR positive gastroenteropancreatic neuroendocrine tumors under the trade name Lutathera.^[92,93] Octreotide has also been conjugated^[92,93] to a large number of cytotoxic agents such as doxorubicin,^[94] periplocyarin^[95] or paclitaxel.^[96] However, none of these compounds passed the preclinical evaluation. An exception needs to be mentioned with a compound developed by Tarveda Therapeutics named PEN-221 (30, Figure 10), which is currently in clinical trial phase 1/2a. This compound combines the targeting properties

of an analogue of octreotide with the killing potency of DM1 and it has been able to eradicate tumors in different xenograft models.^[97]

1.2.3 The linker

The connection between the targeting moiety and the cytotoxic agent is of high relevance as it can dramatically modulate the safety and efficacy of the final construct. An ideal linker should present complete stability in circulation and fast degradation in the lysosomes or in the proteolytically and physiologically enriched extracellular milieu of the tumor. Moreover, the linker usually contains highly hydrophilic moieties to increase the water solubility of the final construct. Linkers can be classified into four main groups according to their mechanism of release: uncleavable, acid-labile, reducible and enzyme sensitive (Scheme 1).^[98,99] Another aspect to take into account is the need to include a self-immolative spacer to increase the release effectivity in many cases.^[100]



Scheme 1. Drug release mechanism of active targeting compounds bearing acid-labile (A), reducible (B) or enzymatically sensitive (C) linkers. X = NH or O.

- **Uncleavable linkers** are characterized to have very good stability in circulation and the release of the drug only occurs in the lysosomes after internalization and hydrolysis of the conjugate. Due to their properties, the usage of non-cleavable linkers is not recommended in the SMDC field but can be useful in ADC development. Indeed, one of the currently approved ADCs, Kadcyla[®], has an uncleavable linker. Using this type of linkers, the bystander effect remains very limited due to the drug release mechanism. Moreover, due to the lysosomal degradation mechanism to release the cytotoxic agent, it is important to choose a payload that is active even if complete degradation does not occur. Despite the success, few ADCs currently under development use a non-cleavable linker because drug release occurs too slow and remains limited to antigen positive cells that internalize the full construct. However, uncleavable linkers remain very useful for conjugates for diagnostic purposes due to their high stability.
- **Acid-labile linkers** rely on the difference between physiological neutral pH and the acidic conditions that can be found in certain cellular compartments (i.e. endosomes pH 5.0 – 6.5, lysosomes pH 4.5 – 5.0) and in the extracellular microenvironment of tumors.^[101] Among others, hydrazones (Scheme 1A) are widely used as acid-labile sensitive linkers. This type of linker is used in two clinically approved ADCs, but their stability needs to be carefully analyzed in each case as it has been proven that sometimes are not stable in circulation.
- **Reducible linkers** mostly based on disulfides are gaining importance, especially in the SMDC field. Glutathione (GSH), a tripeptide capable of reducing disulfide bonds, is essential for cell survival and its concentration is upregulated during oxidative stress and inflammation.^[102] While the concentration of GSH is low in the extracellular space of healthy cells and plasma (~ 10 μM), 1000-fold higher concentrations (~ 10 mM) can be found in the tumor stroma and intracellular compartments of cancer cells. This concentration difference can be used to develop delivery systems based on disulfides or other reducible moieties. The main advantage of disulfides is that the stability and release can be easily tuned by modifying the steric hindrance of the adjacent carbon atoms of the disulfide. Moreover, in some cases it is possible to directly connect the payload and the targeting moiety (Scheme 1B).

However, as many payloads do not contain a free thiol, the incorporation of a self-immolative moiety is required.

- **Enzyme sensitive linkers** are widely used in both the SMDC and the ADC field. Their mechanism of action relies on the overexpression of certain proteases which can selectively cleave known sequences. The cathepsin B-cleavable dipeptide valine-citrulline and closely related analogues (*e.g.* Val-Ala) are the most widely used enzyme sensitive linkers (Scheme 1C). Very recently, it has been shown that this type of linker can be processed in the absence of cathepsin B and multiple proteases are responsible for degradation.^[103] Glycosides such as glucuronide or galactoside are emerging as an alternative to the traditional cathepsin B cleavable linkers. They can be efficiently cleaved by β -glucuronidase and β -galactosidase, respectively.^[104,105]

1.2.4 The payload

Research on new anticancer drugs has been very active since the discovery of the first chemotherapeutic agents. After the discovery of paclitaxel and doxorubicin, it was believed that higher potency would improve the clinical activity because the minimum effective dose would be considerably reduced. Since many cytotoxic agents are derived from natural sources, research in natural products was largely explored. As a result, several highly toxic agents with different modes of actions were discovered (Figure 11).

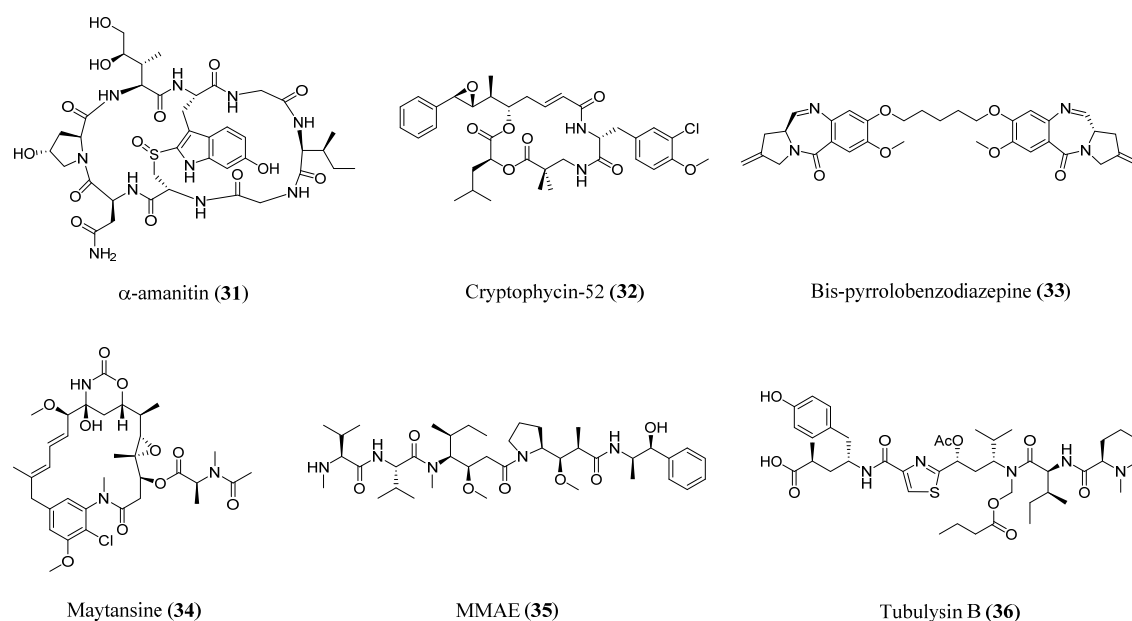


Figure 11. Molecular structures of some highly potent cytotoxic agents.

The new compounds can be subdivided in two main classes: DNA- and RNA- targeting (e.g. amanitins, pyrrolbenzodiazepines) and tubulin interacting agents (e.g. maytansinoids, auristatins, cryptophycins, tubulysins). Despite the higher cytotoxicity of these compounds compared to classical chemotherapeutics, the therapeutic window was not improved due to their low maximum tolerated dose. However, they present enormous potential to be used as cytotoxic agents in a tumor targeted delivery approach.

1.3 Cryptophycin

During a screening campaign to identify new pharmaceuticals, researchers at Merck detected a cyclic depsipeptide with interesting properties. The compound isolated from cyanobacteria *Nostoc sp.* showed remarkable antifungal properties and was named cryptophycin due to its high potency against *Cryptococcus sp.*^[106] Later on, the same compound (cryptophycin-1, Figure 12) was extracted from another strain of cyanobacteria and the total structure was proposed.^[107] However, the subsequent total synthesis identified a wrongly assigned absolute configuration of one stereocenter, which was then corrected.^[108] Further studies allowed the isolation of 18 new analogues from the same strain.^[109] At about the same time, arenastatin A, better known as cryptophycin-24 (**38**, Figure 12), was isolated from the marine sponge *Dysidea arenaria*.^[110] The total structure of this compound was later elucidated and the first total synthesis was performed and improved.^[111–113]

All the discovered cryptophycins can be retrosynthetically divided in four subunits, namely A-D. Unit A represents the most exotic fragment being an α,β -unsaturated δ -hydroxycarboxylic acid with four stereogenic centers and a benzylic epoxide. Fragment B can be derived from D-*O*-methyltyrosine and may contain a chlorine in the 3'-position. β -alanine represents the core of unit C and can be α -mono or α,α -dialkylated. Finally, L-leucic acid constitutes the fragment D.

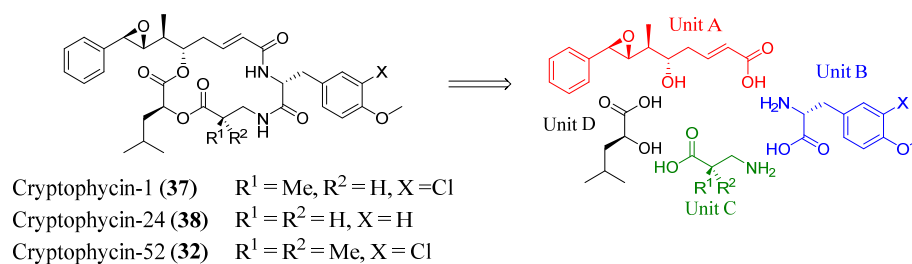


Figure 12. Molecular structures of cryptophycin-1, cryptophycin-24, and cryptophycin-52 and retrosynthetic division.

Shortly after the discovery of cryptophycin-1, biological screening assays showed a high cytotoxicity against several cancer cells lines, even multi-drug resistant (MDR) ones. These properties compromised their applicability as antifungal compounds, but motivated their development as anticancer drugs.^[114]

For this reason, several structure-activity relationship (SAR) studies aiming to find a more active compound were started. These results will be explained more in detail in section 1.3.2, but special attention needs to be paid to the discovery of cryptophycin-52 (**32**, LY355703).^[115] This compound, identified by Eli Lilly, retained the high cytotoxicity of the parent compound and showed an enhanced stability towards hydrolysis, because it contains a dimethyl substitution at the α position of unit C, which protects the susceptible ester between units C and D.^[116] As a result, cryptophycin-52 entered clinical trials phase I and II.^[117–120] From the two clinical trial phase II studies, it was concluded that around 40% of patients obtained a clinical benefit, either with partial response or disease stabilization. However, the activity of cryptophycin-52 was not superior to other drugs that were already available, and neurotoxicity was observed in some cases. The side effects forced a dose reduction and limited, even more, its efficacy. Consequently, further clinical evaluation of the compound was discontinued and opened a new era of research for cryptophycin.

1.3.1 Biological mode of action

Tubulin is a superfamily of globular proteins composed of six different groups although the term tubulin usually refers to the dimers formed by the α - and β -moieties. This heterodimer polymerizes to form the microtubules, a major component of the eukaryotic cytoskeleton. They are essential in many cellular processes such as development and maintenance of cell shape, cell division, and mitosis. In order to fulfill their functions, microtubules undergo a highly dynamic process with a continuous polymerization/depolymerization (Figure 13).^[121]

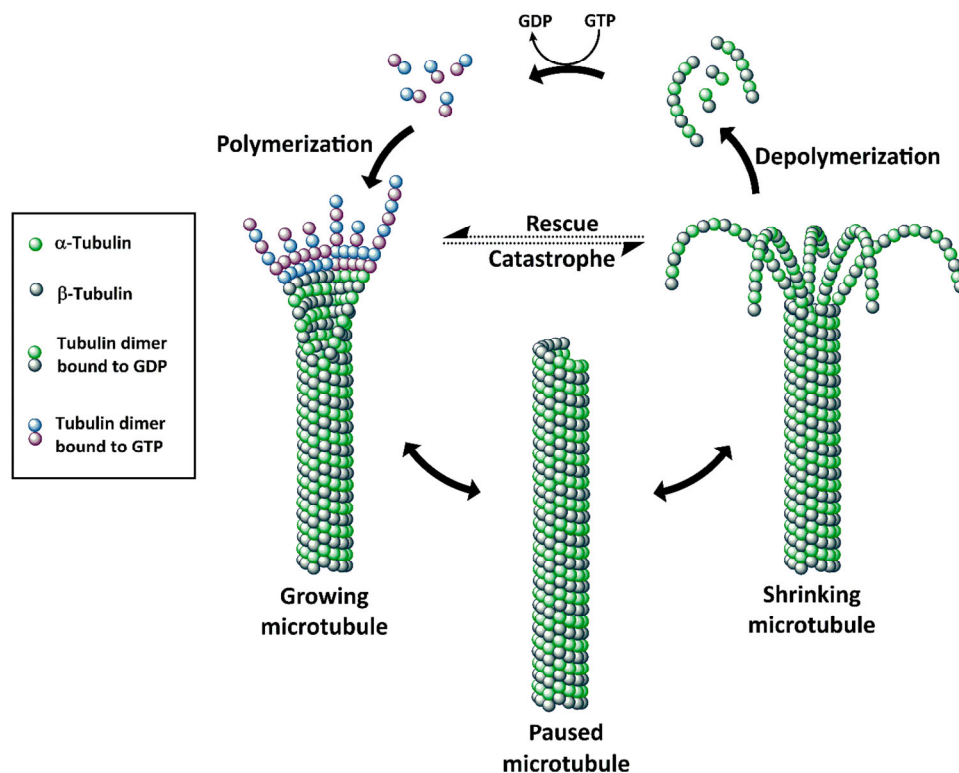


Figure 13. Structure, polymerization and depolymerization dynamics of microtubules.^[122]

α - and β -tubulin are GTPases, which means that each monomer contains a guanosine triphosphate (GTP) molecule. However, the two GTP binding sites present different properties. The GTP of the α -tubulin is located in the non-exchangeable site while the one located at the β -tubulin is exchangeable and susceptible to hydrolysis to form guanosine diphosphate (GDP).

The microtubule formation proceeds in two steps: nucleation and elongation. Shortly after elongation, the GTP of β -tubulin is hydrolyzed to GDP and the rate of this reaction determines their dynamics. Microtubules containing a GDP cap are 100 times more

susceptible to hydrolysis than their GTP cognates. Therefore, a GTP cap favors microtubule growth while shrinkage is promoted in the case that GDP is present.

Because microtubule dynamics are crucial for cell division, disrupting them causes cell cycle arrest in the G2/M phase and induces apoptosis. For this reason, drugs targeting microtubules have emerged as good candidates for cancer treatment.^[123] Depending on their mode of action, microtubule interacting agents can be classified in two main groups: microtubule stabilizers which promote the tubulin polymerization, and microtubule destabilizers which bind to tubulin dimers and block the formation of microtubules.^[124] The activity of microtubule interacting agents is based on their capability to bind to tubulin. Up to now, five binding sites are known: *vinca* alkaloid domain, taxane binding site, colchicine region, maytansine area and laulimalide domain.

Cryptophycin-1 (**37**) has high binding affinity for tubulin and inhibits its polymerization, hence it is a microtubule destabilizer.^[125,126] The same mode of action has also been confirmed for other cryptophycins, such as cryptophycin-52 (**32**).^[127,128] Interestingly, the exact binding mode of cryptophycin to tubulin has not yet been confirmed because no crystal structure of the cryptophycin-tubulin complex has been described. However, different experiments suggest the *vinca* domain as binding site of cryptophycins. First it was shown that binding of vinblastine is impaired upon competition with cryptophycin, while colchicine and paclitaxel binding are not compromised in the same experiment.^[129–131] Moreover, molecular dynamics and molecular docking studies are in agreement with the experimental findings.^[132] Despite the high binding affinity, cryptophycins interact in a non-covalent manner to tubulin as they can be recovered from the tubulin complex upon denaturation.^[133,134]

Furthermore, the activity of cryptophycin is not reduced in MDR cells because it is a poor substrate for the P-glycoprotein efflux pump, a typical cell membrane protein responsible to transport many substances out of cells.^[135]

1.3.2 Structure-activity relationship (SAR) studies

Since the discovery of the first cryptophycin, several SAR studies were initiated. At first, the research was focused in the total synthesis and discovery of new cryptophycins with higher toxicity and increased stability to proteases.^[136–138] As a result, cryptophycin-52 was discovered and brought to clinical trials phase II. With the setback of its failure, SAR studies continued to understand the essential structural requirements for effective binding to tubulin to retain activity. Several analogues with high cytotoxicity have been discovered, but they present the same drawback than the parent compound. They lack tumor selectivity and thus, produce severe side effects.

With the growing interest in tumor targeting, cryptophycins have emerged as potential payload.^[139] Nevertheless, most of the cryptophycins lack a functional group for connection to a homing device. For this reason, in the last years the SAR research has been focused on functionalized cryptophycins that can be used for conjugation in tumor targeting therapy.^[140] As a result, many active analogues have been discovered and allowed the construction of ADCs and SMDCs. The most relevant and active examples will be explained in the next sections.

1.3.2.1 Unit A

The unusual δ -hydroxy acid of unit A has been by far the most explored fragment of cryptophycin. The four consecutive stereocenters represents a challenge from the synthetical point of view and several strategies to obtain the desired diastereomer in short synthetic routes have been explored.^[141–144] From early SAR studies, it was established that the absolute stereochemistry of the four stereocenters is of crucial importance and any modification results in a dramatical reduction of activity. However, certain modifications are tolerated in the benzylic epoxide.^[145] While epoxides with other configurations (*R/S*, *S/R* or *S/S*) than the original (*R/R*) are much less active, the acid-mediated opening of the β -epoxide to obtain the corresponding halohydrin retains the activity of the parent compound (Figure 14).^[146] This can be attributed to their prodrug character as they are converted back to the epoxide under physiological conditions. Despite their higher biological activity *in vitro* and *in vivo*, the chlorohydrins never entered clinical trials because they cannot be formulated as stable solutions.^[147] Later on,

it was discovered that stabilization of cryptophycin-55, the chlorohydrin of cryptophycin-52, and other chlorohydrins is possible upon esterification of the secondary alcohol with glycine while retaining the high activity.^[148] Esterification with other amino acids such as alanine or aminoisobutyric acid has also been studied, with a 50-fold and 1100-fold reduction of activity, respectively.

The *para* position of the aromatic unit A has also been largely explored. The first studies aimed to increase the poor water solubility of the parent compound while retaining the cytotoxicity.^[149–151] For this reason, different polar groups (e.g. alcohols, amines, carboxylic acids) have been introduced. As a result, several analogues have been obtained and some of them are even more potent than the parent compound. Unfortunately, many lost their activity against MDR cells because they became good substrates for the P-glycoprotein transporter and thus, research was discontinued.^[152] Very recently, Sanofi has used some of these analogues to create ADCs.

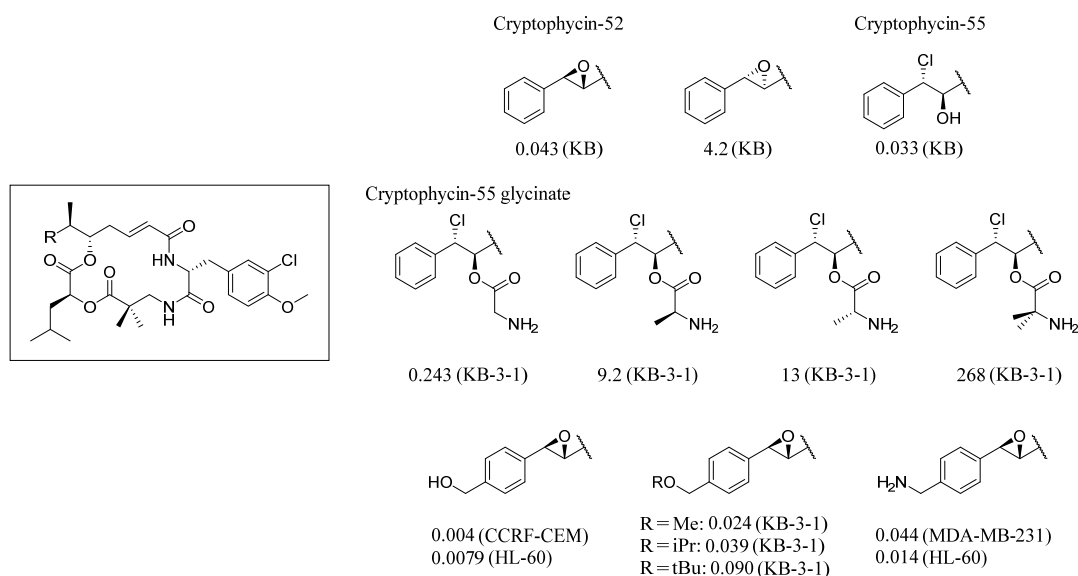


Figure 14. Cytotoxicities of unit A modified cryptophycin-52 analogues (IC₅₀ values in nM). Cell lines: KB and KB-3-1, human cervical carcinoma; CCRF-CEM, human T-cell leukemia; HL-60, human acute myelocytic leukemia; MDA-MB-231, breast carcinoma.

1.3.2.2 Unit B

The basis of the unit B is an *O*-methyl-D-tyrosine which, in most of the natural cryptophycins, is 3'-chlorinated. So far, the activity of cryptophycins has not been improved by modifying the unit B but certain modifications are permitted. The most

important feature of this unit is the absolute configuration since substitution into an *O*-methyl-L-tyrosine leads to a completely inactive cryptophycin (Figure 15).^[113] The methoxy and chloro groups are not indispensable and their absence is tolerated to a certain extent.^[153] In this direction, a slight decrease of activity is observed for the *para*-hydroxy or *para*-amino substituents containing a chlorine in the *meta* position. More interestingly, the *para*-dimethylamino is highly tolerated and there is only a minimal reduction of cytotoxicity compared to the parent compound.^[154]

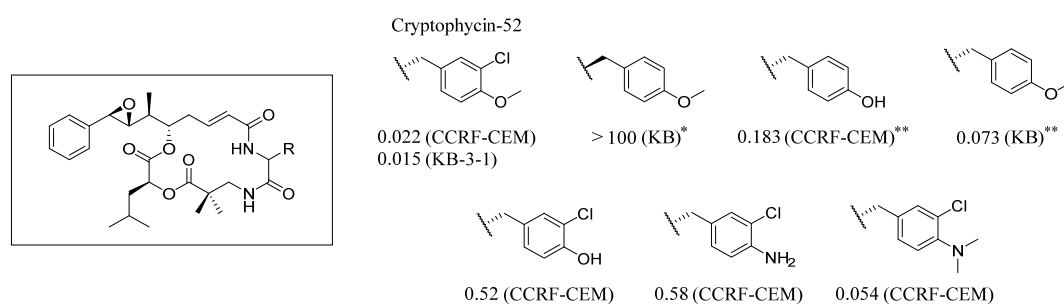


Figure 15. Cytotoxicities of unit B modified cryptophycin analogues (IC_{50} values in nM). Cell lines: KB and KB-3-1, human cervical carcinoma; CCRF-CEM, human T-cell leukemia. * Derived from cryptophycin-24. ** Derived from cryptophycin-1.

1.3.2.3 Unit C

A β -alanine constitutes the backbone of the unit C and the replacement for natural alanine or other α -amino acids dramatically reduces the activity.^[155] However, certain modifications are well tolerated, especially in the α -position. Indeed, cryptophycin-52, the only cryptophycin compound that was tested in clinical trials, contains an extra α -methyl group in the unit C compared to the natural cryptophycin-1 (Figure 16). Other α,α -dialkylated compounds, either linear or cyclic, have been tested and their activity is proportionally reduced with increasing substituent size.^[156] Moreover, their water solubility gets compromised due to their higher lipophilicity and leads to a lower efficiency. For this reason, more recently the incorporation of polar groups in this position has been reported.^[157] Several groups are well tolerated and maintain the potency of the cryptophycin in the subnanomolar range in cervix carcinoma cells (KB-3-1). However, their activity is dramatically reduced in the MDR subclone (KB-V1) probably due to their high amphiphilicity. Interestingly, there seems to be an influence of the stereochemistry of the α -position, but no clear SAR correlation could be obtained.

Finally, small groups can be tolerated in the β -position and, although they always lead to a reduced potency, it can be a good strategy to increase the amide stability between units B and C.

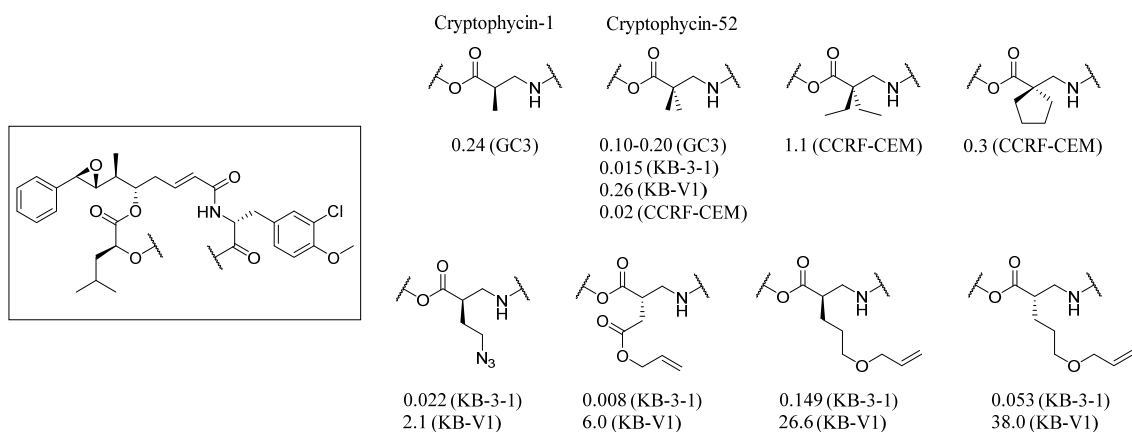


Figure 16. Structure-activity relationship studies of unit C building block (IC₅₀ values in nM). Cell lines: KB-3-1, human cervical carcinoma; KB-V1, P-gp expressing MDR subclone of KB-3-1; CCRF-CEM, human T-cell leukemia; GC3, human colon carcinoma.

1.3.2.4 Unit D

The hydroxy acid of the unit D is amenable to certain modifications and even natural cryptophycins present several alkyl chains. Among them, the isobutyl group is the most commonly found and the most potent one, but the *n*-propyl, *sec*-butyl, and isopropyl groups retain the activity in the nanomolar range (Figure 17).^[109] Moreover, the non-natural neopentyl derivative has shown similar *in vivo* activity to the isobutyl residue.^[158] Interestingly, the inversion of the chiral center does not produce a dramatical loss of activity in contrast to the other stereocenters.^[159] More recently, the synthesis of functionalized cryptophycins has been reported.^[160] The allyl ester cryptophycin can be considered as a precursor of the free carboxylic acid which can be used in targeted therapy. In both cases, they present high cytotoxicity with IC₅₀ values in the low picomolar range against KB-3-1 cells. However, their potency is highly affected in the MDR subclone KB-V1 cells. While the allyl ester retains the potency in the subnanomolar range, the free acid shows a dramatic reduction of activity. This can be attributed to its higher amphiphilicity which makes it a better substrate for the P-gp efflux pump.

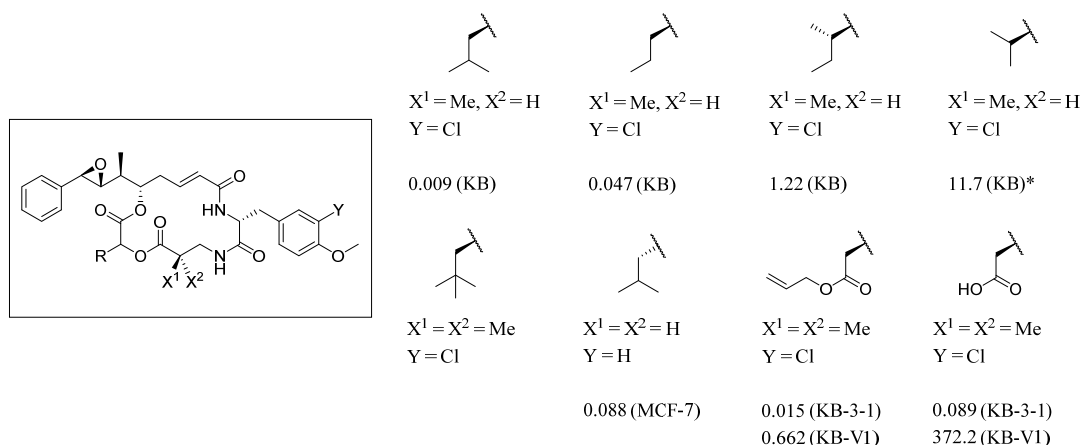


Figure 17. Structure-activity relationship studies of unit D building block (IC₅₀ values in nM). Cell lines: KB and KB-3-1, human cervical carcinoma; KB-V1, P-gp expressing MDR subclone of KB-3-1; MCF-7, human breast adenocarcinoma. *contains a styrene moiety instead of the epoxide.

1.3.3 Conjugates containing cryptophycin as payload

The knowledge obtained from the SAR studies provided the background to create efficient conjugates using cryptophycin as payload for targeted therapy.^[139] The possibility to introduce different functional groups that can be addressed with homing devices and the high activity against MDR cell lines makes cryptophycin a promising agent in this field. Although this strategy has not been largely explored, there is a growing interest on this class of payload as it presents features that are superior to currently used payloads (e.g. maytansinoids, auristatins).

The first ADCs using cryptophycin as payload were reported from Sanofi and used the *para* position of unit A for the conjugation. The cytotoxic agent was connected to the antibody through the protease-sensitive dipeptide Val-Cit and did not use any self-immolative moiety (**39**, Figure 18).^[161] In a similar manner, Genentech used the same drug and linker but they incorporated the *p*-aminobenzyl group as self-immolative linker (**40**, Figure 18).^[162] Although they obtained good *in vivo* and *in vitro* results, respectively, the macrocycle was unstable in mice which resulted in a considerable loss of potency. This instability was translated in a loss of fragments C and D leading to an inactive payload. Interestingly, this metabolization could not be observed in monkey, most probably due to the lower content of hydrolases.

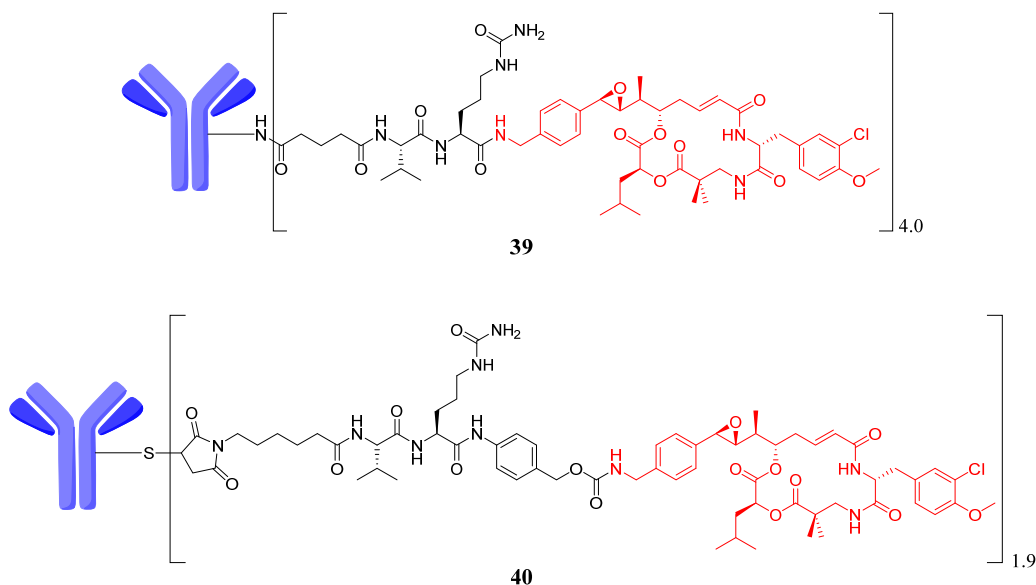


Figure 18. First generation of ADCs featuring cryptophycin as payload. **39** was developed by Sanofi and **40** by Genentech.

Later on, both companies worked on raising the stability using different approaches. Sanofi increased the stability with two modifications in the macrocycle: (i) the incorporation of a methyl group in the β -position of unit C to shield the amide bond between units B and C and (ii) replacement of the scissile ester bond between units C and D by an amide. Consequently, they obtained a cryptophycin that retains the high cytotoxicity of the parent compound and the stability is clearly enhanced.^[163] The conjugation of this payload to an antibody using the protease sensitive Val-Ala dipeptide resulted in a potent ADC that is able to eradicate tumors in nude mice bearing MDA-MB-231 xenografts with only one dose at 5 mg/kg (**41**, Figure 19). Alternatively, Genentech modulated the payload metabolism modifying the conjugation site and the linker.^[164] On a first attempt, they explored the conjugation of the payload to different sites of the antibody and reduced the enzymatic metabolism from more than 40% to 25% in an *in vitro* experiment after 24 h of incubation and thus, remarkably increased the *in vivo* efficacy. A further stability improvement was achieved employing a shorter linker which resulted in a highly stable conjugate *in vitro* and *in vivo* (**42**, Figure 19). However, no therapeutic efficacy has been reported for this last conjugate.

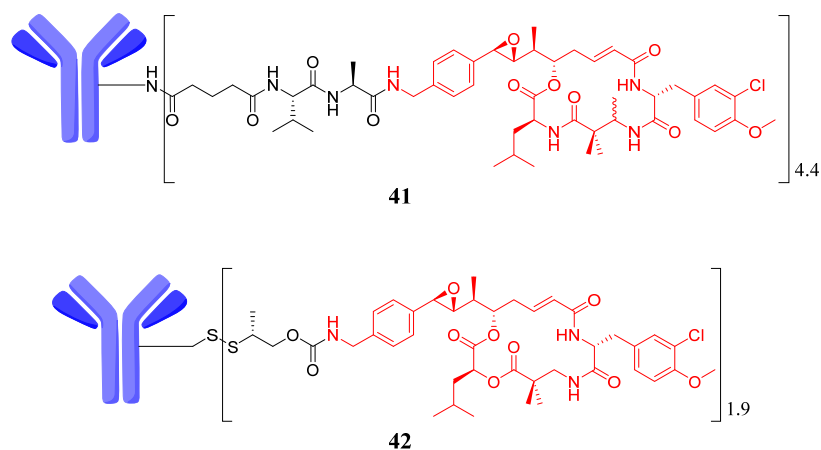


Figure 19. Second generation of ADCs featuring cryptophycin as payload. **41** was developed by Sanofi and **42** by Genentech.

The usage of cryptophycin-55 glycinate as payload in an ADC has been recently acknowledged in a patent (**43**, Figure 20).^[165] In this case, the cytotoxic agent is connected to the HER2 targeting antibody, Trastuzumab, using a protease sensitive Val-Cit dipeptide as linker and a diketopiperazine forming (Pro-Gly) as self-immolative moiety. The cytotoxicity of the construct was evaluated in cell lines expressing different levels of HER2 and showed excellent specificity. However, no further details of stability or therapeutic activity are disclosed.

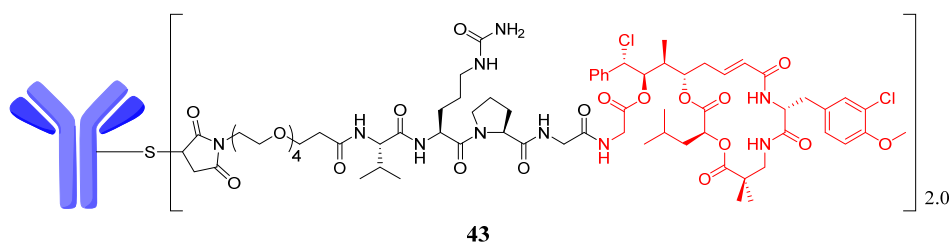


Figure 20. Molecular structure of an ADC using cryptophycin-55 glycinate as payload.

In another embodiment, the growing interest in the SMDC field has motivated the usage of cryptophycin in conjugation to different small molecules. Endocyte was the first to report a conjugate using cryptophycin-55 as payload and folic acid as targeting moiety (**44**, Figure 21).^[166] The compound displayed high cytotoxicity against KB cells with an IC_{50} value in the low nanomolar range and competition experiments showed a decrease of cytotoxicity proving their specificity. However, no *in vivo* results have been reported. Succeeding research connected a cyclic RGD peptide to an azide unit C modified cryptophycin (**45**, Figure 21) using copper(I)-catalyzed alkyne-azide cycloaddition

(CuAAC).^[157] The compound showed good binding affinity to integrins, which are overexpressed in several cancer cells. More interestingly, the incorporation of a carboxyfluorescein moiety between the peptide and the cytotoxic agent was used to study its internalization. Confocal microscopy (picture Figure 21) showed integrin mediated endocytosis of the compound as it ended up in the lysosomal compartment.

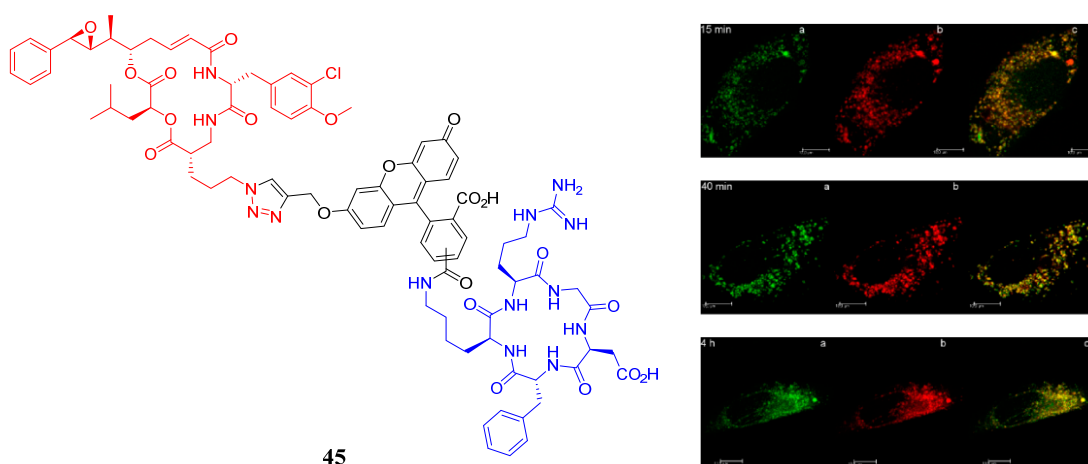
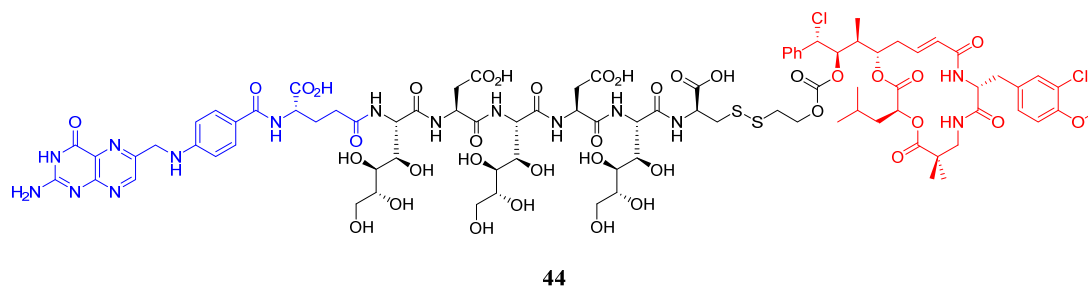


Figure 21. SMDCs using cryptophycin as payload. The confocal microscopy study of compound **45** in WM-115 melanoma cells is shown for (i) 15 min, (ii) 40 min, (iii) 4 h. The compound is shown in green, the lysosomes in red and the overlay clearly proves colocalization.

1.4 References

- [1] B. W. Stewart, C. P. Wild, *World Cancer Report 2014*, **2014**.
- [2] <http://www.who.int/news-room/fact-sheets/detail/cancer> (Accessed on October 14th 2018).
- [3] <https://www.cancer.gov/publications/dictionaries/cancer-terms/def/cancer> (Accessed on October 14th 2018).
- [4] V. T. DeVita, E. Chu, *Cancer Res.* **2008**, *68*, 8643–8653.
- [5] E. Espinosa, P. Zamora, J. Feliu, M. González Barón, *Cancer Treat. Rev.* **2003**, *29*, 515–523.
- [6] K. Cheung-Ong, G. Giaever, C. Nislow, *Chem. Biol.* **2013**, *20*, 648–659.
- [7] D. M. Cheff, M. D. Hall, *J. Med. Chem.* **2017**, *60*, 4517–4532.
- [8] M. Hanif, C. G. Hartinger, *Future Med. Chem.* **2018**, *10*, 615–617.
- [9] L. L. Brunton, B. A. Chabner, B. C. Knollman, *Goodman and Gilman's The Pharmacological Basis of Therapeutics*, McGraw-Hill Education, 12th Edition, **2011**.
- [10] D. A. Gewirtz, *Biochem. Pharmacol.* **1999**, *57*, 727–741.
- [11] M. Binaschi, F. Zunino, G. Capranico, *Stem Cells* **1995**, *13*, 369–379.
- [12] W. N. Hait, E. Rubin, E. Alli, S. Goodin, *Update Cancer Ther.* **2007**, *2*, 1–18.
- [13] E. Martino, G. Casamassima, S. Castiglione, E. Cellupica, S. Pantalone, F. Papagni, M. Rui, A. M. Siciliano, S. Collina, *Bioorg. Med. Chem. Lett.* **2018**, *28*, 2816–2826.
- [14] A. A. M. van der Veldt, N. H. Hendrikse, E. F. Smit, M. P. J. Mooijer, A. Y. Rijnders, W. R. Gerritsen, J. J. M. Van Der Hoeven, A. D. Windhorst, A. A. Lammertsma, M. Lubberink, *Eur. J. Nucl. Med. Mol. Imaging* **2010**, *37*, 1950–1958.
- [15] N. Carelle, E. Piotto, A. Bellanger, J. Germanaud, A. Thuillier, D. Khayat, *Cancer* **2002**, *95*, 155–163.
- [16] J. Sun, Q. Wei, Y. Zhou, J. Wang, Q. Liu, H. Xu, *BMC Syst. Biol.* **2017**, *11*, 87.
- [17] D. Hanahan, R. A. Weinberg, *Cell* **2000**, *100*, 57–70.
- [18] D. Hanahan, R. A. Weinberg, *Cell* **2011**, *144*, 646–674.
- [19] T. Lammers, F. Kiessling, W. E. Hennink, G. Storm, *J. Control. Release* **2012**, *161*, 175–187.
- [20] A. K. Iyer, G. Khaled, J. Fang, H. Maeda, *Drug Discov. Today* **2006**, *11*, 812–818.
- [21] I. Judson, J. A. Radford, M. Harris, J.-Y. Blay, Q. van Hoesel, A. le Cesne, A. T. van Oosterom, M. J. Clemons, C. Kamby, C. Hermans, *et al.*, *Eur. J. Cancer* **2001**, *37*, 870–877.
- [22] A. N. Fader, P. G. Rose, *Int. J. Gynecol. Cancer* **2009**, *19*, 1281–1283.

- [23] B. Říhová, *Adv. Drug Deliv. Rev.* **1998**, *29*, 273–289.
- [24] R. V. J. Chari, *Adv. Drug Deliv. Rev.* **1998**, *31*, 89–104.
- [25] T. M. Allen, *Nat. Rev. Cancer* **2002**, *2*, 750–763.
- [26] M. Srinivasarao, P. S. Low, *Chem. Rev.* **2017**, *117*, 12133–12164.
- [27] G. Köhler, C. Milstein, *Nature* **1975**, *256*, 495–497.
- [28] P. N. Nelson, G. M. Reynolds, E. E. Waldron, E. Ward, K. Giannopoulos, P. G. Murray, *Mol. Pathol.* **2000**, *53*, 111–117.
- [29] R. V. J. Chari, M. L. Miller, W. C. Widdison, *Angew. Chem. Int. Ed.* **2014**, *53*, 3796–3827.
- [30] B. A. Teicher, R. V. J. Chari, *Clin. Cancer Res.* **2011**, *17*, 6389–6397.
- [31] R. V. J. Chari, *Acc. Chem. Res.* **2008**, *41*, 98–107.
- [32] A. W. Tolcher, S. Sugarman, K. A. Gelmon, R. Cohen, M. Saleh, C. Isaacs, L. Young, D. Healey, N. Onetto, W. Slichenmyer, *J. Clin. Oncol.* **1999**, *17*, 478–484.
- [33] A. Beck, L. Goetsch, C. Dumontet, N. Corvaia, *Nat. Rev. Drug Discov.* **2017**, *16*, 315–337.
- [34] J. Lu, F. Jiang, A. Lu, G. Zhang, *Int. J. Mol. Sci.* **2016**, *17*, 561.
- [35] X. Sun, J. F. Ponte, N. C. Yoder, R. Laleau, J. Coccia, L. Lanieri, Q. Qiu, R. Wu, E. Hong, M. Bogalhas, *et al.*, *Bioconjugate Chem.* **2017**, *28*, 1371–1381.
- [36] R. P. Lyon, T. D. Bovee, S. O. Doronina, P. J. Burke, J. H. Hunter, H. D. Neff-Laford, M. Jonas, M. E. Anderson, J. R. Setter, P. D. Senter, *Nat. Biotechnol.* **2015**, *33*, 733–735.
- [37] F. R. Appelbaum, I. D. Bernstein, *Blood* **2017**, *130*, 2373–2376.
- [38] E. Y. Jen, C. W. Ko, J. Eun Lee, P. L. Del Valle, A. Aydanian, C. Jewell, K. J. Norsworthy, D. Przepiorka, L. Nie, J. Liu, *et al.*, *Clin. Cancer Res.* **2018**, *24*, 3242–3246.
- [39] P. D. Senter, E. L. Sievers, *Nat. Biotechnol.* **2012**, *30*, 631–637.
- [40] A. Ballantyne, S. Dhillon, *Drugs* **2013**, *73*, 755–765.
- [41] Y. N. Lamb, *Drugs* **2017**, *77*, 1603–1610.
- [42] B. Sammet, C. Steinkühler, N. Sewald, *Pharm. Pat. Anal.* **2012**, *1*, 65–73.
- [43] R. V. J. Chari, *ACS Med. Chem. Lett.* **2016**, *7*, 974–976.
- [44] G. Casi, D. Neri, *J. Med. Chem.* **2015**, *58*, 8751–8761.
- [45] P. Strop, K. Delaria, D. Foletti, J. M. Witt, A. Hasa-Moreno, K. Poulsen, M. G. Casas, M. Dorywalska, S. Farias, A. Pios, *et al.*, *Nat. Biotechnol.* **2015**, *33*, 694–696.
- [46] P. Agarwal, C. R. Bertozzi, *Bioconjugate Chem.* **2015**, *26*, 176–192.
- [47] E. Perrino, M. Steiner, N. Krall, G. J. L. Bernardes, F. Pretto, G. Casi, D. Neri, *Cancer Res.* **2014**, *74*, 2569–2578.

- [48] A. Dal Corso, R. Gébleux, P. Murer, A. Soltermann, D. Neri, *J. Control. Release* **2017**, *264*, 211–218.
- [49] R. Gébleux, M. Stringhini, R. Casanova, A. Soltermann, D. Neri, *Int. J. Cancer* **2017**, *140*, 1670–1679.
- [50] A. H. Staudacher, M. P. Brown, *Br. J. Cancer* **2017**, *117*, 1736–1742.
- [51] N. Joubert, C. Denevault-Sabourin, F. Bryden, M. C. Viaud-Massuard, *Eur. J. Med. Chem.* **2017**, *142*, 393–415.
- [52] G. Casi, D. Neri, *Mol. Pharm.* **2015**, *12*, 1880–1884.
- [53] N. Krall, J. Scheuermann, D. Neri, *Angew. Chem. Int. Ed.* **2013**, *52*, 1384–1402.
- [54] C. S. Kue, A. Kamkaew, K. Burgess, L. V. Kiew, L. Y. Chung, H. B. Lee, *Med. Res. Rev.* **2016**, *36*, 494–575.
- [55] E. I. Vrettos, G. Mezö, A. G. Tzakos, *Beilstein J. Org. Chem.* **2018**, *14*, 930–954.
- [56] V. Le Joncour, P. Laakkonen, *Bioorg. Med. Chem.* **2017**, *26*, 2797–2806.
- [57] T. Chatzisideri, G. Leonidis, V. Sarli, *Future Med. Chem.* **2018**, *10*, 2201–2226.
- [58] M. Deonarain, G. Yahioğlu, I. Stamatı, A. Pomowski, J. Clarke, B. Edwards, S. Diez-Posada, A. Stewart, *Antibodies* **2018**, *7*, 16.
- [59] M. Werle, A. Bernkop-Schnürch, *Amino Acids* **2006**, *30*, 351–367.
- [60] C. Heinis, T. Rutherford, S. Freund, G. Winter, *Nat. Chem. Biol.* **2009**, *5*, 502–507.
- [61] M. Srinivasarao, C. V. Galliford, P. S. Low, *Nat. Rev. Drug Discov.* **2015**, *14*, 203–219.
- [62] P. S. Low, W. A. Henne, D. D. Doorneweerd, *Acc. Chem. Res.* **2008**, *41*, 120–129.
- [63] M. Fernández, F. Javaid, V. Chudasama, *Chem. Sci.* **2018**, *9*, 790–810.
- [64] J. A. Reddy, L. Xu, N. Parker, M. Vetzal, C. P. Leamon, J. A. Reddy, L. Xu, N. Parker, M. Vetzal, C. P. Leamon, *J. Nucl. Med.* **2014**, *45*, 857–866.
- [65] C. P. Leamon, M. A. Parker, I. R. Vlahov, L.-C. Xu, J. A. Reddy, M. Vetzal, N. Douglas, *Bioconjugate Chem.* **2002**, *13*, 1200–1210.
- [66] G. M. Van Dam, G. Themelis, L. M. A. Crane, N. J. Harlaar, R. G. Pleijhuis, W. Kelder, A. Sarantopoulos, J. S. De Jong, H. J. G. Arts, A. G. J. Van Der Zee, *et al.*, *Nat. Med.* **2011**, *17*, 1315–1319.
- [67] I. R. Vlahov, C. P. Leamon, *Bioconjugate Chem.* **2012**, *23*, 1357–1369.
- [68] J. A. Reddy, R. Dorton, E. Westrick, A. Dawson, T. Smith, L. C. Xu, M. Vetzal, P. Kleindl, I. R. Vlahov, C. P. Leamon, *Cancer Res.* **2007**, *67*, 4434–4442.
- [69] C. P. Leamon, I. R. Vlahov, J. A. Reddy, M. Vetzal, H. K. R. Santhapuram, F. You, A. Bloomfield, R. Dorton, M. Nelson, P. Kleindl, *et al.*, *Bioconjugate Chem.* **2014**, *25*, 560–568.
- [70] J. A. Reddy, R. Dorton, A. Bloomfield, M. Nelson, C. Dircksen, M. Vetzal, P. Kleindl, H. Santhapuram, I. R. Vlahov, C. P. Leamon, *Sci. Rep.* **2018**, *8*, 8943.

- [71] I. R. Vlahov, L. Qi, P. J. Kleindl, H. K. Santhapuram, A. Felten, G. L. Parham, K. Wang, F. You, J. F. Vaughn, S. J. Hahn, *et al.*, *Bioconjugate Chem.* **2017**, *28*, 2921–2931.
- [72] T. Wüstemann, U. Haberkorn, J. Babich, W. Mier, *Med. Res. Rev.* **2019**, *39*, 40–69.
- [73] S. A. Kularatne, K. Wang, H. K. R. Santhapuram, P. S. Low, *Mol. Pharm.* **2009**, *6*, 780–789.
- [74] I. R. Vlahov, J. A. Reddy, A. Bloomfield, R. Dorton, M. Nelson, M. Veltzel, L. C. Paul, *Conjugates for Treating Diseases Caused by PSMA Expressing Cells, WO2014/078484 A1*, **2014**.
- [75] C. Kratochwil, F. L. Giesel, M. Stefanova, M. Benešová, M. Bronzel, A. Afshar-Oromieh, W. Mier, M. Eder, K. Kopka, U. Haberkorn, *J. Nucl. Med.* **2016**, *57*, 1170–1176.
- [76] C. A. Umbricht, M. Benešová, R. Schibli, C. Müller, *Mol. Pharm.* **2018**, *15*, 2297–2306.
- [77] H. Kuo, H. Merkens, Z. Zhang, C. F. Uribe, J. Lau, C. Zhang, N. Colpo, K.-S. Lin, F. Bénard, *Mol. Pharm.* **2018**, *15*, 5183–5191.
- [78] C. T. Supuran, V. Alterio, A. Di Fiore, K. D’Ambrosio, F. Carta, S. M. Monti, G. De Simone, *Med. Res. Rev.* **2018**, *38*, 1799–1836.
- [79] M. Choschzick, E. Oosterwijk, V. Müller, L. Woelber, R. Simon, H. Moch, P. Tennstedt, *Virchows Arch.* **2011**, *459*, 193–200.
- [80] N. Krall, F. Pretto, W. Decurtins, G. J. L. Bernardes, C. T. Supuran, D. Neri, *Angew. Chem. Int. Ed.* **2014**, *53*, 4231–4235.
- [81] N. Krall, F. Pretto, M. Mattarella, C. Müller, D. Neri, *J. Nucl. Med.* **2016**, *57*, 943–949.
- [82] S. Cazzamalli, A. Dal Corso, D. Neri, *Mol. Cancer Ther.* **2016**, *15*, 2926–2936.
- [83] S. Cazzamalli, A. Dal Corso, D. Neri, *J. Control. Release* **2017**, *246*, 39–45.
- [84] N. Krall, F. Pretto, D. Neri, *Chem. Sci.* **2014**, *5*, 3640–3644.
- [85] M. Wichert, N. Krall, W. Decurtins, R. M. Franzini, F. Pretto, P. Schneider, D. Neri, J. Scheuermann, *Nat. Chem.* **2015**, *7*, 241–249.
- [86] S. Cazzamalli, A. Dal Corso, F. Widmayer, D. Neri, *J. Am. Chem. Soc.* **2018**, *140*, 1617–1621.
- [87] S. Cazzamalli, B. Ziffels, F. Widmayer, P. Murer, G. Pellegrini, F. Pretto, S. Wulhfard, D. Neri, *Clin. Cancer Res.* **2018**, *24*, 3656–3667.
- [88] V. Dudutiene, J. Matuliene, A. Smirnov, D. D. Timm, A. Zubriene, L. Baranauskiene, V. Morkunaite, J. Smirnoviene, V. Michailoviene, V. Juozapaitiene, *et al.*, *J. Med. Chem.* **2014**, *57*, 9435–9446.
- [89] I. S. Marks, S. S. Gardeen, S. J. Kurdziel, S. T. Nicolaou, J. E. Woods, S. A. Kularatne, P. S. Low, *Mol. Pharm.* **2018**, *15*, 2289–2296.
- [90] Y. C. Patel, *Front. Neuroendocrinol.* **1999**, *20*, 157–198.

- [91] A. Henninot, J. C. Collins, J. M. Nuss, *J. Med. Chem.* **2018**, *61*, 1382–1414.
- [92] J. Strosberg, G. El-Haddad, E. Wolin, A. Hendifar, J. Yao, B. Chasen, E. Mittra, P. L. Kunz, M. H. Kulke, H. Jacene, *et al.*, *N. Engl. J. Med.* **2017**, *376*, 125–135.
- [93] H. Jadvar, X. Chen, W. Cai, U. Mahmood, *Radiology* **2018**, *286*, 388–400.
- [94] M. Lelle, S. Kaloyanova, C. Freidel, M. Theodoropoulou, M. Musheev, C. Niehrs, G. Stalla, K. Peneva, *Mol. Pharm.* **2015**, *12*, 4290–4300.
- [95] H.-Y. Zhang, W.-Q. Xu, Y.-Y. Zheng, E. Omari-Siaw, Y. Zhu, X. Cao, S.-S. Tong, J.-N. Yu, X.-M. Xu, *Oncotarget* **2016**, *7*, 86326–86338.
- [96] T. Yin, Q. Wu, L. Wang, L. Yin, J. Zhou, M. Huo, *Mol. Pharm.* **2015**, *12*, 3020–3031.
- [97] R. R. Shinde, R. G. Alargova, P. Lim Soo, B. Sweryda-Krawiec, L. Alland, C. Sears, *Targeted Conjugates and Particles and Formulations Thereof, WO2018/081521 A1*, **2018**.
- [98] F. Kratz, I. A. Müller, C. Ryppa, A. Warnecke, *ChemMedChem* **2008**, *3*, 20–53.
- [99] J. R. McCombs, S. C. Owen, *AAPS J.* **2015**, *17*, 339–351.
- [100] A. Alouane, R. Labruère, T. Le Saux, F. Schmidt, L. Jullien, *Angew. Chem. Int. Ed.* **2015**, *54*, 7492–7509.
- [101] Y. Kato, S. Ozawa, C. Miyamoto, Y. Maehata, A. Suzuki, T. Maeda, Y. Baba, *Cancer Cell Int.* **2013**, *13*, 89.
- [102] G. K. Balendiran, R. Dabur, D. Fraser, *Cell Biochem. Funct.* **2004**, *22*, 343–352.
- [103] N. G. Caculitan, J. dela Cruz Chuh, Y. Ma, D. Zhang, K. R. Kozak, Y. Liu, T. H. Pillow, J. Sadowsky, T. K. Cheung, Q. Phung, *et al.*, *Cancer Res.* **2017**, *77*, 7027–7037.
- [104] T. Legigan, J. Clarhaut, I. Tranoy-Opalinski, A. Monvoisin, B. Renoux, M. Thomas, A. Le-Pape, S. Lerondel, S. Papot, *Angew. Chem. Int. Ed.* **2012**, *51*, 11606–11610.
- [105] I. Tranoy-Opalinski, T. Legigan, R. Barat, J. Clarhaut, M. Thomas, B. Renoux, S. Papot, *Eur. J. Med. Chem.* **2014**, *74*, 302–313.
- [106] R. E. Schwartz, C. F. Hirsch, D. F. Sesin, J. E. Flor, M. Chartrain, R. E. Fromtling, G. H. Harris, M. J. Salvatore, J. M. Liesch, K. Yudin, *J. Ind. Microbiol.* **1990**, *5*, 113–124.
- [107] G. Trimurtulu, I. Ohtani, G. M. L. Patterson, R. E. Moore, T. H. Corbett, F. A. Valeriote, L. Demchik, *J. Am. Chem. Soc.* **1994**, *116*, 4729–4737.
- [108] R. A. Barrow, T. Hemscheidt, J. Liang, S. Paik, R. E. Moore, M. A. Tius, *J. Am. Chem. Soc.* **1995**, *117*, 2479–2490.
- [109] T. Golakoti, J. Ogino, C. E. Heltzel, T. Le Husebo, C. M. Jensen, L. K. Larsen, G. M. L. Patterson, R. E. Moore, S. L. Mooberry, T. H. Corbett, *et al.*, *J. Am. Chem. Soc.* **1995**, *117*, 12030–12049.
- [110] M. Kobayashi, S. Aoki, N. Ohyabu, M. Kurosu, W. Wang, I. Kitagawa, *Tetrahedron Lett.* **1994**, *35*, 7969–7972.

- [111] M. Kobayashi, M. Kurosu, N. Ohyabu, W. Wang, S. Fujii, I. Kitagawa, *Chem. Pharm. Bull.* **1994**, *42*, 2196–2198.
- [112] M. Kobayashi, M. Kurosu, W. Wang, I. Kitagawa, *Chem. Pharm. Bull.* **1994**, *42*, 2394–2396.
- [113] M. Kobayashi, W. Wang, N. Ohyabu, M. Kurosu, I. Kitagawa, *Chem. Pharm. Bull.* **1995**, *43*, 1598–1600.
- [114] C. D. Smith, X. Zhang, S. L. Mooberry, G. M. L. Patterson, R. E. Moore, *Cancer Res.* **1994**, *54*, 3779–3784.
- [115] B. D. M. Chen, A. Nakeff, F. Valeriote, *Int. J. Cancer* **1998**, *77*, 869–873.
- [116] M. M. Wagner, D. C. Paul, C. Shih, M. A. Jordan, L. Wilson, D. C. Williams, *Cancer Chemother. Pharmacol.* **1999**, *43*, 115–125.
- [117] J. P. Stevenson, W. Sun, M. Gallagher, R. Johnson, D. Vaughn, L. Schuchter, K. Algazy, S. Hahn, N. Enas, D. Ellis, *et al.*, *Clin. Cancer Res.* **2002**, *8*, 2524–2529.
- [118] C. Sessa, K. Weigang-Köhler, O. Pagani, G. Greim, O. Mor, T. De Pas, M. Burgess, I. Weimer, R. Johnson, *Eur. J. Cancer* **2002**, *38*, 2388–2396.
- [119] M. J. Edelman, D. R. Gandara, P. Hausner, V. Israel, D. Thornton, J. DeSanto, L. A. Doyle, *Lung Cancer* **2003**, *39*, 197–199.
- [120] G. D’Agostino, J. Del Campo, B. Mellado, M. A. Izquierdo, T. Minarik, L. Cirri, L. Marini, J. L. Perez-Gracia, G. Scambia, *Int. J. Gynecol. Cancer* **2006**, *16*, 71–76.
- [121] B. Albertis, D. Bray, J. Lewis, M. Ralf, K. Roberts, J. D. Watson, *Molecular Biology of the Cell*, Garland Science, 3rd Edition, **1994**.
- [122] H. Chen, Z. Lin, K. E. Arnst, D. D. Miller, W. Li, *Molecules* **2017**, *22*, 1281.
- [123] M. A. Jordan, L. Wilson, *Nat. Rev. Cancer* **2004**, *4*, 253–265.
- [124] D. Fanale, G. Bronte, F. Passiglia, V. Calò, M. Castiglia, F. Di Piazza, N. Barraco, A. Cangemi, M. T. Catarella, L. Insalaco, *et al.*, *Anal. Cell. Pathol.* **2015**, Article ID 690916.
- [125] K. Kerksiek, M. R. Mejillano, R. E. Schwartz, G. I. Georg, R. H. Himes, *FEBS Lett.* **1995**, *377*, 59–61.
- [126] S. L. Mooberry, L. Busquets, G. Tien, *Int. J. Cancer* **1997**, *73*, 440–448.
- [127] D. Panda, K. DeLuca, D. Williams, M. A. Jordan, L. Wilson, *Proc. Natl. Acad. Sci. USA* **1998**, *95*, 9313–9318.
- [128] L. Drew, R. L. Fine, T. N. Do, G. P. Douglas, D. P. Petrylak, *Clin. Cancer Res.* **2002**, *8*, 3922–3932.
- [129] C. D. Smith, X. Zhang, *J. Biol. Chem.* **1996**, *271*, 6192–6198.
- [130] S. L. Mooberry, C. R. Taoka, L. Busquets, *Cancer Lett.* **1996**, *107*, 53–57.
- [131] R. Bai, R. E. Schwartz, J. A. Kepler, G. R. Pettit, E. Hamel, *Cancer Res.* **1996**, *56*, 4398–406.
- [132] A. Mitra, D. Sept, *Biochemistry* **2004**, *43*, 13955–13962.

- [133] D. Panda, R. H. Himes, R. E. Moore, L. Wilson, M. A. Jordan, *Biochemistry* **1997**, *36*, 12948–12953.
- [134] D. Panda, V. Ananthnarayan, G. Larson, C. Shih, M. A. Jordan, L. Wilson, *Biochemistry* **2000**, *39*, 14121–14127.
- [135] D. Waghray, Q. Zhang, *J. Med. Chem.* **2018**, *61*, 5108–5121.
- [136] M. Eggen, G. I. Georg, *Med. Res. Rev.* **2002**, *22*, 85–101.
- [137] M. A. Tius, *Tetrahedron* **2002**, *58*, 4343–4367.
- [138] S. Eißler, A. Stoncius, M. Nahrwold, N. Sewald, *Synthesis* **2006**, *22*, 3747–3789.
- [139] C. Weiss, E. Figueras, A. N. Borbely, N. Sewald, *J. Pept. Sci.* **2017**, *23*, 514–531.
- [140] C. Weiss, B. Sammet, N. Sewald, *Nat. Prod. Rep.* **2013**, *30*, 924–40.
- [141] J. Liang, D. W. Hoard, V. Van Khau, M. J. Martinelli, E. D. Moher, R. E. Moore, M. A. Tius, *J. Org. Chem.* **1999**, *64*, 1459–1463.
- [142] S. Eissler, M. Nahrwold, B. Neumann, H.-G. Stammler, N. Sewald, *Org. Lett.* **2007**, *9*, 817–819.
- [143] S. Eißler, B. Neumann, H. G. Stammler, N. Sewald, *Synlett* **2008**, *2*, 273–277.
- [144] K. L. Bolduc, S. D. Larsen, D. H. Sherman, *Chem. Commun.* **2012**, *48*, 6414–6416.
- [145] T. K. Moore, R. E.; Tius, M. A.; Barrow, R. A.; Liang, J.; Corbett, T. H.; Valeriote, F. A.; Hemscheidt, *New Cryptophycins from Synthesis, WO1996040184 A1*, **1996**.
- [146] G. I. Georg, S. M. Ali, V. J. Stella, W. N. Waugh, R. H. Himmes, *Bioorg. Med. Chem. Lett.* **1998**, *8*, 1959–1962.
- [147] R. R. Boinpally, L. Polin, S. L. Zhou, B. R. Jasti, R. A. Wiegand, K. White, J. Kushner, J. P. Horwitz, T. H. Corbett, R. E. Parchment, *Cancer Chemother. Pharmacol.* **2003**, *52*, 25–33.
- [148] J. Liang, R. E. Moore, E. D. Moher, J. E. Munroe, R. S. Al-Awar, D. A. Hay, D. L. Varie, T. Y. Zhang, J. A. Aikins, M. J. Martinelli, *et al.*, *Invest. New Drugs* **2005**, *23*, 213–224.
- [149] R. S. Al-awar, J. E. Ray, R. M. Schultz, S. L. Andis, J. H. Kennedy, R. E. Moore, J. Liang, T. Golakoti, G. V. Subbaraju, T. H. Corbett, *J. Med. Chem.* **2003**, *46*, 2985–3007.
- [150] N. Kotoku, T. Kato, F. Narumi, E. Ohtani, S. Kamada, S. Aoki, N. Okada, S. Nakagawa, M. Kobayashi, *Bioorg. Med. Chem.* **2006**, *14*, 7446–7457.
- [151] S. Eißler, T. Bogner, M. Nahrwold, N. Sewald, *Chem. - A Eur. J.* **2009**, *15*, 11273–11287.
- [152] R. S. Al-Awar, T. H. Corbett, J. E. Ray, L. Polin, J. H. Kennedy, M. M. Wagner, D. C. Williams, *Mol. Cancer Ther.* **2004**, *3*, 1061–1067.
- [153] S. B. Buck, J. K. Huff, R. H. Himes, G. I. Georg, *J. Med. Chem.* **2004**, *47*, 696–702.
- [154] V. F. Patel, S. L. Andis, J. H. Kennedy, J. E. Ray, R. M. Schultz, *J. Med. Chem.* **1999**, *42*, 2588–2603.

- [155] S. Chuan, L. S. Gossett, J. M. Gruber, C. Sue Grossman, S. L. Andis, R. M. Schultz, J. F. Worzalla, T. H. Corbett, J. T. Metz, *Bioorg. Med. Chem. Lett.* **1999**, *9*, 69–74.
- [156] D. L. Varie, C. Shih, D. A. Hay, S. L. Andis, T. H. Corbett, L. S. Gossett, S. K. Janisse, M. J. Martinelli, E. D. Moher, R. M. Schultz, *et al.*, *Bioorg. Med. Chem. Lett.* **1999**, *9*, 369–374.
- [157] M. Nahrwold, C. Weiß, T. Bogner, F. Mertink, J. Conradi, B. Sammet, R. Palmisano, S. R. Gracia, T. Preuße, N. Sewald, *J. Med. Chem.* **2013**, *56*, 1853–1864.
- [158] K. Menon, E. Alvarez, P. Forler, V. Phares, T. Amsrud, C. Shih, R. Al-Awar, B. A. Teicher, *Cancer Chemother. Pharmacol.* **2000**, *46*, 142–149.
- [159] S. B. Buck, J. K. Huff, R. H. Himes, G. I. Georg, *J. Med. Chem.* **2004**, *47*, 3697–3699.
- [160] B. Sammet, T. Bogner, M. Nahrwold, C. Weiss, N. Sewald, *J. Org. Chem.* **2010**, *75*, 6953–6960.
- [161] H. Bouchard, M.-P. Brun, A. Commercon, J. Zhang, *Novel Conjugates, Preparation Thereof, and Therapeutic Use Thereof, US2012/0225089 A1*, **2012**.
- [162] V. A. Verma, T. H. Pillow, L. Depalatis, G. Li, G. L. Phillips, A. G. Polson, H. E. Raab, S. Spencer, B. Zheng, *Bioorg. Med. Chem. Lett.* **2015**, *25*, 864–868.
- [163] A. Bigot, H. Bouchard, M.-P. Brun, F. Clerc, J. Zhang, *Novel Cryptophycin Compounds and Conjugates, Their Preparation and Their Therapeutic Use, WO2017/076998 A1*, **2017**.
- [164] D. Su, K. R. Kozak, J. Sadowsky, S. F. Yu, A. Fourie-O'Donohue, C. Nelson, R. Vandlen, R. Ohri, L. Liu, C. Ng, *et al.*, *Bioconjugate Chem.* **2018**, *29*, 1155–1167.
- [165] M. C. Steinkühler, M. P. Gallinari, B. Osswald, N. Sewald, M. Ritzefeld, M. Frese, E. Figueras, L. Pethő, *Cryptophycin-Based Antibody-Drug Conjugates with Novel Self-Immolative Linkers, WO2016/146638 A1*, **2016**.
- [166] C. P. Leamon, I. R. Vlahov, F. You, P. J. Kleindl, H. K. R. Santhapuram, *Conjugates Containing Hydrophilic Spacer Linkers, WO2009/002993 A1*, **2009**.

Chapter 2 - Objectives

2. Objectives

The main objective of this thesis was to explore the potential of cryptophycin as payload for targeted therapy using small molecules as delivery vehicles. Since cryptophycin display high cytotoxicity towards several cancer cells and is amenable to certain modifications to introduce functional groups, its vectorization using small molecules could enhance the therapeutic activity of the drug while reducing its side effects.

The first part of this thesis (chapter 3) aimed the identification of new highly active cryptophycins containing different functional groups that can be used for conjugation to homing devices. In particular, the synthesis of cryptophycins with modifications in the *para* position of the unit B was envisioned (Figure 22). The study of their biological activity was planned in a cell-based cytotoxicity assay using cervix cancer cells (KB-3-1) and, in case of active compounds, its MDR subclone (KB-V1). Moreover, the obtained compounds could also serve as payloads for the preparation of small molecule-drug conjugates (SMDCs).

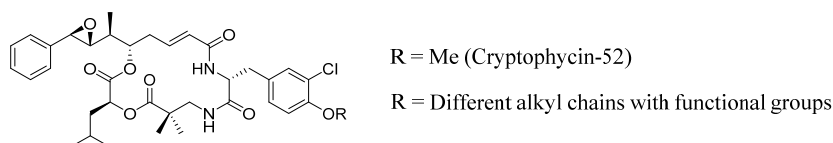


Figure 22. Proposed molecular structures of unit B modified cryptophycin.

The second part (chapters 4 and 5), intended the investigation of cryptophycin-55 glycinate as payload of SMDCs. Different peptides and peptidomimetics targeting receptors or enzymes such as the somatostatin receptor 2 (SSTR2) or carbonic anhydrase 9 (CAIX) were contemplated (Figure 23).

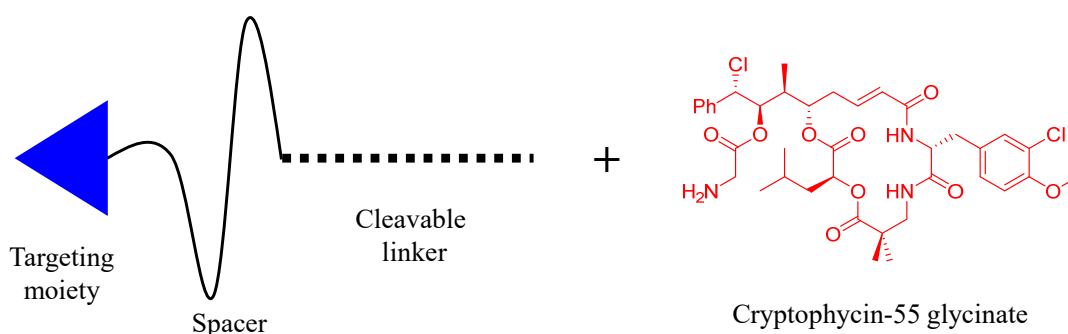
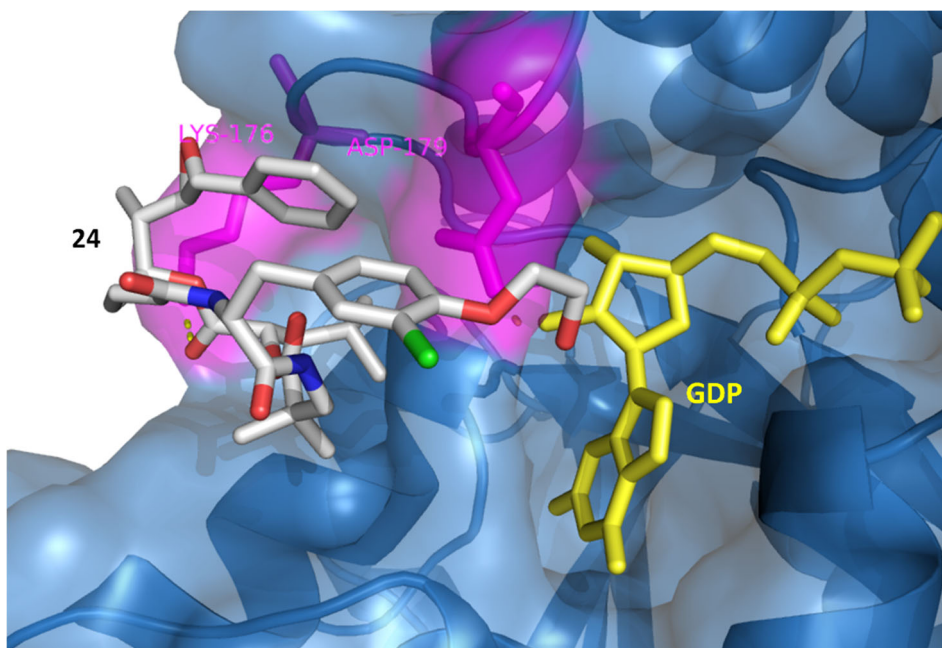


Figure 23. Schematic structure of SMDC using cryptophycin-55 glycinate as payload

In particular, an acetazolamide derivative targeting CAIX and octreotide targeting SSTR2 were considered as ideal and validated targeting moieties to explore the capacity of cryptophycin-55 glycinate as payload. The conjugation between the targeting moiety and the drug was planned through different cleavable linkers containing spacers to increase their hydrophilicity. In order to proof the efficient targeting properties of the prepared conjugates, a series of *in vitro* and *in vivo* experiments were envisioned.

Chapter 3 – Novel analogues of cryptophycin modified in the unit B



This chapter corresponds to the following publication:

Eduard Figueras, Adina Borbély, Mohamed Ismail, Marcel Frese, and Norbert Sewald*.
Novel unit B cryptophycin analogues as payloads for targeted therapy. *Beilstein J. Org. Chem.* **2018**, 14, 1281-1286.

List of author contributions:

Conception and design: E. Figueras and N. Sewald

Synthesis: E. Figueras

Cytotoxic studies: C. Michalek

Molecular docking: M. Ismail

Analysis and interpretation of data: E. Figueras, A. Borbély, M. Ismail, M. Frese, and N. Sewald

Writing the manuscript: E. Figueras

Review and/or revision of the manuscript: E. Figueras, A. Borbély, M. Ismail, M. Frese, and N. Sewald

Study supervision: N. Sewald



Novel unit B cryptophycin analogues as payloads for targeted therapy

Eduard Figueras, Adina Borbély, Mohamed Ismail, Marcel Frese and Norbert Sewald*

Full Research Paper

Open Access

Address:
Department of Chemistry, Organic and Bioorganic Chemistry,
Bielefeld University, Universitätsstraße 25, 33615 Bielefeld, Germany

Email:
Norbert Sewald* - Norbert.sewald@uni-bielefeld.de

* Corresponding author

Keywords:
cryptophycin; cytotoxic agents; novel payloads; tubulin inhibitors;
tumour targeting

Beilstein J. Org. Chem. **2018**, *14*, 1281–1286.
doi:10.3762/bjoc.14.109

Received: 16 February 2018
Accepted: 02 May 2018
Published: 01 June 2018

This article is part of the Thematic Series "Peptide–drug conjugates".

Associate Editor: A. Kirschning

© 2018 Figueras et al.; licensee Beilstein-Institut.
License and terms: see end of document.

Abstract

Cryptophycins are naturally occurring cytotoxins with great potential for chemotherapy. Since targeted therapy provides new perspectives for treatment of cancer, new potent analogues of cytotoxic agents containing functional groups for conjugation to homing devices are required. We describe the design, synthesis and biological evaluation of three new unit B cryptophycin analogues. The *O*-methyl group of the unit B D-tyrosine analogue was replaced by an *O*-(allyloxyethyl) moiety, an *O*-(hydroxyethyl) group, or an *O*-(((azidoethoxy)ethoxy)ethoxyethyl) substituent. While the former two maintain cytotoxicity in the subnanomolar range, the attachment of the triethylene glycol spacer with a terminal azide results in a complete loss of activity. Docking studies of the novel cryptophycin analogues to β -tubulin provided a rationale for the observed cytotoxicities.

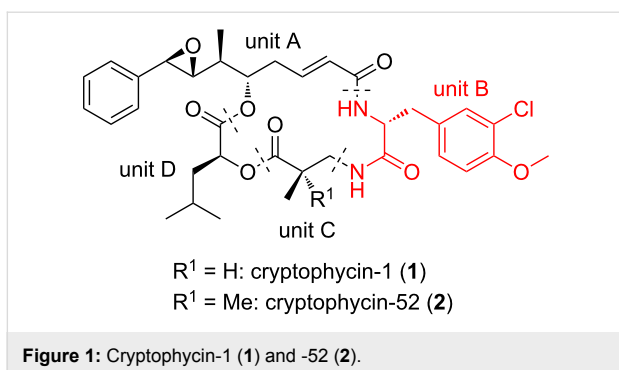
Introduction

Cryptophycins are natural occurring cyclic depsipeptides that were first isolated from cyanobacteria *Nostoc* sp. ATCC 53789 in 1990 [1]. Cryptophycins target tubulin, in particular the peptide site of the vinca domain. They block microtubule formation, inhibiting their assembly and, hence, are antimetabolic agents [2,3]. Their high cytotoxicity prompted manifold studies that were initially focussed on the total synthesis and structure–activity relationships [4–20]. This work resulted in the identification of cryptophycin-52, a highly biologically active analogue of cryptophycin-1 (Figure 1).

Eli Lilly took cryptophycin-52 into clinical trials. Although almost half of the patients obtained a benefit from the treatment,

neurotoxic side effects forced the termination of the clinical trials [21–23]. In order to overcome the side effects of cryptophycin-52 and to better understand the fundamental structure for biological activity, numerous structure–activity relationship studies have been carried out [24–35]. However, like cryptophycin-52, the new analogues were not selective against cancer cells making them not better than its parent.

In recent years the targeted delivery of cytotoxic agents has emerged as a highly promising method to tackle selectivity issues [36–40]. Cryptophycin-52 and many analogues lack an addressable group to conjugate the toxin to a homing device. For this reason, new analogues containing functional groups



that would allow the conjugation of a homing device were developed [41–46]. Some of these functionalized analogues have been recently used for the preparation of antibody–drug conjugates (ADCs) and peptide–drug conjugates (PDCs) [46–51]. Nevertheless, there is still a strong need of novel cryptophycin analogues with maintained activity containing a suitable functional group that would allow the conjugation to the homing device. Cryptophycin-1 contains a methoxy group in the aromatic ring of the unit B, which is a chlorinated derivative of D-tyrosine. Different chains for unit B have been investigated, albeit the elongation of the methoxy group is still unknown. Therefore, in the current study, we embarked on the synthesis of novel cryptophycin analogues containing different substituents at the phenolic hydroxy group of the unit B. We intended to investigate whether the high biological activity of the parent compound is retained and thus, construction of ADCs and PDCs would be feasible. This preparation could be done using trace-

less cleavable linkers that are sensitive to the distinct physiology of the tumour with enhanced level and activity of specific enzymes. The connection between the payload and the linker is of crucial importance since its stability can dramatically change the release and thus, the activity of the compound. For this reason, the included functional groups were designed with the consideration to provide appropriate stability and activity to the future conjugate.

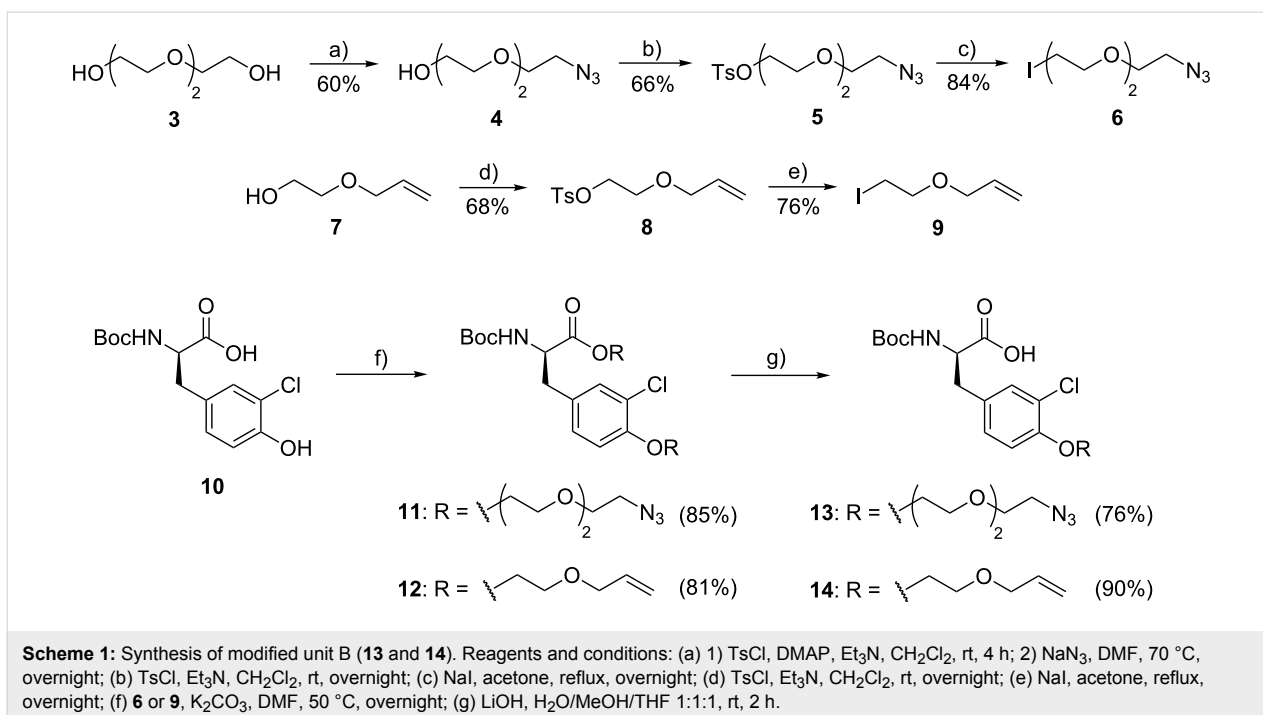
Results and Discussion

Design and synthesis

Previous docking studies have postulated that the methyl group of unit B is not involved in the cryptophycin–tubulin interaction [52]. Moreover, its absence did not produce a dramatic loss of activity [24].

Based on this, we designed cryptophycin analogues modified in the unit B. Instead of the *O*-methyl group that is present in the natural cryptophycin, we attached a hydroxyethyl group or a triethylene glycol chain terminated with an alcohol or azide, respectively. These functional groups would allow the conjugation of the novel cryptophycin analogues across an appropriate linker to an antibody or peptide. Either a virtually uncleavable triazole (introduced by CuAAC) or scissile ester, carbonate, or carbamate moieties were taken into account.

The synthesis of the modified unit B (Scheme 1) started with the preparation of the two different spacers that were later connected to the phenol. Starting from triethylene glycol (3) or



23 were obtained in good purity after column chromatography. The allyl ether in **23** was cleaved using Pd(PPh₃)₄ as Pd(0) source and phenylsilane as scavenger to obtain the cryptophycin analogue **24** in good purity.

Biological evaluation

The biological activity of the modified unit B analogues was determined in a cell viability assay using the human cervix carcinoma cell line KB-3-1 (Table 1). The cryptophycin analogue **22** showed a dramatic loss of activity compared to cryptophycin-52 (**2**), while analogues **23** and **24** showed a reduced cytotoxicity although their IC₅₀ values are still in the low nanomolar range. The observed dramatic loss of activity of analogue **22** could be due to its poor internalization or the modification could alter the interaction with tubulin. In order to get an extensive knowledge of the novel analogues, we embarked in docking and modelling studies, herein reported, and internalization studies are ongoing in our research group.

Table 1: Cytotoxicity of cryptophycin-52 and its unit B analogues.

compd	unit B	IC ₅₀ KB-3-1 (nM)
2	CH ₂ Ph(<i>m</i> -Cl, <i>p</i> -OMe)	0.015
22	CH ₂ Ph(<i>m</i> -Cl, <i>p</i> -(OCH ₂ CH ₂) ₃ N ₃)	195000
23	CH ₂ Ph(<i>m</i> -Cl, <i>p</i> -OCH ₂ CH ₂ OCH ₂ CH ₂ CH ₂)	0.748
24	CH ₂ Ph(<i>m</i> -Cl, <i>p</i> -OCH ₂ CH ₂ OH)	0.184

Docking and modelling of cryptophycin derivatives

There is no X-ray analysis of cryptophycin–tubulin complexes available to provide information on the binding site. Based on biochemical evidence, binding close to the vinca-alkaloid binding site of β-tubulin, the so called “peptide-site”, has been proposed [2,52,53]. We performed a docking study to explain the different affinities of the newly synthesized derivatives. The parent compound **2** scored highest with respect to β-tubulin binding (Table 2). Three hydrogen bonds were detected to key residues in the peptide binding pocket of the vinca domain (Lys176, Val177 and Tyr210). Other than previously reported

Table 2: Binding energies for the different cryptophycin analogues.

compd	binding energy (kJ/mol)	max. binding energy (kJ/mol)	min. binding energy (kJ/mol)
2	36.17	36.17	17.21
22	22.61	22.61	5.44
23	32.20	32.20	10.38
24	32.70	32.70	11.72

[52], the methoxy group of subunit B forms a hydrogen bond with Lys176 (Figure 2). Another binding mode of **2** with high binding affinity and hydrogen bond formation did not involve any interaction of subunit B, yet it was oriented towards the GDP binding site that might influence GTP hydrolysis.

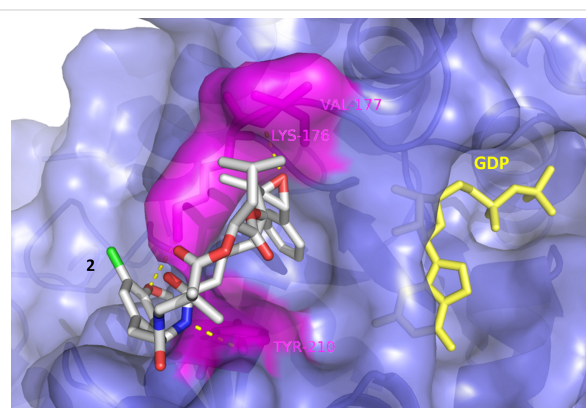


Figure 2: Binding mode of **2**, showing the interaction to the vinca domain peptide binding pocket (blue). Hydrogen bonds are shown as yellow dots with the interacting amino acid residues in magenta.

Compound **22** with the triethylene glycol-based substituent prevents correct binding, the binding energy was decreased and mainly nonspecific interactions outside the binding pocket were observed (Figure 3). This was not the case for the other derivatives **23** and **24** (Figure 4).

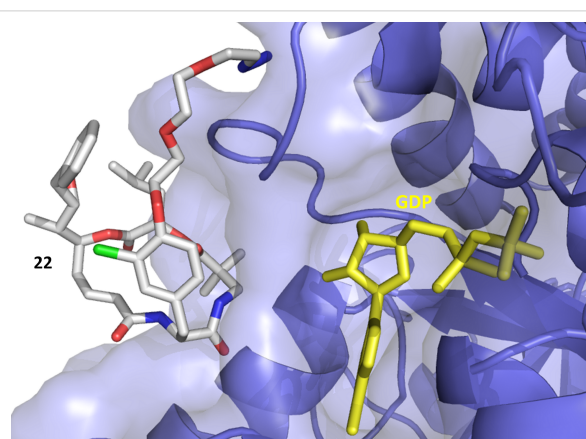


Figure 3: Docking of **22** to the vinca domain of β-tubulin. Surface and backbone of β-tubulin are shown in blue, GDP in yellow. No hydrogen bond formation was detected. The orientation of the azidoethoxyethoxyethyl substituent prevents the inhibitor from the correct interaction with the protein. The epoxide and benzyl group of subunit A are pointing away from the binding pocket.

Besides hydrogen bond formation and binding affinity of inhibitors **2**, **23** and **24**, π-interactions and hydrophobic contacts with the binding pocket of the vinca domain were detected

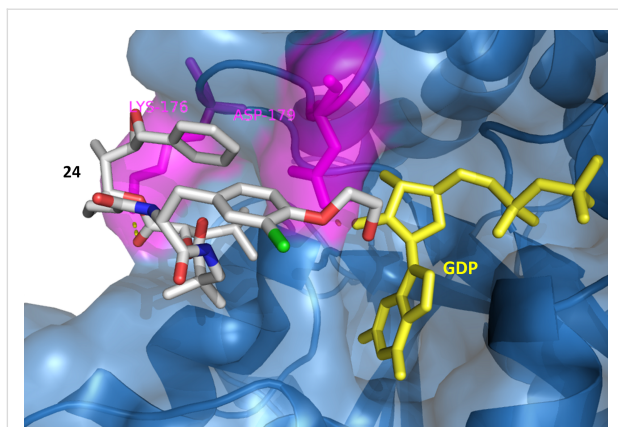


Figure 4: Docking of **24** to β -tubulin. Surface and backbone of β -tubulin are shown in blue, GDP in yellow. H-bonding (yellow dots) was detected with Lys176 and Asp179 in magenta. The benzyl group and the epoxide of subunit A are directed towards the peptide binding pocket, while the hydroxyethyl group is positioned towards the GDP binding pocket forming an H-bond with Asp179.

that would in turn increase the affinity of the inhibitor and its effect on the protein (Supporting Information File 1, Table S1).

Conclusion

In summary, three new cryptophycin analogues with a modified unit B have been designed and successfully synthesized. The novel analogues were less active than cryptophycin-52 in the KB-3-1 cell line. Analogue **22** showed a dramatic loss of activity whereas analogues **23** and **24** showed a reduced activity but were still very cytotoxic.

Supporting Information

Supporting Information File 1

Experimental part and analytical data.

[<https://www.beilstein-journals.org/bjoc/content/supplementary/1860-5397-14-109-S1.pdf>]

Acknowledgements

This project has received funding from the European Union's Horizon 2020 research and innovation programme under the Marie Skłodowska-Curie grant agreement No 642004. The authors like to acknowledge M. Wißbrock, A. Nieß and C. Michalek for technical support.

ORCID® iDs

Eduard Figueras - <https://orcid.org/0000-0002-1853-9974>

Adina Borbély - <https://orcid.org/0000-0002-5506-6555>

Norbert Sewald - <https://orcid.org/0000-0002-0309-2655>

References

- Schwartz, R. E.; Hirsch, C. F.; Sesin, D. F.; Flor, J. E.; Chartrain, M.; Fromtling, R. E.; Harris, G. H.; Salvatore, M. J.; Liesch, J. M.; Yudin, K. *J. Ind. Microbiol.* **1990**, *5*, 113–123. doi:10.1007/BF01573860
- Bai, R.; Schwartz, R. E.; Kepler, J. A.; Pettit, G. R.; Hamel, E. *Cancer Res.* **1996**, *56*, 4398–4406.
- Smith, C. D.; Zhang, X. *J. Biol. Chem.* **1996**, *271*, 6192–6198. doi:10.1074/jbc.271.11.6192
- Barrow, R. A.; Hemscheidt, T.; Liang, J.; Paik, S.; Moore, R. E.; Tius, M. A. *J. Am. Chem. Soc.* **1995**, *117*, 2479–2490. doi:10.1021/ja00114a011
- Kobayashi, M.; Wang, W.; Ohyabu, N.; Kurosu, M.; Kitagawa, I. *Chem. Pharm. Bull.* **1995**, *43*, 1598–1600. doi:10.1248/cpb.43.1598
- de Muys, J.-M.; Rej, R.; Nguyen, D.; Go, B.; Fortin, S.; Lavallée, J.-F. *Bioorg. Med. Chem. Lett.* **1996**, *6*, 1111–1116. doi:10.1016/0960-894X(96)00182-5
- Rej, R.; Nguyen, D.; Go, B.; Fortin, S.; Lavallée, J.-F. *J. Org. Chem.* **1996**, *61*, 6289–6295. doi:10.1021/jo960816b
- Gardinier, K. M.; Leahy, J. W. *J. Org. Chem.* **1997**, *62*, 7098–7099. doi:10.1021/jo971645t
- Norman, B. H.; Hemscheidt, T.; Schultz, R. M.; Andis, S. L. *J. Org. Chem.* **1998**, *63*, 5288–5294. doi:10.1021/jo980536r
- Georg, G. I.; Ali, S. M.; Stella, V. J.; Waugh, W. N.; Himmels, R. H. *Bioorg. Med. Chem. Lett.* **1998**, *8*, 1959–1962. doi:10.1016/S0960-894X(98)00356-4
- Ghosh, A. K.; Bischoff, A. *Org. Lett.* **2000**, *2*, 1573–1575. doi:10.1021/ol000058i
- Eggen, M.; Mossman, C. J.; Buck, S. B.; Nair, S. K.; Bhat, L.; Ali, S. M.; Reiff, E. A.; Boge, T. C.; Georg, G. I. *J. Org. Chem.* **2000**, *65*, 7792–7799. doi:10.1021/jo000767+
- Murakami, N.; Wang, W.; Ohyabu, N.; Ito, T.; Tamura, S.; Aoki, S.; Kobayashi, M.; Kitagawa, I. *Tetrahedron* **2000**, *56*, 9121–9128. doi:10.1016/S0040-4020(00)00766-3
- Murakami, N.; Tamura, S.; Wang, W.; Takagi, T.; Kobayashi, M. *Tetrahedron* **2001**, *57*, 4323–4336. doi:10.1016/S0040-4020(01)00339-8
- Ghosh, A. K.; Swanson, L. *J. Org. Chem.* **2003**, *68*, 9823–9826. doi:10.1021/jo035077v
- Mast, C. A.; Eißler, S.; Stončič, A.; Stämmler, H.-G.; Neumann, B.; Sewald, N. *Chem. – Eur. J.* **2005**, *11*, 4667–4677. doi:10.1002/chem.200500282
- Danner, P.; Bauer, M.; Phukan, P.; Maier, M. E. *Eur. J. Org. Chem.* **2005**, 317–325. doi:10.1002/ejoc.200400558
- Eißler, S.; Neumann, B.; Stämmler, H.-G.; Sewald, N. *Synlett* **2008**, 273–277. doi:10.1055/s-2007-1000868
- Sammet, B.; Radzey, H.; Neumann, B.; Stämmler, H.-G.; Sewald, N. *Synlett* **2009**, 417–420. doi:10.1055/s-0028-1087541
- Sammet, B.; Brax, M.; Sewald, N. *Beilstein J. Org. Chem.* **2011**, *7*, 243–245. doi:10.3762/bjoc.7.32
- Sessa, C.; Weigang-Köhler, K.; Pagani, O.; Greim, G.; Mor, O.; De Pas, T.; Burgess, M.; Weimer, I.; Johnson, R. *Eur. J. Cancer* **2002**, *38*, 2388–2396. doi:10.1016/S0959-8049(02)00489-6
- Stevenson, J. P.; Sun, W.; Gallagher, M.; Johnson, R.; Vaughn, D.; Schuchter, L.; Algazy, K.; Hahn, S.; Enas, N.; Ellis, D.; Thornton, D.; O'Dwyer, P. *J. Clin. Cancer Res.* **2002**, *8*, 2524–2529.
- D'Agostino, G.; Del Campo, J.; Mellado, B.; Izquierdo, M. A.; Minarik, T.; Cirri, L.; Marini, L.; Perez-Gracia, J. L.; Scambia, G. *Int. J. Gynecol. Cancer* **2006**, *16*, 71–76. doi:10.1111/j.1525-1438.2006.00276.x

24. Patel, V. F.; Andis, S. L.; Kennedy, J. H.; Ray, J. E.; Schultz, R. M. *J. Med. Chem.* **1999**, *42*, 2588–2603. doi:10.1021/jm980706s
25. Varie, D. L.; Shih, C.; Hay, D. A.; Andis, S. L.; Corbett, T. H.; Gossett, L. S.; Janisse, S. K.; Martinelli, M. J.; Moher, E. D.; Schultz, R. M.; Toth, J. E. *Bioorg. Med. Chem. Lett.* **1999**, *9*, 369–374. doi:10.1016/S0960-894X(98)00748-3
26. Shih, C.; Gossett, L. S.; Gruber, J. M.; Sue Grossman, C.; Andis, S. L.; Schultz, R. M.; Worzalla, J. F.; Corbett, T. H.; Metz, J. T. *Bioorg. Med. Chem. Lett.* **1999**, *9*, 69–74. doi:10.1016/S0960-894X(98)00682-9
27. Vidya, R.; Eggen, M. J.; Georg, G. I.; Himes, R. H. *Bioorg. Med. Chem. Lett.* **2003**, *13*, 757–760. doi:10.1016/S0960-894X(02)01023-5
28. Buck, S. B.; Huff, J. K.; Himes, R. H.; Georg, G. I. *J. Med. Chem.* **2004**, *47*, 696–702. doi:10.1021/jm030278c
29. Buck, S. B.; Huff, J. K.; Himes, R. H.; Georg, G. I. *J. Med. Chem.* **2004**, *47*, 3697–3699. doi:10.1021/jm030555f
30. Eißler, S.; Bogner, T.; Nahrwold, M.; Sewald, N. *Chem. – Eur. J.* **2009**, *15*, 11273–11287. doi:10.1002/chem.200901750
31. Liu, W. L.; Zhang, J. C.; Jiang, F. Q.; Fu, L. *Arch. Pharm.* **2009**, *342*, 577–583. doi:10.1002/ardp.200900067
32. Nahrwold, M.; Bogner, T.; Eissler, S.; Verma, S.; Sewald, N. *Org. Lett.* **2010**, *12*, 1064–1067. doi:10.1021/ol1000473
33. Weiß, C.; Bogner, T.; Sammet, B.; Sewald, N. *Beilstein J. Org. Chem.* **2012**, *8*, 2060–2066. doi:10.3762/bjoc.8.231
34. Kumar, A.; Kumar, M.; Sharma, S.; Guru, S. K.; Bhushan, S.; Shah, B. A. *Eur. J. Med. Chem.* **2015**, *93*, 55–63. doi:10.1016/j.ejmech.2014.11.068
35. Weiss, C.; Figueras, E.; Borbely, A. N.; Sewald, N. *J. Pept. Sci.* **2017**, *23*, 514–531. doi:10.1002/psc.3015
36. Chari, R. V. J.; Miller, M. L.; Widdison, W. C. *Angew. Chem., Int. Ed.* **2014**, *53*, 3796–3827. doi:10.1002/anie.201307628
37. Srinivasarao, M.; Low, P. S. *Chem. Rev.* **2017**, *117*, 12133–12164. doi:10.1021/acs.chemrev.7b00013
38. Krall, N.; Scheuermann, J.; Neri, D. *Angew. Chem., Int. Ed.* **2013**, *52*, 1384–1402. doi:10.1002/anie.201204631
39. Dal Corso, A.; Pignataro, L.; Belvisi, L.; Gennari, C. *Curr. Top. Med. Chem.* **2016**, *16*, 314–329. doi:10.2174/1568026615666150701114343
40. Le Joncour, V.; Laakkonen, P. *Bioorg. Med. Chem.* **2018**, *26*, 2797–2806. doi:10.1016/j.bmc.2017.08.052
41. Al-awar, R. S.; Ray, J. E.; Schultz, R. M.; Andis, S. L.; Kennedy, J. H.; Moore, R. E.; Liang, J.; Golakoti, T.; Subbaraju, G. V.; Corbett, T. H. *J. Med. Chem.* **2003**, *46*, 2985–3007. doi:10.1021/jm0203884
42. Al-Awar, R. S.; Corbett, T. H.; Ray, J. E.; Polin, L.; Kennedy, J. H.; Wagner, M. M.; Williams, D. C. *Mol. Cancer Ther.* **2004**, *3*, 1061–1067.
43. Kotoku, N.; Kato, T.; Narumi, F.; Ohtani, E.; Kamada, S.; Aoki, S.; Okada, N.; Nakagawa, S.; Kobayashi, M. *Bioorg. Med. Chem.* **2006**, *14*, 7446–7457. doi:10.1016/j.bmc.2006.07.019
44. Sammet, B.; Bogner, T.; Nahrwold, M.; Weiss, C.; Sewald, N. *J. Org. Chem.* **2010**, *75*, 6953–6960. doi:10.1021/jo101563s
45. Weiss, C.; Sammet, B.; Sewald, N. *Nat. Prod. Rep.* **2013**, *30*, 924–940. doi:10.1039/c3np70022d
46. Nahrwold, M.; Weiß, C.; Bogner, T.; Mertink, F.; Conradi, J.; Sammet, B.; Palmisano, R.; Royo Gracia, S.; Preuße, T.; Sewald, N. *J. Med. Chem.* **2013**, *56*, 1853–1864. doi:10.1021/jm301346z
47. Bouchard, H.; Brun, M.-P.; Commerçon, A.; Zhang, J. Novel conjugates, preparation thereof, and therapeutic use thereof. WO Patent WO2011/001052, Jan 6, 2011.
48. Verma, V. A.; Pillow, T. H.; Depalatis, L.; Li, G.; Phillips, G. L.; Polson, A. G.; Raab, H. E.; Spencer, S.; Zheng, B. *Bioorg. Med. Chem. Lett.* **2015**, *25*, 864–868. doi:10.1016/j.bmcl.2014.12.070
49. Steinkuhler, M. C.; Gallinari, M. P.; Osswald, B.; Sewald, N.; Ritzefeld, M.; Frese, M.; Figueras, E.; Pethö, L. Cryptophycin-based antibody-drug conjugates with novel self-immolative linkers. WO Patent WO2016/146638 A1, Sept 22, 2016.
50. Bigot, A.; Bouchard, H.; Brun, M.-P.; Clerc, F.; Zhang, J. Novel cryptophycin compounds and conjugates, their preparation and their therapeutic use. WO Patent WO2017/076998 A1, May 11, 2017.
51. Chen, H.; Lin, Z.; Arnst, K. E.; Miller, D. D.; Li, W. *Molecules* **2017**, *22*, No. 1281. doi:10.3390/molecules22081281
52. Mitra, A.; Sept, D. *Biochemistry* **2004**, *43*, 13955–13962. doi:10.1021/bi0487387
53. Bai, R.; Pettit, G. R.; Hamel, E. *Biochem. Pharmacol.* **1990**, *39*, 1941–1949. doi:10.1016/0006-2952(90)90613-P

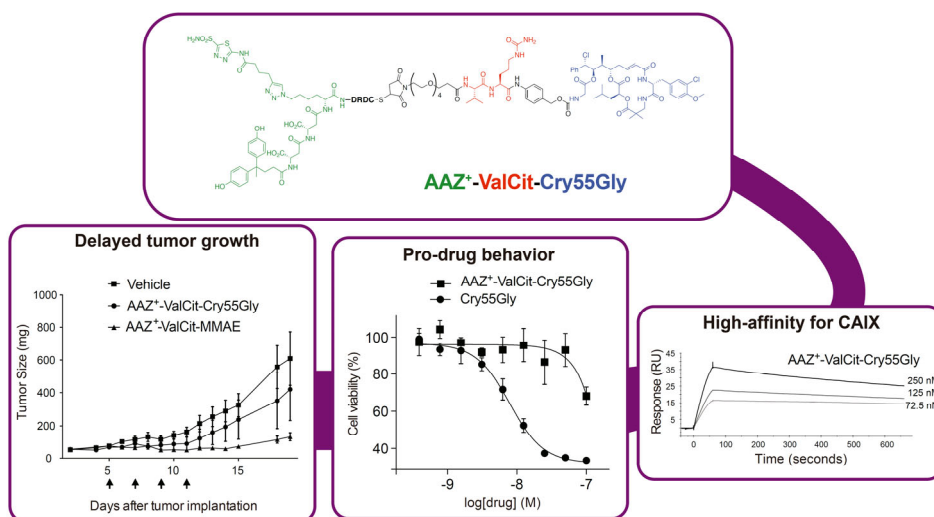
License and Terms

This is an Open Access article under the terms of the Creative Commons Attribution License (<http://creativecommons.org/licenses/by/4.0>), which permits unrestricted use, distribution, and reproduction in any medium, provided the original work is properly cited.

The license is subject to the *Beilstein Journal of Organic Chemistry* terms and conditions: (<https://www.beilstein-journals.org/bjoc>)

The definitive version of this article is the electronic one which can be found at: [doi:10.3762/bjoc.14.109](https://doi.org/10.3762/bjoc.14.109)

Chapter 4 – Cryptophycin conjugate targeting carbonic anhydrase IX



This chapter corresponds to the following publication:

Samuele Cazzamalli,[‡] Eduard Figueras,[‡] Lilla Pethó, Adina Borbély, Christian Steinkühler, Dario Neri,* and Norbert Sewald*. *In vivo* antitumor activity of a novel acetazolamide-cryptophycin conjugate for the treatment of renal cell carcinoma. *ACS Omega*, **2018**, 3 (11), 14726-14731

[‡] Authors contributed equally to this work

List of author contributions:

Conception and design: S. Cazzamalli, E. Figueras, D. Neri, and N. Sewald

Synthesis: E. Figueras, L. Pethő, and S. Cazzamalli

Biological evaluation: S. Cazzamalli

Analysis and interpretation of data: S. Cazzamalli, E. Figueras, L. Pethő, A. Borbély, D. Neri, and N. Sewald

Writing the manuscript: E. Figueras

Review and/or revision of the manuscript: S. Cazzamalli, E. Figueras, L. Pethő, A. Borbély, C. Steinkühler, D. Neri, and N. Sewald

Study supervision: C. Steinkühler, D. Neri, and N. Sewald

In Vivo Antitumor Activity of a Novel Acetazolamide–Cryptophycin Conjugate for the Treatment of Renal Cell Carcinomas

Samuele Cazzamalli,^{†,‡,Ⓜ} Eduard Figueras,^{‡,Ⓜ} Lilla Pethő,^{‡,§} Adina Borbély,[‡] Christian Steinkühler,^{||} Dario Neri,^{*,†} and Norbert Sewald^{*,‡,Ⓜ}

[†]Department of Chemistry and Applied Biosciences, Swiss Federal Institute of Technology (ETH Zürich), Vladimir-Prelog-Weg 4, CH-8093 Zürich, Switzerland

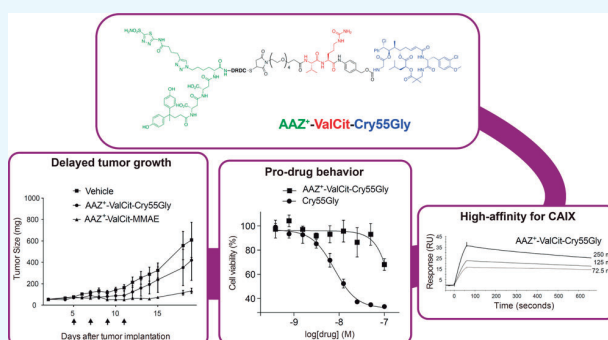
[‡]Department of Chemistry, Organic and Bioorganic Chemistry, Bielefeld University, Universitätsstraße 25, D-33615 Bielefeld, Germany

[§]MTA-ELTE Research Group of Peptide Chemistry, Hungarian Academy of Sciences, Eötvös L. University, H-1117 Budapest, Hungary

^{||}Exiris s.r.l., Via Savona 6, I-00182 Rome, Italy

Supporting Information

ABSTRACT: Traditional chemotherapeutics used in cancer therapy do not preferentially accumulate in tumor tissues. The conjugation to delivery vehicles like antibodies or small molecules has been proposed as a strategy to increase the tumor uptake and improve the therapeutic window of these drugs. Here, we report the synthesis and the biological evaluation of a novel small molecule–drug conjugate (SMDC) comprising a high-affinity bidentate acetazolamide derivative, targeting carbonic anhydrase IX (CAIX), and cryptophycin, a potent microtubule destabilizer. The biological activity of the novel SMDC was evaluated in vitro, measuring binding to the CAIX antigen by surface plasmon resonance and cytotoxicity against SKRC-52 cells. In vivo studies showed a delayed growth of tumors in nude mice bearing SKRC-52 renal cell carcinomas.



1. INTRODUCTION

Most cytotoxic compounds, which are used for cancer chemotherapy, do not accumulate selectively at the site of the disease.^{1,2} The suboptimal biodistribution properties of these drugs limit clinical efficacy and may cause severe side effects.³ Antibodies and small molecules that are able to bind accessible tumor-associated antigens have been proposed as carriers to deliver cytotoxic payloads to the tumor site. The corresponding products are called antibody–drug conjugates (ADCs) and small molecule–drug conjugates (SMDCs), respectively.⁴ Four ADCs (Kadcyla, Adcetris, Besponsa, and Mylotarg) have been approved for cancer treatment.⁵

The prolonged circulatory half-life of ADC products can induce side effects as a result of premature release of the payload. In addition, challenges related to the preparation of ADCs with homogenous drug–antibody ratio, as well as high manufacturing cost, may hinder ADC development.⁶ SMDC products may represent an alternative to ADCs.⁷ Their small size facilitates rapid and uniform diffusion into tissues,⁸ potentially reaching high tumor/organ ratios at earlier time points. Lower cost-of-goods,⁹ lack of immunogenicity,¹⁰ amenability to chemical synthesis, and easier analytical characterization may represent opportunities for SMDC

development compared to ADCs. Promising results from nuclear medicine studies and preclinical experiments have been obtained with certain ligands of folate receptors,¹¹ prostate-specific membrane antigen,¹² somatostatin receptors,¹³ and carbonic anhydrase IX (CAIX),^{3,7,14} indicating that it is possible to target different types of tumors with small organic compounds.

Carbonic anhydrase IX (CAIX) is a transmembrane protein virtually absent in most of the healthy human tissues, with the exception of certain gastrointestinal structures.^{15,16} CAIX represents an ideal target for SMDC development since its expression is enhanced in tumor hypoxia and certain cancer types. A growing body of evidence indicates that binding of antibodies or small ligands to CAIX does not induce receptor internalization.^{3,17–22} We have recently reported the discovery of a noninternalizing acetazolamide derivative from a DNA-encoded library and its use as a delivery vehicle for tumor targeting.^{7,23} An SMDC product based on this ligand, called AAZ², showed a comparable in vivo activity to an ADC

Received: September 11, 2018

Accepted: October 25, 2018

Published: November 2, 2018

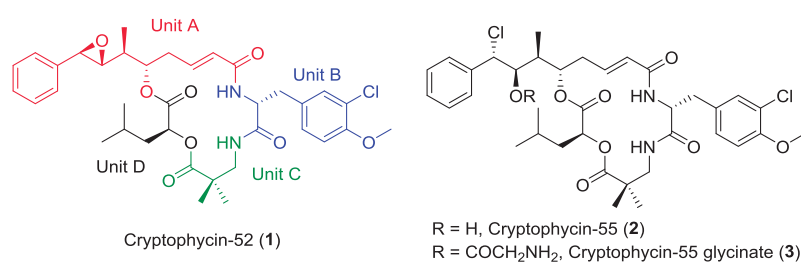
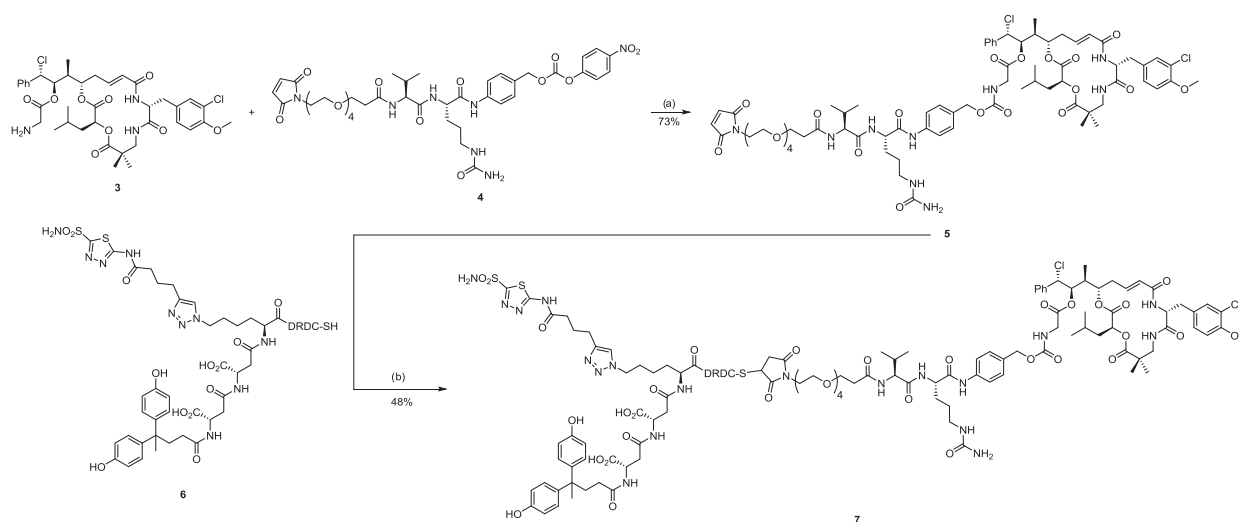


Figure 1. Structures of cryptophycin-52 (1), cryptophycin-55 (2), and cryptophycin-55 glycinate (3).

Scheme 1. Synthesis of an Acetazolamide–Cryptophycin Conjugate^a



^aReagents and conditions: (a) *N,N*-diisopropylethylamine (DIPEA), dimethylformamide (DMF), room temperature (RT), 3 h; (b) Tris buffered saline (TBS), DMF, RT, o.n.

targeting the same antigen.⁷ Moreover, we could show that the anticancer activity of the SMDC can be enhanced by the combination of immune-oncology drugs like antibody–cytokine fusion proteins.¹⁴

Not only the ligands but also the linker–payload combination is significant for the development of efficacious targeted cytotoxic products.^{24,25} In fact, the failure of early ADCs and SMDCs was partially due to the insufficient potency of the chosen payloads. The importance of using more potent cytotoxic agents has been recognized, prompting research in the identification of highly active drugs. Indeed, since the tumor-targeting performance of AAZ and AAZ⁺ decreases at doses above 250 nmol/kg, our groups have searched for cytotoxic payloads, which could potentially outperform conventional drugs used in ADC and SMDC research.

Cryptophycins (Figure 1) are cyclic depsipeptides with a bacterial origin, which show promise as payloads to be used in targeted therapy.²⁶ Cryptophycins display a very high cytotoxicity (typically in the low picomolar range) on a broad variety of cancer cells, including multidrug-resistant ones.²⁷ Initial studies focused on the total synthesis and application of cryptophycins as traditional chemotherapeutics, but disappointing results in monotherapy phase II clinical trials prompted a focus shift toward ligand-based pharmacodelivery approaches.^{28,29} However, the parental compound lacks an addressable functional group for the conjugation to a homing device. Therefore, research has been focused on the generation of cryptophycin derivatives that can be conjugated and

subsequently released, preserving the potent cytotoxicity of the parent compound.^{30–33}

The para position of the aromatic ring of unit A has proven to be a suitable position to be modified, and ADCs using this anchoring point have been produced.^{34–37} Another position that can be modified is the epoxide of unit A. Although this site plays an essential role for the high cytotoxicity, it tolerates certain modifications. Cytotoxicity is retained upon epoxide opening with HCl to give a chlorohydrin, presumably due to the epoxide-forming reverse reaction under physiological conditions. Hence, the secondary alcohol of the chlorohydrin permits conjugation to the homing device, since esterification is an elegant way to stabilize the compound while retaining the cytotoxicity.³⁸

2. RESULTS AND DISCUSSION

The use of cryptophycin payloads has been studied for the preparation of ADCs, but *in vivo* applications of cryptophycin–SMDC have not yet been reported. For this reason, we embarked on a project aiming at the synthesis and biological evaluation of a conjugate bearing a bidentate acetazolamide ligand, cleavable Val-Cit dipeptide with *para*-aminobenzyl self-immolative part, and cryptophycin-55 glycinate as a payload, and studied its biological effect. Cryptophycin-55 glycinate (3) was prepared as previously described with slight modifications.³⁸ The cleavable linker 4 was prepared starting from Fmoc-Val-Cit-PAB; the Fmoc group was removed and a triethylene glycol spacer containing a maleimide moiety was

coupled to increase the solubility of the conjugate and allow the conjugation to the acetazolamide moiety via Michael addition. Then, the alcohol of the *para*-aminobenzyl moiety was activated with bis(4-nitrophenyl) carbonate and the linker 4 was obtained in good yield and purity. Next, linker 4 was coupled to cryptophycin-55 glycinate (3) via carbamate linkage obtaining 5 with satisfactory yield (73%) and purity (Scheme 1). Conjugation of 5 to the acetazolamide ligand 6 yielded the final conjugate 7 (48%) in excellent purity.

The affinity of the novel SMDC (7) to recombinant human CAIX was determined using surface plasmon resonance (SPR) (Figure 2). Conjugate 7 was bound in a concentration-

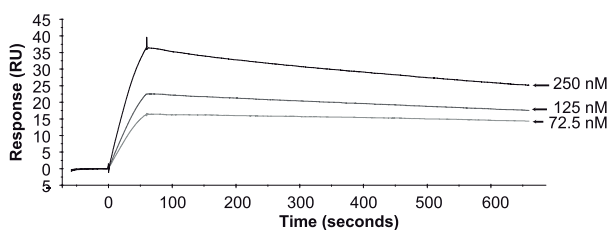


Figure 2. SPR analysis: binding of acetazolamide–cryptophycin conjugate 5 to immobilized CAIX.

dependent manner to immobilized CAIX in agreement with previous data obtained using similar derivatives of AAZ⁺ (i.e., we could calculate an apparent binding constant of 3.4 nM for AAZ⁺-ValCit-Cry55gly, similar to the K_D value previously reported for AAZ⁺-ValCit-MMAE).^{7,14}

An *in vitro* cytotoxicity cell-based assay was performed using the cell line SKRC-52 (Figure 3). The unmodified payload 3

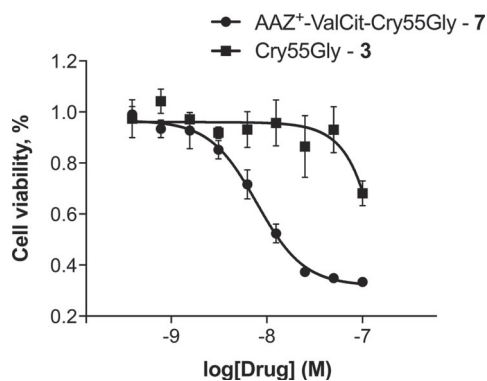


Figure 3. *In vitro* toxicity of cryptophycin-55 glycinate (unconjugated drug) and compound 7 on the SKRC-52 tumor cells.

showed a cytotoxicity in the low nanomolar range (IC_{50} = 7.9 nM). Indeed, cryptophycin-55 glycinate was remarkably less potent than expected when compared to other cell lines.³⁹ Monomethyl auristatin E (MMAE) using the same cell line and protocol showed a IC_{50} of 1.5 nM.²⁴ As expected, conjugate 7 showed a decreased cytotoxicity compared to the unmodified drug, proving the prodrug behavior characteristic of noninternalizing conjugates.

The antitumor activity of compound 7 was investigated *in vivo* in nude mice bearing subcutaneous SKRC-52 renal cell carcinomas (Figure 4). An optimal and safe dose corresponding to 250 nmol/kg was determined on the basis of dose-escalation studies in nude mice (Supporting Information

Figure S5) and previously published biodistribution studies.²⁴ Mice treated with compound 7 enjoyed a therapeutic benefit with a slower tumor growth, especially during the treatment (p = 0.05 at day 14), compared with the control group (saline). In comparison to the lead compound featuring MMAE as the payload administered at the same dose, the therapeutic activity was significantly inferior. Under these experimental conditions, neither acute toxicity nor significant loss of weight could be observed for mice treated with the compounds bearing either cryptophycin or MMAE as the payload.

3. CONCLUSIONS

In summary, we have generated a novel cryptophycin–acetazolamide conjugate targeting CAIX. The SMDC product showed excellent affinity to the target and a noninternalizing behavior in an *in vitro* cytotoxicity assay. The compound exhibited a moderate antitumor effect *in vivo*, which was, however, inferior to that of an analogous compound based on MMAE as the payload. The lower therapeutic activity observed with the cryptophycin-55 glycinate, compared to that of the MMAE conjugate, correlates with the lower *in vitro* potency of the corresponding free drugs and provides a motivation to search for more potent cryptophycin derivatives.

4. EXPERIMENTAL SECTION

4.1. General. The general information about the used materials and methods, NMR, and high-performance liquid chromatography (HPLC) spectra can be found in the Supporting Information.

4.2. Syntheses. **4.2.1. Cryptophycin-55 Glycinate (3).** Cryptophycin-55 was prepared as previously reported.³² Slightly modified protocol from Liang et al. was used to synthesize cryptophycin-55 glycinate.³⁸ Cryptophycin-55 (62 mg, 88 μ mol, 1 equiv), DCC (27.2 mg, 132 μ mol, 1.5 equiv), Boc-glycine (23.1 mg, 132 μ mol, 1.5 equiv), and 4-DMAP (1.07 mg, 8.8 μ mol, 0.1 equiv) were placed under argon atmosphere and dissolved in 1 mL of dry dichloromethane (DCM). The solution was stirred for 2 h 30 min at RT. Then, 2 mL of EtOAc/PE 3:1 was added and the solution was stirred for 10 min. The solution was filtered through Celite, washed with EtOAc/PE 3:1 (100 mL), and the solvent was removed under reduced pressure. The crude was dissolved in 4 mL of dry DCM, 120 μ L of 4 M HCl in dioxane was added, and the solution was stirred overnight at RT. Then, the solvent was removed under reduced pressure and the residue was purified by reversed-phase (RP)-HPLC (method P1) to yield cryptophycin-55 glycinate trifluoroacetate salt (63.4 mg, 82% yield) as a white powder after freeze-drying. ¹H NMR (600 MHz, CDCl₃): δ (ppm) = 0.94 (d, J = 6.5 Hz, 3H, uD-C ^{δ} H₃), 0.99 (d, J = 6.5 Hz, 3H, uD-C ^{δ} H₃), 1.00 (d, J = 7.2 Hz, 3H, uA-C ^{ϵ} HCH₃), 1.08 (s, 3H, uC-C(CH₃)₂), 1.18 (s, 3H, uC-C(CH₃)₂), 1.63–1.68 (m, 1H, uD-C ^{β} H^A), 1.73–1.79 (m, 1H, uD-C ^{γ} H), 1.90–1.95 (m, 1H, uD-C ^{β} H^B), 2.17–2.23 (m, 1H, uA-C ^{γ} H^A), 2.54–2.57 (m, 1H, uA-C ^{γ} H^B), 2.64–2.69 (m, 1H, uA-C ^{ϵ} H), 2.94 (dd, J = 14.5, 8.5 Hz, 1H, uB-C ^{β} H^A), 3.07–3.14 (m, 3H, Gly-H^A, uB-C ^{β} H^B, uC-C ^{β} H^A), 3.34–3.41 (m, uC-C ^{β} H^B), 3.67 (d, J = 16.6 Hz, 1H, Gly-H^B), 3.88 (s, 3H, uB-OCH₃), 4.56 (td, J = 7.8, 5.1 Hz, uB-C ^{α} H), 4.73 (t, J = 10.6 Hz, 1H, uA-C ^{δ} H), 4.81 (d, J = 10.2 Hz, 1H, uA-C ^{η} H), 4.93 (dd, J = 10.9, 2.7 Hz, 1H, uD-C ^{α} H), 5.42 (d, J = 10.2 Hz, 1H, uA-C ^{ζ} H), 5.74 (dd, J = 15.4, 1.8 Hz, 1H, uA-C ^{α} H), 6.27 (br, 1H, uB-NH), 6.52 (ddd, J = 15.2, 11.0, 4.2 Hz, 1H, uA-C ^{β} H),

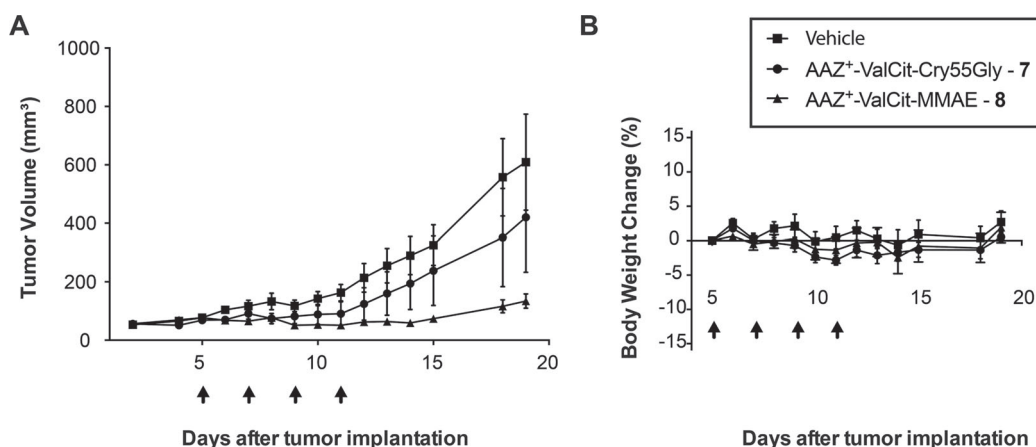


Figure 4. Therapy experiment of conjugates 7 and 8 (250 nmol/kg). (A) Tumor volume changes for different treatment groups. (B) Animal body weight changes during the in vivo efficacy study. Intravenous administration of the corresponding compound is indicated by the arrows.

6.86 (d, $J = 8.4$ Hz, 1H, uB-C^{5'}H), 7.05 (dd, $J = 8.4, 2.2$ Hz, 1H, uB-C^{6'}H), 7.19 (d, $J = 2.2$ Hz, 1H, uB-C^{2'}H), 7.27–7.37 (m, 5H, uA-C^{2'}H).

4.2.2. Maleimide-PEG₄-Val-Cit-PAB-PNP (4). Fmoc-Val-Cit-PABOH (500 mg, 0.83 mmol) was dissolved in *N*-methyl pyrrolidone (10 mL), diethylamine (2 mL) was added, and the solution was stirred overnight at room temperature. Then, the solvent was removed under high vacuum and the obtained oil was resuspended in DCM. The suspension was placed in an ultrasonic bath for 10 min; the solid was filtered off, washed with DCM, and dried in high vacuum to yield H-Val-Cit-PABOH as a beige solid (260 mg, 82% yield).

Maleimide-PEG₄-OH (190 mg, 0.55 mmol, 1.2 equiv) and DIPEA (321 μ L, 1.85 mmol, 4 equiv) were premixed in DMF (6.5 mL) and added to H-Val-Cit-PAB (175 mg, 0.46 mmol, 1 equiv). HATU (209 mg, 0.55 mmol, 1.2 equiv) and HOAt (75 mg, 0.55 mmol, 1.2 equiv) were dissolved in DMF (6.5 mL) and added to the reaction mixture. The solution was stirred at room temperature for 2 h, and then, the solvent was removed under reduced pressure. The product was taken up in MeOH, the solution filtered off, and the filtrate purified by column chromatography using DCM/MeOH (8:2) as an eluent to provide Maleimide-PEG₄-Val-Cit-PABOH as a yellow oil (215 mg, 66% yield).

Maleimide-PEG₄-Val-Cit-PABOH (120 mg, 0.17 mmol, 1 equiv) was dissolved in anhydrous DMF (1.5 mL), and bis(4-nitrophenyl) carbonate (103 mg, 0.34 mmol, 2 equiv) and DIPEA (45 μ L, 0.26 mmol, 1.5 equiv) were added. The solution was stirred at room temperature for 3 h, and then, the solvents were removed under reduced pressure. The product was purified by column chromatography using DCM/MeOH (9:1) as an eluent to obtain 2 as a slightly yellowish solid (95 mg, 64% yield). LC–MS (method A): $t_r = 8.61$ min, 92% purity ($\lambda = 220$ nm). m/z calcd for [C₄₀H₅₄N₇O₁₅]⁺: 872.37 [M + H]⁺; found: 872.36.

4.2.3. Maleimide-PEG₄-Val-Cit-PABC-Cry55-gly (5). 3 (8.7 mg, 9.94 μ mol, 1 equiv) and 4 (9.5 mg, 10.90 μ mol, 1.1 equiv) were dissolved in DMF (0.5 mL), DIPEA (5.2 μ L, 29.82 μ mol, 3 equiv) was added, and the solution was stirred at room temperature for 3 h. Then, it was directly purified by RP-HPLC (method P1); fractions containing the desired product were freeze-dried to afford 5 as a white powder (10.9 mg, 73% yield). LC–MS (method A): $t_r = 10.52$ min, >99% purity ($\lambda =$

220 nm), m/z calcd for [C₇₂H₉₉Cl₂N₉O₂₁]²⁺: 747.82 [M + 2H]²⁺; found: 747.82.

4.2.4. AAZ⁺ (6). Compound 6 was synthesized as previously reported.⁷

4.2.5. AAZ⁺-ValCit-Cry55gly (7). Compound 6 (3.6 mg, 2.51 μ mol, 2.5 equiv) was dissolved in 500 μ L of degassed TBS (pH 7.4). Compound 5 (1.5 mg, 1.00 μ mol, 1.0 equiv) was added as a DMF solution (500 μ L), and the reaction mixture was stirred at room temperature overnight. The crude mixture was diluted in 500 μ L of H₂O and 500 μ L of CH₃CN, and purified by RP-HPLC (method P2). Product-containing fractions were identified by high-resolution mass spectrometry and lyophilized overnight to afford 7 (AAZ⁺-ValCit-Cry55gly; 1.4 mg, 48% yield). LC–MS (method B): $t_r = 3.51$ min, >99% purity ($\lambda = 260$ nm), m/z calcd for [C₁₂₈H₁₇₄Cl₂N₂₆O₄₃S₃]²⁺: 1464.5378 [M + 2H]²⁺; found: 1464.5367; m/z calcd for [C₁₂₈H₁₇₅Cl₂N₂₆O₄₃S₃]³⁺: 976.6943 [M + 3H]³⁺; found: 976.6956

4.3. Surface Plasmon Resonance. Surface plasmon resonance (SPR) experiments were performed at room temperature using a Biacore S200 instrument (GE Healthcare). CMS chips (Series S) and filtered phosphate-buffered saline (PBS) pH 7.4 with dimethyl sulfoxide (DMSO) (5% v/v) as a flow buffer were used for all experiments. Human CAIX was immobilized on the chip to 500 response units (R.U.) using EDC-HCl and NHS according to the manufacturer's instructions. Serial dilutions of compound 7 (AAZ⁺-ValCit-Cry55gly) in a running buffer at a flow rate of 20 μ L/min were used as analytes. The chip surface was regenerated after each cycle by a short treatment with DMSO (50% v/v) in PBS. Sensorgrams were solvent-corrected and the binding kinetics was analyzed with the Biacore S200 evaluation software using the 1:1 Langmuir binding model.

4.4. Cell Culture and In Vitro Cytotoxicity Assay. The human renal cell carcinoma cell line SKRC-52 was kindly provided by Professor E. Oosterwijk (Radboud University Nijmegen Medical Centre, Nijmegen, The Netherlands). Upon thawing, cells were maintained in culture-full growth medium (Roswell Park Memorial Institute (RPMI) added with 10% fetal calf serum (FCS) and 1% antibiotic–antimycotic; Invitrogen) at 37 °C and 5% CO₂. When reaching 90% confluence, cells were detached using trypsin–ethylenediaminetetraacetic acid (EDTA) 0.05% (Invitrogen) and re-seeded at a dilution of 1:6.

SKRC-52 cells were seeded in 96-well plates in RPMI added with 10% FCS (100 μL) at a density of 5×10^3 cells/well. The medium was replaced after 24 h with fresh medium containing different concentrations of test substance (starting concentration of 100 nM, 1:2 dilution steps), and plates were incubated under standard culture conditions. After 72 h, the medium was removed, MTS cell viability dye (20 μL , Promega) was added in 150 μL of fresh medium, the plates were incubated for 2 h under standard culture conditions, and the absorbance at 490 nm was measured on a Spectra Max Paradigm multimode plate reader (Molecular Devices; background correction was performed by measuring the absorbance at 630 nm). Experiments were performed in triplicates, and the average cell viability was calculated as measured background-corrected absorbance divided by the absorbance of untreated control wells. IC_{50} values were determined by fitting data to the four-parameter logistic equation, using Prism 7 software (GraphPad Software) for data analysis.

4.5. Animal Studies. The animal studies were performed in accordance with Swiss animal welfare laws and regulations (license number 27/2015, granted by Veterinäramt des Kantons Zürich).

4.5.1. Tumor Implantation. SKRC-52 cells were grown as described above to 80% confluence and detached with trypsin–EDTA 0.05% (Life Technologies). Cells were rinsed once with Hank's balanced salt solution (HBSS, pH 7.4), and counted and suspended again in HBSS to give a final concentration of 3.4×10^7 cells/mL. Aliquots of 5×10^6 cells (150 μL of the suspension) were injected subcutaneously into the right flank of athymic BALB/c nu/nu mice (8–10 weeks old females, Janvier).

4.5.2. Dose Escalation. Athymic BALB/c nu/nu mice (females, 8–10 weeks old, no tumors, Janvier) were injected intravenously with different doses of compound 7 (AAZ⁺-ValCit-Cry5Sgly; 10, 25, 125, 250, and 500 nmol/kg; $n = 1$ per group) five times, once every two days (starting from day 1; Figure S5). None of the doses tested resulted in a significant acute body weight loss.

4.5.3. Therapy Experiment. Tumors were allowed to grow to an average volume of 75 mm³. Three groups (5 mice each) were formed randomly. The treatment was started by intravenously injecting a solution of AAZ⁺-ValCit-Cry5Sgly (compound 7), AAZ⁺-ValCit-MMAE (compound 8), or vehicle (PBS containing 1% of DMSO) (lateral tail vein) at 250 nmol/kg. All compounds were prepared and injected as solutions in sterile PBS containing 1% DMSO. The mice were weighed, and the tumor sizes were monitored daily with an electronic caliper. Tumor volume calculation was done by multiplying (long side) \times (short side) \times (short side) \times 0.5. Once the termination criteria were reached, the animals were sacrificed. GraphPad Prism 7 was used for data analysis (regular two-way ANOVA followed by Bonferroni test).

■ ASSOCIATED CONTENT

● Supporting Information

The Supporting Information is available free of charge on the ACS Publications website at DOI: 10.1021/acsomega.8b02350.

Materials and methods, characterization of new compounds, and dose-escalation graph (PDF)

■ AUTHOR INFORMATION

Corresponding Authors

*E-mail: neri@pharma.ethz.ch (D.N.).

*E-mail: norbert.sewald@uni-bielefeld.de (N.S.).

ORCID

Samuele Cazzamalli: 0000-0003-0510-5664

Norbert Sewald: 0000-0002-0309-2655

Author Contributions

[†]S.C. and E.F. contributed equally to this work.

Notes

The authors declare the following competing financial interest(s): D.N. is a co-founder and shareholder of Philogen (www.philogen.com), a Swiss-Italian Biotech company that operates in the field of ligand-based pharmacodelivery.

■ ACKNOWLEDGMENTS

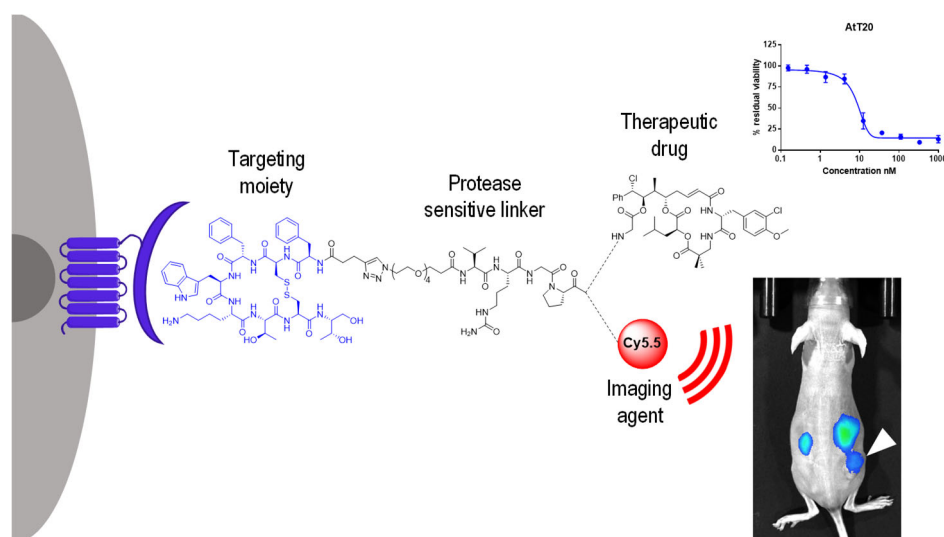
This project has received funding from the European Union's Horizon 2020 research and innovation programme under the Marie Skłodowska-Curie grant agreement No 642004 (ETN MAGICBULLET). The authors gratefully acknowledge financial support from ETH Zürich, the Swiss National Science Foundation (Project Nos. 310030B_163479/1 and SINERGIA CRSII2_160699/1), ERC Advanced Grant "ZauberKugel" (670603), and Kommission für Technologie und Innovation (Grant No. 17072.1). The authors acknowledge M. Wißbrock, A. Nieß, and C. Michalek for technical support.

■ REFERENCES

- (1) van der Veldt, A. A. M.; Hendrikse, N. H.; Smit, E. F.; Mooijer, M. P. J.; Rijnders, A. Y.; Gerritsen, W. R.; Van Der Hoeven, J. J. M.; Windhorst, A. D.; Lammertsma, A. A.; Lubberink, M. Biodistribution and Radiation Dosimetry of ¹¹C-Labelled Docetaxel in Cancer Patients. *Eur. J. Nucl. Med. Mol. Imaging* **2010**, *37*, 1950–1958.
- (2) van der Veldt, A. A. M.; Lubberink, M.; Mathijssen, R. H. J.; Loos, W. J.; Herder, G. J. M.; Greuter, H. N.; Comans, E. F. I.; Rutten, H. B.; Eriksson, J.; Windhorst, A. D.; et al. Toward Prediction of Efficacy of Chemotherapy: A Proof of Concept Study in Lung Cancer Patients Using [¹¹C]Docetaxel and Positron Emission Tomography. *Clin. Cancer Res.* **2013**, *19*, 4163–4173.
- (3) Krall, N.; Pretto, F.; Decurtins, W.; Bernardes, G. J. L.; Supuran, C. T.; Neri, D. A Small-Molecule Drug Conjugate for the Treatment of Carbonic Anhydrase IX Expressing Tumors. *Angew. Chem., Int. Ed.* **2014**, *53*, 4231–4235.
- (4) Srinivasarao, M.; Low, P. S. Ligand-Targeted Drug Delivery. *Chem. Rev.* **2017**, *117*, 12133–12164.
- (5) Carter, P. J.; Lazar, G. A. Next Generation Antibody Drugs: Pursuit of the "High-Hanging Fruit". *Nat. Rev. Drug Discovery* **2018**, *17*, 197–223.
- (6) Beck, A.; Goetsch, L.; Dumontet, C.; Corvaia, N. Strategies and Challenges for the next Generation of Antibody–drug Conjugates. *Nat. Rev. Drug Discovery* **2017**, *16*, 315–337.
- (7) Cazzamalli, S.; Dal Corso, A.; Widmayer, F.; Neri, D. Chemically Defined Antibody- and Small Molecule-Drug Conjugates for in Vivo Tumor Targeting Applications: A Comparative Analysis. *J. Am. Chem. Soc.* **2018**, *140*, 1617–1621.
- (8) Yuan, F.; Dellian, M.; Fukumura, D.; Leunig, M.; Berk, D. A.; Torchilin, V. P.; Jain, R. K. Vascular Permeability in a Human Tumor Xenograft: Molecular Size Dependence and Cutoff Size. *Cancer Res.* **1995**, *55*, 3752–3756.
- (9) Firer, M. A.; Gellerman, G. Targeted Drug Delivery for Cancer Therapy: The Other Side of Antibodies. *J. Hematol. Oncol.* **2012**, *5*, 70.
- (10) Jefferis, R. Posttranslational Modifications and the Immunogenicity of Biotherapeutics. *J. Immunol. Res.* **2016**, No. 5358272.

- (11) Leamon, C. P.; Parker, M. A.; Vlahov, I. R.; Xu, L.-C.; Reddy, J. A.; Vetzell, M.; Douglas, N. Synthesis and Biological Evaluation of EC20: A New Folate-Derived, 99m Tc-Based Radiopharmaceutical. *Bioconjugate Chem.* **2002**, *13*, 1200–1210.
- (12) Hillier, S. M.; Maresca, K. P.; Lu, G.; Merkin, R. D.; Marquis, J. C.; Zimmerman, C. N.; Eckelman, W. C.; Joyal, J. L.; Babich, J. W. ^{99m}Tc-Labeled Small-Molecule Inhibitors of Prostate-Specific Membrane Antigen for Molecular Imaging of Prostate Cancer. *J. Nucl. Med.* **2013**, *54*, 1369–1376.
- (13) Ginj, M.; Zhang, H.; Waser, B.; Cescato, R.; Wild, D.; Wang, X.; Erchevgy, J.; Rivier, J.; Mäcke, H. R.; Reubi, J. C. Radiolabeled Somatostatin Receptor Antagonists Are Preferable to Agonists for in Vivo Peptide Receptor Targeting of Tumors. *Proc. Natl. Acad. Sci. U.S.A.* **2006**, *103*, 16436–16441.
- (14) Cazzamalli, S.; Ziffels, B.; Widmayer, F.; Murer, P.; Pellegrini, G.; Pretto, F.; Wulhfard, S.; Neri, D. Enhanced Therapeutic Activity of Non-Internalizing Small Molecule-Drug Conjugates Targeting Carbonic Anhydrase IX in Combination With Targeted Interleukin-2. *Cancer Res.* **2018**, *24*, 3656–3667.
- (15) Wichert, M.; Krall, N. Targeting Carbonic Anhydrase IX with Small Organic Ligands. *Curr. Opin. Chem. Biol.* **2015**, *26*, 48–54.
- (16) Supuran, C. T.; Alterio, V.; Fiore, A. Di; D'Ambrosio, K.; Carta, F.; Monti, S. M.; De Simone, G. Inhibition of Carbonic Anhydrase IX Targets Primary Tumors, Metastases, and Cancer Stem Cells: Three for the Price of One. *Med. Res. Rev.* **2018**, 1799.
- (17) Krall, N.; Pretto, F.; Neri, D. A Bivalent Small Molecule-Drug Conjugate Directed against Carbonic Anhydrase IX Can Elicit Complete Tumour Regression in Mice. *Chem. Sci.* **2014**, *5*, 3640–3644.
- (18) Perrino, E.; Steiner, M.; Krall, N.; Bernardes, G. J. L.; Pretto, F.; Casi, G.; Neri, D. Curative Properties of Noninternalizing Antibody-Drug Conjugates Based on Maytansinoids. *Cancer Res.* **2014**, *74*, 2569–2578.
- (19) Dorywalska, M.; Dushin, R.; Moine, L.; Farias, S. E.; Zhou, D.; Navaratnam, T.; Lui, V.; Hasa-Moreno, A.; Casas, M. G.; Tran, T.-T.; et al. Molecular Basis of Valine-Citrulline-PABC Linker Instability in Site-Specific ADCs and Its Mitigation by Linker Design. *Mol. Cancer Ther.* **2016**, *15*, 958–970.
- (20) Dal Corso, A.; Cazzamalli, S.; Gébleux, R.; Mattarella, M.; Neri, D. Protease-Cleavable Linkers Modulate the Anticancer Activity of Noninternalizing Antibody – Drug Conjugates. *Bioconjugate Chem.* **2017**, *28*, 1826–1833.
- (21) Dal Corso, A.; Gébleux, R.; Murer, P.; Soltermann, A.; Neri, D. A Non-Internalizing Antibody-Drug Conjugate Based on an Anthracycline Payload Displays Potent Therapeutic Activity in Vivo. *J. Controlled Release* **2017**, *264*, 211–218.
- (22) Marks, I. S.; Gardeen, S. S.; Kurdziel, S. J.; Nicolaou, S. T.; Woods, J. E.; Kularatne, S. A.; Low, P. S. Development of a Small Molecule Tubulysin B Conjugate for Treatment of Carbonic Anhydrase IX Receptor Expressing Cancers. *Mol. Pharm.* **2018**, *15*, 2289–2296.
- (23) Wichert, M.; Krall, N.; Decurtins, W.; Franzini, R. M.; Pretto, F.; Schneider, P.; Neri, D.; Scheuermann, J. Dual-Display of Small Molecules Enables the Discovery of Ligand Pairs and Facilitates Affinity Maturation. *Nat. Chem.* **2015**, *7*, 241–249.
- (24) Cazzamalli, S.; Dal Corso, A.; Neri, D. Acetazolamide Serves as Selective Delivery Vehicle for Dipeptide-Linked Drugs to Renal Cell Carcinoma. *Mol. Cancer Ther.* **2016**, *15*, 2926–2936.
- (25) Cazzamalli, S.; Dal Corso, A.; Neri, D. Linker Stability Influences the Anti-Tumor Activity of Acetazolamide-Drug Conjugates for the Therapy of Renal Cell Carcinoma. *J. Controlled Release* **2017**, *246*, 39–45.
- (26) Weiss, C.; Figueras, E.; Borbely, A. N.; Sewald, N. Cryptophycins: Cytotoxic Cyclodepsipeptides with Potential for Tumor Targeting. *J. Pept. Sci.* **2017**, *23*, 514–531.
- (27) Schwartz, R. E.; Hirsch, C. F.; Sesin, D. F.; Flor, J. E.; Chartrain, M.; Fromtling, R. E.; Harris, G. H.; Salvatore, M. J.; Liesch, J. M.; Yudin, K. Pharmaceuticals from Cultured Algae. *J. Ind. Microbiol.* **1990**, *5*, 113–124.
- (28) Eißler, S.; Stoncius, A.; Nahrwold, M.; Sewald, N. The Synthesis of Cryptophycins. *Synthesis* **2006**, 3747–3789.
- (29) D'Agostino, G.; Del Campo, J.; Mellado, B.; Izquierdo, M. A.; Minarik, T.; Cirri, L.; Marini, L.; Perez-Gracia, J. L.; Scambia, G. A Multicenter Phase II Study of the Cryptophycin Analog LY355703 in Patients with Platinum-Resistant Ovarian Cancer. *Int. J. Gynecol. Cancer* **2006**, *16*, 71–76.
- (30) Sammet, B.; Bogner, T.; Nahrwold, M.; Weiss, C.; Sewald, N. Approaches for the Synthesis of Functionalized Cryptophycins. *J. Org. Chem.* **2010**, *75*, 6953–6960.
- (31) Nahrwold, M.; Weiß, C.; Bogner, T.; Mertink, F.; Conradi, J.; Sammet, B.; Palmisano, R.; Gracia, S. R.; Preuß, T.; Sewald, N. Conjugates of Modified Cryptophycins and RGD-Peptides Enter Target Cells by Endocytosis. *J. Med. Chem.* **2013**, *56*, 1853–1864.
- (32) Weiss, C.; Sammet, B.; Sewald, N. Recent Approaches for the Synthesis of Modified Cryptophycins. *Nat. Prod. Rep.* **2013**, *30*, 924–940.
- (33) Figueras, E.; Borbély, A.; Ismail, M.; Frese, M.; Sewald, N. Novel Unit B Cryptophycin Analogues as Payloads for Targeted Therapy. *Beilstein J. Org. Chem.* **2018**, *14*, 1281–1286.
- (34) Eißler, S.; Bogner, T.; Nahrwold, M.; Sewald, N. Efficient Synthesis of Cryptophycin-52 and Novel Para-Alkoxyethyl Unit A Analogues. *Chem. - Eur. J.* **2009**, *15*, 11273–11287.
- (35) Verma, V. A.; Pillow, T. H.; Depalatis, L.; Guangmin, L.; Phillips, G. L.; Polson, A. G.; Raab, H. E.; Spencer, S.; Zheng, B. The Cryptophycins as Potent Payloads for Antibody Drug Conjugates. *Bioorg. Med. Chem. Lett.* **2015**, *25*, 864–868.
- (36) Bigot, A.; Bouchard, H.; Brun, M.-P.; Clerc, F.; Zhang, J. WO2017/076998A1, 2017.
- (37) Chen, H.; Lin, Z.; Arnst, K. E.; Miller, D. D.; Li, W. Tubulin Inhibitor-Based Antibody-Drug Conjugates for Cancer Therapy. *Molecules* **2017**, *22*, No. 1281.
- (38) Liang, J.; Moore, R. E.; Moher, E. D.; Munroe, J. E.; Al-Awar, R. S.; Hay, D. A.; Varie, D. L.; Zhang, T. Y.; Aikins, J. A.; Martinelli, M. J.; et al. Cryptophycins-309, 249 and Other Cryptophycin Analogs: Preclinical Efficacy Studies with Mouse and Human Tumors. *Invest. New Drugs* **2005**, *23*, 213–224.
- (39) Steinkühler, M. C.; Gallinari, M. P.; Osswald, B.; Sewald, N.; Ritzefeld, M.; Frese, M.; Figueras, E.; Pethö, L. WO2016/146638A1, 2016.

Chapter 5 – Cryptophycin conjugates targeting the somatostatin receptor 2



This chapter corresponds to the following publication:

Eduard Figueras,[‡] Ana Martins,[‡] Adina Borbély, Vadim Le Joncour, Paola Cordella, Raffaella Perego, Daniela Modena, Paolo Pagani, Simone Esposito, Giulio Auciello, Marcel Frese, Paola Gallinari, Pirjo Laakkonen, Christian Steinkühler, and Norbert Sewald*. Octreotide conjugates for tumor targeting and imaging. *Submitted*.

[‡] Authors contributed equally to this work

List of author contributions:

Conception and design: E. Figueras, A. Martins, A. Borbély, P. Gallinari, C. Steinkühler, and N. Sewald

Synthesis: E. Figueras

Binding affinity: D. Modena

***In vitro* cytotoxicity, receptor internalization, *in vitro* and *in vivo* imaging, *in vivo* antitumor activity:** A. Martins

Pharmacokinetics: A. Martins and P. Cordella

Plasma stability: A. Borbély

Cathepsin B assays: P. Cordella

Analysis and interpretation of data: All authors

Writing the manuscript: E. Figueras and A. Martins

Review and/or revision of the manuscript: All authors

Study supervision: P. Laakkonen, P. Gallinari, C. Steinkühler, and N. Sewald

Octreotide Conjugates for Tumor Targeting and Imaging

Eduard Figueras,^{a,†} Ana Martins,^{a,b,†} Adina Borbély,^a Vadim Le Joncour,^c Paola Cordella,^d Raffaella Perego,^d Daniela Modena,^d Paolo Pagani,^d Simone Esposito,^c Giulio Auciello,^c Marcel Frese,^a Paola Gallinari,^b Pirjo Laakkonen,^c Christian Steinkühler,^{b,d} and Norbert Sewald^{a,*}

^a Department of Chemistry, Organic and Bioorganic Chemistry, Bielefeld University, Universitätsstraße 25, DE-33615 Bielefeld, Germany

^b Exiris srl, Via di Castel Romano 100, IT-00128 Rome, Italy

^c Translational Cancer Medicine, Research Programs Unit, Haartmaninkatu 8, FI-00014 University Helsinki, Finland

^d Italfarmaco SpA, Via dei Lavoratori 54, IT-20092 Cinisello Balsamo, Italy

^e IRBM Science Park SpA, Via Pontina Km. 30,600, IT-00071 Pomezia, Italy

KEYWORDS: Tumor Targeting, Small Molecule Drug Conjugates, Cryptophycin, Cytotoxic Payloads, Imaging

ABSTRACT: Tumor targeting has emerged as an advantageous approach to improve the efficacy and safety of cytotoxic agents or radiolabeled ligands that do not preferentially accumulate in the tumor tissue. The somatostatin receptors (SSTRs) belong to the G-protein-coupled receptor superfamily and are overexpressed in many neuroendocrine tumors (NETs). SSTRs can be efficiently targeted with octreotide, a cyclic octapeptide derived from native somatostatin. The conjugation of cargoes to octreotide represents an attractive approach for effective tumor targeting. In this study, we conjugated octreotide to cryptophycin, a highly cytotoxic decapeptide, through the protease cleavable Val-Cit dipeptide linker using two different self-immolative moieties. The biological activity was investigated *in vitro* and the stability of the conjugates was largely influenced by the self-immolative part. Replacement of cryptophycin by the infrared cyanine dye Cy5.5 was exploited to elucidate the tumor targeting properties of the conjugates *in vitro* and *in vivo*. The compound efficiently and selectively internalized in cells overexpressing SSTR2 and accumulated in xenografts for prolonged time. Our results on the *in vivo* properties indicate that octreotide may serve as an efficient delivery vehicle for tumor targeting.

INTRODUCTION

Cancer therapy has experienced several paradigm changes during the last decade from small molecule drugs over targeted therapy with antibody-drug conjugates (ADCs) to approaches in immuno-oncology. Originally tumor therapy was based on cytotoxic drugs as mono or combination therapy (alkylating agents like cisplatin, chlorambucil, procarbazine, carmustine; antimetabolites like methotrexate, cytarabine, gemcitabine; microtubule-binding agents like vinblastine, paclitaxel, or topoisomerase inhibitors). Traditional chemotherapeutics (e.g. paclitaxel, doxorubicin) usually do not preferentially accumulate in tumors but affect all tissues, which leads to detrimental side effects.¹ Thus, targeted therapy with antibody-drug conjugates (ADCs) and, more recently, with small molecule-drug conjugates (SMDCs), has emerged as a viable alternative to enlarge the therapeutic window.²⁻⁶ With the approvals of Adcetris[®] (Seattle Genetics/Millennium), Kadcyla[®] (Genentech/Roche), Besponsa[®] (Wyeth/Pfizer), the re-approval of Mylotarg[®] (Wyeth/Pfizer) and more than 80 ADCs in clinical trial pipelines, ADCs are to be considered a new class of pharmaceuticals. Compared to classical cytotoxic drugs, ADCs have the benefit of higher specificity towards tumor cells and controllable release mechanisms at the site of action. Small molecule-mediated targeting represents advantages in terms of the straightforward organic synthesis of

SMDCs and their uniform structure compared to antibodies. Indeed, small molecule ligands have been used to efficiently target tumors expressing the folate receptor,⁷ prostate-specific membrane antigen (PSMA),⁸ carbonic anhydrase IX (CAIX),⁹⁻¹¹ and somatostatin receptors (SSTRs).¹²

The somatostatin receptors (SSTRs) belong to the G-protein-coupled receptor family and can be subdivided into five different subtypes (SSTR1-SSTR5). Many neuroendocrine tumors (NETs) overexpress the somatostatin receptor genes, especially SSTR2, followed by SSTR1 and SSTR5.¹³ Octreotide is a short synthetic octapeptide derived from the natural somatostatin with high affinity and selectivity for SSTR2. Moreover, it has a better metabolic stability and half-life than somatostatin due to the incorporation of D-amino acids and a disulfide bridge.¹⁴ As a result, octreotide has been used to specifically deliver a large number of cytotoxic agents such as paclitaxel,¹⁵ doxorubicin,¹⁶ periplocymarin¹⁷ or periplogenin.¹⁸ Moreover, octreotide is routinely used in clinical practice for tumor diagnostic imaging (e.g. OctreoScan, ⁶⁸Ga-DOTATATE).^{19,20}

In this regard, the usage of potent cytotoxic agents is an attractive approach to increase the efficacy and reduce the dosage. Hence, cryptophycins, potent microtubule destabilizers, represent promising agents to be conjugated to octreotide for tumor targeting.²¹

Cryptophycins are naturally occurring cyclic depsipeptides that were first isolated from cyanobacteria.²² They target tubulin and block the microtubule formation leading to high cytotoxicity against many cancer cell lines. Moreover, they are a weak substrate for the P-gp efflux pump and, consequently, the cytotoxicity is only slightly reduced in multidrug-resistant (MDR) cancer cells.²³ Due to these characteristics, several cryptophycin analogues were investigated as chemotherapeutics, and cryptophycin-52 (LY-355703) was brought to the clinics by Eli Lilly. However, the clinical development was discontinued during phase II because of side effects and insufficient efficacy.^{24,25} Subsequent research focused on several structure-activity relationship studies.^{26–30} Special emphasis was put on the introduction of a functional group enabling conjugation to a homing device for targeted tumor therapy.^{31–37}

Sanofi and Genentech developed cryptophycin derivatives as payloads in the ADC field.^{38–40} In particular, cryptophycin modified in the *para* position of the phenyl ring in unit A has been used in this context, but has shown to be highly unstable in murine plasma, which made the use of these conjugates impossible for preclinical development of new ADCs. Stability problems of the macrocycle could subsequently be overcome by applying modifications in the payload⁴¹ or changing the anchoring point to the antibody.⁴² In strong contrast, very little is known about small molecules conjugated to cryptophycin as delivery agents.⁴³

We have recently communicated the application of acetazolamide as a homing device to deliver cryptophycin-55 glycinate to tumors overexpressing carbonic anhydrase IX. This is the first report showing *in vivo* data of a SMDC comprising cryptophycin.⁴⁴ Here we describe the employment of cryptophycin-55 glycinate as potent payload to be released in

tumors overexpressing SSTR2 using octreotide as delivery vehicle. These findings demonstrate that efficient tumor delivery can be achieved with small molecules such as octreotide and that cryptophycin is a valid payload for targeted tumor therapy.

RESULTS AND DISCUSSION

Design and Synthesis of octreotide-cryptophycin conjugates

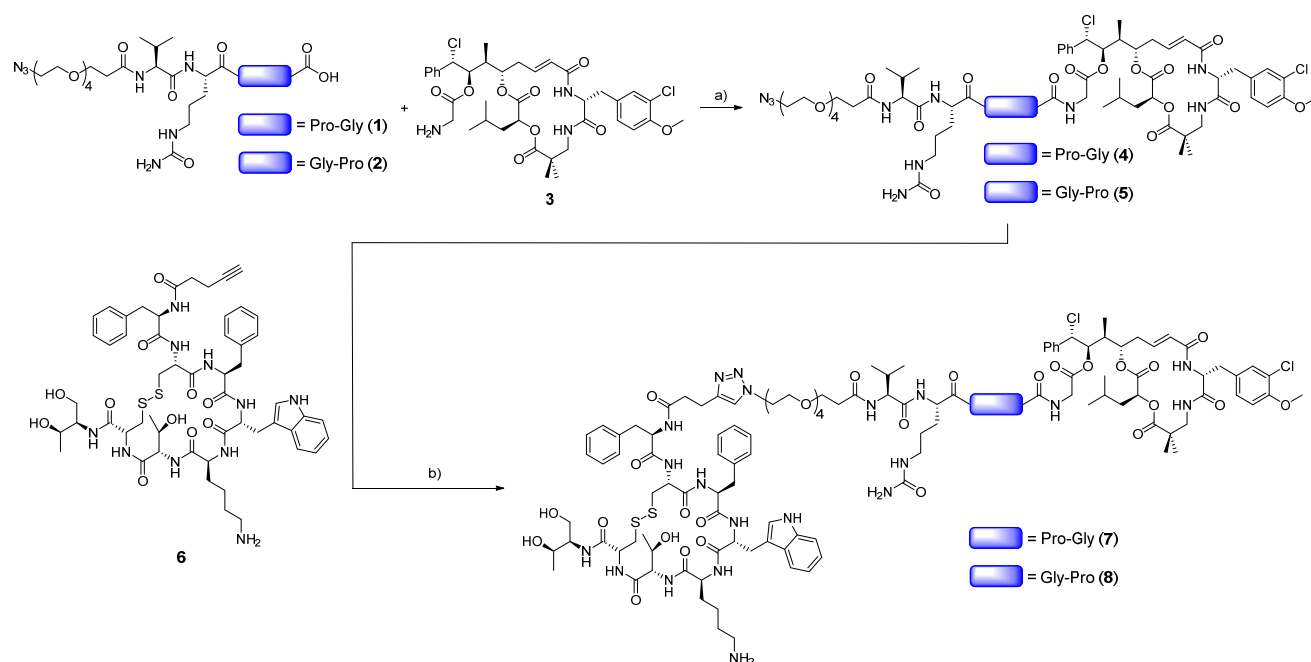
Cryptophycin-55 glycinate was selected as the payload and octreotide as the targeting moiety to develop cryptophycin conjugates targeting SSTR2. The payload was connected to the C-terminus of the cathepsin B-cleavable dipeptide sequence Val-Cit across two different self-immolative dipeptides (Gly-Pro or Pro-Gly) designed to form a diketopiperazine.⁴⁵ The N-terminus contained an azide moiety for subsequent copper(I)-catalyzed alkyne-azide cycloaddition (CuAAC) to an alkyne functionalized octreotide.

The conjugate synthesis started with the preparation of the linkers (**1** and **2**) using solid-phase peptide synthesis (SPPS), followed by coupling to cryptophycin-55 glycinate (**3**) across an amide bond (Scheme 1) to obtain compounds **4** and **5** in excellent purities and good yields (54–79%). The final CuAAC reaction of compounds **4** and **5** with alkyne functionalized octreotide **6** resulted to the conjugates **7** and **8**.

Binding affinity

The binding affinity of the conjugates was evaluated *in vitro* using a radioligand binding competition assay with human SSTR2 and was compared to octreotide. Conjugates **7** and **8** displayed a low nanomolar IC₅₀ affinities (0.62 nM and 1.3 nM, respectively) comparable to the value of the free ligand octreotide (0.5 nM) (Figure 1A).

Scheme 1. Synthesis of octreotide-cryptophycin conjugates **7** and **8**



Reagents and conditions: a) **1** or **2** (2 eq), PyBOP (2 eq), HOBt·H₂O (2.25 eq), DIPEA (2.5 eq), DMF, RT, 4 h; b) CuSO₄·5H₂O (0.6 eq), sodium ascorbate (0.4 eq), DMF/H₂O (1:1), 40 °C, 24 h.

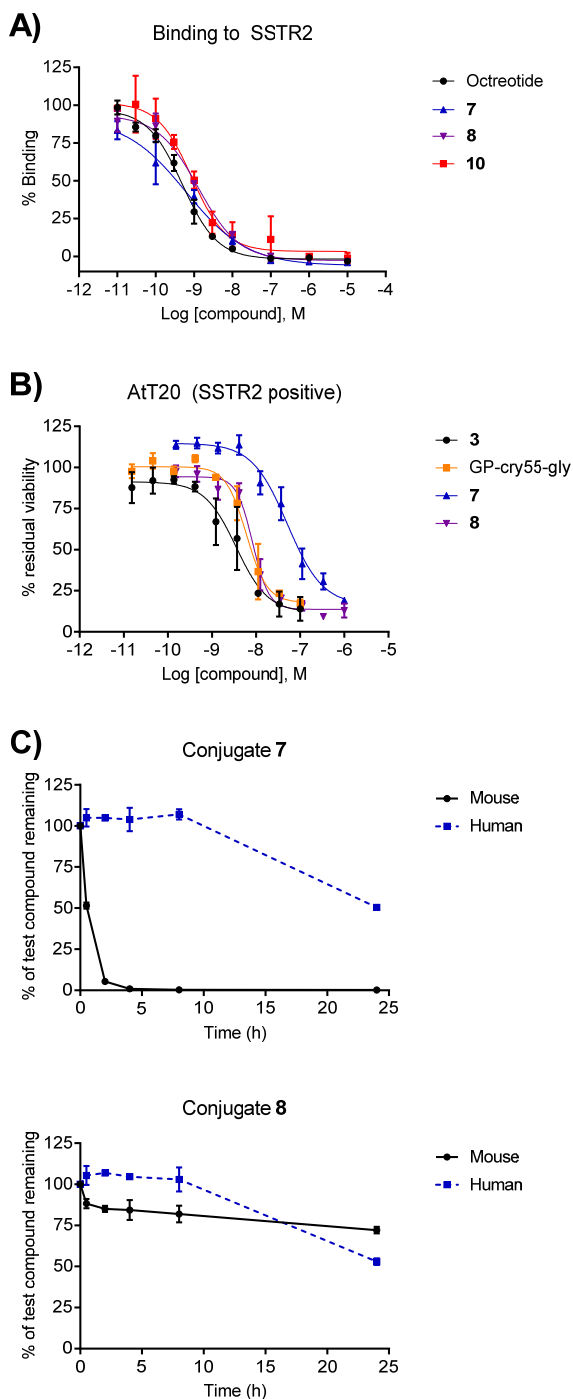


Figure 1. (A) Binding affinity towards SSTR2 of free ligand (octreotide), conjugates **7**, **8**, and **10**. (B) *in vitro* cytotoxicity of the compounds **3**, **7**, and **8** and metabolite Gly-Pro-Cry-55gly in the AtT20 cell line. (C) Plasma stability of conjugates **7** and **8** in murine and human plasma.

In vitro cytotoxicity

AtT20 murine pituitary cancer cells were incubated with increasing concentrations of compounds **7** and **8** to determine their cytotoxicity, which was compared to free payload **3** (Figure 1B). Cryptophycin-55 glycinate showed high potency with an IC_{50} in the low nanomolar range (3.53 nM). Unexpectedly, the activity of conjugates **7** and **8** was remarkably different. While conjugate **8** maintained the high cytotoxicity (IC_{50}

of 8.37 nM), compound **7** showed a reduced cytotoxicity (IC_{50} = 51.23 nM), albeit still in the nanomolar range.

Plasma stability

The stability of conjugates **7** and **8** was evaluated *in vitro* at 37 °C in murine and human plasma. The stability was dramatically influenced by the self-immolative moiety (Figure 1C). Compound **7** exhibited poor stability in mouse plasma ($t_{1/2}$ = 30 min) and moderate stability in human plasma ($t_{1/2}$ = 23 h). Conversely, conjugate **8** was remarkably stable in mouse plasma ($t_{1/2}$ > 24 h) and also slightly more stable in human plasma compared to compound **7** ($t_{1/2}$ = 24 h). The sufficient stability of compound **8** compared to the circulatory half-life (104 min, Figure 2B) close to that measured for octreotide acetate in humans justified the further investigation of its biological activity.

Receptor and conjugate internalization

In the absence of somatostatin, SSTR2 localizes primarily at the plasma membrane and is known to be rapidly internalized upon ligand binding. However, the rate and extent of internalization can vary widely depending on the agonist and its binding affinity.⁴⁶ When evaluating the ability to induce internalization of the receptor in a SSTR2-positive cell model both conjugates induced internalization of SSTR2, which localized to the trans-Golgi network/late endosomal compartment (Figure 2A).⁴⁷ To investigate the tumor homing properties of octreotide conjugates *in vivo* and to confirm that they internalized into the cells, the more stable conjugate **8** was selected and the cytotoxic moiety was replaced by the infrared dye Cy5.5 for the visualization of the conjugate. The dye was coupled to the spacer **2** across an amide bond (Scheme S1) to obtain the intermediate **9** that was then “clicked” to **6** using CuAAC to obtain the fluorescently labeled conjugate **10** with satisfactory yield and excellent purity. We obtained low nanomolar IC_{50} when the affinity of compound **10** towards SSTR2 was measured using radioligand displacement. This confirmed that introduction of the fluorescent dye did not alter the affinity compared to the free ligand (Figure 1A). SSTR2 expressing AtT20 cells showed effective internalization of the construct after only 10 min in live cell confocal microscopy analyses. In addition, high concentration of the conjugate could be detected at the perinuclear space, similar to the receptor itself, upon 30 min of incubation (Figure S1). The internalization could be efficiently competed with a 100-fold excess of the free ligand confirming internalization by the receptor mediated endocytosis. Moreover, no internalization was observed in A549 cells that express low levels of SSTR2.

In vivo tumor imaging

The tumor-targeting ability of conjugate **10** was evaluated in mice bearing AtT20 xenografts that express high levels of SSTR2. Compound **10** was administered intravenously at 1 mg/kg and whole-body imaging at different time points was performed (Figure 2C). A high percentage of the conjugate could be detected in liver and kidneys at early time points, correspondent to the clearance pattern of radiolabeled octreotide derivatives.⁴⁸ However, preferential accumulation of the compound **10** in the tumor over the healthy tissues not involved in the compound excretion could be observed and the conjugate showed good homing properties with detection in the tumor up to 7 days.

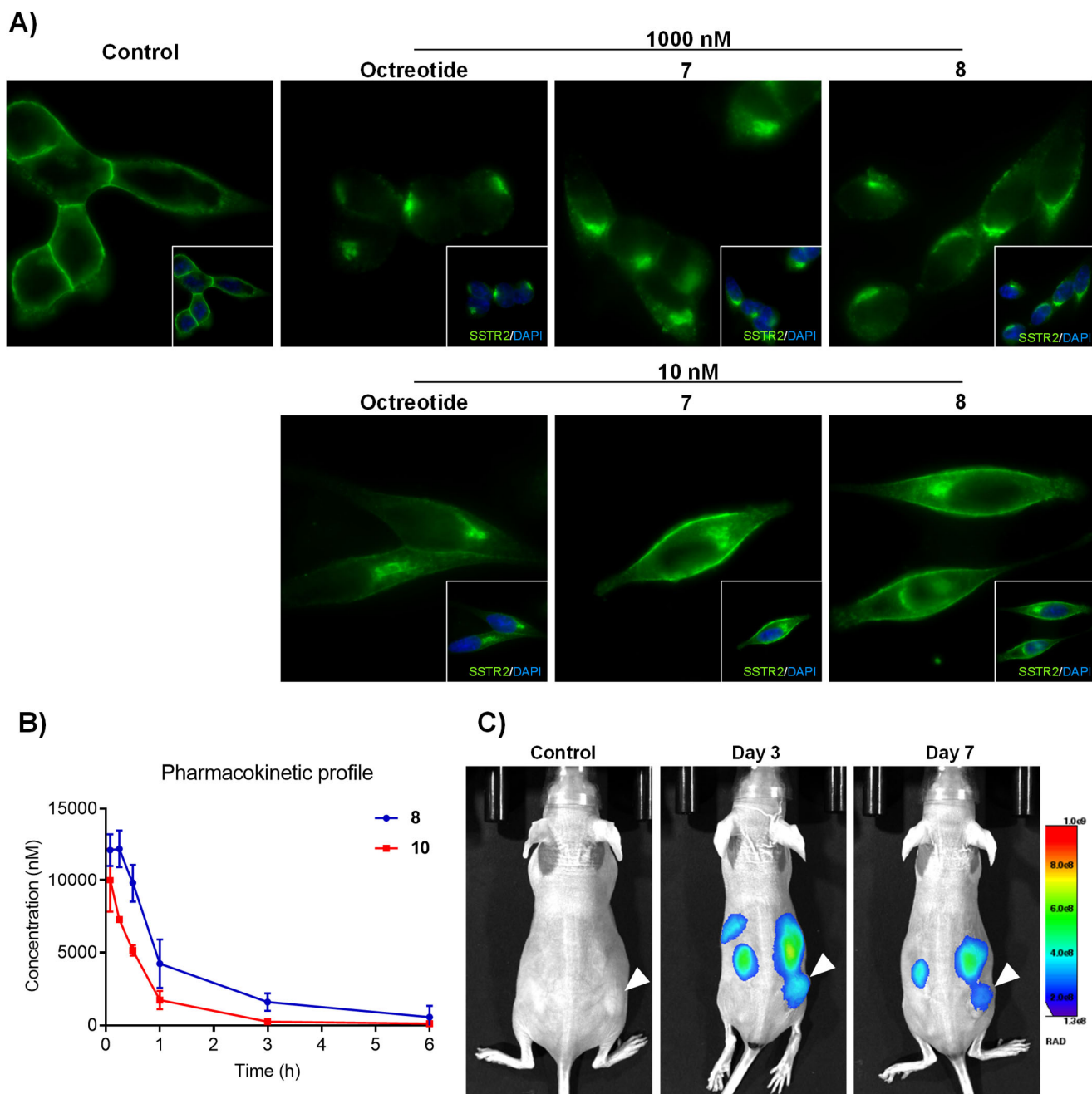


Figure 2. (A) Concentration-dependent internalization of SSTR2 in AtT20 cells. Cells were treated for 30 min at 37 °C with 10 or 1000 nM of octreotide and corresponding octreotide-cryptophycin conjugates **7** and **8**. (B) Pharmacokinetic profile of conjugates **8** and **10** in heterozygous NCR mice. (C) *In vivo* tumor targeting of the infrared derivative of conjugate **8** using the AtT20 xenograft-bearing mice. Animals were injected intravenously with 1 mg/kg of conjugate **10** and whole-body images were taken at the indicated timepoints.

In vivo antitumor activity

On the basis of the above results, the *in vivo* antitumor efficacy of conjugate **8** was evaluated in AtT20 tumor-bearing mice. The maximum tolerated dose of the conjugate was determined by dose escalation experiments. The compound was well tolerated up to 10 mg/kg, the highest tested dose (data not shown). Mice were treated with compound **8** (5 mg/kg) once weekly for 3 weeks and the tumor volume was compared to groups treated with vehicle (2% DMSO in water) or a mixture of unconjugated cryptophycin and octreotide (Figure S3). However, no therapeutic benefit could be observed upon ad-

ministration of **8**. The lack of activity presumably is attributed to insufficient payload release (*vide infra*).

Cathepsin B stability

Cleavage of the conjugate **8** by cathepsin B was studied to elucidate the reasons for the lack of *in vivo* efficacy (Figure 3). The compound was highly stable in the buffer used for the experiment in the absence of enzyme (90% remaining after 6 hours of incubation) but it was readily cleaved upon addition of cathepsin B (1 U/mL). A small amount of compound was already metabolized at $t = 0$, suggesting a high reactivity of the enzyme towards conjugate **8**, which was confirmed by the

fast decrease of the substrate during the first hour of incubation. As expected, the enzymatic cleavage led to the formation of Gly-Pro-Cry-55gly. However, the release of this metabolite was not followed by a self-immolation of the dipeptide, as no cryptophycin-55 glycinate (**3**) was found. Further qualitative analysis did not show the presence of other metabolites (e.g. cryptophycin-55, cryptophycin-52). The cytotoxicity of the metabolite was evaluated using the same protocol than the conjugate and free drug in AtT20 cells. The IC₅₀ value of the metabolite was maintained in the low nanomolar range (6.05 nM) and was comparable to the free payload **3** and conjugate **8**.

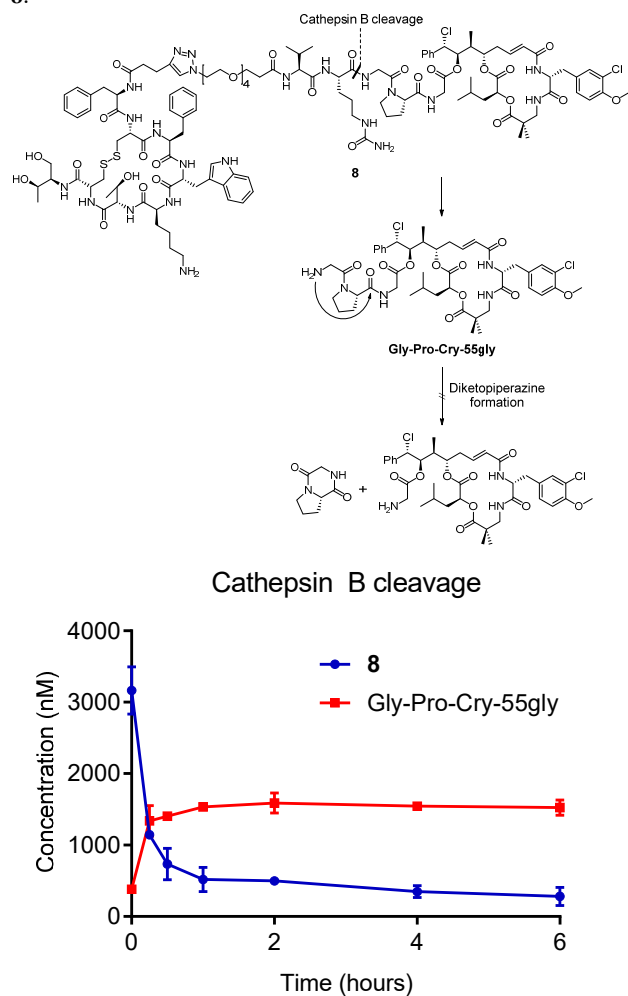


Figure 3. Cathepsin B cleavage and self-immolation mechanism (top) and *in vitro* stability of conjugate **8** in presence of cathepsin B and quantification of the main metabolite (bottom). Compound **8** (5 μ M) was rapidly cleaved in the presence of the enzyme (1 U/mL) already at t_0 , releasing the drug containing metabolite Gly-Pro-Cry-55gly.

CONCLUSIONS

Here we validate octreotide as an appropriate delivery vehicle to tumors overexpressing SSTR2 and cryptophycin-55 glycinate as payload. The generated conjugates with cryptophycin showed good binding affinity to the receptor. The dipeptide spacer between the enzyme-labile moiety and the drug largely influenced the metabolism and cytotoxicity. While the conjugate containing the dipeptide Pro-Gly showed instability

in plasma and reduced cytotoxicity compared to the free drug, the product with the Gly-Pro sequence was highly stable and its cytotoxicity was comparable to the unconjugated payload. The replacement of the payload for the infrared fluorophore Cy5.5 did not alter the binding properties and the labeled compound was internalized selectively by the AtT20 cells. The homing properties of **10** were studied in nude mice bearing AtT20 tumors. Pharmacokinetic and *in vivo* imaging studies showed that, upon i.v. injection, a fluorescent signal becomes rapidly associated with the tumor and persists there for many days despite very rapid clearance of the conjugate from circulation. This observation points to a fundamental difference of the peptide conjugate with respect to antibody-drug conjugates. While the latter have long plasma half-lives and only slowly penetrate into tumor tissues, peptide conjugates are small enough to rapidly reach their intra-tumoral targets, where they can be trapped due to specific interaction with the cognate receptor. The unbound conjugate gets rapidly cleared, mostly by glomerular filtration, thereby avoiding unwanted toxicities to normal tissues. ADCs, in contrast will expose the whole organism to released toxin for a long period of time, thereby potentially giving rise to side effects. In line with this notion, several ADCs directed against solid tumor targets have recently failed in the clinic due to low therapeutic indices. Our octreotide-cryptophycin conjugate, albeit being well tolerated and having the desired pharmacokinetic profile, did not show any therapeutic benefit upon administration at the selected dosing regimen. Cathepsin B cleavage studies proved efficient enzymatic cleavage of the sensitive dipeptide Val-Cit and release of the metabolite Gly-Pro-Cry-55gly, which did not detectably react by further self-immolation to release cryptophycin-55 glycinate under the test conditions. It is possible that the *in vitro* cytotoxicity of the obtained metabolite is insufficient to lead to a sustained *in vivo* efficacy. The translation of the promising *in vitro* results to an *in vivo* model is currently under investigation. The system might benefit from a different linker, which affords efficient release of the free payload and longer residence *in vivo*.

EXPERIMENTAL SECTION

Synthesis of N₃-PEG4-Val-Cit-Pro-Gly (1) and N₃-PEG4-Val-Cit-Gly-Pro (2): Self-immolative linkers **1** and **2** were synthesized manually using standard SPPS. First amino acid was loaded to chlorotrityl resin by reacting the corresponding amino acid (1.5 eq) and DIPEA (3 eq) in anhydrous DCM for 3 h at RT. Then, MeOH (1 mL) was added, the resin stirred 10 minutes and then was washed with DMF (6 x 1 min) and DCM (1 x 1 min). The resin was dried with diethyl ether and Fmoc test was performed to check the loading. Elongation of the sequence was performed by sequential Fmoc removal and coupling of the corresponding amino acid. Fmoc group was removed by treating the resin with a mixture of piperidine/DMF (3:7, 2 + 10 min). Coupling of the Fmoc amino acids (4 eq) was performed by treatment with DIC (4 eq) and Oxyma (4 eq) in DMF under stirring at RT for 2 h. **13** (2 eq) coupling was performed with DIC (2 eq), Oxyma (2 eq) and DIPEA (2 eq) in DMF under stirring at RT for 6 h. Final cleavage was performed with TFA/H₂O/TIS (95:2.5:2.5) for 2 h at RT. Product was purified by reversed-phase HPLC (method P1). **1**: HPLC-MS: $t_R = 5.33$ min, >99% purity ($\lambda = 220$ nm), $m/z = 702.43$ (702.38 [M+H]⁺); **2**: HPLC-MS: $t_R =$

5.52 min, 91% purity ($\lambda = 220$ nm), $m/z = 702.48$ (702.38 $[M+H]^+$).

Synthesis of N₃-PEG4-Val-Cit-Pro-Gly-Cry-55gly (4): Cryptophycin-55 glycinate trifluoroacetate prepared as previously described⁴⁴ (5 mg, 5.7 μ mol, 1 eq), **1** (8 mg, 11.4 μ mol, 2 eq), PyBOP (5.9 mg, 11.4 μ mol, 2 eq) and HOBt·H₂O (2 mg; 12.8 μ mol; 2.25 eq) were placed under argon atmosphere and dissolved with anhydrous DMF (0.5 mL). DIPEA (2.5 μ L, 14.3 μ mol, 2.5 eq) was added and the reaction mixture was stirred at RT for 4 h. Then, the solution was directly purified by RP-HPLC (method P3). Freeze-drying of fractions containing the product afforded **4** (4.5 mg, 54% yield) as white powder. **HPLC-MS:** $t_R = 9.57$ min, >99% purity ($\lambda = 220$ nm), $m/z = 1445.69$ (1445.65 $[M+H]^+$); 723.35 (723.33 $[M+2H]^{2+}$). **HRMS (ESI-MS):** m/z calculated for C₆₇H₁₀₀Cl₂N₁₂O₁₉ $[M+2H]^{2+}$ 723.3297; found 723.3291.

Synthesis of N₃-PEG4-Val-Cit-Gly-Pro-Cry-55gly (5): Cryptophycin-55 glycinate trifluoroacetate (10 mg, 0.011 mmol, 1 eq), **2** (16 mg, 0.022 mmol, 2 eq), PyBOP (11.9 mg, 0.022 mmol, 2 eq) and HOBt·H₂O (3.9 mg; 0.026 mmol; 2.25 eq) were placed under argon atmosphere and dissolved with anhydrous DMF (0.5 mL). DIPEA (5 μ L, 0.028 mmol, 2.5 eq) was added and the reaction mixture was stirred at RT for 4 h. Then, the solution was directly purified by RP-HPLC (method P2). Freeze-drying of fractions containing the product afforded **5** (13 mg, 79% yield) as white powder. **HPLC-MS:** $t_R = 9.54$ min, 97% purity ($\lambda = 220$ nm), $m/z = 1445.67$ (1445.65 $[M+H]^+$); 723.34 (723.33 $[M+2H]^{2+}$). **HRMS (ESI-MS):** m/z calculated for C₆₇H₁₀₀Cl₂N₁₂O₁₉ $[M+2H]^{2+}$ 723.3297; found 723.3291.

Synthesis of 4-pentynoyl-octreotide (α -CH₂CH₂C \equiv CH) (6): Octreotide acetate was ϵ -mono-Boc-protected as previously described.⁴⁹ Octreotide(ϵ -Boc) (69 mg, 0.056 mmol, 1 eq), was dissolved in a 1:1 solution of ethanol and 0.2 M borate buffer (pH = 8.5) to a final concentration of 2 mg/mL. Then, 4-pentynoic acid succinimidyl ester (109 mg, 0.56 mmol, 10 eq) was added and the solution was stirred at RT overnight. The crude was purified by RP-HPLC (method P1) to obtain Octreotide (ϵ -Boc, α -CH₂CH₂C \equiv CH) (53 mg, 80% yield). Finally, the Boc group was removed with TFA/H₂O/TIS (95:2.5:2.5) for 5 min at RT, the solvents were immediately evaporated, and the crude residue was purified by RP-HPLC (method P1) to give **6** (46 mg, 85% yield) as a white powder after freeze-drying. **HPLC-MS:** $t_R = 5.97$ min, 96% purity ($\lambda = 220$ nm), $m/z = 1099.47$ (1099.47 $[M+H]^+$); 550.24 (550.24 $[M+2H]^{2+}$). **HRMS (ESI-MS):** m/z calculated for C₅₄H₇₁N₁₀O₁₀S₂ $[M+H]^+$ 1099.4740; found 1099.4775; calculated for C₅₄H₇₂N₁₀O₁₀S₂ $[M+2H]^{2+}$ 550.2406; found 550.2429.

Synthesis of 7: Azide **4** (6 mg, 0.004 mmol, 1 eq), alkyne **6** (5 mg, 0.004 mmol, 1 eq), CuSO₄·5H₂O (0.6 mg, 0.6 eq) and sodium ascorbate (0.3 mg, 0.4 eq) were placed under argon atmosphere and dissolved with a degassed solution of DMF/H₂O (1:1, 0.5 mL). The solution was stirred for 24 h at 40 °C and was directly purified by RP-HPLC (method P4). Freeze-drying of desired fractions afforded **7** (5.6 mg, 51% yield) as white powder. **HPLC-MS:** $t_R = 7.47$ min, 98% purity ($\lambda = 220$ nm), $m/z = 1272.62$ (1272.56 $[M+2H]^{2+}$); 848.75 (848.71 $[M+3H]^{3+}$). **HRMS (ESI-MS):** m/z calculated for C₁₂₁H₁₇₁Cl₂N₂₂O₃₀S₂ $[M+3H]^{3+}$ 848.7111; found 848.7122.

Synthesis of 8: Azide **5** (10.8 mg, 0.007 mmol, 1 eq), alkyne **6** (8.5 mg, 0.007 mmol, 1 eq), CuSO₄·5H₂O (1.1 mg, 0.6 eq) and sodium ascorbate (0.6 mg, 0.4 eq) were placed under argon atmosphere and dissolved with a degassed solution of DMF/H₂O (1:1, 0.5 mL). The solution was stirred for 24 h at 40 °C and was directly purified by RP-HPLC (method P2). Freeze-drying of desired fractions afforded **8** (12 mg, 60% yield) as white powder. **HPLC-MS:** $t_R = 7.50$ min, 98% purity ($\lambda = 220$ nm), $m/z = 1272.58$ (1272.56 $[M+2H]^{2+}$); 848.72 (848.71 $[M+3H]^{3+}$). **HRMS (ESI-MS):** m/z calculated for C₁₂₁H₁₇₁Cl₂N₂₂O₃₀S₂ $[M+3H]^{3+}$ 848.7111; found 848.7139.

Binding affinity: Compounds were solubilized with 100% DMSO at a concentration of 10 mM and diluted with assay buffer (25 mM HEPES pH 7.4, 5 mM MgCl₂, 1 mM CaCl₂, 10 μ g/mL Saponin, 0.5% protease free BSA). The dilution of test compound (50 μ L, maximum final DMSO concentration 3%), radioligand 3-[125I] iodotyrosyl111 Somatostatin 14 (Perkin Elmer, NEX389, 25 μ L, 0.4 nM) and membrane extract (recombinant CHO-K1-SST2 (NP_001041.1), 25 μ L, 0.2 μ g) were successively added to a 96-well plate and incubated at 25 °C for 60 min. It was filtered over GF/B Unifilter plate (Perkin Elmer, 6005177, pre-soaked in 0.5% PEI for 2 h at room temperature) with a Filtermate Harvester (Perkin Elmer). After rinsing the filters 6 times with 0.5 mL of ice-cold washing buffer (25 mM HEPES pH 7.4, 5 mM MgCl₂, 1 mM CaCl₂), 50 μ L of Microscint 20 (Packard) was added to the filters and the samples were incubated 15 min on an orbital shaker and then counted with a TopCount™ for 1 min/well. Binding affinity was determined in duplicates by plotting the dose-response data to a nonlinear regression with variable slope.

In vitro cytotoxicity: To evaluate the cytotoxicity of conjugates and metabolites, AtT20/D16v-F2 murine pituitary tumor cells obtained from American Type Culture Collection (ATCC, Bethesda, MD, USA) were used. Cell viability was determined by the MTT (3-(4,5-dimethylthiazol-2-yl)-2,5-diphenyltetrazolium bromide) assay. Briefly, cells in DMEM supplemented with 10% FBS, 1% L-glutamine and 1% penicillin/streptomycin, were seeded in 96-well culture plates (3000 cells/well) and incubated overnight in a humidified, 37 °C, 5% CO₂ atmosphere to allow adherence. The following day cells were treated with serial dilutions of each compound starting at 100 nM for free drugs and 1000 nM for each one of the conjugates and incubated as described for 2 h. 0.1% DMSO served as a control. After incubation, cells were washed once, media replaced, and incubation continued for further 70 h. At the end of treatment, 5 μ L of MTT solution (5 mg/mL in deionized H₂O, Sigma #M5655) was added to each well and cells were incubated for another 2 hours. Finally, 100 μ L of lysis buffer (10% SDS, 10 mM HCl) was added, and cells placed in the incubator overnight for the formazan crystal solubilization. Absorbance at 540 nm was measured using a FLUOstar Omega (BMG Labtech) microplate reader and the growth inhibition ratio was calculated. Blank controls detecting cell-free media absorbance were performed in parallel. Three experimental replicates were used. The half-maximal inhibitory concentration values (IC₅₀) were obtained from viability curves using GraphPad Prism 6. Cell viability was expressed as percentage relative to the respective control conditions.

Plasma stability: The sample preparation and the metabolic analysis of the conjugates was carried out similarly to the previously described method.⁵⁰ Shortly, in a 96-well plate each conjugate and the control compound, procaine (3 mM, stock solution in DMSO) in three replicates were diluted with 250 μ L of plasma to give a 3 μ M concentration and incubated at 37 °C. At each sample collecting time point an aliquot of 30 μ L was transferred into a 96-deep well plate and the reaction was stopped with 120 μ L of acetonitrile containing 0.1% formic acid and 0.4 μ g/mL of warfarin as internal standard (IS). This mixture was centrifuged at 1100 \times g for 30 min at 4 °C and 50 μ L of supernatant was transferred into a clean 96 deep-well plate and diluted with 50 μ L of 0.1% formic acid in water. Samples were stored at -80 °C until analyses. Stability was determined based on LC-HRMS analysis of the disappearance of the compound as a function of incubation time, using area ratio (analyte peak area vs internal standard peak area). The elimination constant *k* is calculated by plotting mean disappearance values on a semi-logarithmic scale and fitting with a best fit linear regression. The half-life ($t_{1/2}$) expressed in hours is derived using equation: $t_{1/2} = \ln 2 / (-k)$.

Receptor and conjugate internalization: For the immunofluorescence studies of SSTR2 internalization, AtT20/D16v-F2 cells were grown overnight in 8-well chamber slides (Nunc® Lab-Tek®, Sigma-Aldrich, St. Louis, MO) previously coated with poly-D-lysine (10 μ g/mL, Sigma-Aldrich, St. Louis, MO). Cells were treated with concentrations ranging from 10 to 1000 nM of either octreotide-cryptophycin conjugates or with octreotide as positive control, for 30 min at 37 °C. To stop the internalization process and fix the cells, wells were rinsed twice with cold PBS and fixed with ice cold methanol for 7 min. Then, the non-specific binding sites were blocked with PBS containing 10% fetal bovine serum for 60 min at room temperature, and cells were incubated for another 60 min with rabbit anti-SSTR2 primary antibody (UMB-1, Abcam #ab134152) diluted 1:200 in blocking solution. Next, wells were rinsed 3 times for 5 min with PBS followed by incubation in the dark with the secondary antibody Alexa Fluor 488 goat anti-rabbit diluted 1:600 in blocking solution for 60 min. Nuclei were visualized by DAPI staining (1 μ L/mL in PBS, Tocris) for 15 min. Finally, wells were rinsed, chambers removed, and coverslips mounted with Mowiol 4-88 antifading solution (Sigma). Images were generated using the Zeiss AxioImager upright epifluorescence microscope with a 100 \times oil immersion objective. The real-time internalization of the labeled conjugate **10** was acquired using a Zeiss LSM880 confocal microscope coupled to an environmental chamber allowing a 37 °C, 5% CO₂ atmosphere. Briefly, the AtT20/D16v-F2 murine pituitary tumor cells that express high levels of SSTR2 and the human epithelial lung carcinoma A549 cells with low SSTR2 expression were grown overnight as described above. On the day of the experiment, either 1 μ M of the fluorescently labeled conjugate **10** alone or a mixture of that with 100-fold excess of free octreotide were prepared in phenol red-free media (1% DMSO final) and warmed up to 37 °C. Image acquisition was performed using a 40 \times water immersion objective and started shortly after the solutions were added to the cells. One frame was acquired every 30 s for a total of 60 frames. Brightfield was used to visualize the cellular bodies.

Pharmacokinetics: To evaluate the pharmacokinetic profile of conjugate **8** and its fluorescein-labeled analog **10**, four-week-old female heterozygous NCR mice from Charles River were used. Animals were injected intravenously with 2.5 mg/kg (in 2% DMSO in water, dosed at 0.5 mg/mL) of each conjugate. Terminal blood samples were collected via cardiac puncture from animals under deep anesthesia at different time points (5, 15, 30, 60, 180, and 360 min, *n*=3). Samples were rapidly transferred to lithium heparin-coated tubes, kept on ice and subsequently centrifuged at 2000 \times g, 4 °C for 10 minutes. After centrifugation plasma was collected, and samples kept at -20 °C until analyses.

Tumor targeting studies: The fluorescence-labeled conjugate **10** (1 mg/kg in 2% DMSO in water) was injected intravenously in nude mice bearing AtT20 tumors. At each time point whole body imaging was acquired using the Lago optical imaging system (Spectral Instruments Imaging) while mice were under isoflurane anesthesia (2.5%/20% O₂).

Cathepsin B degradation: An aqueous solution of L-cysteine (0.28 M) was diluted 1:10 in acetate buffer/EDTA 1 mM pH 5.5, to achieve a working solution of 28 mM of L-cysteine. This solution was used to dilute cathepsin B to 1.11 U/mL. The cathepsin B solution was pre-incubated at 37 °C for 15 min and then split into 45 μ L aliquots in Eppendorf tubes, with two replicates for each incubation time. 5 μ L of substrate solution (50 μ M in MeOH/H₂O (1:1)) were added to each tube for a final concentration of 5 μ M. Tubes corresponding to t_0 contained 100 μ L of 1% HCOOH in MeOH and were put in ice bath to inhibit the reaction. All the other tubes were incubated at 37 °C in an oscillating thermostatic bath and the reaction was stopped at the following incubation times: 0.25, 0.5, 1, 2, 4 and 6 hours, as described for t_0 samples. Samples were then centrifuged for 10 min at 14000 rpm at 4 °C and filtered through regenerated cellulose syringe filters prior to injection in the HPLC/MS system. Control solutions containing 5 μ M substrate in acetate buffer pH 5.5/EDTA 1 mM/L-cysteine 28 mM were also prepared and incubated up to 6 hours at 37 °C in the absence of the enzyme to check the substrate stability under incubation conditions. Substrates and their possible cleavage products (Gly-Pro-Cry-55gly, Cry-55gly and Cry-55) were quantified *via* calibration curves prepared in acetate buffer/EDTA/L-cysteine in the range 25-5000 nM.

ASSOCIATED CONTENT

Supporting information

The supporting information is available free of charge on the ACS publication website at DOI: XXX

General methods and instrumentation, scheme S1 and synthesis of compounds **9-13**, characterization of intermediates and final products, live cell imaging confocal microscopy pictures, and *in vivo* antitumor efficacy.

AUTHOR INFORMATION

Corresponding author

* E-mail: norbert.sewald@uni-bielefeld.de

ORCID

Eduard Figueras: 0000-0002-1853-9974

Ana Martins: 0000-0002-2620-1754

Adina Borbély: 0000-0002-5506-6555

Vadim Le Joncour: 0000-0001-8153-8563

Simone Esposito: 0000-0002-9351-3109

Marcel Frese: 0000-0002-2232-7755

Pirjo Laakkonen: 0000-0002-9620-095X

Christian Steinkühler: 0000-0001-8341-9699

Norbert Sewald: 0000-0002-0309-2655

Author contributions

E.F. and A.M. contributed equally to this work.

Notes

A.M. is an employee of Exiris. P.C., R.P., D.M., and P.P. are employees of Italfarmaco. S.E. and G.A. are employees of IRBM. P.G. is a shareholder of Exiris. C.S. is an employee of Italfarmaco and a shareholder of Exiris.

ACKNOWLEDGMENTS

This project has received funding from the European Union's Horizon 2020 research and innovation programme under the Marie Skłodowska-Curie grant agreement No 642004 (ETN MAGICBULLET). The authors want to acknowledge M. Wißbrock, A. Nieß, and C. Michalek for technical support. The Biomedicum Imaging Unit is acknowledged for their assistance in microscopy and *in vivo* imaging, and Kromnigon for their S-Split 488 filter.

REFERENCES

- (1) Malhotra, V.; Perry, M. C. Classical Chemotherapy: Mechanisms, Toxicities and the Therapeutic Window. *Cancer Biol. Ther.* **2003**, *2* (Sup 1), 1–3.
- (2) Böhme, D.; Beck-Sickingler, A. G. Drug Delivery and Release Systems for Targeted Tumor Therapy. *J. Pept. Sci.* **2015**, *21* (3), 186–200.
- (3) Casi, G.; Neri, D. Antibody-Drug Conjugates and Small Molecule-Drug Conjugates: Opportunities and Challenges for the Development of Selective Anticancer Cytotoxic Agents. *J. Med. Chem.* **2015**, *58* (22), 8751–8761.
- (4) Krall, N.; Scheuermann, J.; Neri, D. Small Targeted Cytotoxics: Current State and Promises from DNA-Encoded Chemical Libraries. *Angew. Chem. Int. Ed.* **2013**, *52* (5), 1384–1402.
- (5) Srinivasarao, M.; Low, P. S. Ligand-Targeted Drug Delivery. *Chem. Rev.* **2017**, *117* (19), 12133–12164.
- (6) Chatzisideri, T.; Leonidis, G.; Sarli, V. Cancer-Targeted Delivery Systems Based on Peptides. *Future Med. Chem.* **2018**, *10* (18), 2201–2226.
- (7) Vlahov, I. R.; Qi, L.; Kleindl, P. J.; Santhapuram, H. K.; Felten, A.; Parham, G. L.; Wang, K.; You, F.; Vaughn, J. F.; Hahn, S. J.; *et al.* Latent Warheads for Targeted Cancer Therapy: Design and Synthesis of pro-Pyrrolobenzodiazepines and Conjugates. *Bioconjugate Chem.* **2017**, *28*, 2921–2931.
- (8) Umbricht, C. A.; Benešová, M.; Schibli, R.; Müller, C. Preclinical Development of Novel PSMA-Targeting Radioligands: Modulation of Albumin-Binding Properties to Improve Prostate Cancer Therapy. *Mol. Pharm.* **2018**, *15* (6), 2297–2306.
- (9) Marks, I. S.; Gardeen, S. S.; Kurdziel, S. J.; Nicolaou, S. T.; Woods, J. E.; Kularatne, S. A.; Low, P. S. Development of a Small Molecule Tubulysin B Conjugate for Treatment of Carbonic Anhydrase IX Receptor Expressing Cancers. *Mol. Pharm.* **2018**, *15* (6), 2289–2296.
- (10) Cazzamalli, S.; Dal Corso, A.; Widmayer, F.; Neri, D. Chemically Defined Antibody- and Small Molecule-Drug Conjugates for *In Vivo* Tumor Targeting Applications: A Comparative Analysis. *J. Am. Chem. Soc.* **2018**, *140* (5), 1617–1621.
- (11) Cazzamalli, S.; Dal Corso, A.; Neri, D. Acetazolamide Serves as Selective Delivery Vehicle for Dipeptide-Linked Drugs to Renal Cell Carcinoma. *Mol. Cancer Ther.* **2016**, *15* (12), 2926–2936.
- (12) Ginj, M.; Zhang, H.; Waser, B.; Cescato, R.; Wild, D.; Wang, X.; Ercegyi, J.; Rivier, J.; Mäcke, H. R.; Reubi, J. C. Radiolabeled Somatostatin Receptor Antagonists Are Preferable to Agonists for *In Vivo* Peptide Receptor Targeting of Tumors. *Proc. Natl. Acad. Sci. U. S. A.* **2006**, *103* (44), 16436–16441.
- (13) Reubi, J. C.; Waser, B.; Schaer, J.-C.; Laissue, J. A. Somatostatin Receptor Sst1-Sst5 Expression in Normal and Neoplastic Human Tissues Using Receptor Autoradiography with Subtype-Selective Ligands. *Eur. J. Nucl. Med.* **2001**, *28* (7), 836–846.
- (14) Froidevaux, S.; Eberle, A. N. Somatostatin Analogs and Radiopeptides in Cancer Therapy. *Biopolym. (Pept Sci)* **2002**, *66* (3), 161–183.
- (15) Yin, T.; Wu, Q.; Wang, L.; Yin, L.; Zhou, J.; Huo, M. Well-Defined Redox-Sensitive Poly(ethylene Glycol)-Paclitaxel Prodrug Conjugate for Tumor-Specific Delivery of Paclitaxel Using Octreotide for Tumor Targeting. *Mol. Pharm.* **2015**, *12* (8), 3020–3031.
- (16) Lelle, M.; Kaloyanova, S.; Freidel, C.; Theodoropoulou, M.; Musheev, M.; Niehrs, C.; Stalla, G.; Peneva, K. Octreotide-Mediated Tumor-Targeted Drug Delivery via a Cleavable Doxorubicin-Peptide Conjugate. *Mol. Pharm.* **2015**, *12* (12), 4290–4300.
- (17) Zhang, H.-Y.; Xu, W.-Q.; Zheng, Y.-Y.; Omari-Siaw, E.; Zhu, Y.; Cao, X.; Tong, S.-S.; Yu, J.-N.; Xu, X.-M. Octreotide-Periplocymarin Conjugate Prodrug for Improving Targetability and Anti-Tumor Efficiency: Synthesis, *In Vitro* and *In Vivo* Evaluation. *Oncotarget* **2016**, *7* (52), 86326–86338.
- (18) Zhang, H.-Y.; Xu, W.-Q.; Wang, Y.-W.; Omari-Siaw, E.; Wang, Y.; Zheng, Y.-Y.; Cao, X.; Tong, S.-S.; Yu, J.-N.; Xu, X.-M. Tumor Targeted Delivery of Octreotide-Periplogenin Conjugate: Synthesis, *In Vitro* and *In Vivo* Evaluation. *Int. J. Pharm.* **2016**, *502* (1–2), 98–106.
- (19) Maxwell, J. E.; Howe, J. R. Imaging in Neuroendocrine Tumors: An Update for the Clinician. *Int. J. Endocr. Oncol.* **2015**, *2* (2), 159–168.
- (20) Pauwels, E.; Cleeren, F.; Bormans, G.; Deroose, C. M. Somatostatin Receptor PET Ligands - the next Generation for Clinical Practice. *Am. J. Nucl. Med. Mol. Imaging* **2018**, *8* (5), 311–331.
- (21) Weiss, C.; Figueras, E.; Borbély, A. N.; Sewald, N. Cryptophycins: Cytotoxic Cyclodepsipeptides with Potential for Tumor Targeting. *J. Pept. Sci.* **2017**, *23*, 514–531.
- (22) Schwartz, R. E.; Hirsch, C. F.; Sesin, D. F.; Flor, J. E.; Chartrain, M.; Fromtling, R. E.; Harris, G. H.; Salvatore, M. J.; Liesch, J. M.; Yudin, K. Pharmaceuticals from Cultured Algae. *J. Ind. Microbiol.* **1990**, *5*, 113–124.
- (23) Smith, C. D.; Zhang, X.; Mooberry, S. L.; Patterson, G. M. L.; Moore, R. E. Cryptophycin: A New Antimicrotubule Agent Active against Drug-Resistant Cells. *Cancer Res.* **1994**, *54* (14), 3779–3784.
- (24) Edelman, M. J.; Gandara, D. R.; Hausner, P.; Israel, V.; Thornton, D.; DeSanto, J.; Doyle, L. A. Phase 2 Study of Cryptophycin 52 (LY355703) in Patients Previously Treated with Platinum Based Chemotherapy for Advanced Non-Small Cell Lung Cancer. *Lung Cancer* **2003**, *39* (2), 197–199.
- (25) D'Agostino, G.; Del Campo, J.; Mellado, B.; Izquierdo, M. A.; Minarik, T.; Cirri, L.; Marini, L.; Perez-Gracia, J. L.; Scambia, G. A Multicenter Phase II Study of the Cryptophycin Analog LY355703 in Patients with Platinum-Resistant Ovarian Cancer. *Int. J. Gynecol. Cancer* **2006**, *16* (1), 71–76.
- (26) Eißler, S.; Bogner, T.; Nahrwold, M.; Sewald, N. Efficient Synthesis of Cryptophycin-52 and Novel Para-Alkoxyethyl Unit A Analogues. *Chem. - A Eur. J.* **2009**, *15* (42), 11273–11287.

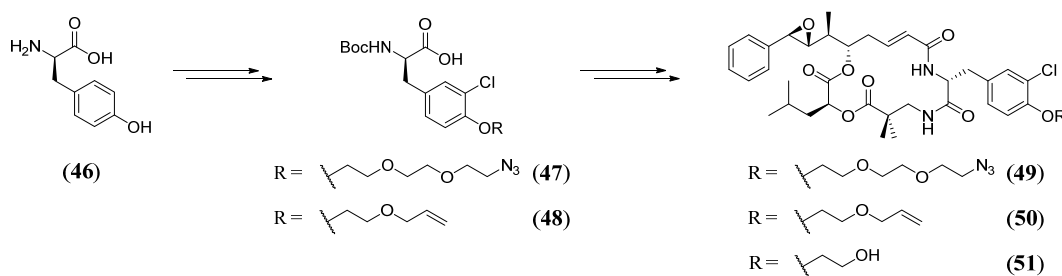
- (27) Wen, L. L.; Jian, C. Z.; Fa, Q. J.; Fu, L. Synthesis and Cytotoxicity Studies of New Cryptophycin Analogues. *Arch. Pharm. (Weinheim)*. **2009**, *342* (10), 577–583.
- (28) Nahrwold, M.; Bogner, T.; Eissler, S.; Verma, S.; Sewald, N. "Clicktophycin-52": A Bioactive Cryptophycin-52 Triazole Analogue. *Org. Lett.* **2010**, *12* (5), 1064–1067.
- (29) Weiß, C.; Bogner, T.; Sammet, B.; Sewald, N. Total Synthesis and Biological Evaluation of Fluorinated Cryptophycins. *Beilstein J. Org. Chem.* **2012**, *8*, 2060–2066.
- (30) Kumar, A.; Kumar, M.; Sharma, S.; Guru, S. K.; Bhushan, S.; Shah, B. A. Design and Synthesis of a New Class of Cryptophycins Based Tubulin Inhibitors. *Eur. J. Med. Chem.* **2015**, *93*, 55–63.
- (31) Al-Awar, R. S.; Corbett, T. H.; Ray, J. E.; Polin, L.; Kennedy, J. H.; Wagner, M. M.; Williams, D. C. Biological Evaluation of Cryptophycin 52 Fragment A Analogues: Effect of the Multidrug Resistance ATP Binding Cassette Transporters on Antitumor Activity. *Mol. Cancer Ther.* **2004**, *3* (9), 1061–1067.
- (32) Kotoku, N.; Kato, T.; Narumi, F.; Ohtani, E.; Kamada, S.; Aoki, S.; Okada, N.; Nakagawa, S.; Kobayashi, M. Synthesis of 15,20-Triamide Analogue with Polar Substituent on the Phenyl Ring of Arenastatin A, an Extremely Potent Cytotoxic Spongian Dipeptide. *Bioorg. Med. Chem.* **2006**, *14* (22), 7446–7457.
- (33) Sammet, B.; Bogner, T.; Nahrwold, M.; Weiss, C.; Sewald, N. Approaches for the Synthesis of Functionalized Cryptophycins. *J. Org. Chem.* **2010**, *75* (20), 6953–6960.
- (34) Nahrwold, M.; Weiß, C.; Bogner, T.; Mertink, F.; Conradi, J.; Sammet, B.; Palmisano, R.; Gracia, S. R.; Preuß, T.; Sewald, N. Conjugates of Modified Cryptophycins and RGD-Peptides Enter Target Cells by Endocytosis. *J. Med. Chem.* **2013**, *56* (5), 1853–1864.
- (35) Weiss, C.; Sammet, B.; Sewald, N. Recent Approaches for the Synthesis of Modified Cryptophycins. *Nat. Prod. Rep.* **2013**, *30* (7), 924–940.
- (36) Figueras, E.; Borbély, A.; Ismail, M.; Frese, M.; Sewald, N. Novel Unit B Cryptophycin Analogues as Payloads for Targeted Therapy. *Beilstein J. Org. Chem.* **2018**, *14*, 1281–1286.
- (37) Liang, J.; Moore, R. E.; Moher, E. D.; Munroe, J. E.; Al-Awar, R. S.; Hay, D. A.; Varie, D. L.; Zhang, T. Y.; Aikins, J. A.; Martinelli, M. J.; *et al.* Cryptophycins-309, 249 and Other Cryptophycin Analogs: Preclinical Efficacy Studies with Mouse and Human Tumors. *Invest. New Drugs* **2005**, *23* (3), 213–224.
- (38) Bouchard, H.; Brun, M.-P.; Commerçon, A.; Zhang, J. Novel Conjugates, Preparation Thereof, and Therapeutic Use Thereof, WO 2011/001052, **2011**.
- (39) Verma, V. A.; Pillow, T. H.; Depalatis, L.; Li, G.; Phillips, G. L.; Polson, A. G.; Raab, H. E.; Spencer, S.; Zheng, B. The Cryptophycins as Potent Payloads for Antibody Drug Conjugates. *Bioorg. Med. Chem. Lett.* **2015**, *25* (4), 864–868.
- (40) Chen, H.; Lin, Z.; Arnst, K. E.; Miller, D. D.; Li, W. Tubulin Inhibitor-Based Antibody-Drug Conjugates for Cancer Therapy. *Molecules* **2017**, *22*, 1281.
- (41) Bigot, A.; Bouchard, H.; Brun, M.-P.; Clerc, F.; Zhang, J. Novel Cryptophycin Compounds and Conjugates, Their Preparation and Their Therapeutic Use, WO2017/076998 A1, **2017**.
- (42) Su, D.; Kozak, K. R.; Sadowsky, J.; Yu, S. F.; Fourie-O'Donohue, A.; Nelson, C.; Vandlen, R.; Ohri, R.; Liu, L.; Ng, C.; *et al.* Modulating Antibody-Drug Conjugate Payload Metabolism by Conjugation Site and Linker Modification. *Bioconjugate Chem.* **2018**, *29* (4), 1155–1167.
- (43) Leamon, C. P.; Vlahov, I. R.; You, F.; Kleindl, P. J.; Santhapuram, H. K. R. Conjugates Containing Hydrophilic Spacer Linkers, WO2009/002993 A1, **2009**.
- (44) Cazzamalli, S.; Figueras, E.; Pethő, L.; Borbély, A.; Steinkühler, C.; Neri, D.; Sewald, N. In Vivo Antitumor Activity of a Novel Acetazolamide-Cryptophycin Conjugate for the Treatment of Renal Cell Carcinomas. *ACS Omega* **2018**, *3* (11), 14726–14731.
- (45) Manabe, S.; Machida, H.; Aihara, Y.; Yasunaga, M.; Ito, Y.; Matsumura, Y. Development of a Diketopiperazine-Forming Dipeptidyl Gly-Pro Spacer for Preparation of an Antibody-Drug Conjugate. *Medchemcomm* **2013**, *4* (5), 792–796.
- (46) Liu, Q.; Cescato, R.; Dewi, D. A.; Rivier, J.; Reubi, J.-C.; Schonbrunn, A. Receptor Signaling and Endocytosis Are Differentially Regulated by Somatostatin Analogs. *Mol. Pharmacol.* **2005**, *68* (1), 90–101.
- (47) Cescato, R.; Schulz, S.; Waser, B.; Eltschinger, V.; E. Rivier, J.; Wester, H.-J.; Culler, M.; Ginj, M.; Liu, Q.; Schonbrunn, A.; *et al.* Internalization of Sst2, Sst3, and Sst5 Receptors: Effects of Somatostatin Agonists and Antagonists. *J. Nucl. Med.* **2006**, *47* (3), 502–511.
- (48) Fani, M.; Nicolas, G. P.; Wild, D. Somatostatin Receptor Antagonists for Imaging and Therapy. *J. Nucl. Med.* **2017**, *58* (Supplement 2), 61S–66S.
- (49) Morpurgo, M.; Monfardini, C.; Hofland, L. J.; Sergi, M.; Orsolini, P.; Dumont, J. M.; Veronese, F. M. Selective Alkylation and Acylation of α and ϵ Amino Groups with PEG in a Somatostatin Analogue: Tailored Chemistry for Optimized Bioconjugates. *Bioconjugate Chem.* **2002**, *13* (6), 1238–1243.
- (50) Esposito, S.; Mele, R.; Ingenito, R.; Bianchi, E.; Bonelli, F.; Monteagudo, E.; Orsatti, L. An Efficient Liquid Chromatography-High Resolution Mass Spectrometry Approach for the Optimization of the Metabolic Stability of Therapeutic Peptides. *Anal. Bioanal. Chem.* **2017**, *409* (10), 2685–2696.

Chapter 6 – Summary

6. Summary

In the last years, cancer treatment has shifted towards a targeted therapy approach. Antibody- and small molecule-drug conjugates have shown enhanced selectivity and efficacy compared to traditional chemotherapeutics. Thus, the possibility to selectively deliver cytotoxic agents that are highly potent but cannot be administered as stand-alone agents opened new opportunities. In this context, the conjugation of cryptophycin to a delivery vehicle could be translated in a significant antitumor activity.

In the first part (chapter 3), the cytotoxic influence of different modifications in the *para* position of unit B was investigated. The *O*-methyl group was replaced by an *O*-(allyloxyethyl) moiety or an *O*-(((azidoethoxy)ethoxy)ethoxyethyl) substituent. The former can be used as a precursor for an alcohol functionalized cryptophycin while the later can be submitted to the mild conditions of the Staudinger reduction to obtain a free amine. The synthesis of the modified unit B (**47** and **48**, Scheme 2) proceeded through a linear sequence of 4 steps starting with D-Tyrosine (**46**, Scheme 2). Then, the modified unit B were coupled to the unit ADC to obtain the linear cryptophycins that were then macrocyclized under pseudo-high dilution conditions. Subsequent diol to epoxide transformation led to modified cryptophycins **49** and **50**.



Scheme 2. Schematic synthetic route towards unit B modified cryptophycins (**49-51**).

Their cytotoxicity was determined in human cervix carcinoma cell line KB-3-1 (Table 1). A dramatical loss of activity was observed for the analogue **49**. However, compound **50** retained the high cytotoxicity of the parent compound cryptophycin-52 (**32**). With these results in hand, compound **49** was not further investigated and alcohol deprotection of **50** was achieved using $\text{Pd}(\text{PPh}_3)_4$ as Pd(0) source and phenylsilane as scavenger. The obtained cryptophycin analogue **51** was 4-fold more active than its protected cognate and only a 12-fold reduction compared to cryptophycin-52 was observed. Next, the

cytotoxicity of the compounds **50** and **51** was investigated in the MDR cell line KB-V1. Differently than in the non MDR KB-3-1, compound **50** was more active than **51**. This could be attributed to the increased amphiphilicity produced for the free alcohol. Remarkably, compounds **50** and **51** showed an IC₅₀ value in the low nanomolar range which make them promising agents to be used in targeted therapy.

Finally, their binding affinity using molecular docking calculations was investigated. Cryptophycin-52 showed the highest binding energy followed by **51**, **50**, and **49**, which provided a rationale for the observed cytotoxicities in KB-3-1 cells.

Compound	Cytotoxic activity		Binding energy (kJ/mol)
	IC ₅₀ KB-3-1 (nM)	IC ₅₀ KB-V1 (nM)	
Cryptophycin-52 (32)	0.015	0.26	36.17
49	195000	-	22.61
50	0.748	14.5	32.20
51	0.184	42.1	32.70

Table 1. Biological evaluation using a cell-based assay in human cervix carcinoma (KB-3-1) and its MDR subclone (KB-V1), and binding energies using molecular docking for cryptophycin-52 (**32**) and novel analogues (**49-51**).

In the second part (chapters 4 and 5), cryptophycin-55 glycinate was conjugated to small molecules targeting different antigens. The glycinate ester of cryptophycin-55 was observed to provide stability, maintained high cytotoxicity *in vitro*, and showed antitumor activity *in vivo*. The recent conjugation of this drug to an antibody and the promising *in vitro* properties showed from the obtained ADC, motivated us to explore its usage in conjugation to small molecules.

In chapter 4, cryptophycin-55 glycinate was conjugated to the protease sensitive Val-Cit dipeptide including *para*-aminobenzoyl moiety as self-immolative spacer via carbamate bond. A maleimide moiety was included in the *N*-terminus to allow conjugation to the homing device via Michael addition. Conjugation to the bidentate acetazolamide targeting carbonic anhydrase IX was successfully achieved, and the final conjugate was obtained in excellent purity (**52**, Figure 24).

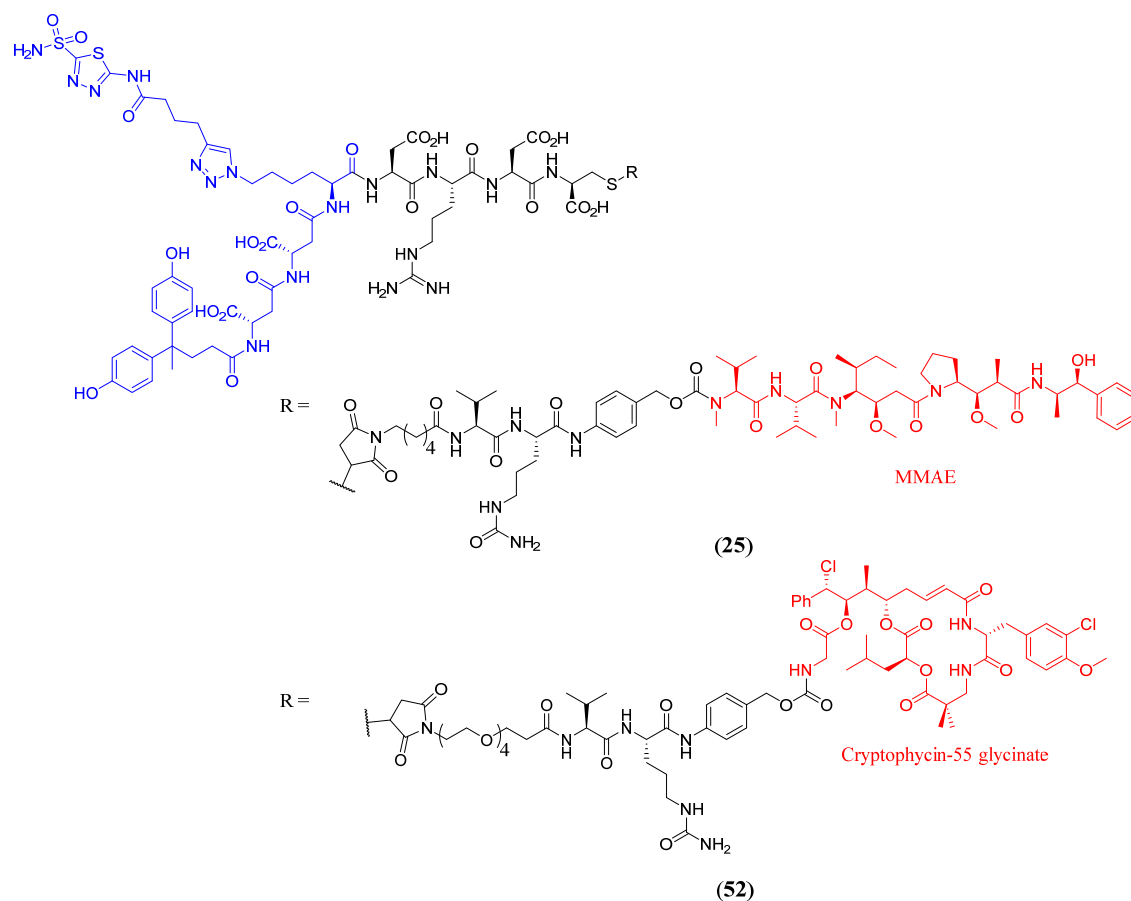


Figure 24. Molecular structures of acetazolamide conjugates targeting CAIX using MMAE (**25**) or cryptophycin-55 glycinate (**52**) as payload.

The biological activity of **52** was compared to the lead compound **25** (Figure 24). Compound **52** showed a binding affinity of 3.4 nM using surface plasmon resonance (SPR) towards recombinant human CAIX, which was in the same range than the isolated ligand ($K_d = 2.6$ nM) and slightly better than lead compound **25** ($K_d = 10$ nM). The cytotoxicity of **52** was investigated in an *in vitro* cell-based assay using the renal cell carcinoma SKRC-52. Conjugate **52** showed a prodrug behavior characteristic of noninternalizing conjugates which is translated to a reduced cytotoxicity compared to the activity of the free payload cryptophycin-55 glycinate ($IC_{50} = 7.9$ nM). Cryptophycin-55 glycinate was less potent than monomethyl auristatin E (MMAE, $IC_{50} = 1.5$ nM) used in the conjugate **25**. Finally, the therapeutic activity of **52** was studied in nude mice bearing SKRC-52 tumors and compared to **25** using an optimal and safe dose of 250 nmol/kg based on previous biodistribution studies. Mice that were treated with the cryptophycin-acetazolamide conjugate (**52**) enjoyed a therapeutic benefit with a slower tumor growth compared with the control group (saline). However, the activity was remarkably inferior

to the lead compound **25**, which can be attributed to the lower cytotoxicity of the free payload in this concrete cell line.

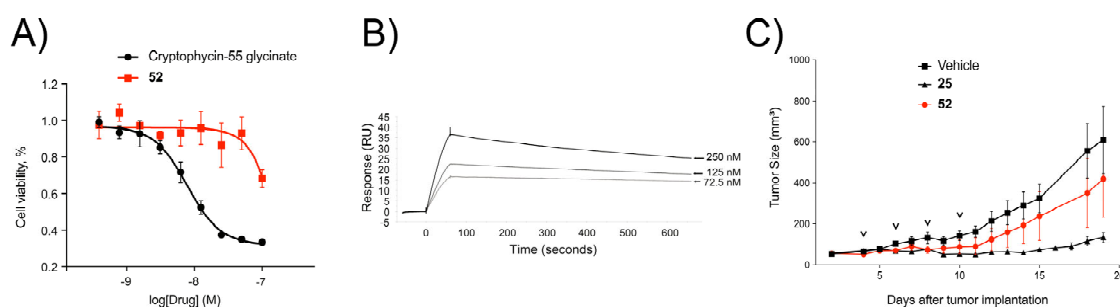


Figure 25. Biological evaluation of conjugate **52**. (A) *in vitro* toxicity of conjugate **52** and cryptophycin-55 glycinate in SKRC-52 renal carcinoma. (B) SPR analysis of **52** to immobilized CAIX. (C) Tumor volume changes for different treatment groups in nude mice bearing SKRC-52 tumors.

In chapter 5, cryptophycin-55 glycinate was conjugated to the protease sensitive dipeptide Val-Cit including a novel diketopiperazine self-immolative linker based on the dipeptide Pro-Gly or Gly-Pro. The conjugation was done via amide bond and the linker included an azide moiety to allow conjugation to alkyne functionalized octreotide targeting the somatostatin receptor 2 (SSTR2) by click chemistry. Conjugation was successfully achieved using copper(I)-catalyzed alkyne-azide cycloaddition (CuAAC), and two cryptophycin-octreotide conjugates (**53** and **54**, Figure 26), differing in their self-immolative moiety, were successfully obtained.

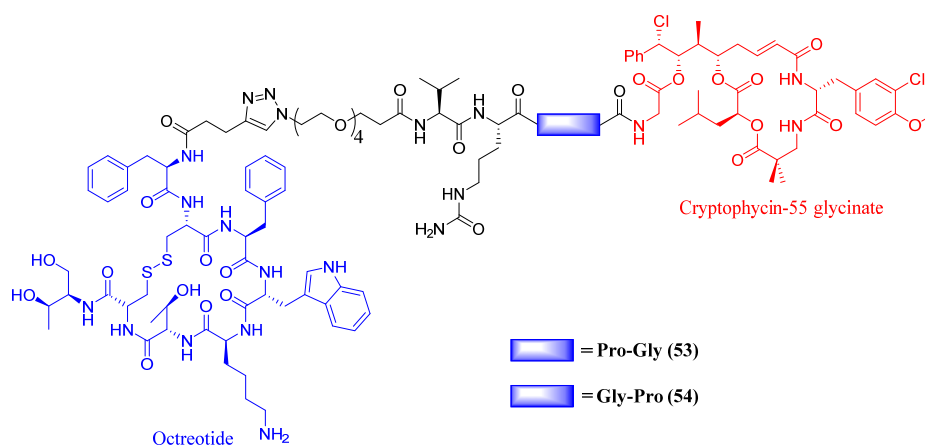


Figure 26. Molecular structures of octreotide conjugates targeting SSTR2 using cryptophycin as payload (**53** and **54**).

Their binding affinity against SSTR2 was measured using radioligand binding displacement. **53** and **54** showed a low nanomolar IC_{50} affinity (0.62 nM and 1.3 nM, respectively), comparable to the isolated octreotide ligand ($IC_{50} = 0.5$ nM).

The bioactivity of **53** and **54** was evaluated with an *in vitro* cytotoxicity assay using AtT20 pituitary mouse cells (Figure 27). The activity was remarkably different depending on the linker. Conjugate **54** retained the high cytotoxicity of the free payload (IC₅₀ of 8.37 nM and 3.53 nM, respectively), while compound **53** was remarkably less active (IC₅₀ = 51.23 nM).

The stability of conjugates **53** and **54** was studied in murine and human plasma (Figure 27). The resistance to the proteases of plasma was largely influenced by the self-immolative moiety. Compound **53** was especially labile to murine plasma with a half-life of 30 min while **54** was remarkably stable ($t_{1/2} > 24$ h). In human plasma they exhibited similar stability with half-lives of 23 h and 24 h for **53** and **54**, respectively.

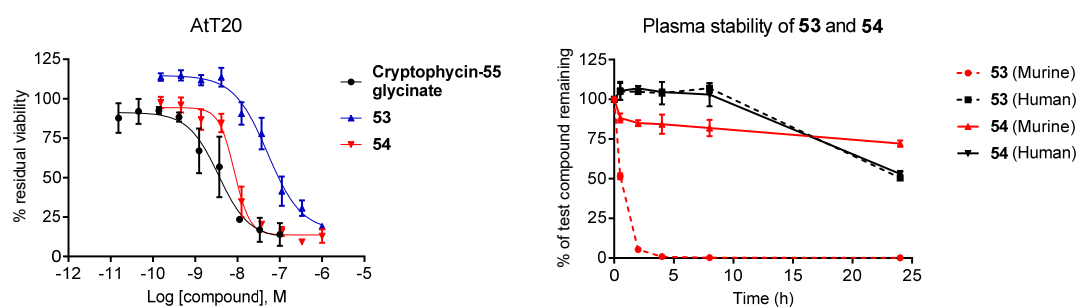


Figure 27. *In vitro* cytotoxicity of cryptophycin-55 glycinate, conjugates **53** and **54** in AtT20 cell line (left) and stability of conjugates **53** and **54** in murine and human plasma (right).

Both conjugates induced the internalization of SSTR2 at 1000 and 10 nM. The homing properties of lead compound **54** were studied by replacing cryptophycin-55 glycinate with the infrared dye Cy5.5 (**55**, Figure 28).

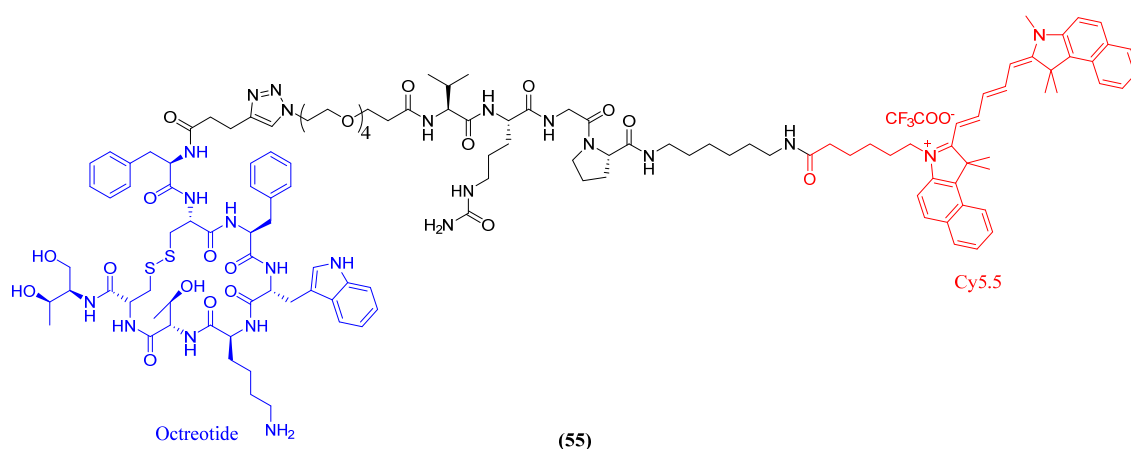


Figure 28. Molecular structure of octreotide-Cy5.5 conjugate **55**.

In vitro cell imaging of **55** in AtT20 (SSTR2 positive) cells showed effective internalization after only 10 min of incubation. The internalization was efficiently competed by 100-fold excess of octreotide and no internalization was observed in A549 (SSTR2 negative) cell line, proving the receptor mediated endocytosis of the conjugate. The tumor-targeting ability of **55** was evaluated in nude mice bearing AtT20 tumors (Figure 29). The compound was administered intravenously at 1 mg/kg and whole-body images at different time points were taken. A high percentage of compound could be observed in clearing organs (i.e. liver and kidneys) at early time points. However, preferential accumulation of conjugate **55** in the tumor over the healthy tissues that are not involved in the compound excretion could be observed and the compound showed good homing properties with detection in the tumor up to 7 days.

The therapeutic activity of **54** was evaluated in AtT20 tumor-bearing mice. Dose escalation of the compound showed good tolerability up to 10 mg/kg (the highest tested dose). Mice were treated with compound **54** once weekly at 5 mg/kg for 3 weeks and the tumor volume was compared to vehicle (Figure 29). No therapeutic benefit could be observed at the selected regimen.

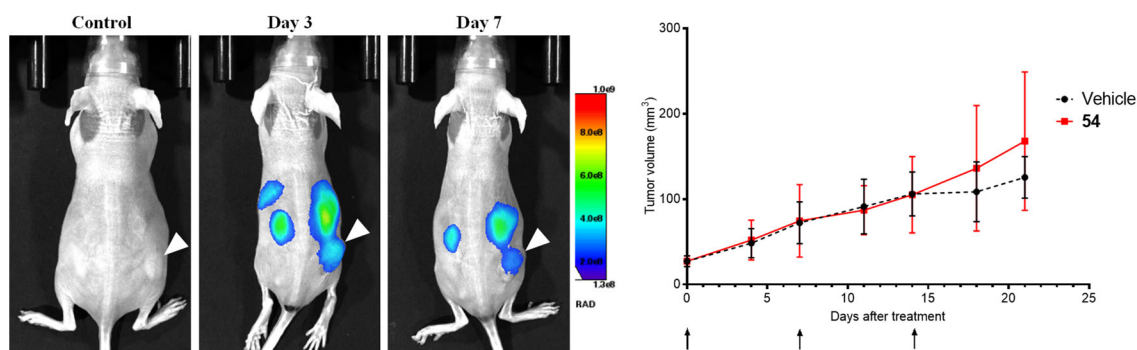


Figure 29. *In vivo* tumor targeting of **55** (left) and *in vivo* antitumor efficacy of conjugate **54** (right) in AtT20 xenografts.

The drug release of **54** by cathepsin B was studied to understand the lack of efficacy *in vivo*. The compound was rapidly metabolized in the presence of enzyme and the expected Gly-Pro-Cry-55gly metabolite was released. This metabolite was not further transformed by self-immolation of the dipeptide. The cytotoxicity of Gly-Pro-Cry-55gly was evaluated in a cell-based assay using AtT20 cells and it showed low nanomolar activity ($IC_{50} = 6.05$ nM). The high *in vitro* cytotoxicity of the metabolite indicates that the lack of *in vivo* efficacy is unlikely to be related to the absence of self-immolation.

Chapter 7 - Appendix

7.1 – Appendix I: supporting information of chapter 3

Supporting Information

for

**Novel unit B cryptophycin analogues as payloads for tar-
geted therapy**

Eduard Figueras, Adina Borbély, Mohamed Ismail, Marcel Frese and Norbert Sewald*

Address: Department of Chemistry, Organic and Bioorganic Chemistry, Bielefeld University,
Universitätsstraße 25, 33615 Bielefeld, Germany

Email: Norbert Sewald - Norbert.sewald@uni-bielefeld.de

*Corresponding author

Experimental part and analytical data

Table of contents

1) General methods	S2
2) Synthesis of modified unit B.....	S5
3) Synthesis of new cryptophycins.....	S10
4) NMR, HPLC and mass spectra	S19
5) References.....	S40

1) General methods

All reactions requiring anhydrous conditions were performed under argon atmosphere. DMF was dried over 4 Å molecular sieves, CH₂Cl₂ was distilled from CaH₂, THF and DME were distilled from sodium/benzophenone. Anhydrous acetone and ethylene glycol were purchased from commercial sources. All the other chemicals and solvents (HPLC-grade or reagent-grade quality), unless otherwise stated, were purchased from commercial sources and used without further purification. Silica for flash chromatography was purchased from Macherey-Nagel 40–63 μM (230-400 mesh). Reactions were monitored by thin layer chromatography using aluminium-backed plates coated with silica gel 60 F254 from Merck; visualization was accomplished with UV light or staining with potassium permanganate or cerium molybdate solution.

Liquid chromatography–mass spectrometry

LC–MS was conducted using an Agilent 1200 series consisting of an autosampler, degasser, binary pump, column oven and diode array detector coupled to an Agilent 6220 accurate-mass TOF MS. A Hypersil Gold C₁₈ (150 mm × 2.1 mm, 3 μm particle size) was used as column.

Eluent A: H₂O/CH₃CN/HCOOH = 95/5/0.1 and eluent B: H₂O/CH₃CN/HCOOH = 5/95/0.1.

Method A:

Flow rate: 300 μl/min

0 min	100% A	0% B
10 min	2% A	98% B
11 min	2% A	98% B
11.5 min	100% A	0% B
15 min	100% A	0% B

High-resolution mass spectrometry

High resolution mass spectra were recorded on an Agilent 6220 accurate-mass TOF LC/MS. Samples were injected through an Agilent 1200 series. Hypersil Gold C₁₈ (50 mm × 2.1 mm, 1.9 μm particle size) was used as a column. Same solvents than HPLC–MS were used and a linear gradient from 0 to 98% B over 4 minutes was employed.

The mass spectrometer was externally calibrated using Agilent tuning mix prior to measurement.

NMR spectroscopy

NMR spectra were recorded on a Bruker Avance 400 (^1H : 400 MHz, ^{13}C : 100 MHz), Avance 500HD (^1H : 500 MHz, ^{13}C : 126 MHz) or Avance 600 (^1H : 600 MHz, ^{13}C : 151 MHz) at 298 K. Chemical shifts were referenced to residual nondeuterated solvent signal (CDCl_3 : ^1H : 7.26 ppm; ^{13}C : 77.16 ppm). Coupling constants (J) are reported in Hz with the following abbreviations used to indicate splitting: s = singlet, d = doublet, t = triplet, q = quartet, m = multiplet, br = broad signal. The acronyms uA, uB, uC and uD describe signals pertaining to cryptophycin units A–D.

Cell lines

Biological tests: The KB-3-1 cells were cultivated as monolayer in DMEM (Dulbecco's modified Eagle medium) with glucose (4.5 g/L), L-glutamine, sodium pyruvate, phenol red (PAA) and supplemented with 10% foetal calf serum (FCS). The cells were maintained at 37 °C and 5.3% CO_2 /humidified air. On the day before the test, the cells were detached with trypsin/ethylenediaminetetraacetic acid (EDTA) solution (0.05% / 0.02% in phosphate buffered saline solution PBS; PAA) and plated in sterile 96-well plates in a density of 10 000 cells in 100 μL medium per well. The dilution series of the compounds were prepared from stock solutions in DMSO of concentrations of 1 mM or 10 mM. The stock solutions were diluted with culture medium (10% FCS). The dilution (100 μL) was added to the wells. Each concentration was tested in six replicates. The control contained the same concentration of DMSO as the first dilution. After incubation for 72 h at 37 °C and 5.3% CO_2 /humidified air, 30 μL of an aqueous resazurin solution (175 μM) was added to each well. Again, the cells were incubated at the same conditions for 6 h. Then the fluorescence was measured using a TECAN infinite M200. The excitation was effected at a wavelength of 530 nm, whereas the emission was recorded at a wavelength of 588 nm. The IC_{50} values were calculated as a sigmoidal dose response curve using GraphPad Prism (version 4.03). The IC_{50} values equal the drug concentrations, at which vitality is 50%.

Docking and molecular dynamic simulation

The $\alpha\beta$ -tubulin structure was obtained from protein data bank (pdb: 1jff). The α -subunit of the protein was removed, the β -subunit was modified by adding the missing hydrogens and

the ligand (taxol) was removed. Structures of the different tested cryptophycin derivatives were built by Yasara structure with the correct stereochemistry. Both the beta subunit of tubulin and cryptophycin derivatives were energy minimized using the Yasara2 force field before using in further experiments.

Docking was performed by Yasara structure using Autodock [1], the simulation cell was defined around the vinca domain residues of the energy minimized beta subunit for docking of all cryptophycin derivatives. Docking results were analysed based on the B-factor (binding energy) calculated by Yasara, compounds with correct positioning and high binding energies were used for further analysis.

Molecular dynamic simulation was done by Yasara structure; the selected docking modes were used for simulation. Simulation cell was extended 10 Å around the whole structure and filled with water of 0.99 g ml⁻¹ density and randomized molecule orientation, AMBER15IPQ with its default parameters was used as force field for running the simulation up to 1 ns. Simulation was also performed on the Apo structure for comparative analysis using same parameters.

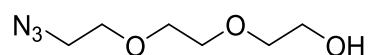
Table S1: Interaction of the cryptophycin derivatives with key amino acid residues within the vinca domain.

Inhibitor	Subunit*	Hydrophobic contact	Pi interaction
2	A	S174, Y210, V177, Y224	Y210
	B	Y210, E207, D211	Y210
22	C	K176	–
	D	V177	–
23	A	K176, S174, V177, E207	Y210
	B	S174, Y224, V177, D179	–
24	A	V177, S178	–
	C	P222, Y224	–
	D	E207, Y224	–

* subunit of cryptophycin molecule.

2) Synthesis of modified unit B

2-(2-(2-Azidoethoxy)ethoxy)ethan-1-ol (4)

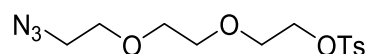


Triethylene glycol (10 g, 66.6 mmol, 1 equiv) was monotosylated as previously described and used without column chromatography purification [2]. The crude was dissolved in anhydrous DMF (28 mL) under inert atmosphere and NaN₃ (1.83 g, 28.2 mmol, 2 equiv) was added. The solution was stirred overnight at 70 °C. Then, the DMF was removed under reduced pressure and the residue was dissolved in DCM (100 mL) and HCl 0.5 M (100 mL), the layers were separated and the aqueous layer was further extracted with DCM (100 mL). The combined organic layers were dried over Na₂SO₄ and the solvent was removed under reduced pressure. The crude was purified by column chromatography using DCM/MeOH (99:1 → 96:4) as eluent to afford 1.75 g (60% yield) of **4** as a colourless oil.

¹H-NMR (400 MHz, CDCl₃): δ (ppm) = 3.40 (t, *J* = 5.0 Hz, 2H, CH₂N₃), 3.62 (m, 2H, CH₂CH₂OH), 3.67-3.70 (m, 6H, CH₂), 3.75 (m, 2H, CH₂OH).

¹³C-NMR (100 MHz, CDCl₃): δ (ppm) = 50.7, 61.8, 70.1, 70.4, 70.7, 72.5.

2-(2-(2-Azidoethoxy)ethoxy)ethyl 4-methylbenzenesulfonate (5)

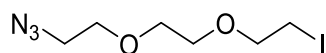


2-(2-(2-Azidoethoxy)ethoxy)ethan-1-ol (1.67 g, 9.53 mmol, 1 equiv) was monotosylated as previously described and the crude was purified by column chromatography using hexane/ethyl acetate (7:3) as eluent to obtain 2.07 g (66% yield) of **5** as colourless oil.

¹H-NMR (400 MHz, CDCl₃): δ (ppm) = 2.44 (s, 3H, CH₃), 3.36 (t, *J* = 5.1 Hz, 2H, CH₂N₃), 3.60 (s, 4H, CH₂), 3.64 (m, 2H, CH₂), 3.70 (m, 2H, CH₂CH₂OSO₂), 4.16 (m, 2H, CH₂OS₂), 7.34 (d, *J* = 8.0 Hz, 2H, C^{ar}H), 7.79 (d, *J* = 8.3 Hz, 2H, SO₂C^{ar}C^{ar}H).

¹³C-NMR (100 MHz, CDCl₃): δ (ppm) = 21.8, 50.8, 68.9, 69.4, 70.2, 70.7, 70.9, 128.1, 129.9, 133.1, 144.9.

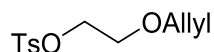
1-Azido-2-(2-(2-iodoethoxy)ethoxy)ethane (6)



2-(2-(2-Azidoethoxy)ethoxy)ethyl 4-methylbenzenesulfonate (1.2 g, 3.64 mmol, 1 equiv) and NaI (2.18 g, 14.64 mmol, 4 equiv) were dissolved in anhydrous acetone (28 mL) under inert atmosphere and it was refluxed overnight. Then, the solvent was removed under reduced pressure and the crude was dissolved in DCM (100 mL), washed with H₂O (100 mL) and brine (100 mL). The organic layer was dried over Na₂SO₄ and the solvent was removed under reduced pressure to obtain 0.87 g (84% yield) of **6** as colourless oil.

¹H-NMR (400 MHz, CDCl₃): δ (ppm) = 3.27 (t, J = 6.8 Hz, 2H, CH₂I), 3.40 (t, J = 5.0 Hz, 2H, CH₂N₃), 3.68-3.71 (m, 6H, CH₂), 3.77 (t, J = 6.8 Hz, 2H, CH₂CH₂I).

2-(Allyloxy)ethyl 4-methylbenzenesulfonate (8)

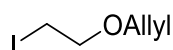


2-Allyloxyethanol (5 g, 48.9 mmol, 1 equiv) was tosylated as previously described and the crude product was purified by column chromatography using PE/EtOAc (8:2) as eluent to obtain 8.48 g (68% yield) of **8** as colourless oil.

¹H-NMR (500 MHz, CDCl₃): δ (ppm) = 2.44 (s, 3H, CH₃), 3.62 (t, J = 4.8 Hz, 2H, CH₂OAllyl), 3.93 (d, J = 5.6 Hz, 2H, OCH₂CH), 4.16 (t, J = 4.8 Hz, 2H, CH₂OSO₂), 5.15 (dd, J = 10.6, 1.5 Hz, 1H, CH=CH^{cis}H^{trans}), 5.21 (dd, J = 17.3, 1.5 Hz, 1H, CH=CH^{cis}H^{trans}), 5.81 (ddt, J = 16.3, 10.8, 5.6 Hz, 1H, CH=CH₂), 7.33 (d, J = 8.0 Hz, 1H, CH^{ar}), 7.79 (d, J = 8.0 Hz, 1H, CH^{ar}).

¹³C-NMR (126 MHz, CDCl₃): δ (ppm) = 21.7, 67.5, 69.4, 72.2, 117.5, 128.1, 129.9, 133.1, 134.2, 144.9.

3-(2-Iodoethoxy)prop-1-ene (9)



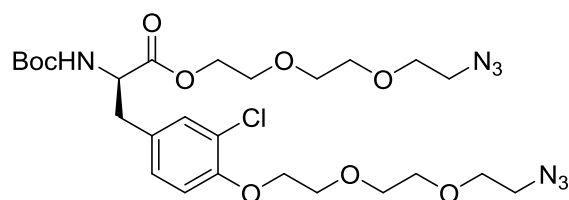
2-(Allyloxy)ethyl 4-methylbenzenesulfonate (8.45 g, 33.0 mmol, 1 equiv) and NaI (19.8 g, 131.9 mmol, 4 equiv) were dissolved in anhydrous acetone (65 mL) under inert atmosphere and it was refluxed overnight. Then, the solvent was removed under reduced pressure and the

crude was dissolved in DCM (150 mL), washed with H₂O (150 mL) and brine (150 mL). The organic layer was dried over Na₂SO₄ and the solvent was removed under reduced pressure to obtain 5.32 g (76% yield) of **9** as colourless oil.

¹H-NMR (500 MHz, CDCl₃): δ (ppm) = 3.26 (t, J = 6.8 Hz, 2H, CH₂I), 3.70 (t, J = 6.8 Hz, 2H, CH₂CH₂I), 4.04 (d, J = 5.6 Hz, 2H, OCH₂CH), 5.21 (d, J = 10.4 Hz, 1H, CH=CH^{cis}H^{trans}), 5.30 (dd, J = 17.3, 1.5 Hz, 1H, CH=CH^{cis}H^{trans}), 5.91 (ddt, J = 16.7, 11.1, 5.6 Hz, 1H, CH=CH₂).

¹³C-NMR (126 MHz, CDCl₃): δ (ppm) = 3.0, 70.8, 71.9, 117.7, 134.5.

Boc-D-Tyr(3-Cl,(OCH₂CH₂)₃N₃)-(OCH₂CH₂)₃N₃ (**11**)

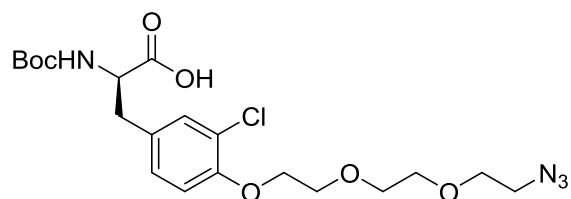


Boc-D-Tyr(3-Cl)-OH (1.1 g, 3.49 mmol, 1 equiv), K₂CO₃ (2.12 g, 15.35 mmol, 4.4 equiv) and **6** (2.2 g, 7.72 mmol, 2.2 equiv) were placed under argon atmosphere, dissolved with anhydrous DMF (22 mL) and the solution was stirred overnight at 50 °C. Then, it was diluted with EtOAc (150 mL) and H₂O (150 mL), the layers were separated and the aqueous layer was further extracted with EtOAc (150 mL). The combined organic layers were washed with brine (200 mL), dried over Na₂SO₄ and the solvent was removed under reduced pressure. The crude was purified by column chromatography using PE/EtOAc (1:1) as eluent to obtain 1.88 g (85% yield) of **11** as colourless oil.

¹H-NMR (400 MHz, CDCl₃): δ (ppm) = 1.43 (s, 9H, (CH₃)₃C), 2.99 (dd, J = 14.0, 5.7 Hz, 1H, CH₂- β), 3.07 (dd, J = 14.0, 5.7 Hz, 1H, CH₂- β), 3.38 (m, 4H, CH₂N₃), 3.65-3.72 (m, 12H, OCH₂CH₂O), 3.77-3.80 (m, 2H, OCH₂), 3.90 (t, J = 4.9 Hz, 2H, C^{ar}OCH₂CH₂), 4.16 (t, J = 4.9 Hz, 2H, C^{ar}OCH₂CH₂), 4.23-4.34 (m, 2H, OCH₂), 4.55 (q, J = 6.3 Hz, 1H, C ^{α} H), 5.01 (d, J = 8.1 Hz, NH, 1H), 6.86 (d, J = 8.4 Hz, 1H, C⁵H), 6.99 (dd, J = 8.4, 2.2 Hz, 1H, C⁶H), 7.16 (d, J = 2.2 Hz, 1H, C²H).

¹³C-NMR (100 MHz, CDCl₃): δ (ppm) = 28.4, 37.2, 50.8, 50.8, 54.4, 64.6, 69.0, 69.1, 69.7, 70.2, 70.2, 70.8, 70.8, 70.9, 71.2, 80.1, 113.8, 123.0, 128.7, 129.6, 131.3, 153.5, 155.1, 171.7.

Boc-D-Tyr(3-Cl,(OCH₂CH₂)₃N₃)-OH (**13**)

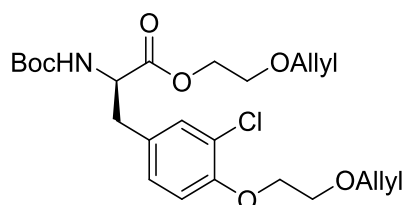


11 (0.72 g, 1.14 mmol, 1 equiv) was dissolved in MeOH/THF (1:1, 6 mL total) and LiOH·H₂O (72 mg, 1.71 mmol, 1.5 equiv) in H₂O (3 mL) was added dropwise and the solution was stirred for 2 h at rt. Then, H₂O (30 mL) was added and the pH was adjusted to 3 with 1M KHSO₄. The solution was extracted with EtOAc (3 x 30 mL) and the combined organic layers were thoroughly washed with 1 M HCl (3 x 50 mL) and brine (50 mL). The organic layer was dried over Na₂SO₄ and the solvent was removed under reduced pressure to obtain 0.41 g (76% yield) of **13** as white solid.

¹H-NMR (400 MHz, CDCl₃, rotamers): δ (ppm) = 1.34/1.43 (2 s, 9H, (CH₃)₃C), 2.85 (m, 0.3H, C^βH^AH^B), 2.98 (dd, *J* = 14.4, 6.3 Hz, 0.7H, C^βH^AH^B), 3.11 (dd, *J* = 14.4, 5.4 Hz, 1H, C^βH^AH^B), 3.38 (t, *J* = 5.1 Hz, 2H, CH₂N₃), 3.67-3.70 (m, 4H, OCH₂), 3.78-3.80 (m, 2H, OCH₂), 3.91 (t, *J* = 5.1 Hz, 2H, C^{ar}OCH₂CH₂), 4.16 (t, *J* = 5.1 Hz, 2H, C^{ar}OCH₂), 4.35 (m, 0.3H, C^αH), 4.53 (q, *J* = 6.5 Hz, 0.7H, C^αH), 5.00 (d, *J* = 7.5 Hz, 0.7H, NH), 6.28 (br, 0.3H, NH), 6.87 (d, *J* = 8.4 Hz, 1H, C⁵H), 7.02 (dd, *J* = 8.4, 2.2 Hz, 1H, C⁶H), 7.19 (br m, 1H, C²H).

¹³C-NMR (100 MHz, CDCl₃): δ (ppm) = 28.4, 36.8, 50.8, 54.4, 69.1, 69.7, 70.2, 70.9, 71.2, 80.6, 113.9, 123.1, 128.7, 129.5, 131.3, 153.6, 155.5, 175.4.

Boc-D-Tyr(3-Cl,CH₂CH₂OAllyl)-OCH₂CH₂OAllyl (**12**)



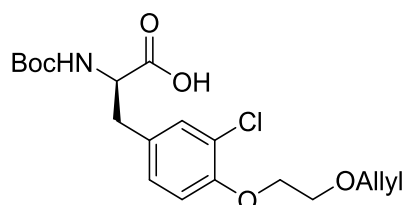
Boc-D-Tyr(3-Cl)-OH (1 g, 3.16 mmol, 1 equiv), K₂CO₃ (1.92 g, 13.90 mmol, 4.4 equiv) and **9** (1.47 g, 6.95 mmol, 2.2 equiv) were placed under argon atmosphere, dissolved with anhydrous DMF (20 mL) and the solution was stirred overnight at 50 °C. Then, it was diluted with EtOAc (150 mL) and H₂O (150 mL), the layers were separated and the aqueous layer was

further extracted with EtOAc (150 mL). The combined organic layers were washed with brine (200 mL), dried over Na₂SO₄ and the solvent was removed under reduced pressure. The crude was purified by column chromatography using PE/EtOAc (4:1) as eluent to obtain 1.24 g (81% yield) of **12** as colourless oil.

¹H-NMR (500 MHz, CDCl₃): δ (ppm) = 1.42 (s, 9H, (CH₃)₃C), 2.99 (dd, *J* = 14.2, 5.9 Hz, 1H, CH₂-β), 3.07 (dd, *J* = 14.2, 5.9 Hz, 1H, CH₂-β), 3.59-3.66 (m, 2H, COOCH₂CH₂), 3.84 (t, *J* = 4.9 Hz, 2H, C^{ar}OCH₂CH₂), 4.02 (d, *J* = 5.6 Hz, 2H, COO(CH₂)₂OCH₂), 4.13 (d, *J* = 5.6 Hz, C^{ar}O(CH₂)₂OCH₂), 4.16 (t, *J* = 4.9 Hz, 2H, C^{ar}OCH₂), 4.22-4.26 (m, 1H, COOCH^AH^B), 4.30-4.34 (m, 1H, COOCH^AH^B), 4.55 (q, *J* = 6.4 Hz, 1H, C^αH), 5.00 (d, *J* = 8.2 Hz, NH, 1H), 5.20 (d, *J* = 10.4 Hz, 2H, CH=CH^{cis}H^{trans}), 5.28 (d, *J* = 16.3 Hz, 1H, CH=CH^{cis}H^{trans}), 5.32 (d, *J* = 16.3 Hz, 1H, CH=CH^{cis}H^{trans}), 5.86-5.97 (m, 2H, CH=CH₂), 6.86 (d, *J* = 8.3 Hz, 1H, C⁵H), 6.99 (dd, *J* = 8.3, 2.2 Hz, 1H, C⁶H), 7.15 (d, *J* = 2.2 Hz, 1H, C²H).

¹³C-NMR (126 MHz, CDCl₃): δ (ppm) = 28.4, 37.2, 54.5, 64.6, 67.7, 68.4, 69.1, 72.2, 72.6, 80.1, 113.9, 117.3, 117.6, 123.1, 128.7, 129.7, 131.4, 134.4, 134.7, 153.6, 155.1, 171.7.

Boc-D-Tyr(3-Cl,CH₂CH₂OAllyl)-OH (**14**)



12 (1.23 g, 2.55 mmol, 1 equiv) was dissolved in MeOH/THF (1:1, 13 mL total) and LiOH·H₂O (0.16 g, 3.83 mmol, 1.5 equiv) in H₂O (6.5 mL) was added dropwise and the solution was stirred for 2 h at rt. Then, H₂O (50 mL) was added and the pH was adjusted to 3 with 1M KHSO₄. The solution was extracted with EtOAc (3 × 50 mL) and the combined organic layers were thoroughly washed with 1 M HCl (3 × 50 mL) and brine (50 mL). The organic layer was dried over Na₂SO₄ and the solvent was removed under reduced pressure to obtain 0.92 g (90% yield) of **14** as white solid.

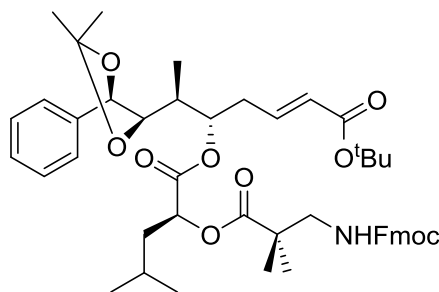
¹H-NMR (500 MHz, CDCl₃, rotamers): δ (ppm) = 1.33/1.42 (2 s, 9H, (CH₃)₃C), 2.81-2.85 (m, 0.3H, C^βH^AH^B), 2.99 (dd, *J* = 14.0, 6.4 Hz, 0.7H, C^βH^AH^B), 3.12 (dd, *J* = 14.2, 5.6 Hz, 1H, C^βH^AH^B), 3.85 (t, *J* = 4.9 Hz, 2H, C^{ar}OCH₂CH₂), 4.13 (d, *J* = 5.6 Hz, C^{ar}O(CH₂)₂OCH₂), 4.16 (t, *J* = 4.9 Hz, 2H, C^{ar}OCH₂), 4.34 (m, 0.3H, C^αH), 4.53 (q, *J* = 6.4 Hz, 0.7H, C^αH), 5.00

(d, $J = 8.2$ Hz, NH, 0.6H), 5.20 (d, $J = 10.4$ Hz, 1H, $\text{CH}=\text{CH}^{\text{cis}}\text{H}^{\text{trans}}$), 5.32 (d, $J = 17.3$ Hz, 1H, $\text{CH}=\text{CH}^{\text{cis}}\text{H}^{\text{trans}}$), 5.93 (ddt, $J = 16.5, 10.9, 5.6$ Hz, 1H, $\text{CH}=\text{CH}_2$), 6.43 (d, $J = 7.4$ Hz, 0.3H, NH), 6.87 (d, $J = 8.3$ Hz, 1H, C^5H), 7.01 (d, $J = 8.3$ Hz, 1H, C^6H), 7.19 (br m, 1H, C^2H).

^{13}C -NMR (126 MHz, CDCl_3): δ (ppm) = 28.2, 28.4, 36.9, 54.4, 68.4, 69.1, 72.6, 80.5, 113.9, 117.5, 123.1, 128.7, 129.6, 131.3, 134.6, 153.6, 155.4, 175.5.

3) Synthesis of new cryptophycins

uA[acetone]DC (**17**)



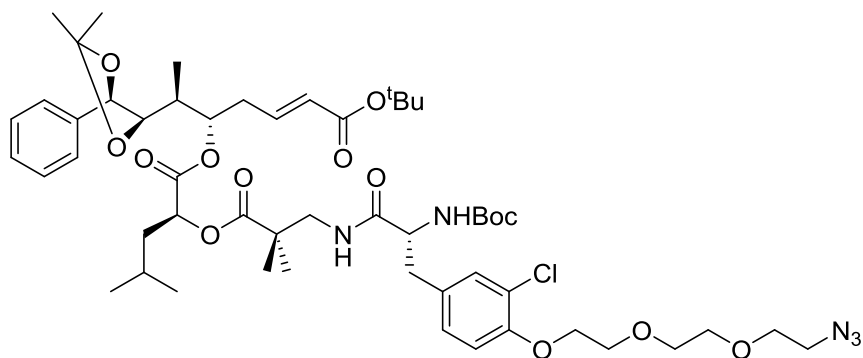
Unit A synthesized as previously described [3] (300 mg, 0.80 mmol, 1 equiv), unit CD (360 mg, 0.80 mmol, 1 equiv) and 4-DMAP (25 mg, 0.2 mmol, 0.25 equiv) were placed in a round bottomed flask under argon atmosphere. Anhydrous THF (10 mL) was added and the solution was cooled down to 0 °C. Et_3N (225 μL , 1.6 mmol, 2 equiv) and 2,4,6-trichlorobenzoyl chloride (255 μL , 1.6 mmol, 2 equiv) were added dropwise and the solution was stirred at 0 °C for 3 h. Then, a 10% citric acid solution (25 mL) was added and the solution warmed up to rt. Solution was extracted with EtOAc (3 \times 50 mL), the combined organic layers were washed with sat. NaHCO_3 (100 mL) and brine (100 mL), dried over MgSO_4 and the solvent was removed under reduced pressure. The product was purified by column chromatography using PE/EtOAc (9:1 \rightarrow 8:2) as eluent to obtain 520 mg (80% yield) of **17** as colourless oil.

^1H -NMR (600 MHz, CDCl_3): δ (ppm) = 0.90 (d, $J = 6.5$ Hz, 3H, uD- $\text{C}^\delta\text{H}_3$), 0.95 (d, $J = 6.5$ Hz, 3H, uD- $\text{C}^\delta\text{H}_3$), 1.09 (d, $J = 7.0$ Hz, 3H, uA- $\text{C}^\varepsilon\text{HCH}_3$), 1.21 (s, 3H, uA- $\text{C}(\text{CH}_3)_2$), 1.23 (s, 3H, uA- $\text{C}(\text{CH}_3)_2$), 1.46 (br s, 12H, uA- $\text{C}(\text{CH}_3)_3$ and uC- $\text{C}(\text{CH}_3)_2$), 1.52 (s, 3H, uC- $\text{C}(\text{CH}_3)_2$), 1.57-1.61 (m, 1H, uD- C^γH), 1.71-1.80 (m, 2H, uD- C^βH_2), 1.92-1.97 (m, 1H, uA- $\text{C}^\varepsilon\text{H}$), 2.34-2.43 (m, 2H, uA- $\text{C}^\gamma\text{H}_2$), 3.36 (d, $J = 6.6$ Hz, 2H, uC- CH_2NH), 3.83 (dd, $J = 8.8, 2.5$ Hz, 1H, uA- C^ζH), 4.23 (t, $J = 7.5$ Hz, 1H, CHCH_2 , Fmoc), 4.34 (dd, $J = 10.6, 7.6$ Hz, 1H, $\text{CHCH}^{\text{A}}\text{H}^{\text{B}}$, Fmoc), 4.37 (dd, $J = 10.6, 7.6$ Hz, 1H, $\text{CHCH}^{\text{A}}\text{H}^{\text{B}}$, Fmoc), 4.70 (d, $J = 8.8$ Hz, 1H, uA- C^ηH),

5.01 (dd, $J = 10.1, 3.5$ Hz, 1H, uD-C $^{\alpha}$ H), 5.05 (td, $J = 6.9, 4.5$ Hz, 1H, uA-C $^{\delta}$ H), 5.58 (d, $J = 15.6$ Hz, 1H, uA-C $^{\alpha}$ H), 5.98 (t, $J = 6.6$ Hz, 1H, NH), 6.58 (dt, $J = 15.6, 7.3$ Hz, 1H, uA-C $^{\beta}$ H), 7.29-7.40 (m, 9H, uA-C $^{\alpha r}$ H, C $^{\alpha r}$ H, Fmoc), 7.63 (d, $J = 7.5$ Hz, 1H, C $^{\alpha r}$ H, Fmoc), 7.65 (d, $J = 7.5$ Hz, 1H, C $^{\alpha r}$ H, Fmoc), 7.76 (d, $J = 7.5$ Hz, 2H, C $^{\alpha r}$ H, Fmoc).

$^{13}\text{C-NMR}$ (151 MHz, CDCl_3): δ (ppm) = 9.8, 21.5, 22.5, 23.1, 23.3, 25.0, 27.2, 27.3, 28.2, 33.7, 35.6, 39.6, 44.1, 47.4, 49.4, 66.9, 71.0, 75.7, 80.3, 80.4, 82.0, 109.1, 120.0, 125.4, 125.4, 126.4, 126.8, 127.1, 127.2, 127.7, 128.7, 128.9, 137.6, 141.3, 141.4, 141.4, 144.2, 144.2, 157.1, 165.4, 170.9, 176.1.

Seco-uA[acetonide]-DCB[OCH $_2$ CH $_2$ OCH $_2$ CH $_2$ OCH $_2$ CH $_2$ N $_3$] (**18**)



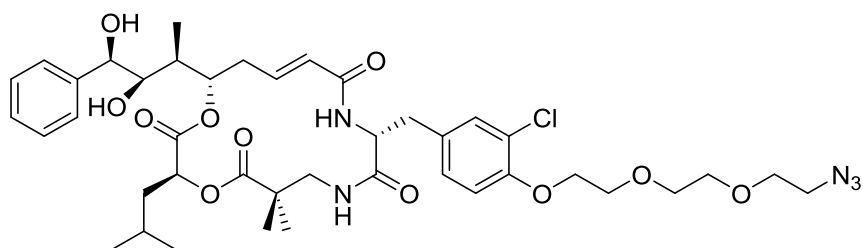
17 (290 mg, 0.35 mmol, 1 equiv) was dissolved in anhydrous DMF (2 mL) under argon atmosphere. Then, piperidine (175 μL , 1.75 mmol, 5 equiv) was added and the solution stirred at rt for 2 h. After this time the solvents were removed under reduced pressure. **13** (220 mg, 0.45 mmol, 1.3 equiv) was dissolved in anhydrous CH_2Cl_2 (1 mL) under argon atmosphere and the solution was cooled down to 0 $^{\circ}\text{C}$. Then, Et_3N (160 μL , 1.12 mmol, 3.2 equiv) and deprotected unit ADC in anhydrous CH_2Cl_2 (1 mL) were added dropwise. Then, HOAt (78 mg, 0.57 mmol, 1.6 equiv) was added as a solid. After complete dissolution, EDC·HCl (109 mg, 0.57 mmol, 1.6 equiv), was added and the mixture stirred overnight while gradually warmed to rt. Then, H_2O (45 mL) and EtOAc (45 mL) were added, the layers were separated and the organic layer was washed with 5% KHSO_4 (45 mL) and saturated NaHCO_3 (45 mL), it was dried over MgSO_4 and the solvent was removed under reduced pressure. The product was purified by column chromatography using PE/EtOAc (3:2) as eluent to obtain 190 mg (51% yield) of **18** as white solid.

$^1\text{H-NMR}$ (600 MHz, CDCl_3): δ (ppm) = 0.87 (d, $J = 6.4$ Hz, 3H, uD-C $^{\delta}$ H $_3$), 0.90 (d, $J = 6.4$ Hz, 3H, uD-C $^{\delta}$ H $_3$), 1.12 (d, $J = 6.9$ Hz, 3H, uA-C $^{\epsilon}$ HCH $_3$), 1.15 (s, 3H, uC-C(CH $_3$) $_2$), 1.16 (s,

3H, uC-C(CH₃)₂), 1.37 (s, 9H, uB-C(CH₃)₃), 1.42 (s, 9H, uA-C(CH₃)₃), 1.45 (s, 3H, uA-C(CH₃)₂), 1.51 (s, 3H, uA-C(CH₃)₂), 1.52-1.54 (m, 1H, uD-C^γH), 1.65-1.69 (m, 2H, uD-C^βH₂), 1.92-1.97 (m, 1H, uA-C^εH), 2.35-2.42 (m, 2H, uA-C^γH₂), 2.81 (dd, *J* = 14.0, 7.3 Hz, 1H, uB-C^βH^AH^B), 3.07 (dd, *J* = 14.0, 5.8 Hz, 1H, uB-C^βH^AH^B), 3.27 (dd, *J* = 13.2, 5.0 Hz, 1H, uC-CH^AH^BNH), 3.38 (t, *J* = 5.1 Hz, 2H, uB-CH₂N₃), 3.50 (dd, *J* = 13.2, 7.8 Hz, 1H, uC-CH^AH^BNH), 3.67-3.69 (m, 4H, uB-CH₂), 3.77-3.79 (m, 2H, uB-CH₂), 3.87-3.89 (m, 3H, uB-C^{ar}OCH₂CH₂, uA-C^ζH), 4.14 (m, 2H, uB-C^{ar}OCH₂), 4.28 (m, 1H, uB-C^αH), 4.69 (d, *J* = 8.7 Hz, 1H, uA-C^ηH), 4.91 (dd, *J* = 9.6, 3.7 Hz, 1H, uD-C^αH), 5.03 (m, 1H, uA-C^δH), 5.19 (d, *J* = 8.1 Hz, 1H, uB-NH), 5.60 (d, *J* = 15.6 Hz, 1H, uA-C^αH), 6.52 (dt, *J* = 15.4, 7.6 Hz, 1H, uA-C^βH), 6.84 (d, *J* = 8.3 Hz, 1H, uB-C⁵H), 7.01 (dd, *J* = 8.3, 2.1 Hz, 1H, uB-C⁶H), 7.18 (s, 1H, uB-C²H), 7.28-7.40 (m, 5H, uA-C^{ar}H).

¹³C-NMR (151 MHz, CDCl₃): δ (ppm) = 9.4, 21.6, 22.5, 23.1, 23.3, 25.0, 27.1, 27.2, 28.2, 28.4, 33.6, 35.8, 38.0, 39.6, 43.8, 47.3, 50.8, 55.9, 69.1, 69.7, 70.2, 70.9, 71.1, 71.3, 75.9, 79.8, 80.4, 80.5, 82.0, 109.1, 113.8, 122.9, 126.5, 127.2, 128.7, 128.7, 128.8, 130.6, 131.4, 137.5, 141.6, 153.3, 155.2, 165.2, 171.3, 171.4, 176.0.

uA[diol]-uB[OCH₂CH₂OCH₂CH₂OCH₂CH₂N₃]-Cryptophycin-52 (**20**)



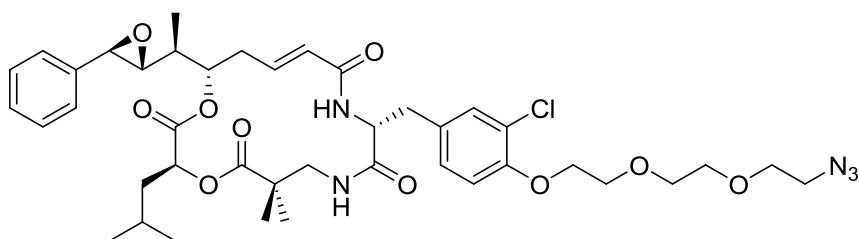
18 (165 mg, 0.16 mmol, 1 equiv) was dissolved in CH₂Cl₂ (1.75 mL), H₂O (0.2 mL) and TFA (1.70 mL) and the solution was stirred for 2 h at rt. The solvents were removed under reduced pressure and the product dried in HV overnight over KOH. The product was dissolved in DMF (10 mL) and transferred into a syringe. HATU (90 mg, 0.24 mmol, 1.5 equiv) and HOAt (33 mg, 0.24 mmol, 1.5 equiv) were dissolved in DMF (10 mL) and transferred into a second syringe. These two solutions were added to a stirred solution of DIPEA (84 μL, 0.48 mmol, 3equiv) in DMF (27.5 mL) at a rate of 0.01 mL/h using a dual channel syringe pump. Once the addition was complete, the mixture was stirred for another 2 h. Then, the solvent was removed, the crude dissolved with EtOAc (50 mL) and washed with saturated NaHCO₃ (50 mL) and brine (50 mL). The organic layer was dried over MgSO₄ and the solvent removed under reduced pressure. The product was purified by column chromatography using PE/EtOAc (1:4) as eluent to obtain 28 mg (21% yield) of **20** as white solid.

¹H-NMR (600 MHz, CDCl₃): δ (ppm) = 0.86 (d, J = 6.1 Hz, 3H, uD-C ^{δ} H₃), 0.92 (d, J = 6.1 Hz, 3H, uD-C ^{δ} H₃), 0.98 (s, 3H, uC-C(CH₃)₂), 1.00 (d, J = 7.0 Hz, 3H, uA-C ^{ϵ} HCH₃), 1.13 (s, 3H, uC-C(CH₃)₂), 1.52-1.66 (m, 4H, uD-C ^{γ} H, uD-C ^{β} H₂, uA-C ^{ϵ} H), 2.15-2.20 (m, 1H, uA-C ^{γ} H^AH^B), 2.66-2.70 (m, 1H, uA-C ^{γ} H^AH^B), 3.01-3.05 (m, 2H, uB-C ^{β} H₂), 3.26 (dd, J = 13.8, 6.1 Hz, 1H, uC-CH^AH^BNH), 3.30 (dd, J = 13.8, 6.5 Hz, 1H, uC-CH^AH^BNH), 3.38 (t, J = 5.1 Hz, 2H, uB-CH₂N₃), 3.67 (m, 4H, uB-CH₂), 3.74 (d, J = 8.6 Hz, 1H, uA-C ^{ζ} H), 3.76-3.78 (m, 2H, uB-CH₂), 3.89 (t, J = 4.9 Hz, 2H, uB-C^{ar}OCH₂CH₂), 4.15 (t, J = 4.9 Hz, 2H, uB-C^{ar}OCH₂), 4.32 (br, 2H, 2xOH), 4.56 (d, J = 8.6 Hz, 1H, uA-C ^{η} H), 4.83 (q, J = 6.6 Hz, 1H, uB-C ^{α} H), 4.94 (td, J = 8.0, 3.0 Hz, 1H, uA-C ^{δ} H), 5.11 (dd, J = 10.4, 3.4 Hz, 1H, uD-C ^{α} H), 5.68 (d, J = 15.8 Hz, 1H, uA-C ^{α} H), 6.04 (d, J = 9.1 Hz, 1H, uB-NH), 6.29 (dt, J = 15.4, 7.2 Hz, 1H, uA-C ^{β} H), 6.86 (d, J = 8.3 Hz, 1H, uB-C⁵H), 6.98 (t, J = 6.2 Hz, uC-NH), 7.01 (dd, J = 8.3, 2.2 Hz, 1H, uB-C⁶H), 7.18 (d, J = 2.2 Hz, 1H, uB-C²H), 7.30-7.36 (m, 5H, uA-C^{ar}H).

¹³C-NMR (151 MHz, CDCl₃): δ (ppm) = 9.3, 21.3, 22.8, 23.2, 23.5, 24.9, 34.7, 35.9, 36.8, 39.1, 42.9, 46.6, 50.8, 54.0, 69.1, 69.6, 70.1, 70.8, 71.2, 74.7, 75.9, 76.8 (overlapped with solvent signal), 114.2, 123.3, 126.3, 127.0, 128.5, 128.7, 129.0, 129.9, 131.2, 139.6, 140.5, 153.6, 165.9, 171.0, 171.0, 176.3.

HPLC-MS: T_R = 9.98 min, >99% purity (λ = 220 nm), m/z = 830.38 (830.37 [M+H]⁺)

uB[OCH₂CH₂OCH₂CH₂OCH₂CH₂N₃]-Cryptophycin-52 (**22**)



The diol of **20** (20 mg, 24.1 μ mol, 1 equiv) was transformed to the corresponding epoxide using a procedure previously described in the literature [4]. Final purification by column chromatography with PE/EtOAc (1:3) as eluent and subsequent lyophilization afforded 7 mg (36% yield over 3 steps) of **22** as a white solid.

¹H-NMR (600 MHz, CDCl₃): δ (ppm) = 0.77 (d, J = 7.2 Hz, 3H, uD-C ^{δ} H₃), 0.78 (d, J = 7.2 Hz, 3H, uD-C ^{δ} H₃), 1.18 (d, J = 6.9 Hz, 3H, uA-C ^{ϵ} HCH₃), 1.20 (s, 3H, uC-C(CH₃)₂), 1.23 (s, 3H, uC-C(CH₃)₂), 1.33-1.37 (m, 2H, uD-C ^{β} H₂), 1.50-1.52 (m, 1H, uD-C ^{γ} H), 1.89-1.92 (m, 1H, uA-C ^{ϵ} H), 2.43 (m, 1H, uA-C ^{γ} H^AH^B), 2.75-2.78 (m, 1H, uA-C ^{γ} H^AH^B), 2.81 (dd, J = 7.1,

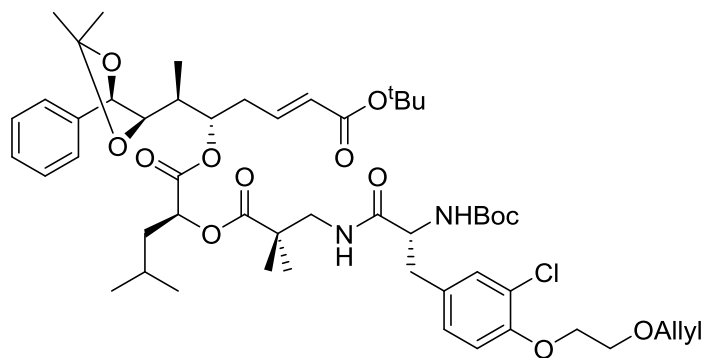
1.9 Hz, 1H, uA-C^εH), 3.10 (d, $J = 6.1$ Hz, 2H, uB-C^βH₂), 3.27 (dd, $J = 13.3, 5.0$ Hz, 1H, uC-CH^AH^BNH), 3.37-3.40 (m, 2H, uC-CH^AH^BNH, uB-CH₂N₃), 3.67-3.69 (m, 5H, uA-C^ηH, uB-CH₂), 3.77-3.79 (m, 2H, uB-CH₂), 3.90 (t, $J = 4.9$ Hz, 2H, uB-C^{ar}OCH₂CH₂), 4.17 (t, $J = 4.9$ Hz, 2H, uB-C^{Ar}OCH₂), 4.85-4.87 (m, 1H, uB-C^αH), 4.89-4.93 (m, 1H, uA-C^δH), 5.04 (dd, $J = 10.7, 3.7$ Hz, 1H, uD-C^αH), 5.73 (d, $J = 8.7$ Hz, uB-NH), 5.78 (d, $J = 15.5$ Hz, uA-C^αH), 6.46 (dt, $J = 15.5, 7.5$ Hz, uA-C^βH), 6.88 (d, $J = 8.4$ Hz, 1H, uB-C⁵H), 6.97 (t, $J = 7.0$ Hz, uC-NH), 7.05 (dd, $J = 8.4, 2.2$ Hz, 1H, uB-C⁶H), 7.21 (d, $J = 2.2$ Hz, 1H, uB-C²H), 7.24-7.25 (m, 2H, uA-C^{ar}H), 7.30-7.36 (m, 3H, uA-C^{ar}H).

¹³C-NMR (151 MHz, CDCl₃): δ (ppm) = 13.5, 21.0, 23.0, 23.1, 23.7, 24.7, 34.3, 35.9, 39.1, 39.3, 43.0, 46.5, 50.9, 54.2, 59.6, 64.3, 69.2, 69.7, 70.2, 70.8, 70.9, 71.3, 76.8 (overlapped with solvent signal), 114.2, 123.3, 125.8, 127.0, 128.5, 128.8, 129.8, 131.2, 136.8, 138.4, 153.7, 165.5, 170.6, 170.7, 176.6.

HPLC-MS: $T_R = 11.25$ min, >99% purity ($\lambda = 220$ nm), $m/z = 812.37$ (812.36 [M+H]⁺)

HRMS (ESI-MS): m/z calculated for C₄₁H₅₅ClN₅O₁₀ [M+H]⁺ 812.3632; found 812.3626

Seco-uA[acetone]-DCB[OCH₂CH₂OCH₂CHCH₂] (**19**)



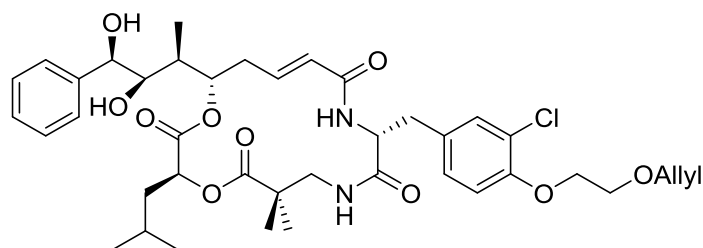
17 (500 mg, 0.62 mmol, 1 equiv) was dissolved in anhydrous DMF (4 mL) under argon atmosphere. Then, piperidine (305 μ L, 3.1 mmol, 5 equiv) was added and the solution stirred at rt for 2 h. After this time the solvents were removed under reduced pressure. **14** (320 mg, 0.81 mmol, 1.3 equiv) was dissolved in anhydrous CH₂Cl₂ (2 mL) under argon atmosphere and the solution was cooled down to 0 °C. Then, Et₃N (275 μ L, 1.97 mmol, 3.2 equiv) and deprotected unit ADC in anhydrous CH₂Cl₂ (2 mL) were added dropwise. Then, HOAt (135 mg, 0.99 mmol, 1.6 equiv) was added as a solid. After complete dissolution, EDC·HCl (190 mg, 0.99 mmol, 1.6 equiv), was added and the mixture stirred overnight while gradually warmed to rt. Then, H₂O (75 ml) and EtOAc (75 mL) were added, the layers were separated and the organic

layer was washed with 5% KHSO₄ (75 mL) and saturated NaHCO₃ (75 mL), it was dried over MgSO₄ and the solvent was removed under reduced pressure. The product was purified by column chromatography using PE/EtOAc (7:3) as eluent to obtain 350 mg (59% yield) of **19** as white solid.

¹H-NMR (600 MHz, CDCl₃): δ (ppm) = 0.84 (d, J = 6.3 Hz, 3H, uD-C ^{δ} H₃), 0.91 (d, J = 6.3 Hz, 3H, uD-C ^{δ} H₃), 1.08 (s, 3H, uC-C(CH₃)₂), 1.11 (d, J = 7.0 Hz, 3H, uA-C ^{ϵ} HCH₃), 1.17 (s, 3H, uC-C(CH₃)₂), 1.34 (s, 9H, uB-C(CH₃)₃), 1.43 (s, 3H, uA-C(CH₃)₂), 1.47 (s, 9H, uA-C(CH₃)₃), 1.48 (s, 3H, uA-C(CH₃)₂), 1.66-1.74, m, 3H, uD-C ^{γ} H, uD-C ^{β} H₂), 1.85-1.90 (m, 1H, uA-C ^{ϵ} H), 2.27-2.33 (m, 1H, uA-C ^{γ} H₂), 2.50-2.54 (m, 1H, uA-C ^{γ} H₂), 2.83 (dd, J = 13.6, 9.9 Hz, 1H, uB-C ^{β} H^AH^B), 3.22-3.28 (m, 2H, uB-C ^{β} H^AH^B, uC-CH^AH^BNH), 3.61 (dd, J = 13.4, 8.3 Hz, 1H, uC-CH^AH^BNH), 3.81-3.83 (m, 3H, C^{ar}OCH₂CH₂, uA-C ^{ζ} H), 4.12 (dt, J = 5.7, 1.4 Hz, 2H, C^{ar}O(CH₂)₂OCH₂), 4.14 (t, J = 5.0 Hz, 2H, C^{ar}OCH₂), 4.41 (q, J = 9.1 Hz, 1H, uB-C ^{α} H), 4.70 (d, J = 8.9 Hz, 1H, uA-C ^{η} H), 4.89 (dd, J = 10.2, 3.0 Hz, 1H, uD-C ^{α} H), 5.08 (t, J = 8.5 Hz, 1H, uA-C ^{δ} H), 5.19 (dq, J = 10.3, 1.4 Hz, 1H, CH=CH^{trans}H^{cis}), 5.31 (dq, J = 17.3, 1.6 Hz, 1H, CH=CH^{trans}H^{cis}), 5.68 (d, J = 15.5 Hz, 1H, uA-C ^{α} H), 5.79 (d, J = 8.7 Hz, 1H, uB-NH), 5.92 (ddt, J = 17.3, 10.8, 5.6 Hz, 1H, CH=CH₂), 6.74 (ddd, J = 15.2, 8.9, 5.3 Hz, 1H, uA-C ^{β} H), 6.85 (d, J = 8.3 Hz, 1H, uB-C ^{ζ} H), 7.09 (dd, J = 8.5, 2.1 Hz, 1H, uB-C ^{δ} H), 7.13-7.15 (m, 1H, uC-NH), 7.26-7.37 (m, 6H, uB-C ^{$2'$} H, uA-C^{ar}H).

¹³C-NMR (151 MHz, CDCl₃): δ (ppm) = 9.7, 21.3, 22.0, 23.3, 24.9, 27.2, 27.3, 28.4, 28.4, 34.9, 35.7, 37.7, 39.5, 44.0, 47.6, 56.3, 60.5, 68.4, 69.2, 70.5, 72.6, 75.6, 79.6, 80.2, 80.5, 82.0, 109.1, 114.0, 117.3, 122.9, 125.9, 126.7, 128.6, 128.9, 131.4, 131.6, 134.8, 137.7, 142.1, 153.2, 155.9, 166.0, 170.9, 172.0, 175.6.

uA[diol]-uB[OCH₂CH₂OCH₂CHCH₂]-Cryptophycin-52 (**21**)



19 (310 mg, 0.32 mmol, 1 equiv) was dissolved in CH₂Cl₂ (3.5 mL), H₂O (0.35 mL) and TFA (3.5 mL) and the solution was stirred for 2 h at rt. The solvents were removed under reduced pressure and the product dried in HV overnight over KOH. The product was dissolved in DMF (16.7 mL) and transferred

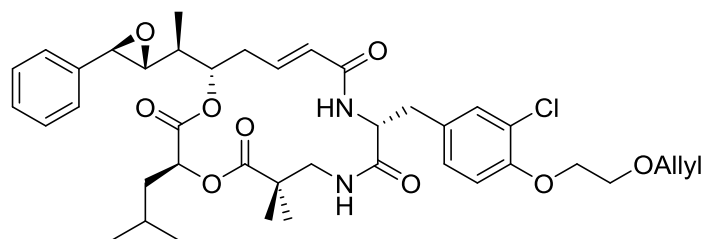
into a syringe. HATU (182 mg, 0.48 mmol, 1.5 equiv) and HOAt (65 mg, 0.48 mmol, 1.5 equiv) were dissolved in DMF (16.7 mL) and transferred into a second syringe. These two solutions were added to a stirred solution of DIPEA (168 μ L, 0.96 mmol, 3 equiv) in DMF (15 mL) at a rate of 0.01 mL/h using a dual channel syringe pump. Once the addition was complete, the mixture was stirred for another 2 h. Then, the solvent was removed, the crude dissolved with EtOAc (100 mL) and washed with saturated NaHCO₃ (100 mL) and brine (100 mL). The organic layer was dried over MgSO₄ and the solvent was removed under reduced pressure. The product was purified by column chromatography using PE/EtOAc (1:4) as eluent to obtain 60 mg (25% yield) of **21** as white solid.

¹H-NMR (600 MHz, CDCl₃): δ (ppm) = 0.85 (d, J = 6.6 Hz, 3H, uD-C ^{δ} H₃), 0.91 (d, J = 6.6 Hz, 3H, uD-C ^{δ} H₃), 0.97 (d, J = 7.0 Hz, 3H, uA-C ^{ϵ} HCH₃), 1.14 (s, 3H, uC-C(CH₃)₂), 1.21 (s, 3H, uC-C(CH₃)₂), 1.41-1.47 (m, 2H, uA-C ^{ϵ} H, uD-C ^{β} H₂), 1.60-1.64 (m, 1H, uD-C ^{γ} H), 1.74-1.79 (m, 1H, uD-C ^{β} H₂), 2.18-2.24 (m, 1H, uA-C ^{γ} H₂), 2.39-2.43 (m, 1H, uA-C ^{γ} H₂), 2.90 (dd, J = 14.6, 9.3 Hz, 1H, uB-C ^{β} H^AH^B), 3.08 (dd, J = 14.6, 4.8 Hz, 1H, uB-C ^{β} H^AH^B), 3.13 (dd, J = 13.5, 3.9 Hz, 1H, uC-CH^AH^BNH), 3.33 (dd, J = 13.5, 8.2 Hz, 1H, uC-CH^AH^BNH), 3.50 (br, 1H, uA-OH), 3.67 (br, 1H, uA-OH), 3.75 (d, J = 8.3 Hz, 1H uA-C ^{ζ} H), 3.81 (t, J = 4.9 Hz, 2H, C^{ar}OCH₂CH₂), 4.09-4.12 (m, 4H, C^{ar}O(CH₂)₂OCH₂, C^{ar}OCH₂), 4.53 (d, J = 8.3 Hz, 1H, uA-CⁿH), 4.68 (td, J = 8.2, 4.9 Hz, 1H, uB-C ^{α} H), 4.85 (dd, J = 10.1, 3.6 Hz, 1H, uD-C ^{α} H), 5.03-5.06 (m, 1H, uA-C ^{δ} H), 5.18 (dq, J = 10.4, 1.5 Hz, 1H, CH=CH^{trans}H^{cis}), 5.30 (dq, J = 17.4, 1.7 Hz, 1H, CH=CH^{trans}H^{cis}), 5.72 (d, J = 15.2 Hz, 1H, uA-C ^{α} H), 5.91 (ddt, J = 17.2, 10.8, 5.5 Hz, 1H, CH=CH₂), 6.18 (d, J = 7.8 Hz, 1H, uB-NH), 6.68 (ddd, J = 15.1, 10.8, 4.2 Hz, 1H, uA-C ^{β} H), 6.82 (d, J = 8.4 Hz, 1H, uB-C^{5'}H), 7.00 (dd, J = 8.4, 2.1 Hz, 1H, uB-C^{6'}H), 7.16 (d, J = 2.1 Hz, 1H, uB-C^{2'}H), 7.24-7.32 (m, 6H, uA-C^{ar}H, uC-NH).

¹³C-NMR (151 MHz, CDCl₃): δ (ppm) = 9.7, 21.7, 22.9, 23.1, 23.1, 24.9, 35.3, 36.2, 38.1, 39.7, 42.8, 46.6, 54.7, 68.4, 69.1, 71.2, 72.5, 74.9, 75.8, 76.6, 114.0, 117.3, 123.1, 124.5, 127.0, 128.2, 128.3, 128.7, 130.4, 130.9, 134.7, 140.9, 142.7, 153.5, 165.7, 170.6, 170.9, 177.6.

HPLC-MS: T_R = 10.35 min, >99% purity (λ = 220 nm), m/z = 757.35 (757.35 [M+H]⁺)

uB[OCH₂CH₂OCH₂CHCH₂]-Cryptophycin-52 (**23**)



The diol of **21** (40 mg, 52.9 μmol, 1 equiv) was transformed to the corresponding epoxide using a procedure previously described in the literature [4]. Final purification by column chromatography with PE/EtOAc (1:2) as eluent and subsequent lyophilization afforded 24 mg (61% yield over 3 steps) of **23** as a white solid.

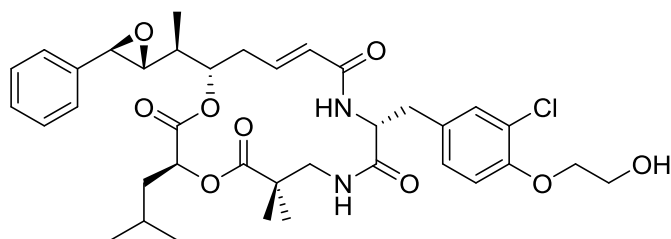
¹H-NMR (600 MHz, CDCl₃): δ (ppm) = 0.82 (d, *J* = 6.5 Hz, 3H, uD-C^δH₃), 0.84 (d, *J* = 6.5 Hz, 3H, uD-C^δH₃), 1.14 (d, *J* = 6.9 Hz, 3H, uA-C^εHCH₃), 1.15 (s, 3H, uC-C(CH₃)₂), 1.21 (s, 3H, uC-C(CH₃)₂), 1.28-1.32 (m, 1H, uD-C^γH), 1.62-1.73 (m, 2H, uD-C^βH₂), 1.75-1.81 (m, 1H, uA-C^εH), 2.41-2.47 (m, 1H, uA-C^γH₂), 2.55-2.59 (m, 1H, uA-C^γH₂), 2.92 (dd, *J* = 7.5, 2.0 Hz, 1H, uA-C^ζH), 3.02 (dd, *J* = 14.5, 7.7 Hz, 1H, uB-C^βH^AH^B), 3.08 (m, 2H, uB-C^βH^AH^B, uC-CH^AH^BNH), 3.40 (dd, *J* = 13.6, 8.6 Hz, 1H, uC-CH^AH^BNH), 3.68 (d, *J* = 2.0 Hz, 1H, uA-C^ηH), 3.83 (t, *J* = 4.9 Hz, C^{ar}OCH₂CH₂), 4.12 (dt, *J* = 5.6, 1.5 Hz, 2H, C^{ar}O(CH₂)₂OCH₂), 4.15 (t, *J* = 4.9 Hz, 2H, C^{ar}OCH₂), 4.72 (td, *J* = 7.7, 4.9 Hz, 1H, uB-C^αH), 4.83 (dd, *J* = 10.2, 3.5 Hz, 1H, uD-C^αH), 5.17-5.21 (m, 2H, uA-C^δH, CH=CH^{trans}H^{cis}), 5.32 (dq, *J* = 17.4, 1.7 Hz, 1H, CH=CH^{trans}H^{cis}), 5.63 (d, *J* = 7.8 Hz, uB-NH), 5.71 (dd, *J* = 15.1, 1.8 Hz, 1H, uA-C^αH), 5.93 (ddt, *J* = 17.3, 10.8, 5.6 Hz, 1H, CH=CH₂), 6.75 (ddd, *J* = 15.0, 10.6, 4.3 Hz, 1H, uA-C^βH), 6.85 (d, *J* = 8.4 Hz, 1H, uB-C⁵H), 7.01 (dd, *J* = 8.4, 2.2 Hz, 1H, uB-C⁶H), 7.18 (d, *J* = 2.2 Hz, 1H, uB-C²H), 7.21 (dd, *J* = 8.9, 3.5 Hz, 1H, uC-NH), 7.23-7.25 (m, 2H, uA-C^{ar}H), 7.31-7.37 (m, 3H, uA-C^{ar}H).

¹³C-NMR (151 MHz, CDCl₃): δ (ppm) = 13.7, 21.4, 22.9, 23.0, 24.7, 35.5, 37.0, 39.5, 40.8, 42.9, 46.6, 54.5, 59.2, 63.2, 68.4, 69.2, 71.3, 72.6, 76.0, 114.2, 117.4, 123.4, 124.8, 125.7, 128.3, 128.7, 128.9, 130.0, 131.0, 134.7, 136.9, 141.9, 153.7, 165.1, 170.5, 170.6, 178.1.

HPLC-MS: T_R = 11.53 min, 98% purity (λ = 220 nm), *m/z* = 739.33 (739.34 [M+H]⁺)

HRMS (ESI-MS): *m/z* calculated for C₄₀H₅₂ClN₂O₉ [M+H]⁺ 739.3356; found 739.3359

uB[OCH₂CH₂OH]-Cryptophycin-52 (**24**)



23 (5 mg, 6.8 μ mol, 1 equiv) and Pd(PPh₃)₄ (0.8 mg, 0.68 μ mol, 10%) were dissolved with anhydrous and degassed CH₂Cl₂ (1 mL). Phenylsilane (4.2 μ L, 34 μ mol, 5 equiv) was added and the solution was stirred at rt for 7 h. Then, the solvent was removed by bubbling air and the product was purified by column chromatography using PE/EtOAc (1:2) as eluent and subsequent lyophilization afforded 2 mg (42% yield) of **24** as white solid.

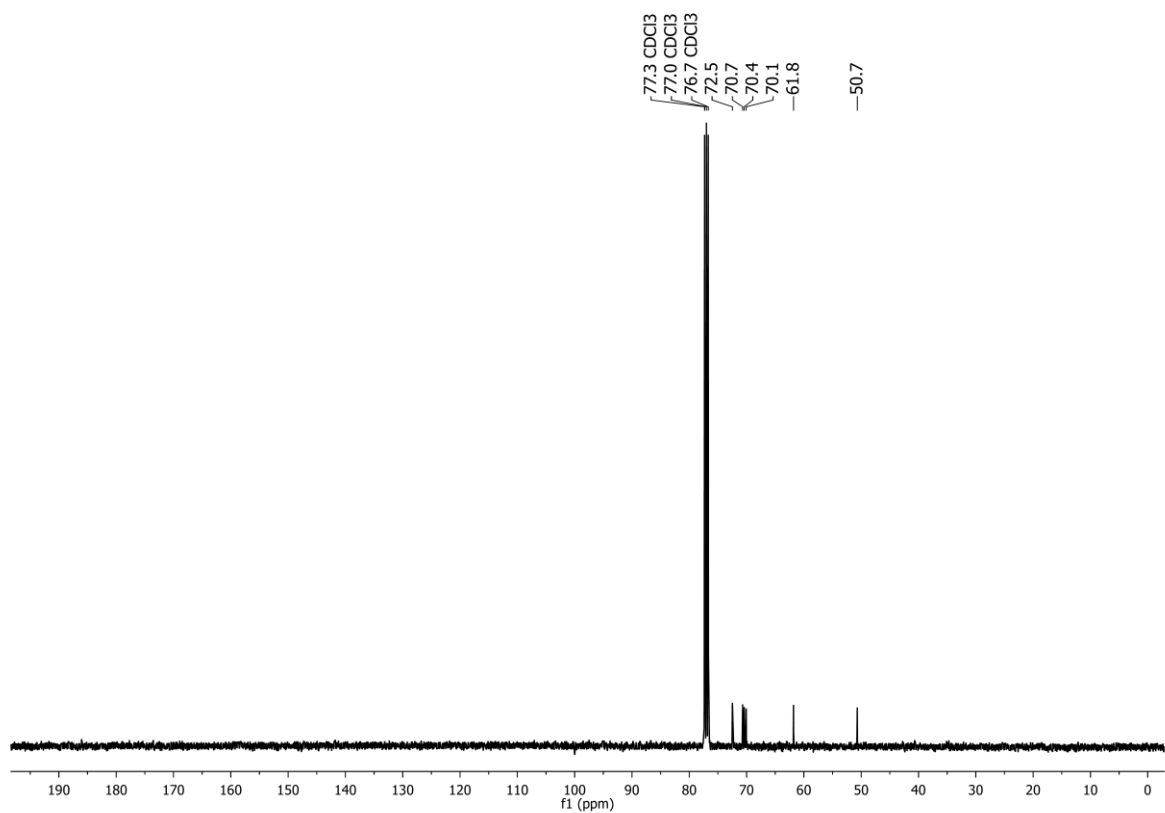
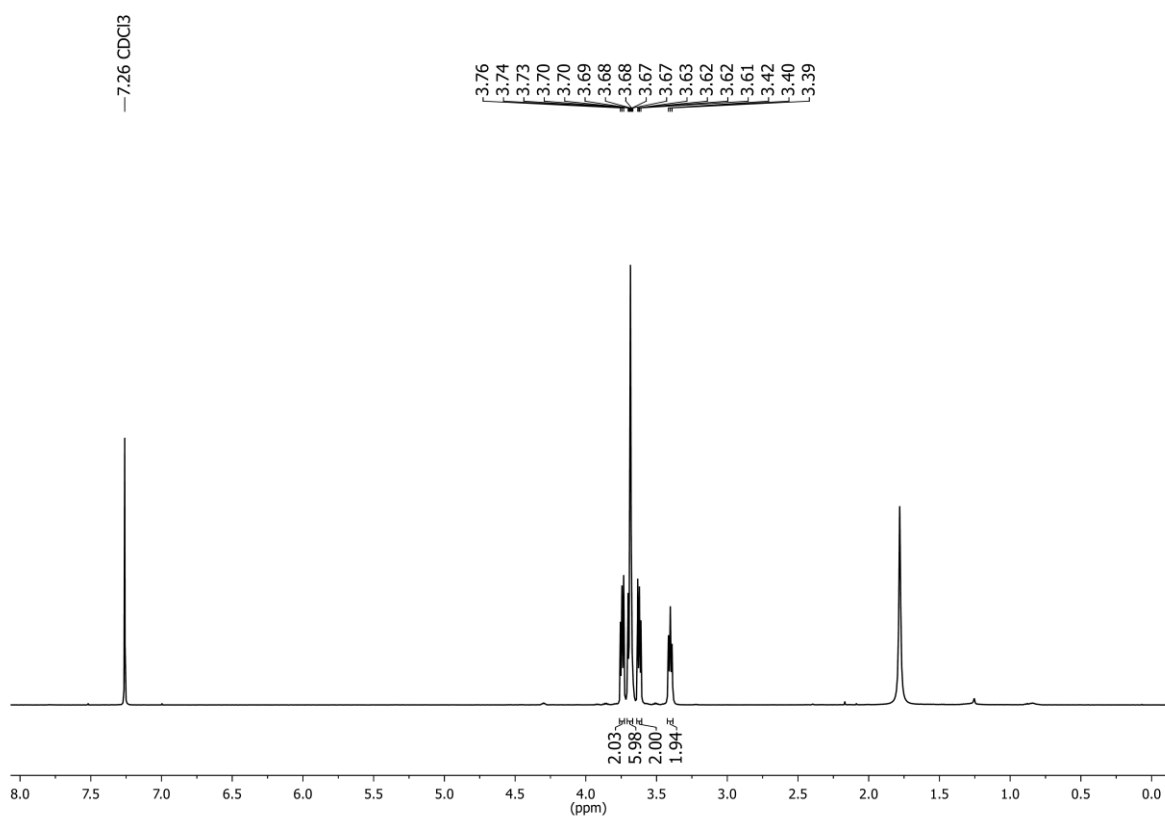
¹H-NMR (600 MHz, CDCl₃): δ (ppm) = 0.83 (d, J = 6.4 Hz, 3H, uD-C ^{δ} H₃), 0.84 (d, J = 6.4 Hz, 3H, uD-C ^{δ} H₃), 1.14-1.15 (m, 6H, uA-C ^{ϵ} HCH₃, uC-C(CH₃)₂), 1.22 (s, 3H, uC-C(CH₃)₂), 1.30-1.34 (m, 1H, uD-C ^{γ} H), 1.66-1.74 (m, 2H, uD-C ^{β} H₂), 1.77-1.80 (m, 1H, uA-C ^{ϵ} H), 2.14-2.18 (br s, 1H, OH), 2.42-2.48 (m, 1H, uA-C ^{γ} H₂), 2.56-2.59 (m, 1H, uA-C ^{γ} H₂), 2.92 (d, J = 7.3 Hz, 1H, uA-C ^{ζ} H), 3.05-3.13 (m, 3H, uB-C ^{β} H₂, uC-CH^AH^BNH), 3.40 (dd, J = 13.6, 8.3 Hz, 1H, uC-CH^AH^BNH), 3.68 (s, 1H, uA-CⁿH), 3.98 (s, 2H, C^{ar}OCH₂CH₂), 4.12 (t, J = 4.1 Hz, 2H, C^{ar}OCH₂), 4.75 (q, J = 6.5 Hz, 1H, uB-C ^{α} H), 4.83 (dd, J = 10.0, 3.7 Hz, 1H, uD-C ^{α} H), 5.19-5.21 (m, 1H, uA-C ^{δ} H), 5.44 (d, J = 7.8 Hz, uB-NH), 5.72 (d, J = 15.2 Hz, 1H, uA-C ^{α} H), 6.76 (ddd, J = 15.0, 10.5, 4.4 Hz, 1H, uA-C ^{β} H), 6.86 (d, J = 8.2 Hz, 1H, uB-C ^{ζ} H), 7.04 (d, J = 8.2 Hz, 1H, uB-C ^{δ} H), 7.18-7.25 (m, 3H, uB-C ^{$2'$} H, uA-C^{ar}H), 7.34-7.38 (m, 3H, uA-C^{ar}H).

HPLC-MS: T_R = 10.61 min, >99% purity (λ = 220 nm), m/z = 699.31 (699.30 [M+H]⁺)

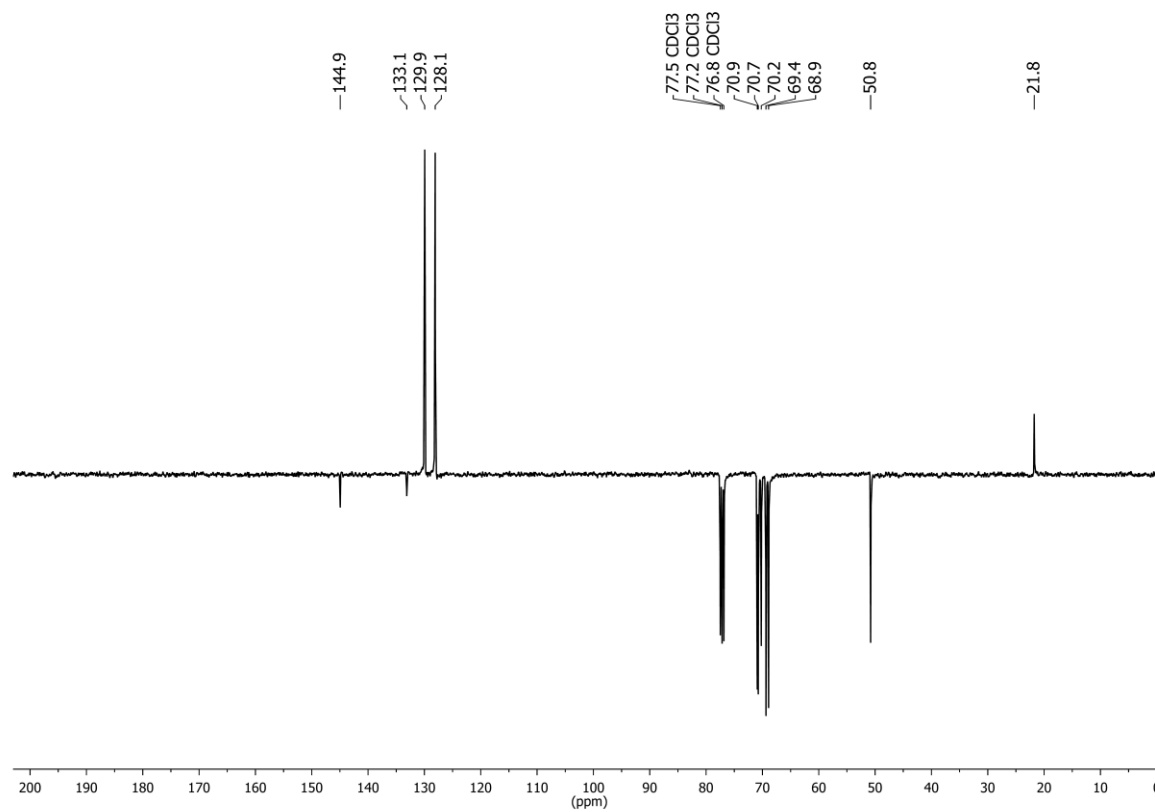
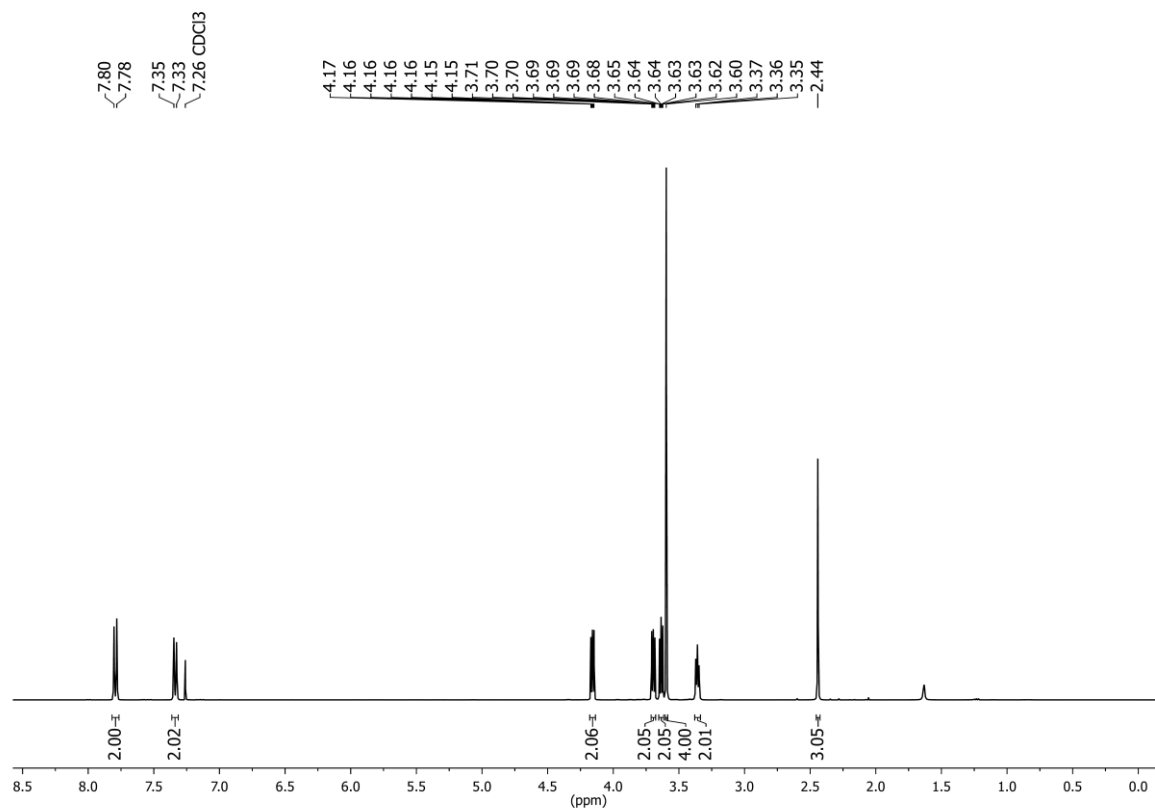
HRMS (ESI-MS): m/z calculated for C₃₇H₄₈ClN₂O₉ [M+H]⁺ 699.3043; found 699.3047

4) NMR, HPLC and mass spectra

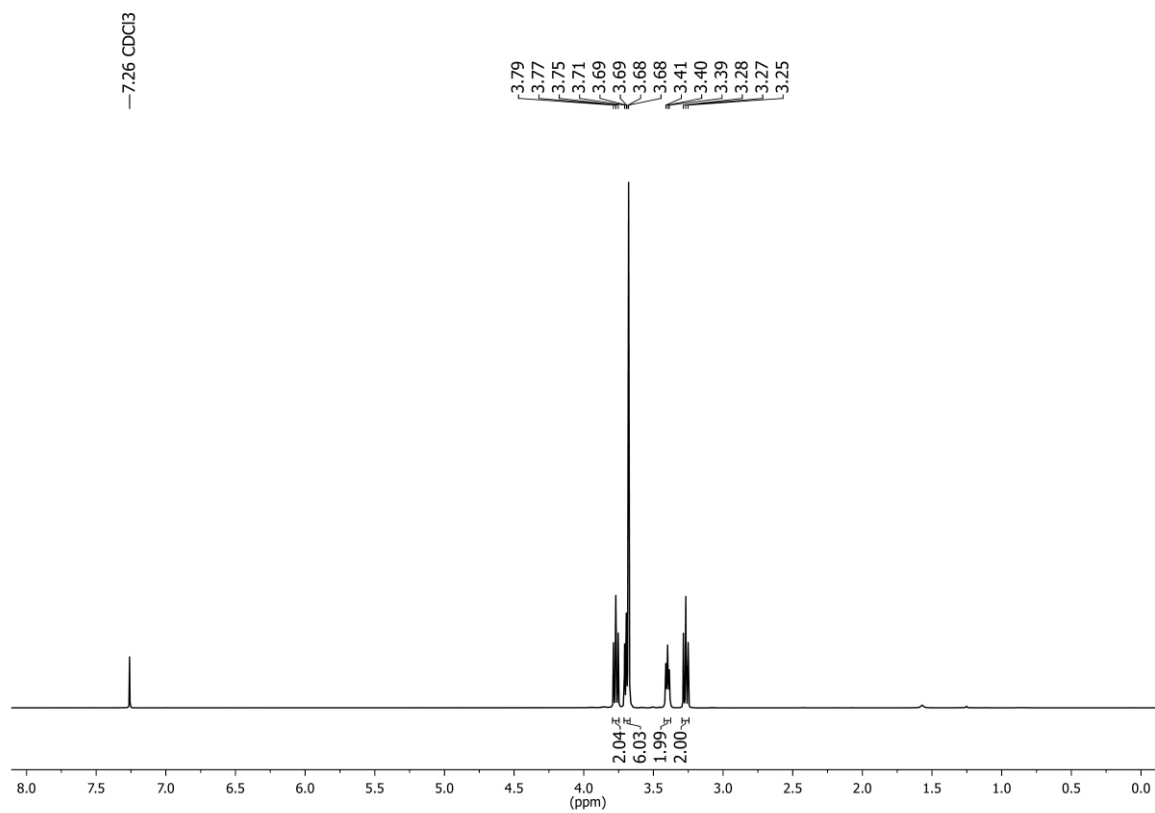
4: ^1H -NMR and ^{13}C -NMR



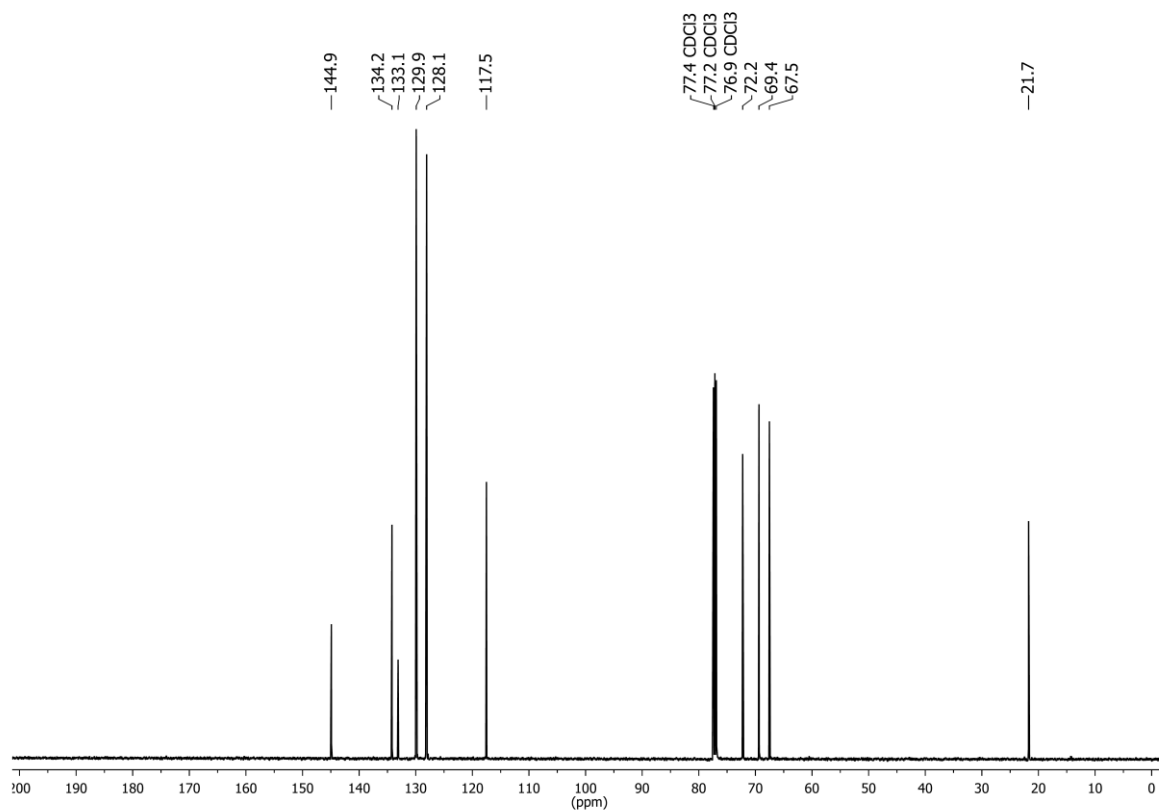
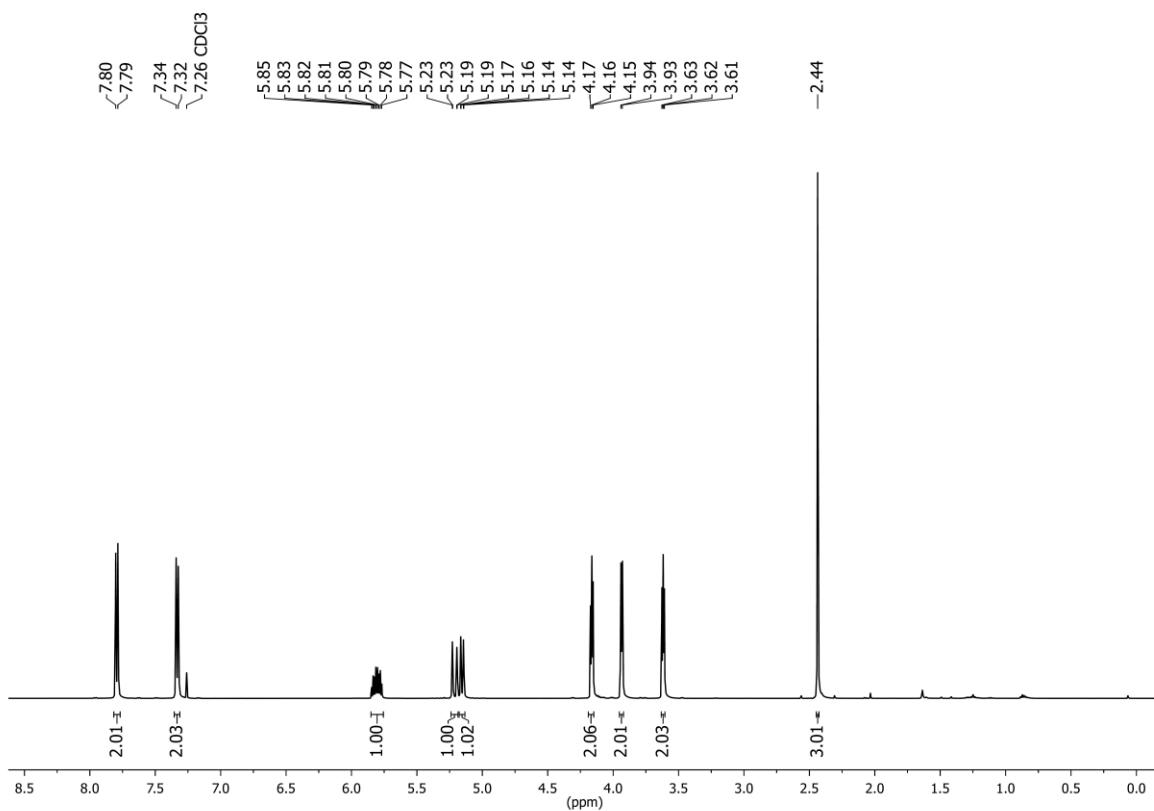
5: ^1H -NMR and ^{13}C -NMR



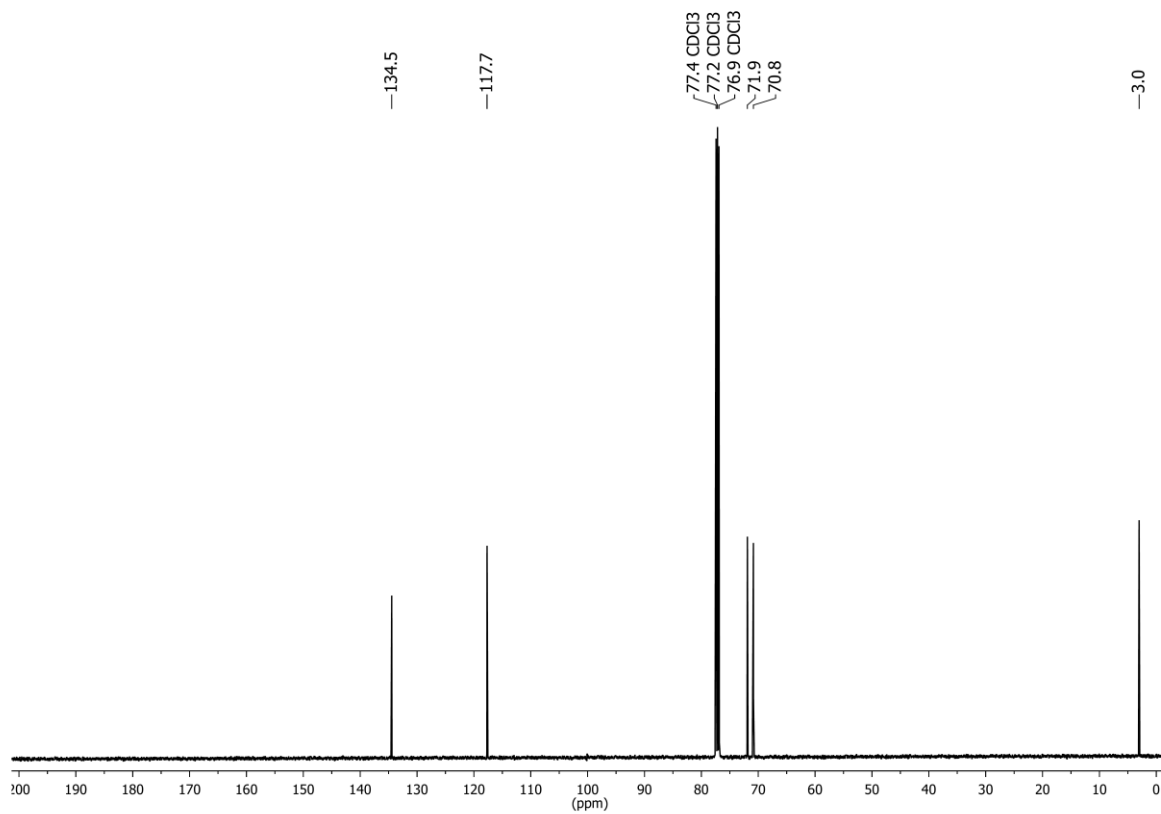
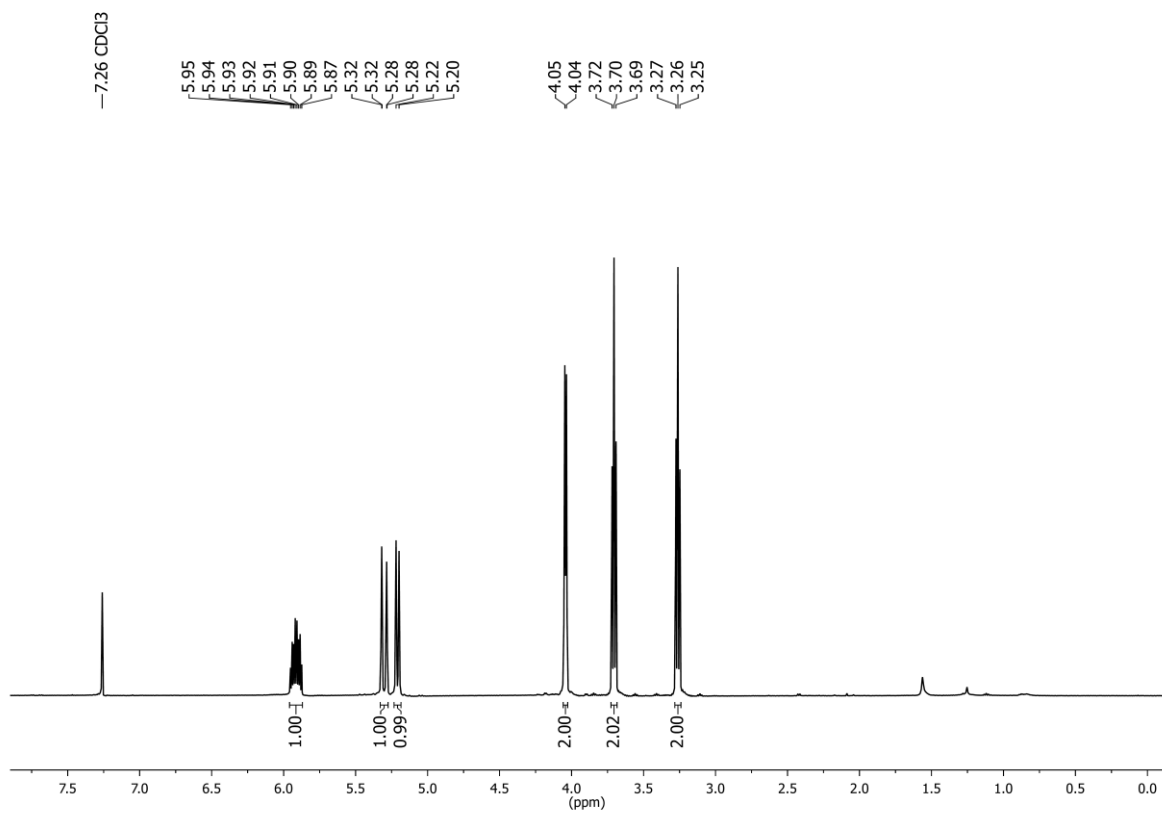
6: $^1\text{H-NMR}$



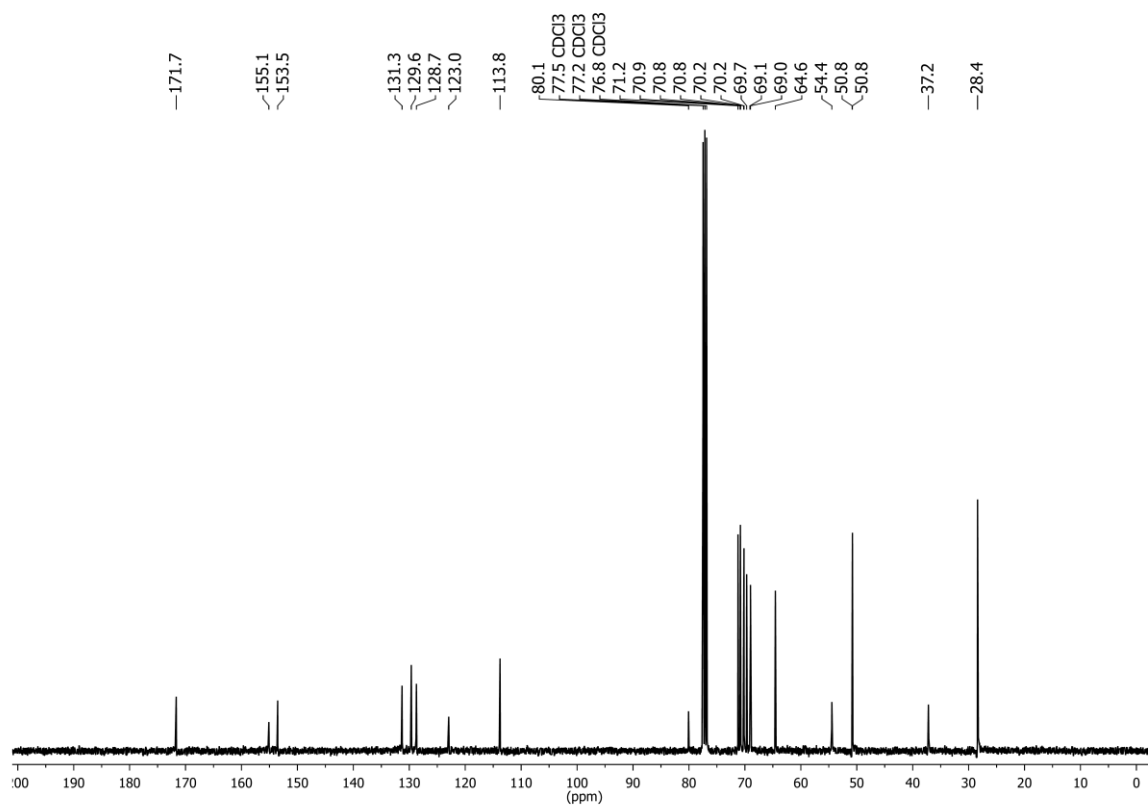
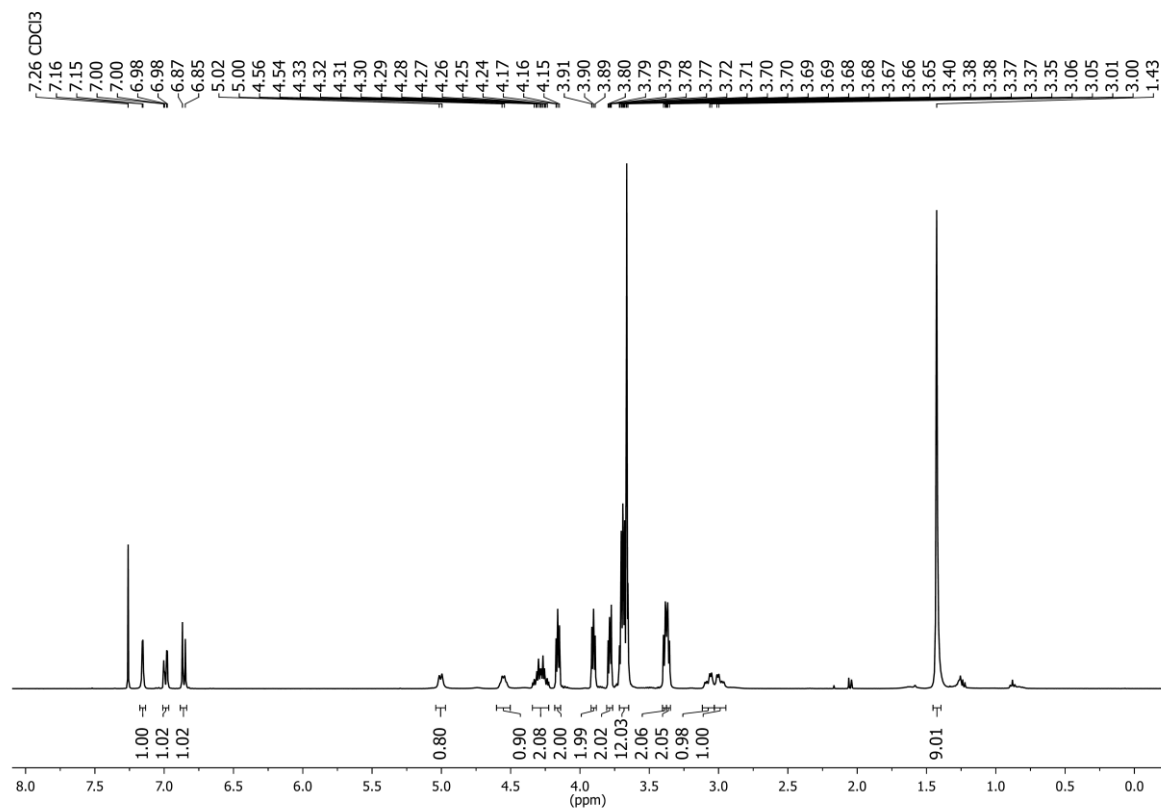
8: ^1H -NMR and ^{13}C -NMR



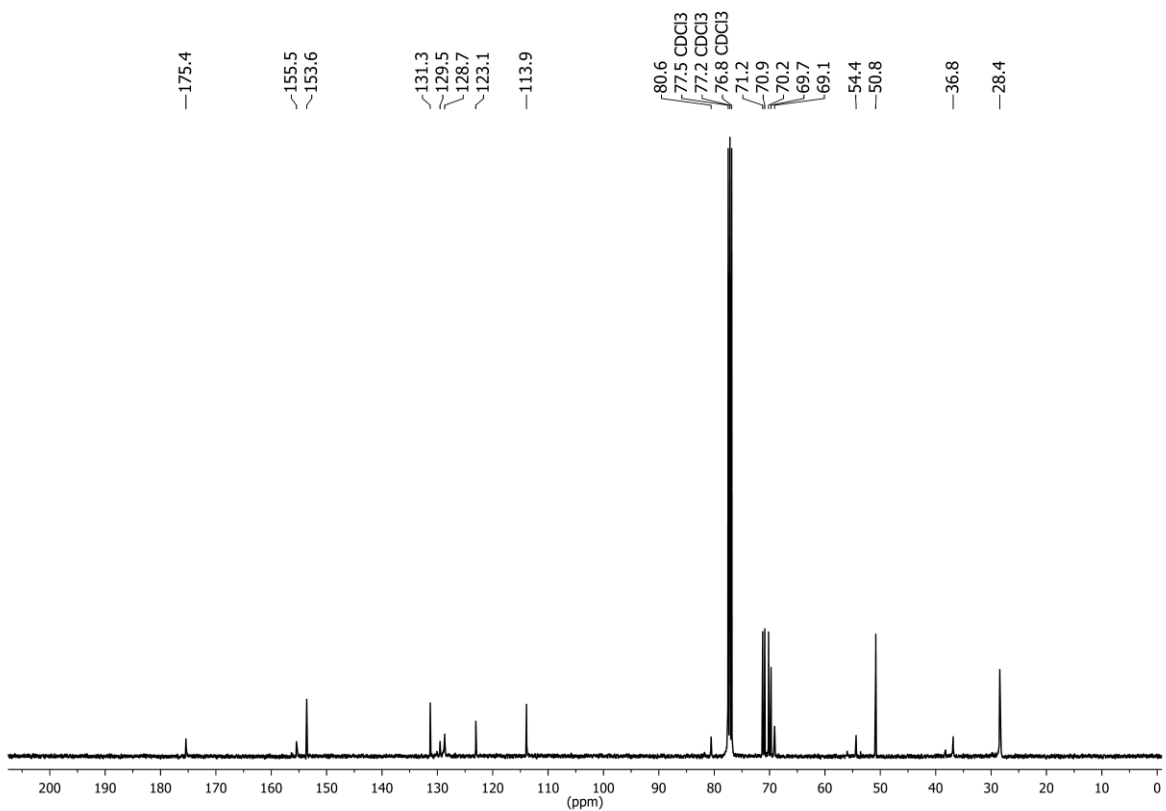
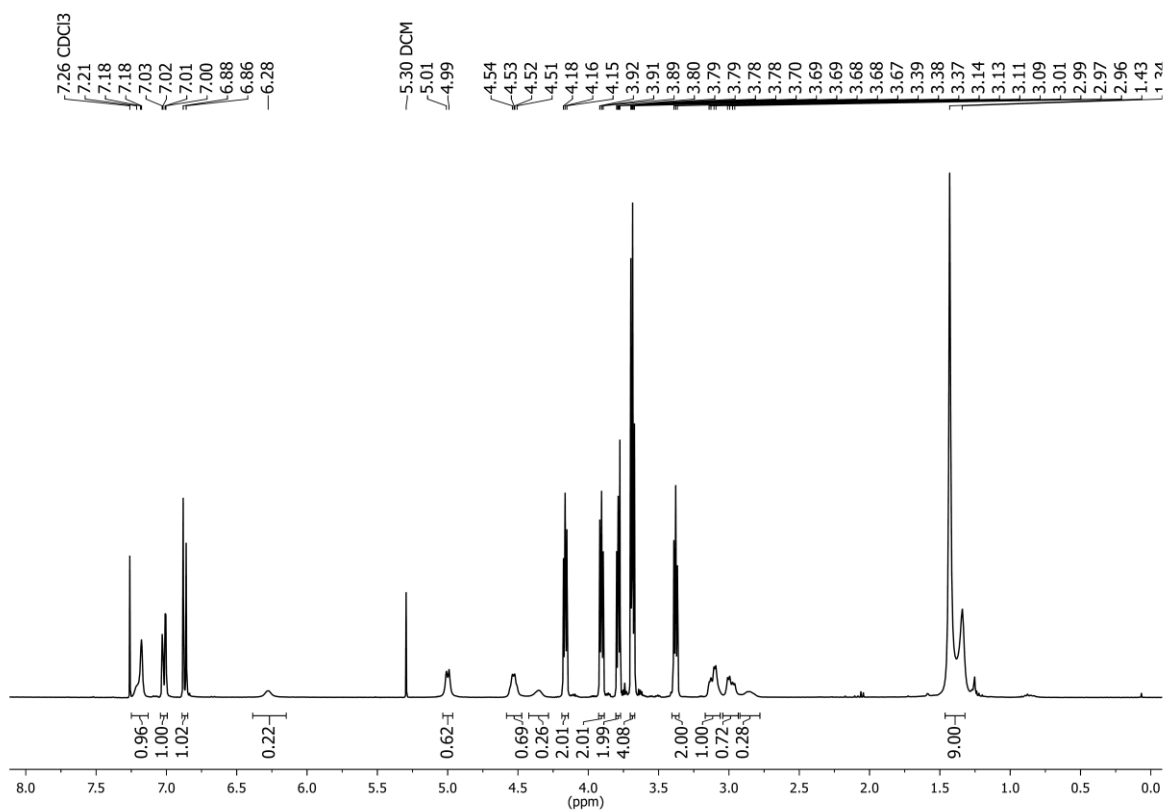
9: ^1H -NMR and ^{13}C -NMR



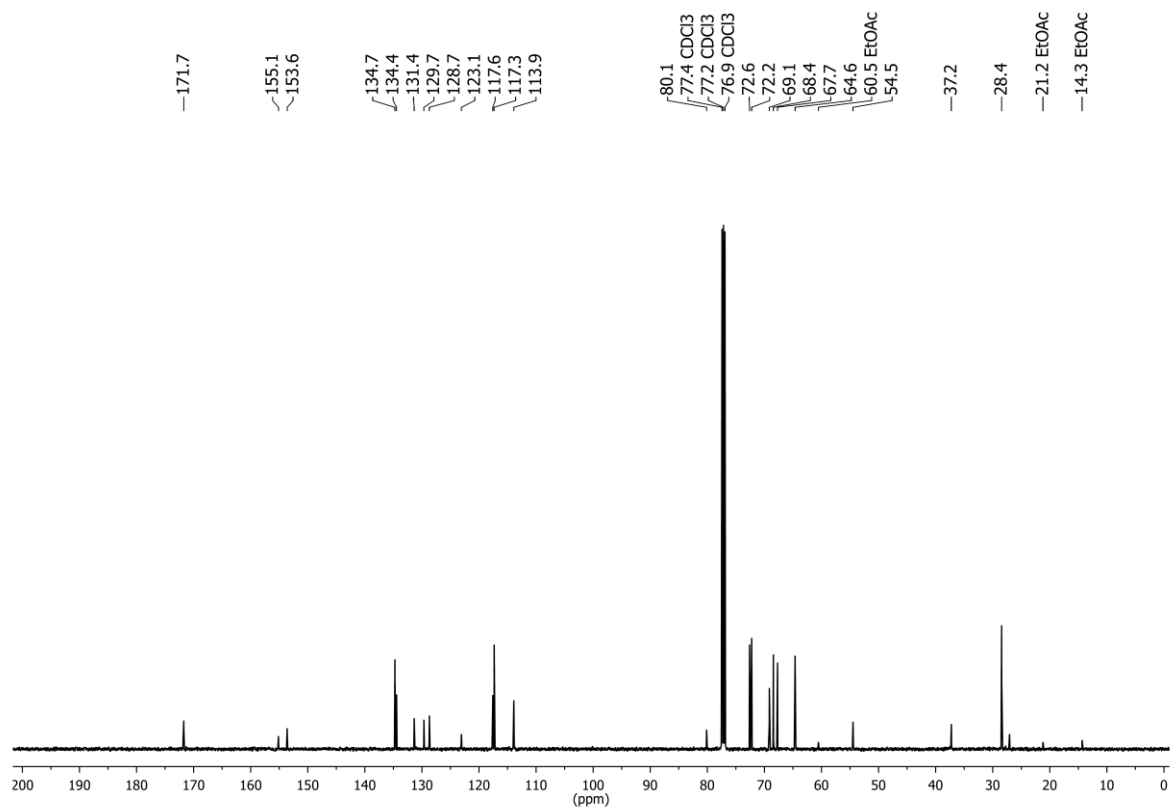
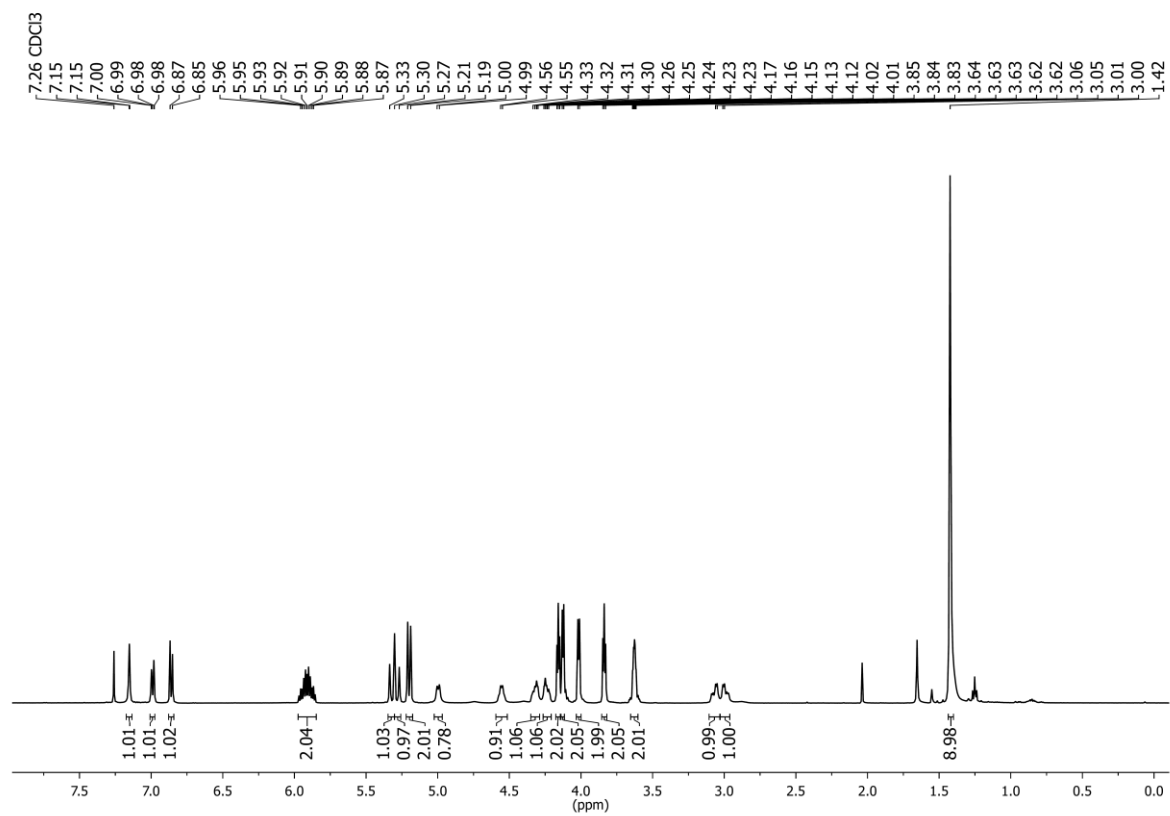
11: $^1\text{H-NMR}$ and $^{13}\text{C-NMR}$



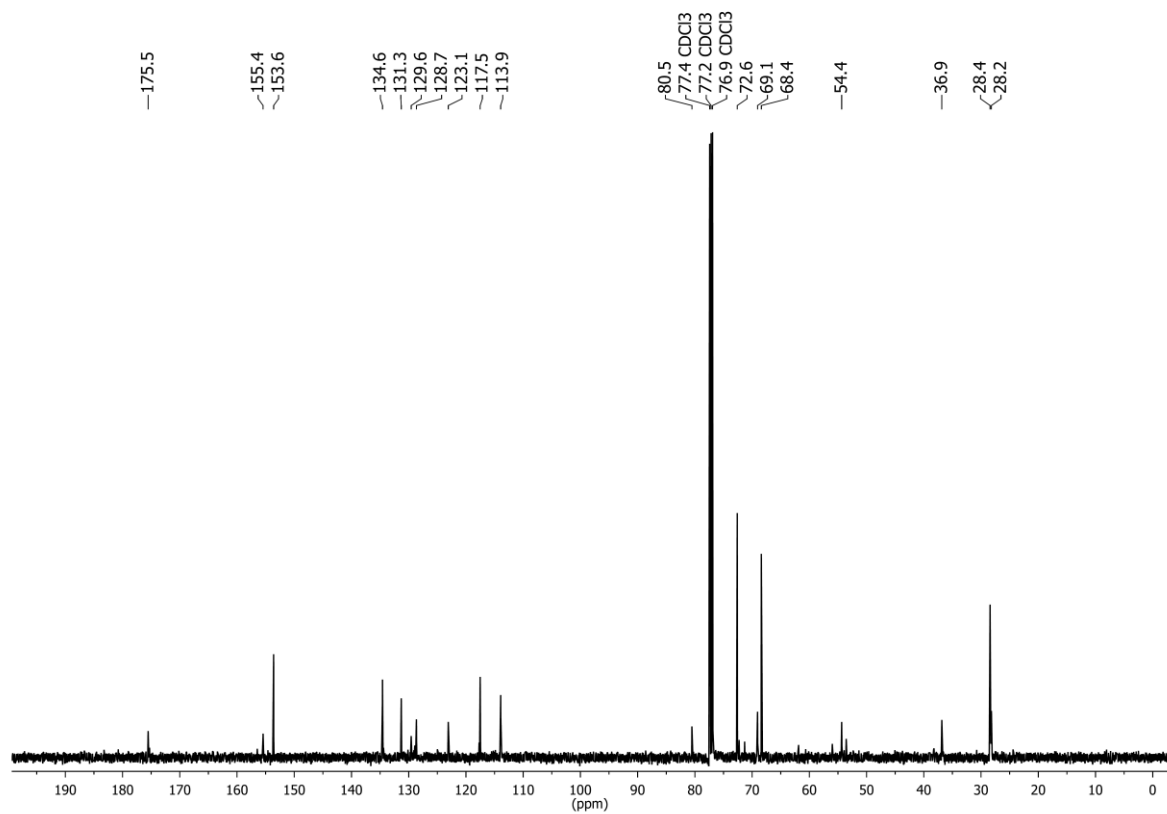
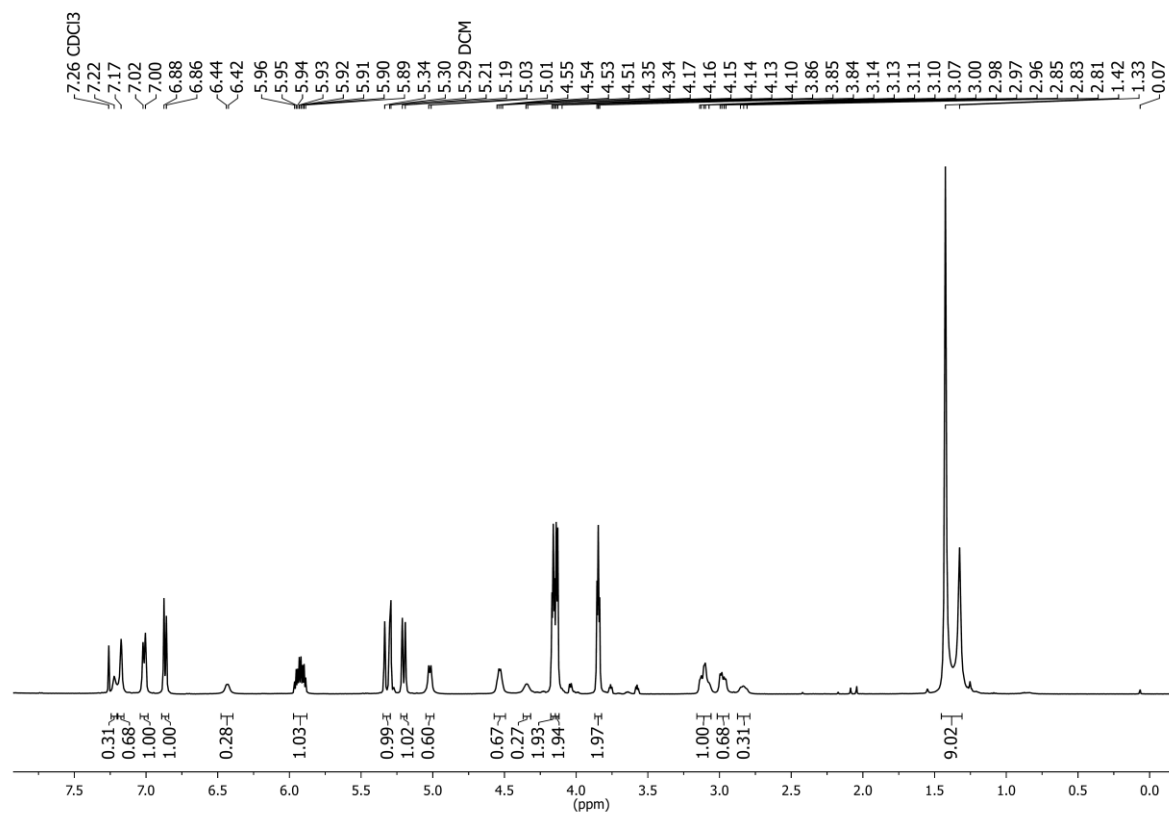
13: ¹H-NMR and ¹³C-NMR



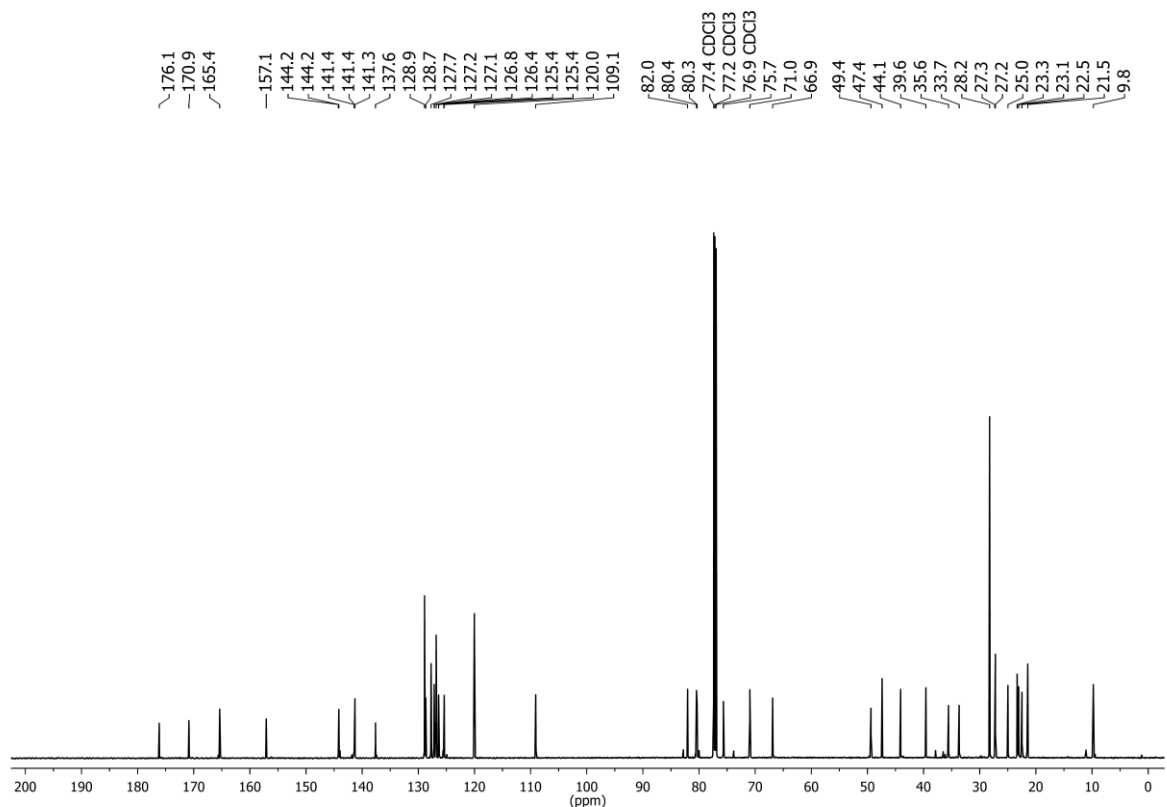
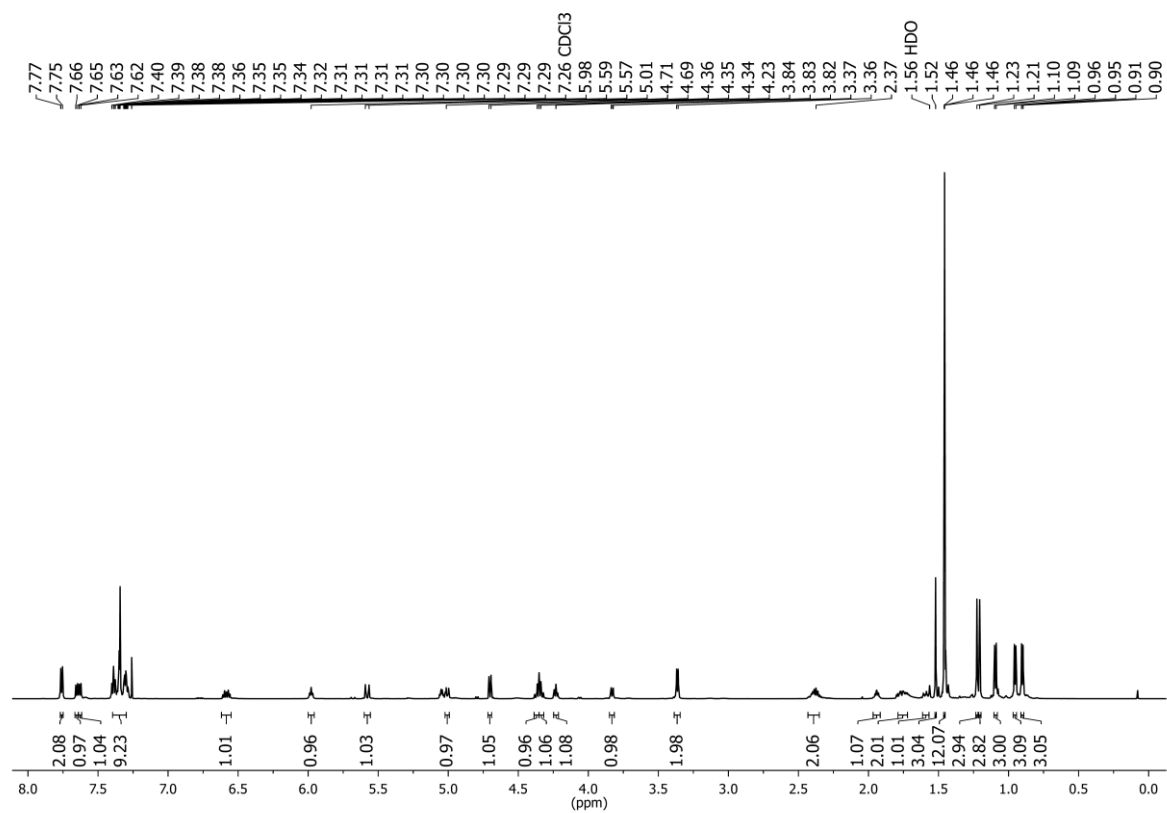
12: $^1\text{H-NMR}$ and $^{13}\text{C-NMR}$



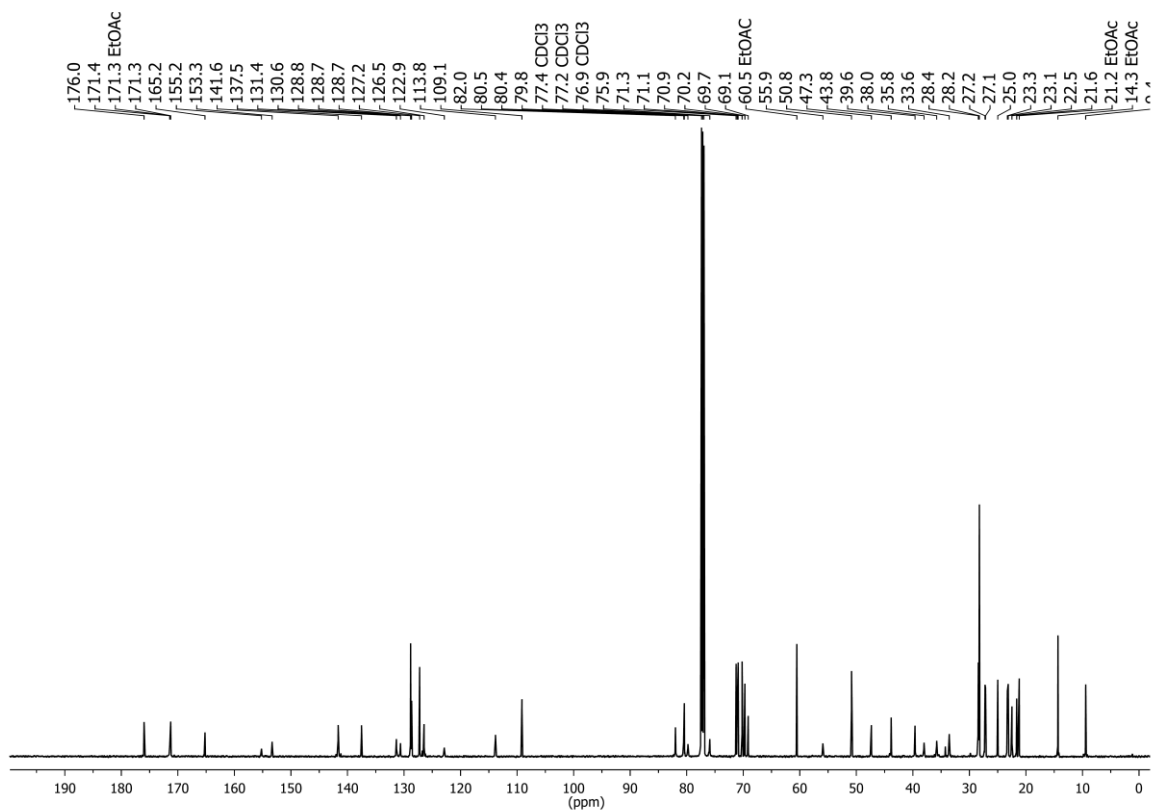
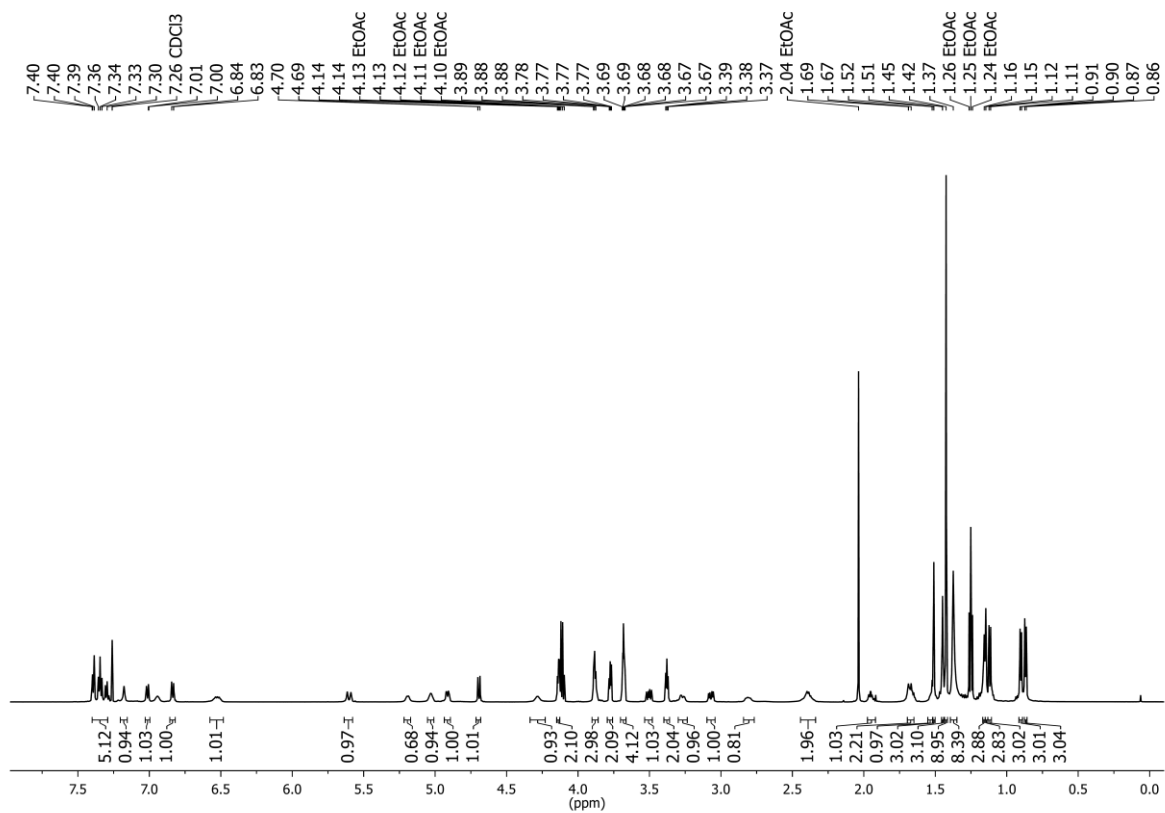
14: $^1\text{H-NMR}$ and $^{13}\text{C-NMR}$



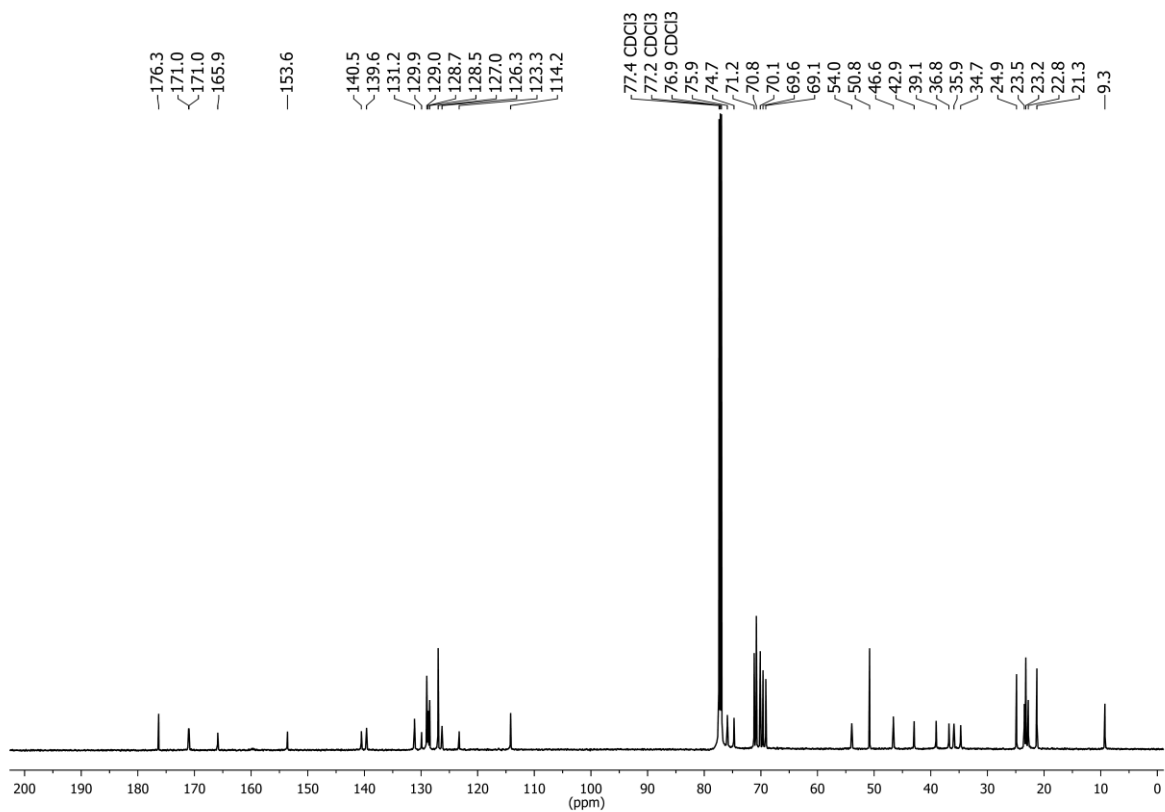
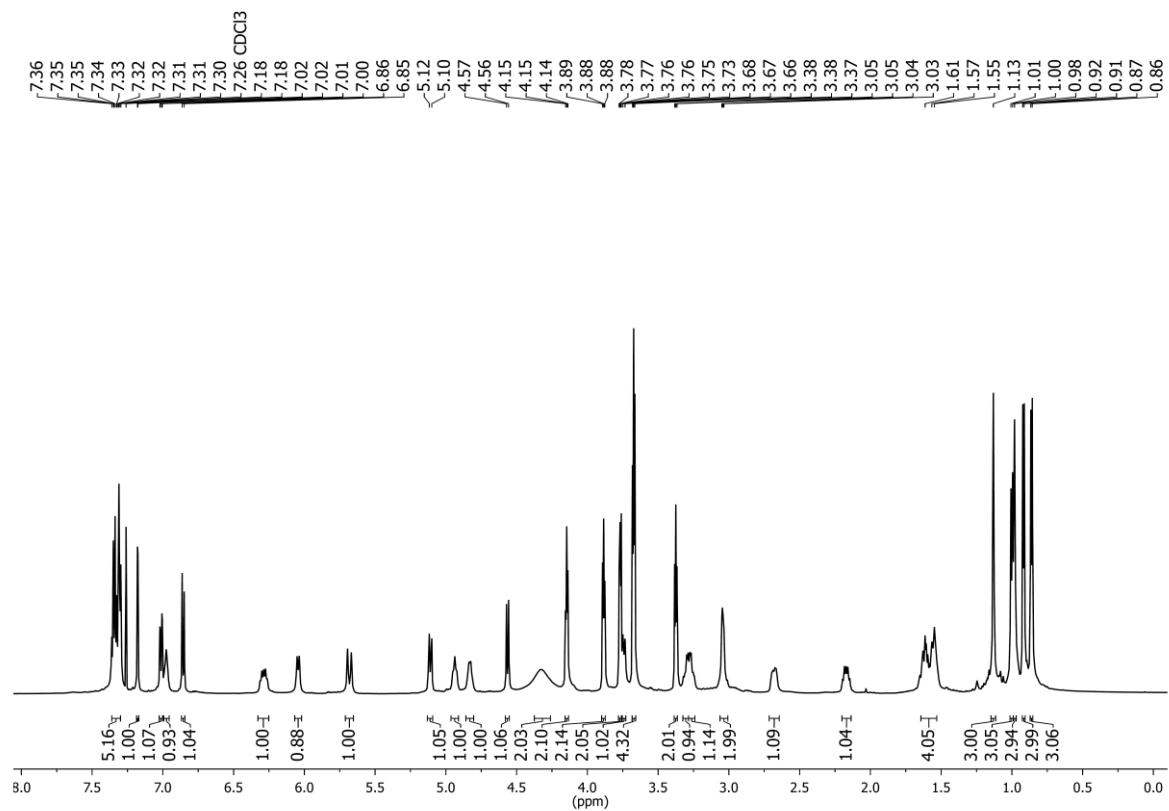
17: $^1\text{H-NMR}$ and $^{13}\text{C-NMR}$

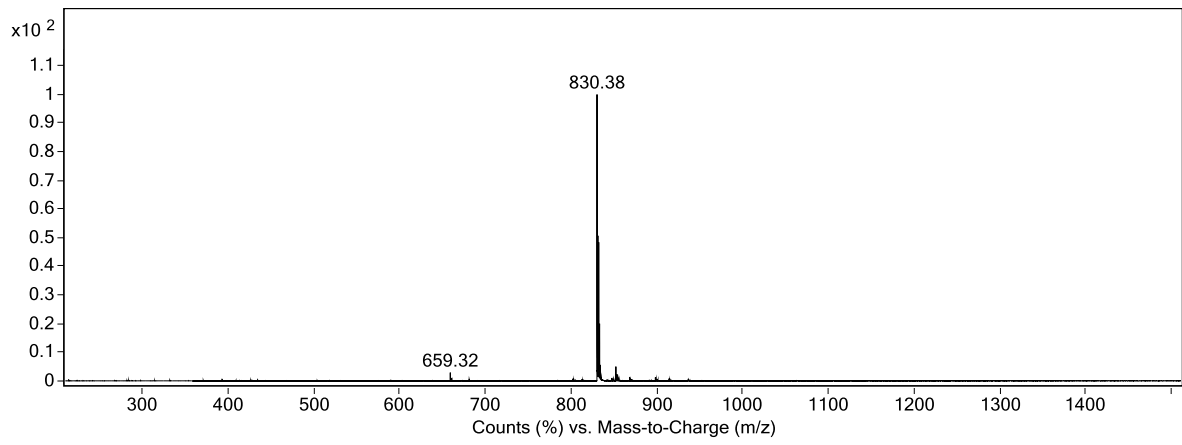
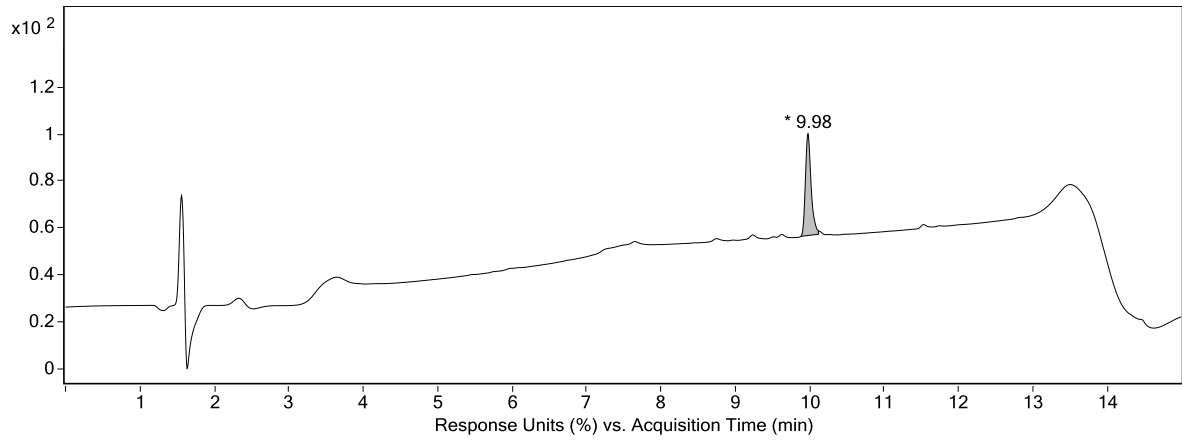


18: ^1H -NMR and ^{13}C -NMR

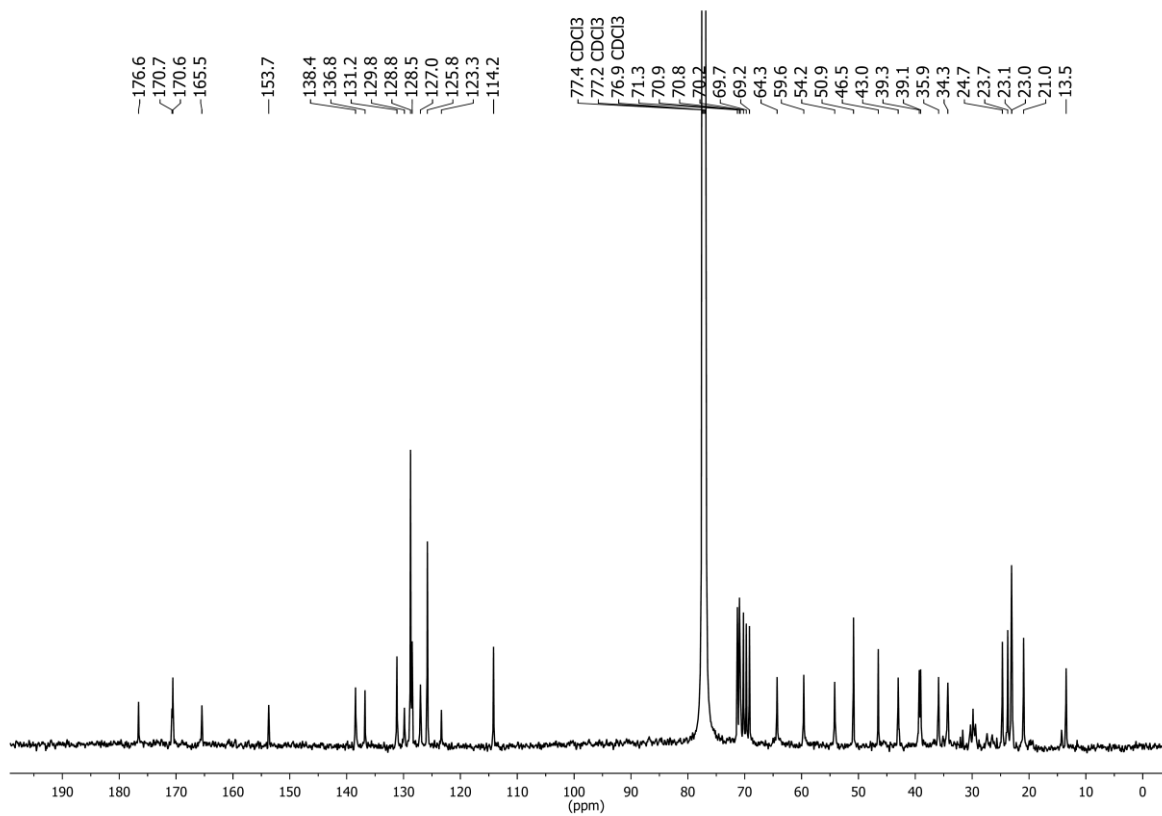
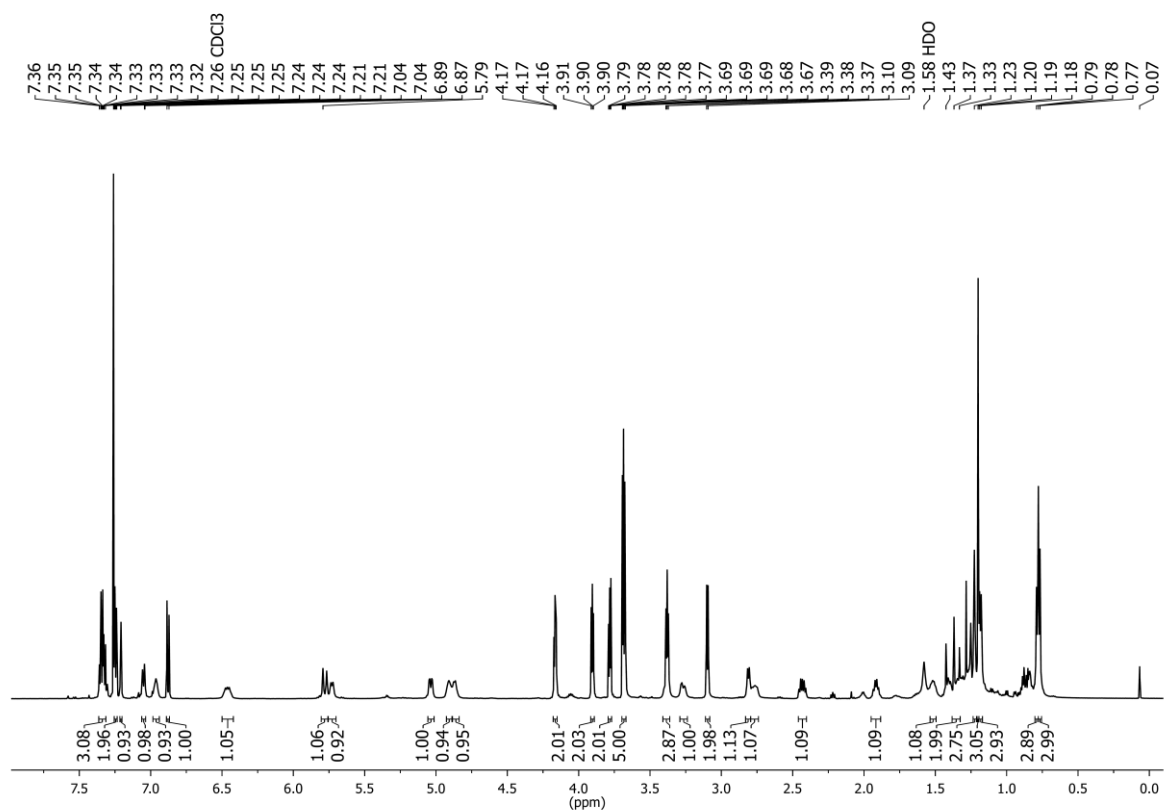


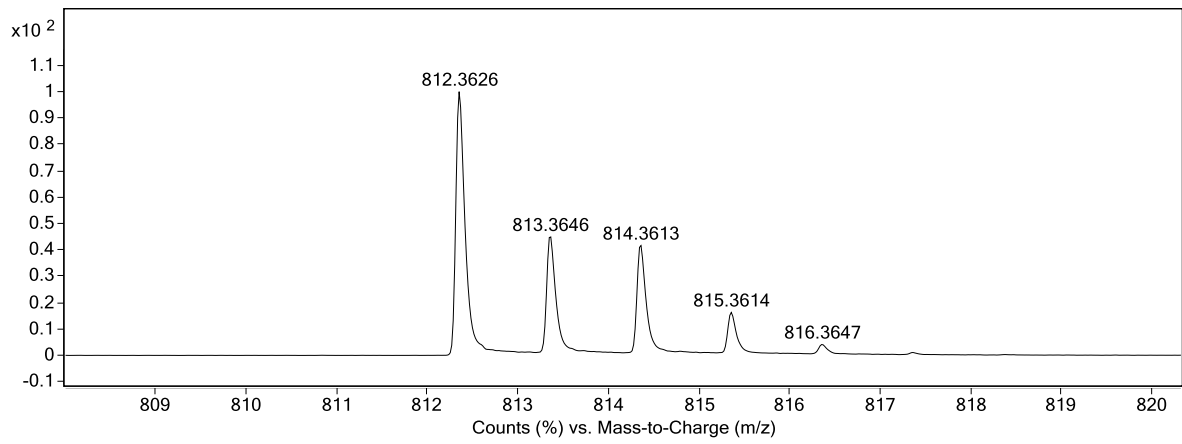
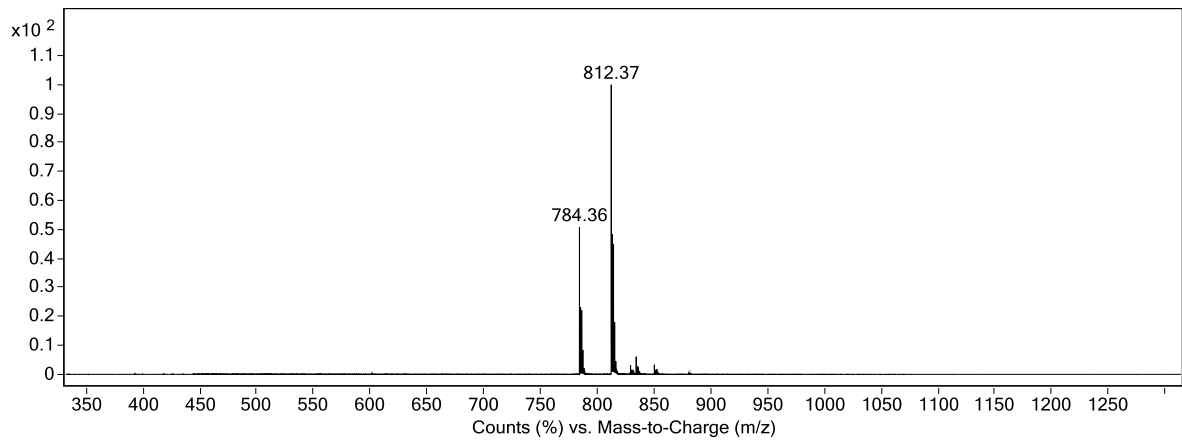
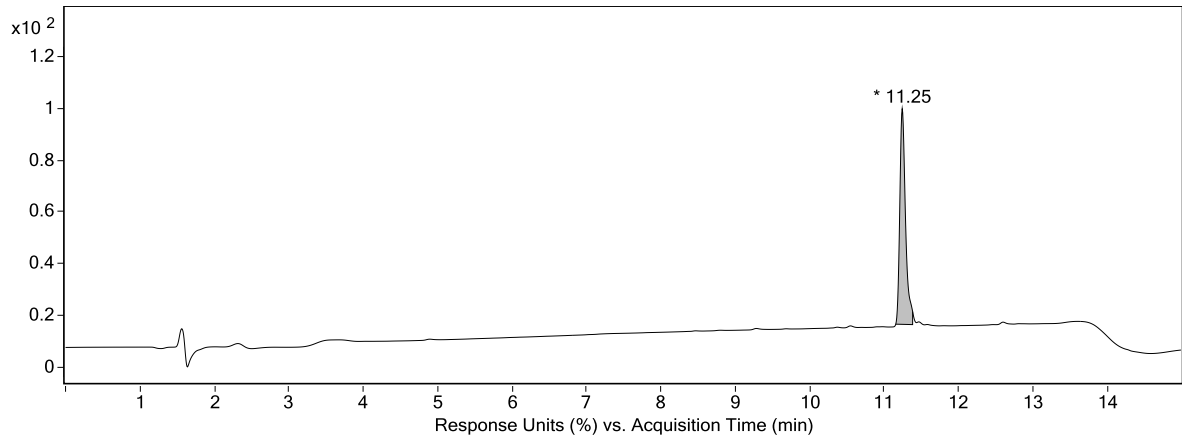
20: $^1\text{H-NMR}$, $^{13}\text{C-NMR}$ and HPLC-MS



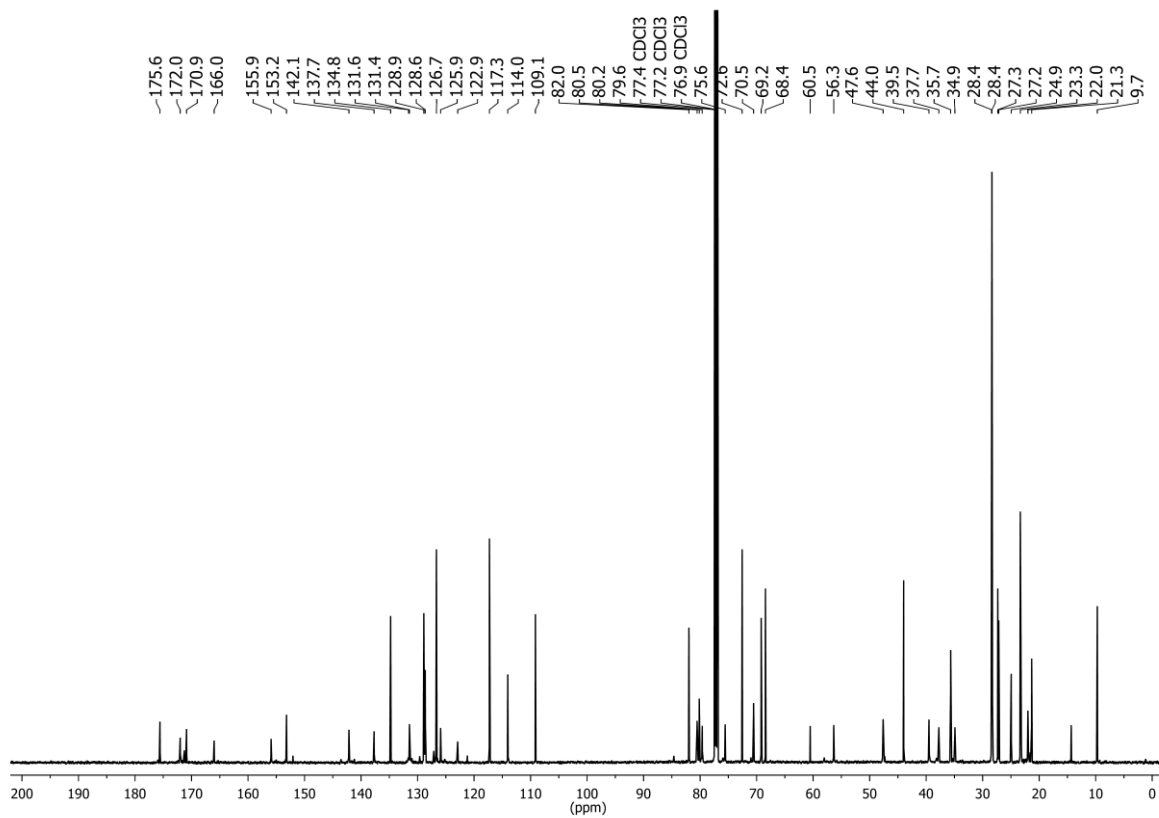
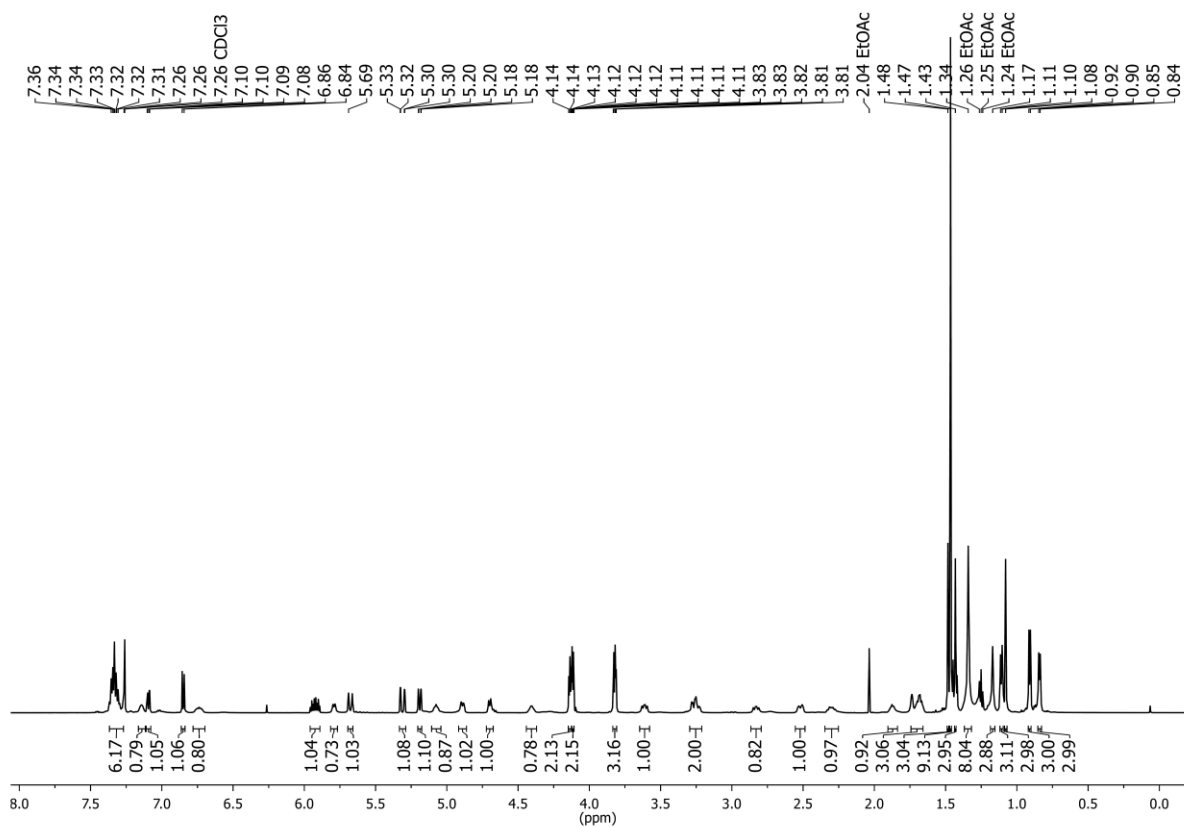


22: ¹H-NMR, ¹³C-NMR, HPLC-MS and HRMS

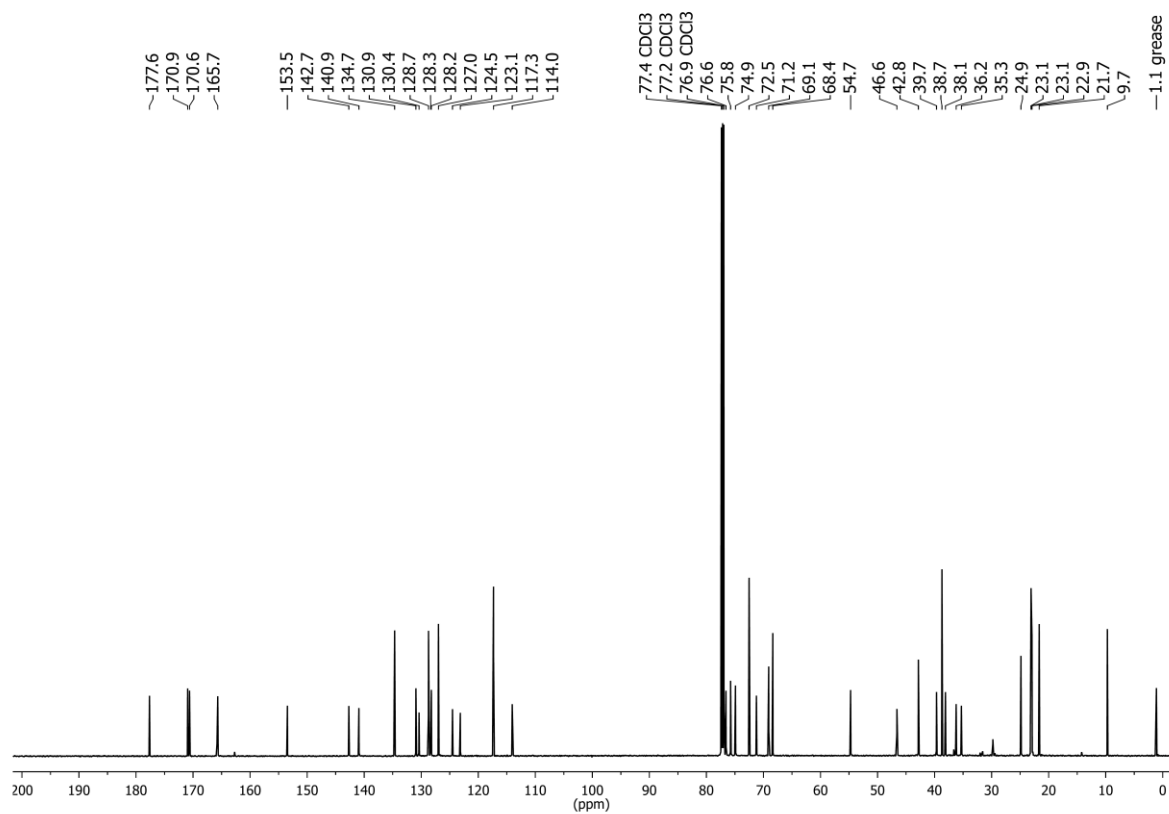
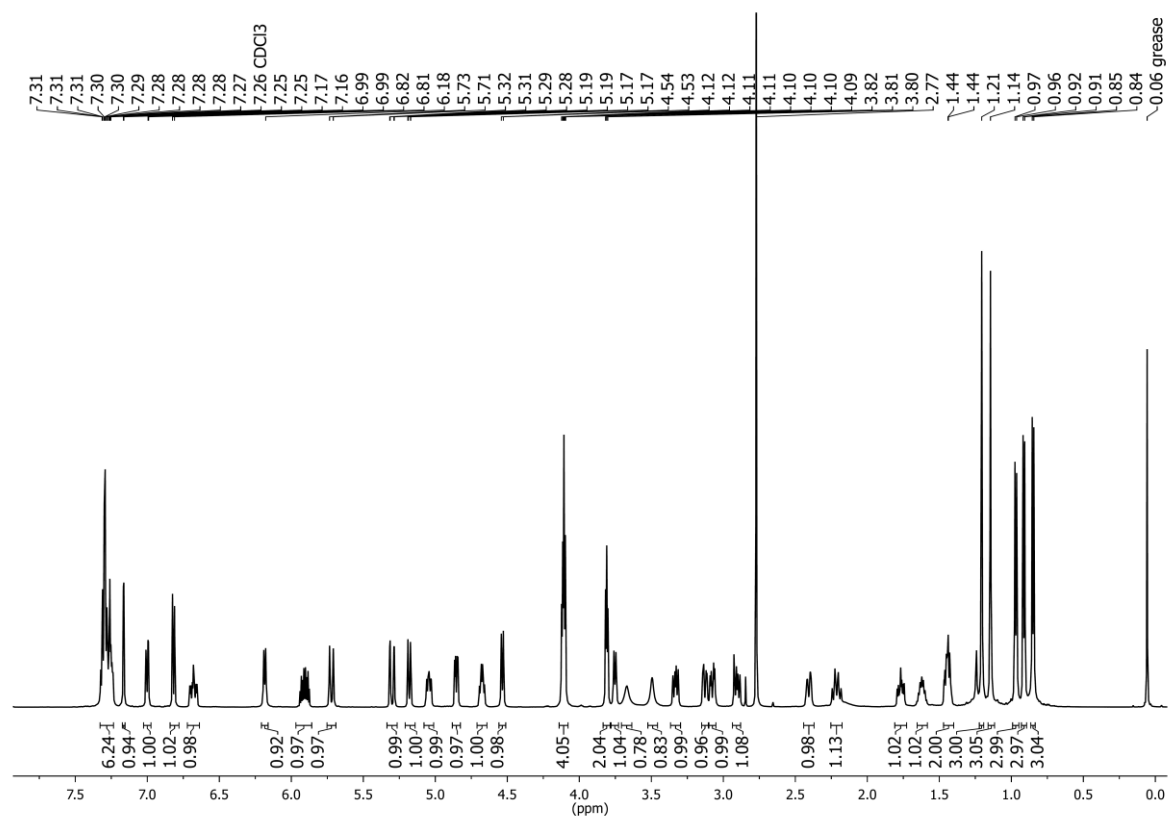


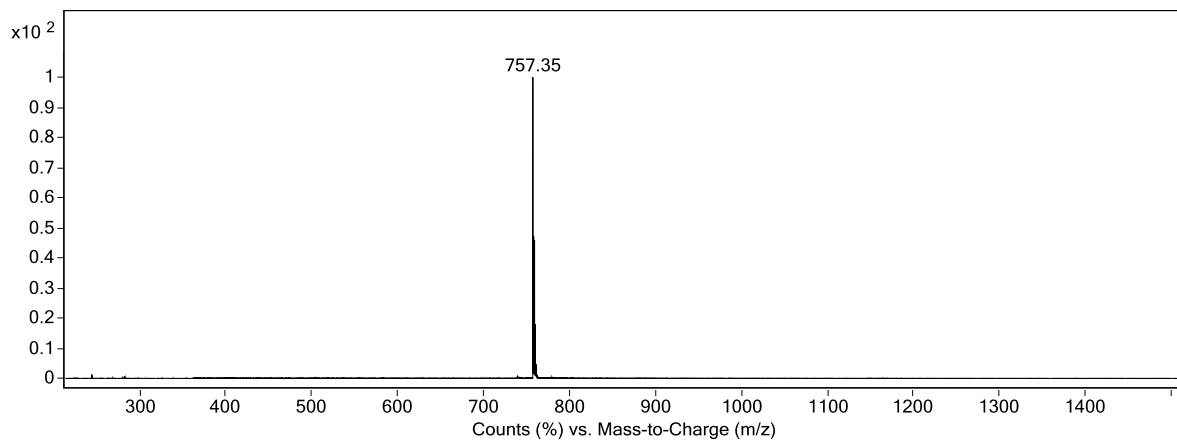
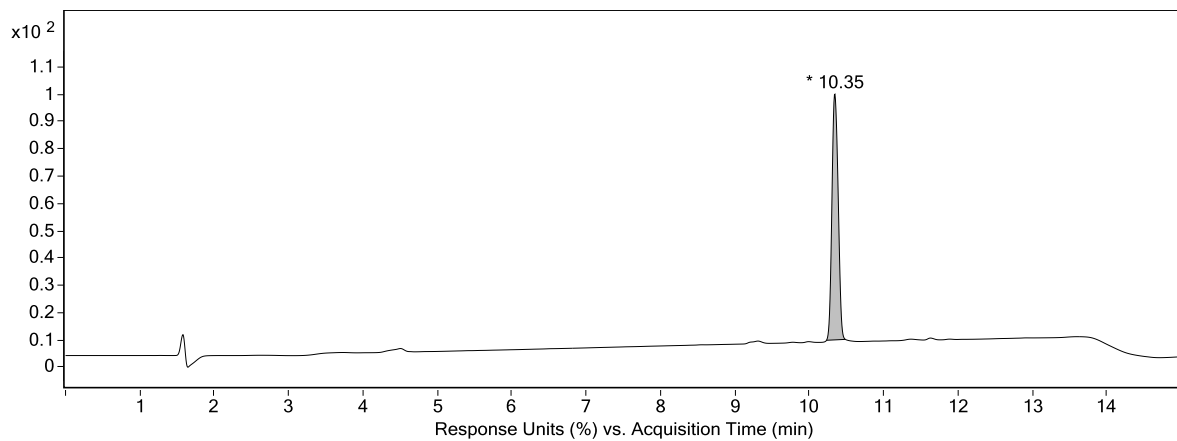


19: $^1\text{H-NMR}$ and $^{13}\text{C-NMR}$

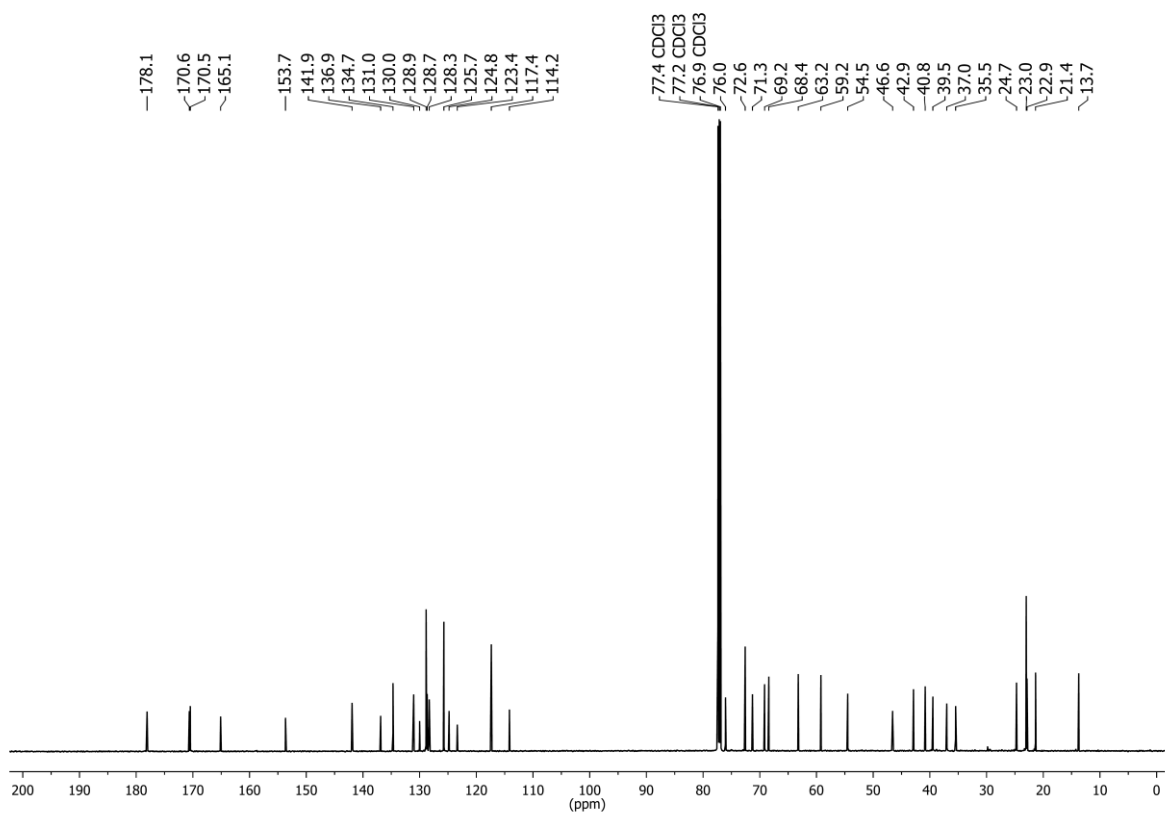
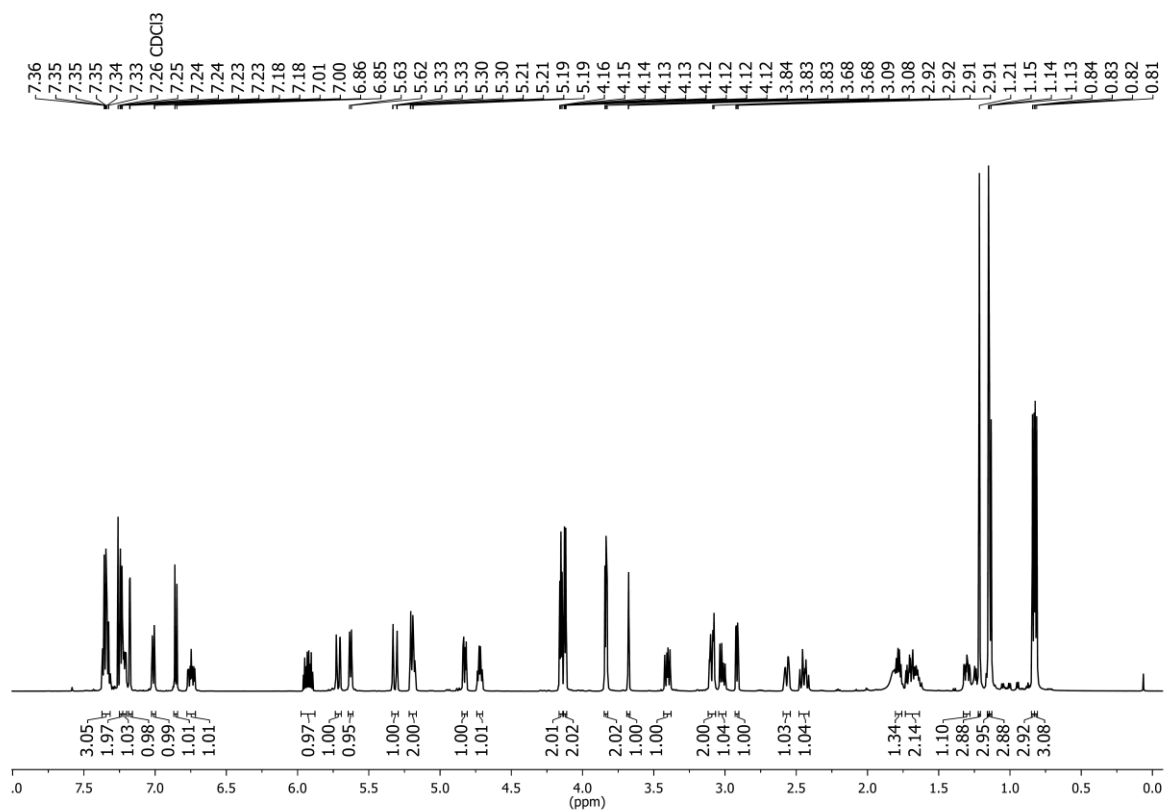


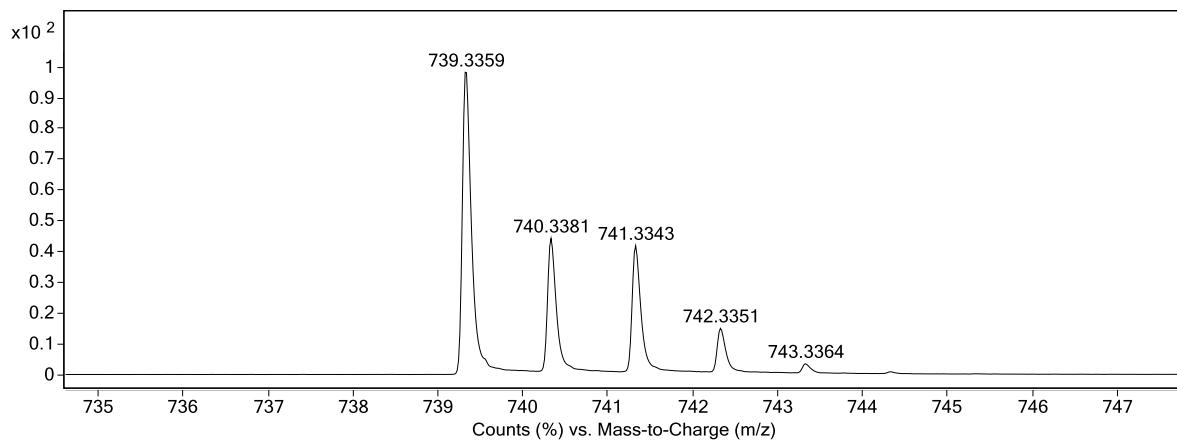
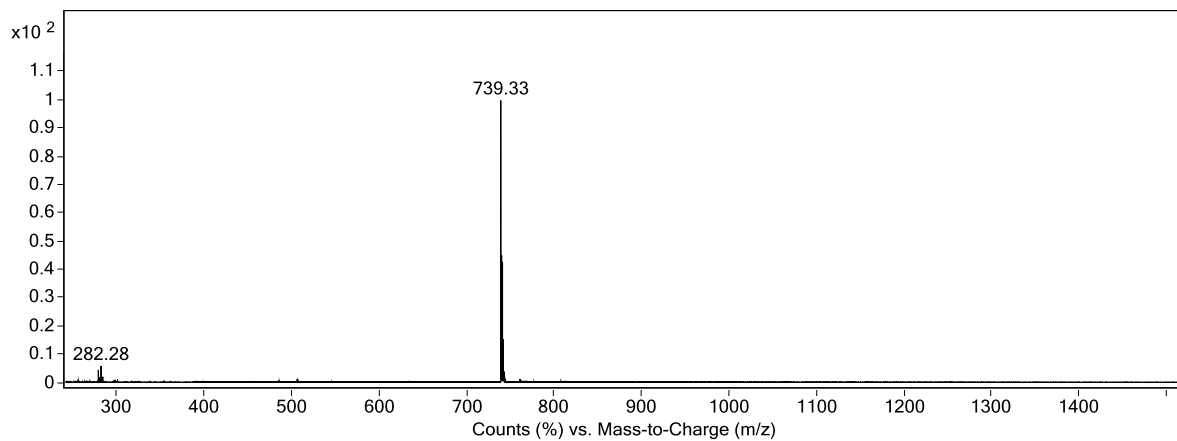
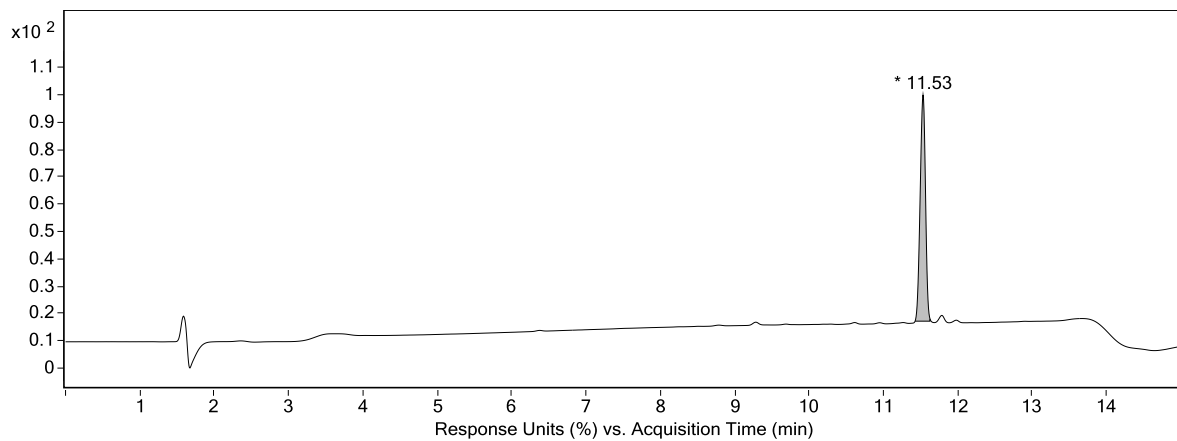
21: $^1\text{H-NMR}$, $^{13}\text{C-NMR}$ and HPLC-MS



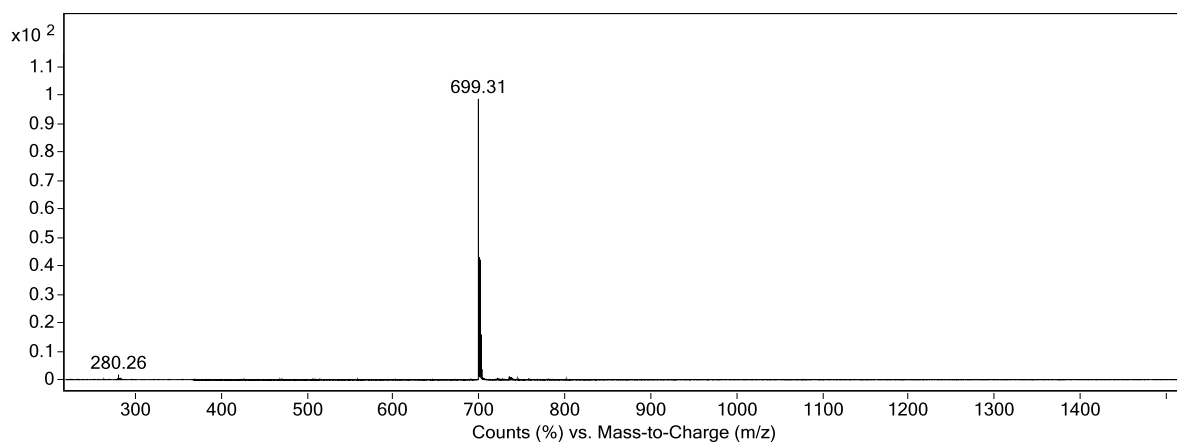
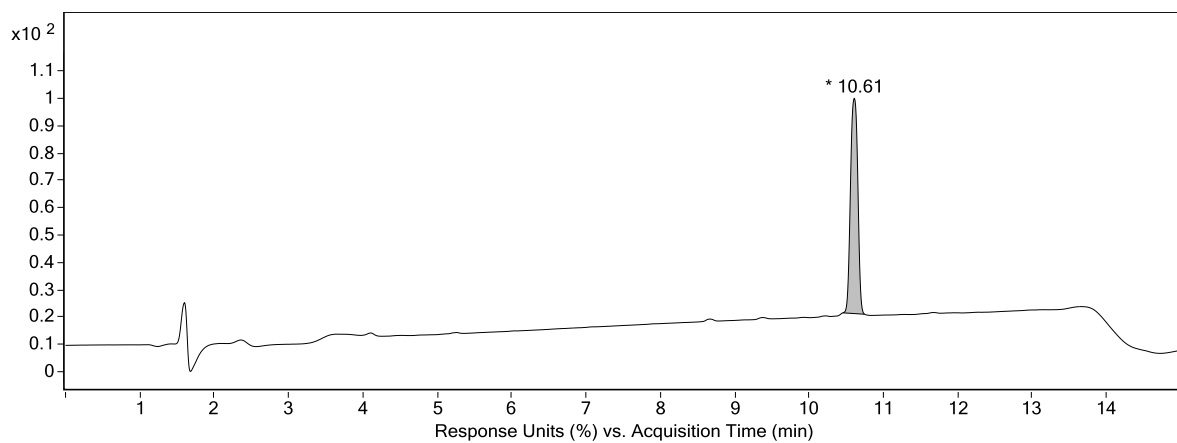
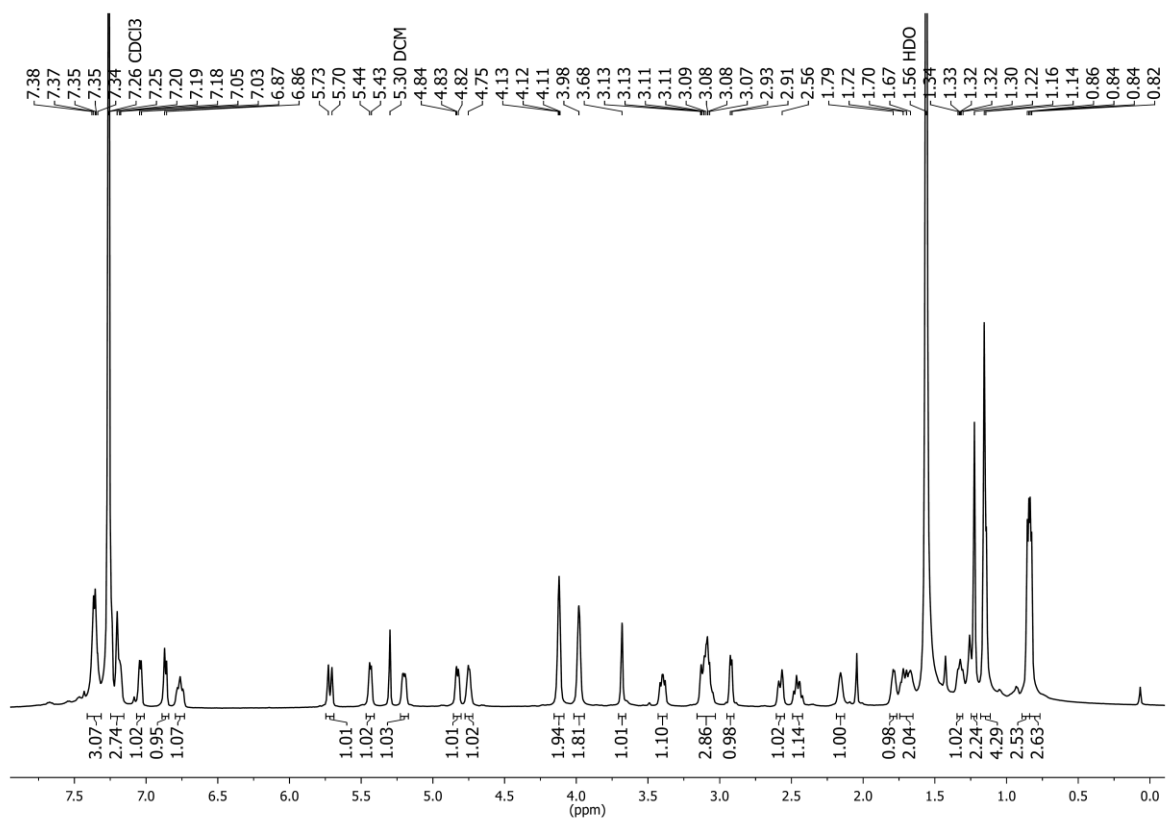


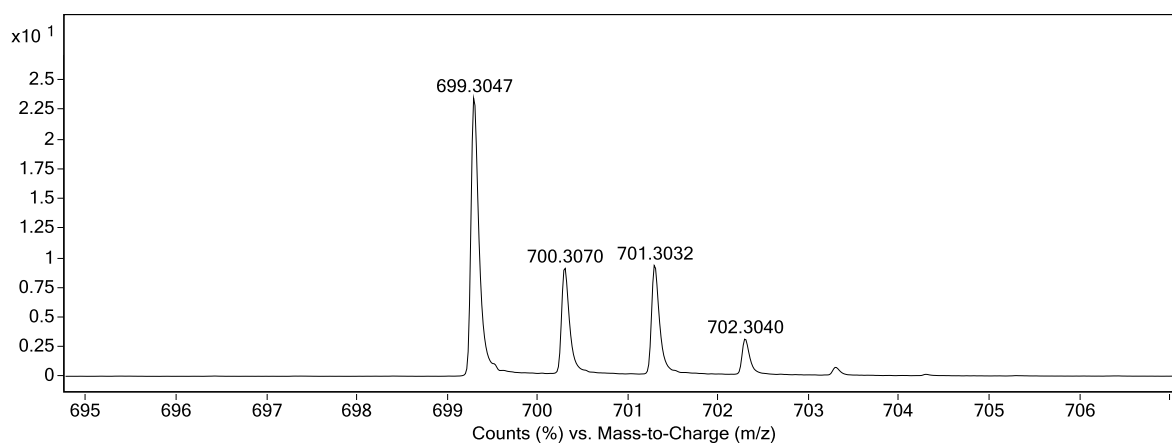
23: $^1\text{H-NMR}$, $^{13}\text{C-NMR}$, HPLC-MS and HRMS





24: ¹H-NMR, HPLC-MS and HRMS





5) References

- [1] G. M. Morris, D. S. Goodsell, R. S. Halliday, R. Huey, W. E. Hart, R. K. Belew, A. J. Olson, *J. Comput. Chem.* **1998**, *19*, 1639–1662.
- [2] L. Börjesson, C. J. Welch, *Acta Chem. Scand.* **1991**, *45*, 621–626.
- [3] S. Eissler, M. Nahrwold, B. Neumann, H.-G. Stammeler, N. Sewald, *Org. Lett.* **2007**, *9*, 817–819.
- [4] M. Nahrwold, C. Weiß, T. Bogner, F. Mertink, J. Conradi, B. Sammet, R. Palmisano, S. Royo Gracia, T. Preuße, N. Sewald, *J. Med. Chem.* **2013**, *56*, 1853–1864.

7.2 – Appendix II: supporting information of chapter 4

Supporting information

for

***In vivo* anti-tumor activity of a novel acetazolamide-cryptophycin conjugate for the treatment of renal cell carcinoma**

Samuele Cazzamalli,^{a,†} Eduard Figueras,^{b,†} Lilla Pethő,^{b,c} Adina Borbély,^b Christian Steinkühler,^d Dario Neri,^{a,*} and Norbert Sewald^{b,*}

^a Department of Chemistry and Applied Biosciences, Swiss Federal Institute of Technology (ETH Zürich), Vladimir-Prelog-Weg 4, CH-8093 Zürich, Switzerland

^b Department of Chemistry, Organic and Bioorganic Chemistry, Bielefeld University, Universitätsstraße 25, D-33615 Bielefeld, Germany

^c MTA-ELTE Research Group of Peptide Chemistry, Hungarian Academy of Sciences, Eötvös L. University, H-1117 Budapest, Hungary

^d Exiris s.r.l., Via Savona 6, I-00182 Rome, Italy

† These authors contributed equally to this work

* Corresponding author

Email: Dario Neri* - neri@pharma.ethz.ch

Norbert Sewald* - Norbert.sewald@uni-bielefeld.de

Table of contents

List of abbreviations	3
General remarks and procedures	4
NMR and HPLC-MS of compounds 3, 4, 5 and 7	6
References	10

List of abbreviations

δ	Chemical shift
Cit	Citruline
DCC	<i>N,N'</i> -Dicyclohexylcarbodiimide
DCM	Dichloromethane
DIPEA	<i>N,N'</i> -Diisopropylethylamine
4-DMAP	4-Dimethylaminopyridine
DMSO	Dimethyl sulfoxide
DMF	<i>N,N'</i> -dimethylformamide
EDC·HCl	<i>N</i> -(3-Dimethylaminopropyl)- <i>N'</i> -ethylcarbodiimide hydrochloride
EtOAc	Ethyl acetate
FCS	Fetal calf serum
HATU	1-[Bis(dimethylamino)methylene]-1H-1,2,3-triazolo[4,5-b]pyridinium 3-oxid hexafluorophosphate
HOAt	1-Hydroxy-7-azabenzotriazole
LC-MS	Liquid Chromatography - Mass Spectrometry
MMAE	Monomethyl Auristatin E
NHS	N-Hydroxysuccinimide
NMR	Nuclear magnetic resonance
PABOH	<i>p</i> -aminobenzyl alcohol
PABC	<i>p</i> -aminobenzyl carbamate/carbonate
PBS	Phosphate buffered saline
PE	Petroleum ether
RP-HPLC	Reverse phase – High Performance Liquid Chromatography
RPMI	Roswell Park Memorial Institute
SPR	Surface plasmon resonance
TBS	Tris buffered saline
Val	Valine

General remarks and procedures

All reactions requiring anhydrous conditions were performed under argon atmosphere. DMF was dried over 4Å molecular sieves and DCM was distilled from CaH₂. Peptide grade DMF for solid phase synthesis was bought from ABCR. H-Cys(Trt)-2-CT-polystyrene resin was purchased from RAPP Polymere. Maleimidocaproyl-ValCit-PABC-MMAE was purchased from Levena Biopharma (No.9 Weidi Road, Qixia District, Nanjing, 210046, China). All the other chemicals and solvents (HPLC-grade or reagent-grade quality), unless otherwise stated, were purchased from commercial sources and used without further purification.

NMR spectroscopy

NMR spectra were recorded on a Bruker Avance 600 (¹H: 600 MHz) at 298 K. Chemical shifts were referenced to residual nondeuterated solvent signal (CDCl₃: ¹H: 7.26 ppm). Coupling constants (*J*) are reported in Hz with the following abbreviations used to indicate splitting: s = singlet, d = doublet, t = triplet, q = quartet, m = multiplet, br = broad signal. The acronyms uA, uB, uC and uD describe signals pertaining to cryptophycin units A-D.

Liquid chromatography - mass spectrometry

LC-MS were conducted using an Agilent 1200 series consisting of an autosampler, degasser, binary pump, column oven and diode array detector coupled to an Agilent 6220 accurate-mass TOF LC/MS. A Hypersil Gold C₁₈ (150 mm x 2.1 mm, 3 μm particle size) was used as a column.

Eluent A: H₂O/CH₃CN/HCCO₂H = 95/5/0.1 and eluent B: H₂O/CH₃CN/HCCO₂H = 5/95/0.1.

Method A:

Flow rate:	300 μL/min	
0 min	100% A	0% B
10 min	2% A	98% B
11 min	2% A	98% B
11.5 min	100% A	0% B
15 min	100% A	0% B

Method B:

Alternatively, Ultra Performance Liquid Chromatography - High Resolution Mass Spectrometry (UPLC-HRMS) were recorded on a Waters Acquity UPLC H-Class System with PDA UV detector coupled to a Waters Xevo G2-XS QTOF, using an ACQUITY UPLC BEH C₁₈ Column (130 Å, 50 mm x 2.1 mm, 1.7 µm particle size) at a flow rate of 0.6 mL/min with linear gradients of solvents A and B (A = H₂O with 0.1% FA, B = CH₃CN with 0.1% FA).

Preparative reversed phase - high performance liquid chromatography

Preparative RP-HPLC were performed on a MERCK-HITACHI unit (controller: D-7000, pump: L7150, detector: L7420, UV-absorption measured at λ = 220 nm).

Eluent A: H₂O/CH₃CN/TFA = 95/5/0.1 and eluent B: H₂O/CH₃CN/TFA = 5/95/0.1

Method P1:

Column: Macherey-Nagel Nucleosil C₁₈ (250 mm x 10 mm, 7 µm particle size)

Flow rate: 4 mL/min

0 min	100% A	0% B
2 min	100% A	0% B
25 min	0% A	100% B
30 min	0% A	100% B
35 min	100% A	0% B

Alternatively, Preparative RP-HPLC were performed on a Waters Alliance HT RP-HPLC with PDA UV detector.

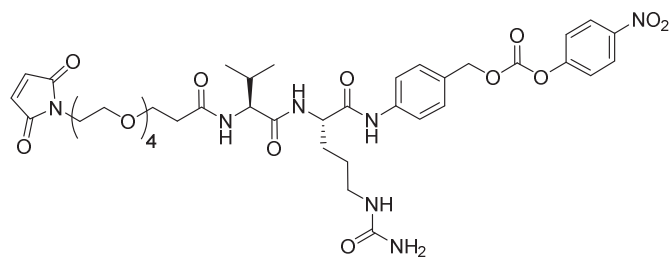
Method P2:

Column: Synergi C₁₈ Polar-RP 80Å (150 mm x 10 mm, 4µm particle size)

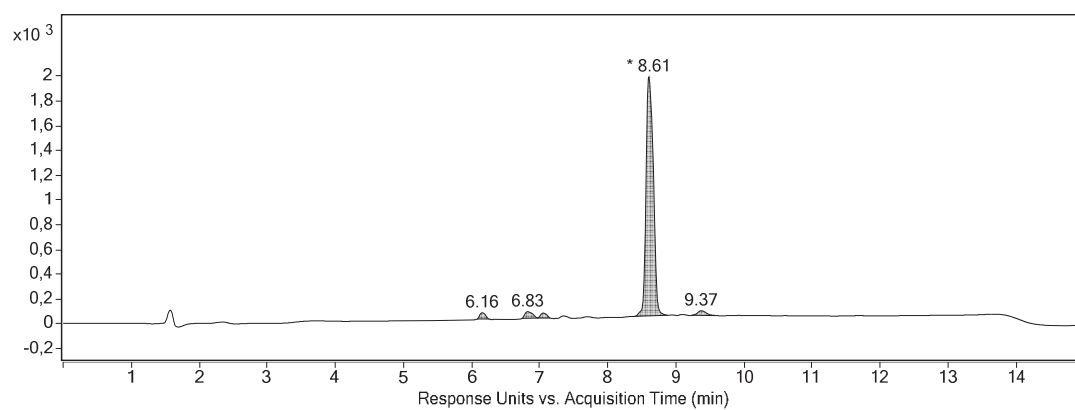
Flow rate: 4 mL/min

Linear gradients of solvents A and B (A = H₂O with 0.1% TFA, B = CH₃CN with 0.1% TFA): from 5% to 80% of B in 20 minutes.

Maleimide-PEG₄-Val-Cit-PABC-PNP (4):



a)



b)

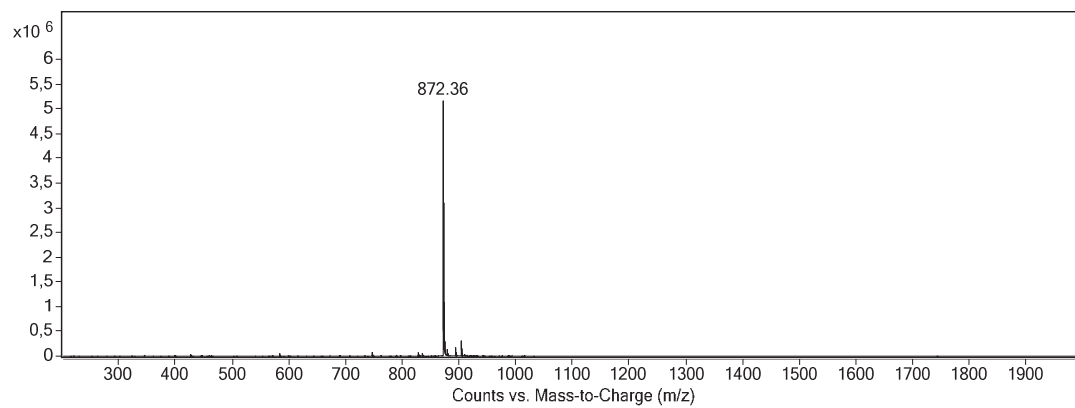
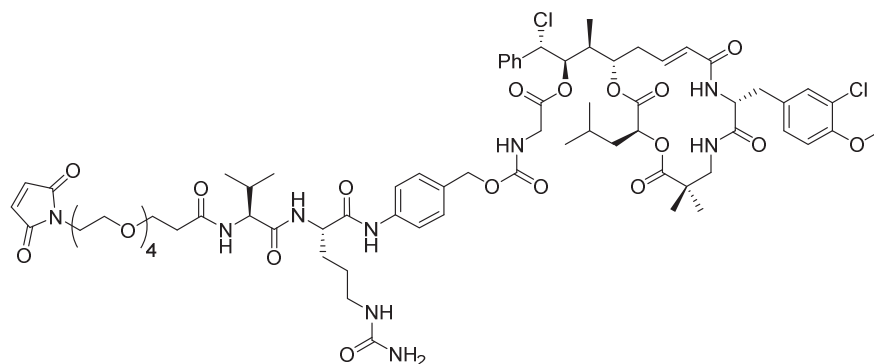
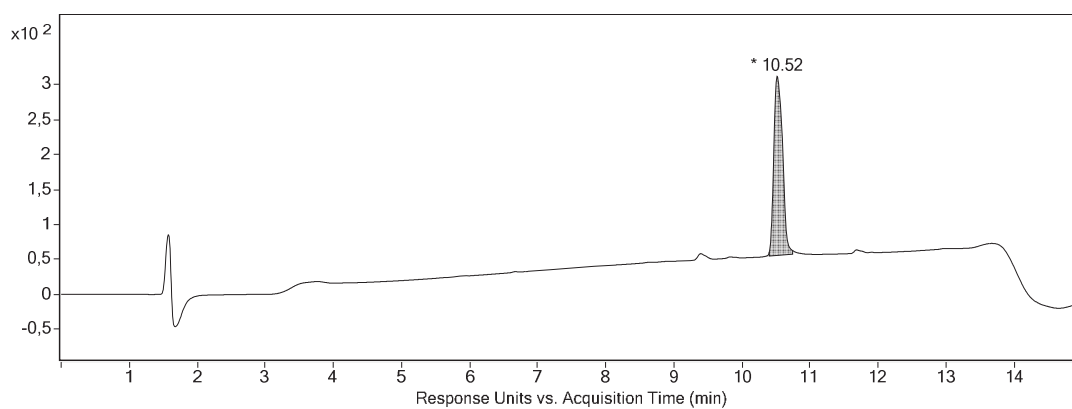


Figure S2: a) HPLC chromatogram ($\lambda = 220$ nm) b) MS spectra of compound **4**

Maleimide-PEG₄-Val-Cit-PABC-Cry55-gly (5):



a)



b)

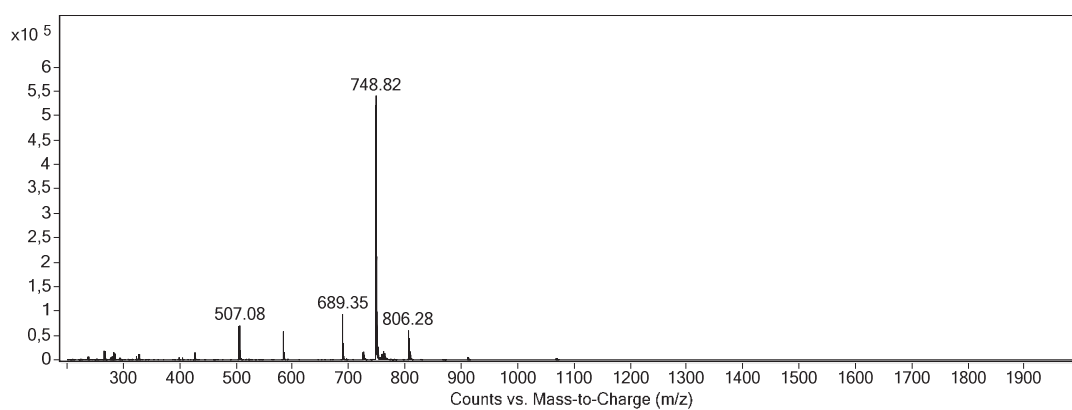
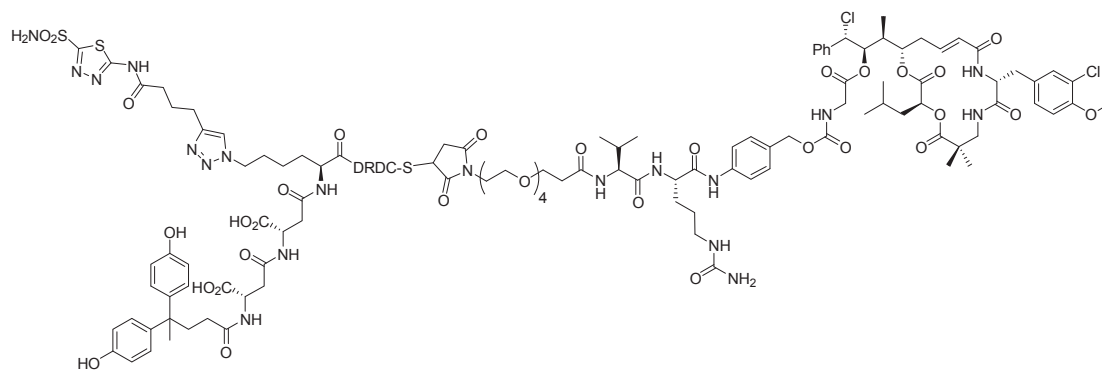
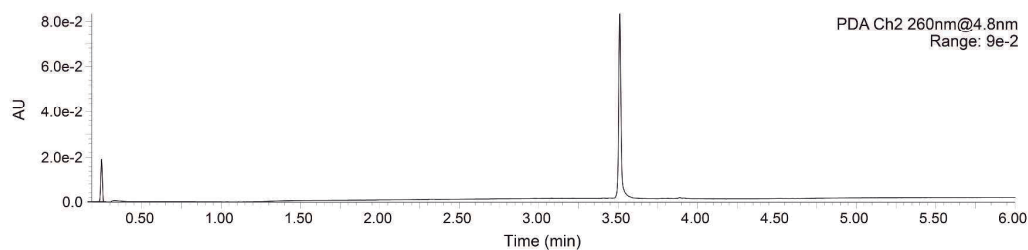


Figure S3: a) HPLC chromatogram ($\lambda = 220$ nm) b) MS spectra of compound **5**

AAZ⁺-ValCit-Cry55gly (7):



a)



b)

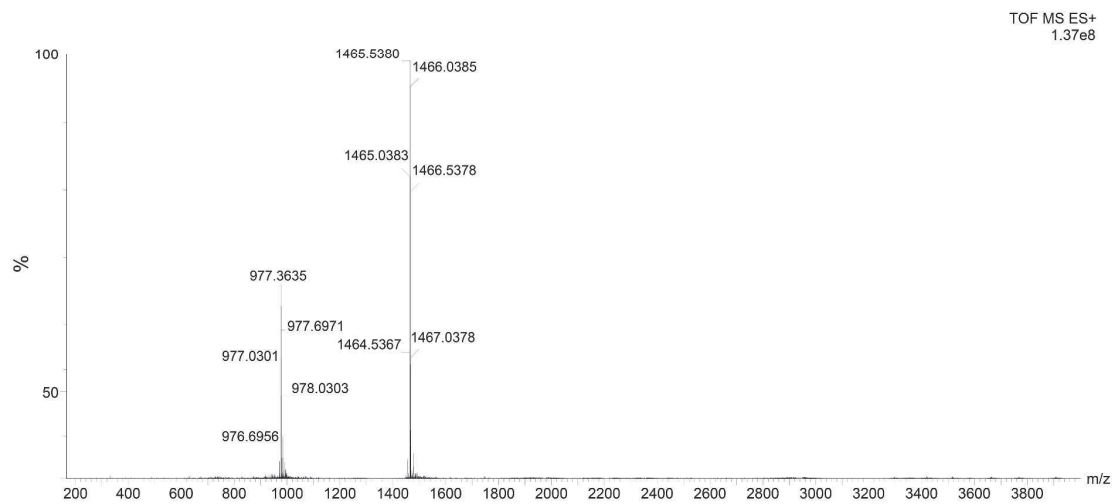
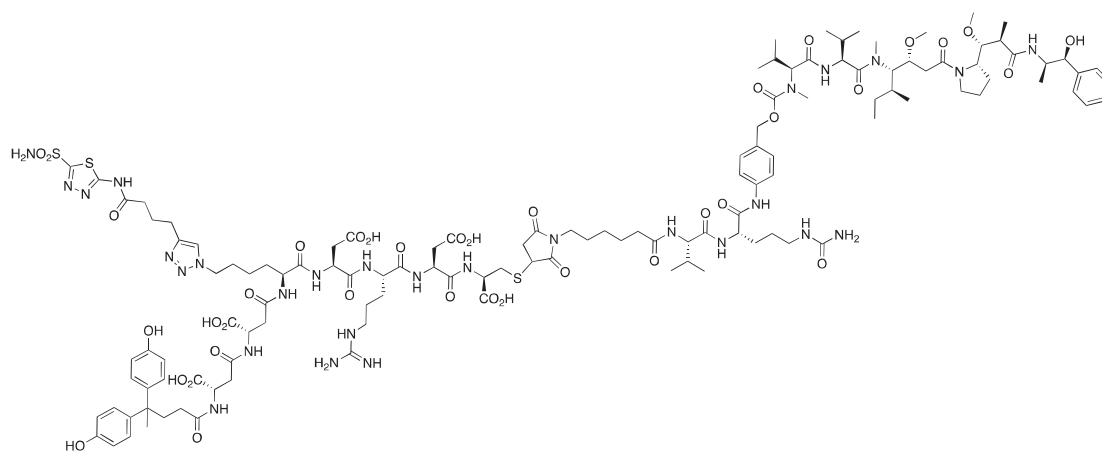


Figure S4: a) HPLC chromatogram ($\lambda = 260 \text{ nm}$) b) HRMS spectra of compound 7

AAZ⁺-ValCit-MMAE (8):



Compound 8 was synthesized as previously reported.¹

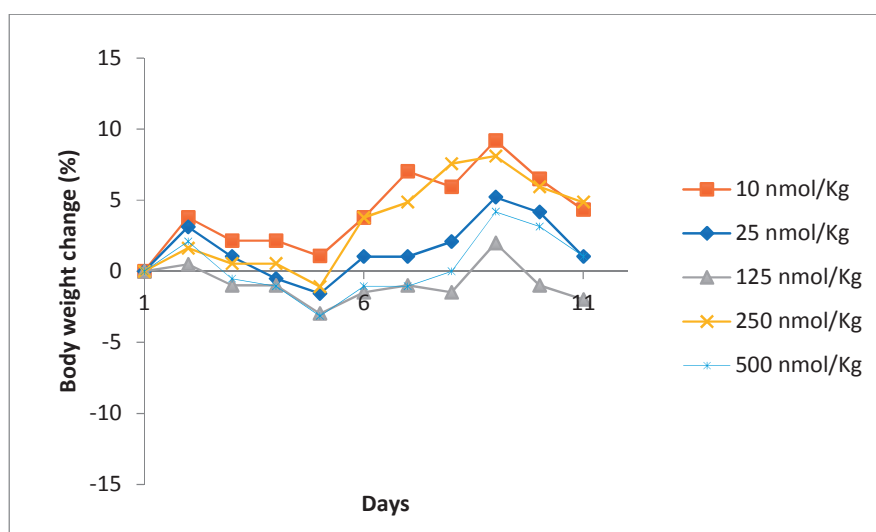


Figure S5: Dose escalation studies of compound 7

References

- (1) Cazzamalli, S.; Dal Corso, A.; Widmayer, F.; Neri, D. Chemically Defined Antibody- and Small Molecule-Drug Conjugates for in Vivo Tumor Targeting Applications: A Comparative Analysis. *J. Am. Chem. Soc.* **2018**, *140* (5), 1617–1621.

7.3 – Appendix III: supporting information of chapter 5

Supporting information

Octreotide Conjugates for Tumor Targeting and Imaging

Eduard Figueras,^{a,†} Ana Martins,^{a,b,†} Adina Borbély,^a Vadim Le Joncour,^c Paola Cordella,^d Raffaella Perego,^d Daniela Modena,^d Paolo Pagani,^d Simone Esposito,^c Giulio Auciello,^c Marcel Frese,^a Paola Gallinari,^b Pirjo Laakkonen,^c Christian Steinkühler,^{b,d} and Norbert Sewald^{a,*}

^a Department of Chemistry, Organic and Bioorganic Chemistry, Bielefeld University, Universitätsstraße 25, DE-33615 Bielefeld, Germany

^b Exiris srl, Via Via di Castel Romano 100, IT-00128 Rome, Italy

^c Translational Cancer Medicine, Research Programs Unit, Haartmaninkatu 8, FI-00014 University Helsinki, Finland

^d Italfarmaco SpA, Via dei Laboratori 54, IT-20092 Cinisello Balsamo, Italy

^e IRBM Science Park SpA, Via Pontina Km. 30,600, IT-00071 Pomezia, Italy

Author Information

† These authors contributed equally to this work

* Corresponding author

E-mail: norbert.sewald@uni-bielefeld.de

Table of contents

1) General methods.....	3
2) Synthesis of octreotide-Cy5.5 conjugate.....	7
3) Synthesis of PEG spacer	9
4) NMR, HPLC ($\lambda = 220$ nM) and mass spectra	11
5) Confocal microscopy	21
6) <i>In vivo</i> experiments	21

1) General methods

All reactions requiring anhydrous conditions were performed under argon atmosphere. DMF was dried over 4 Å molecular sieves, CH₂Cl₂ was distilled from CaH₂, THF was distilled from sodium/benzophenone. All the other chemicals and solvents (HPLC-grade or reagent-grade quality), unless otherwise stated, were purchased from commercial sources and used without further purification. Silica for flash chromatography was purchased from Macherey-Nagel 40-63 µm (230-400 mesh). Reactions were monitored by thin layer chromatography using aluminium-backed plates coated with silica gel 60 F254 from Merck; visualization was accomplished with UV light or staining with potassium permanganate or cerium molybdate solution.

High performance liquid chromatography - mass spectrometry

HPLC-MS was conducted using an Agilent 1200 series consisting of an autosampler, degasser, binary pump, column oven and diode array detector coupled to an Agilent 6220 accurate-mass TOF LC/MS. A Phenomenex Luna[®] 3 µm C18(2) 100 Å (100 mm x 2 mm) was used as column.

Eluent A: H₂O/CH₃CN/HCO₂H = 95/5/0.1 and eluent B: H₂O/CH₃CN/HCO₂H = 5/95/0.1.

Flow rate: 300 µL/min

0 min	100% A	0% B
10.0 min	2% A	98% B
11.0 min	2% A	98% B
11.5 min	100% A	0% B
15.0 min	100% A	0% B

High resolution mass spectrometry

High resolution mass spectra were recorded on an Agilent 6220 accurate-mass TOF LC/MS. Samples were injected through an Agilent 1200 series. Same solvents and column than HPLC-MS were used and a linear gradient from 0 to 98% B at 250 µL/min over 4 minutes was employed.

The mass spectrometer was externally calibrated using Agilent tuning mix prior to measurement.

Preparative reversed phase - high performance liquid chromatography

Preparative RP-HPLC was performed on a MERCK-HITACHI unit (controller: D-7000, pump: L7150, detector: L7420, UV-absorption measured at $\lambda = 220$ nm).

Eluent A: H₂O/CH₃CN/TFA = 95/5/0.1 and eluent B: H₂O/CH₃CN/TFA = 5/95/0.1

Method P1:

Column: Macherey-Nagel Nucleosil C₁₈ (250 mm x 21 mm, 10 μ m particle size)

Flow rate: 10 mL/min

0-2 min	100% A	0% B
35 min	0% A	100% B
40 min	0% A	100% B
45 min	100% A	0% B

Method P2:

Column: Macherey-Nagel Nucleosil C₁₈ (250 mm x 21 mm, 10 μ m particle size)

Flow rate: 10 mL/min

0-5 min	100% A	0% B
50 min	0% A	100% B
55 min	0% A	100% B
60 min	100% A	0% B

Method P3:

Column: Macherey-Nagel Nucleosil C₁₈ (250 mm x 10 mm, 7 μ m particle size)

Flow rate: 4 mL/min

0-15 min	100% A	0% B
60 min	0% A	100% B
65 min	0% A	100% B
70 min	100% A	0% B

Method P4:

Column: Macherey-Nagel Nucleosil C₁₈ (250 mm x 10 mm, 7 μ m particle size)

Flow rate: 4 mL/min

0-15 min	100% A	0% B
75 min	0% A	100% B
80 min	0% A	100% B
85 min	100% A	0% B

UPLC-HRMS conditions for plasma stability studies

Samples were analyzed on a system consisting of a Dionex Ultimate 3000 RS Pump coupled with (a) Dionex Ultimate 3000 RS from Thermo Scientific (Bremen, Germany) autosampler or (b) PAL LSI from CTC Analytics AG (Zwingen, Switzerland) autosampler. UPLC Peptide BEH C18 (50 mm x 2.1 mm, 1.7 μm , 130 \AA) column from Waters (Wexford, Ireland) at 40 $^{\circ}\text{C}$ was used for chromatographic separation at a flow rate of 400 $\mu\text{L}/\text{min}$ with a linear gradient composed of mobile phase A (0.1% formic acid in water) and B (0.1% formic acid in CH_3CN). A volume of (a) 2 μL or (b) 5 μL was injected.

Gradient:

0 min	99.5% A	0.5% B
4.0 min	5% A	95% B
5.0 min	5% A	95% B
5.1 min	99.5% A	0.5% B
6.0 min	99.5% A	0.5% B

All analyses were performed on a Q-Exactive OrbitrapTM mass spectrometer (Thermo Scientific) in ESI positive full scan/data-dependent MS/MS (FS-dd-MS/MS). Each cycle contains four scan events: Full Scan with m/z range (a) 150-1600 or (b) 200-2000 and resolution 35,000 FWHM at 200 m/z , mass accuracy: 5 ppm, followed by three MS/MS fragmentation scans with resolution 17,500 FWHM at 200 m/z over the three most abundant ions (Top N = 3) of the full-MS spectrum. The IS warfarin was detected in FS using the $[\text{M}+\text{H}]^+$ at m/z : 309.1121. Analysis of data was performed with XCalibur software. (a) was used for mouse plasma stability while (b) was used for human plasma stability.

HPLC-MS conditions for pharmacokinetic analysis

Samples were analyzed using a HPLC (Nexera, Shimadzu) connected to an Orbitrap Qexactive Focus (Thermo Scientific). A Jupiter C18 300 \AA (50 mm x 2 mm) 5 μm particle size was used as column.

Eluent A: $\text{H}_2\text{O}/\text{CH}_3\text{CN}/\text{HCO}_2\text{H} = 90/10/0.1$ and eluent B: $\text{CH}_3\text{CN}/\text{HCO}_2\text{H} 99.9/0.1$.

Flow rate: 400 $\mu\text{L}/\text{min}$

0 min	60% A	40% B
2.5 min	40% A	60% B

2.6 min	0% A	100% B
4.0 min	0% A	100% B
4.1 min	60% A	40% B
6.0 min	60% A	40% B

HPLC-MS conditions for cathepsin B cleavage studies

Samples were analyzed using a HPLC (Prominence, Shimadzu) connected to a triple quadrupole mass spectrometer (API4000, Sciex). A Jupiter C18 300 Å (50 mm x 2 mm) 5 µm particle size was used as column.

Eluent A: H₂O/CH₃CN/HCO₂H = 90/10/0.1 and eluent B: ACN/HCO₂H 99.9/0.1.

Flow rate: 200 µL/min

0 min	60% A	40% B
5.0 min	60% A	40% B
5.1 min	0% A	100% B
7.0 min	0% A	100% B
7.1 min	60% A	40% B
10 min	60% A	40% B

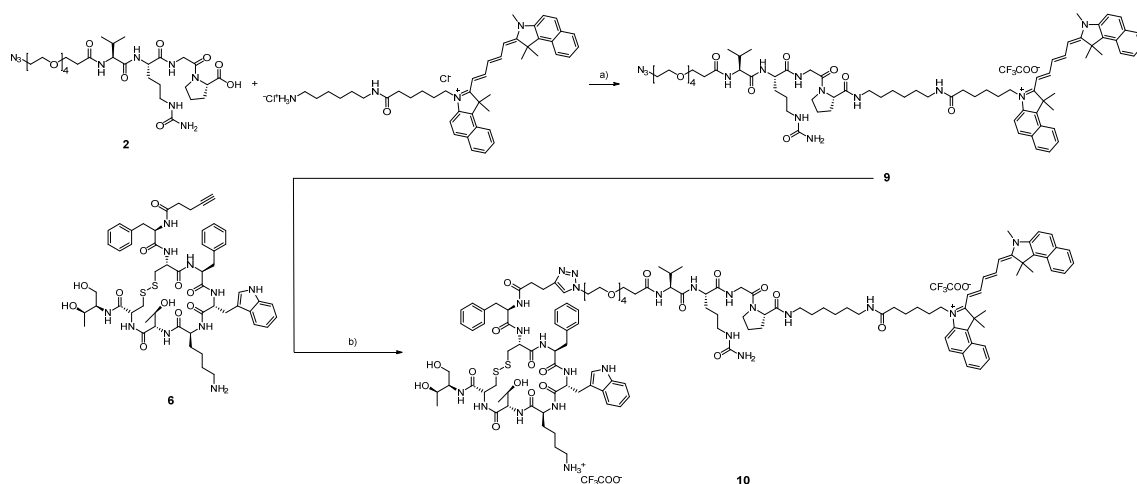
NMR spectroscopy

NMR spectra were recorded on a Bruker Avance 500 or Avance 500HD spectrometer (¹H: 500 MHz) at 298 K. Chemical shifts were referenced to residual nondeuterated solvent signal (CDCl₃: ¹H: 7.26 ppm). Coupling constants (*J*) are reported in Hz with the following abbreviations used to indicate splitting: s = singlet, t = triplet, m = multiplet.

Photo spectrophotometer

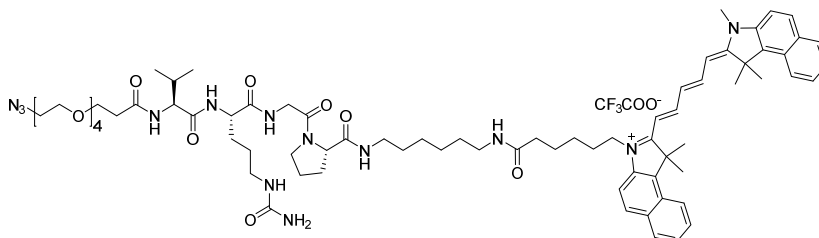
Photo spectrometry was recorded in a UV-3100 PC from VWR®.

2) Synthesis of octreotide-Cy5.5 conjugate



Scheme S1. Synthesis of octreotide-cy5.5 conjugate **10**. Reagents and conditions: a) PyBOP (2 eq), HOBt·H₂O (2.25 eq), DIPEA (2.5 eq), DMF, RT, 4 h; b) CuSO₄·5H₂O (0.6 eq), sodium ascorbate (0.4 eq), DMF/H₂O (1:1), 40 °C, 24 h.

Synthesis of N₃-PEG4-Val-Cit-Gly-Pro-Cy5.5 (**9**):

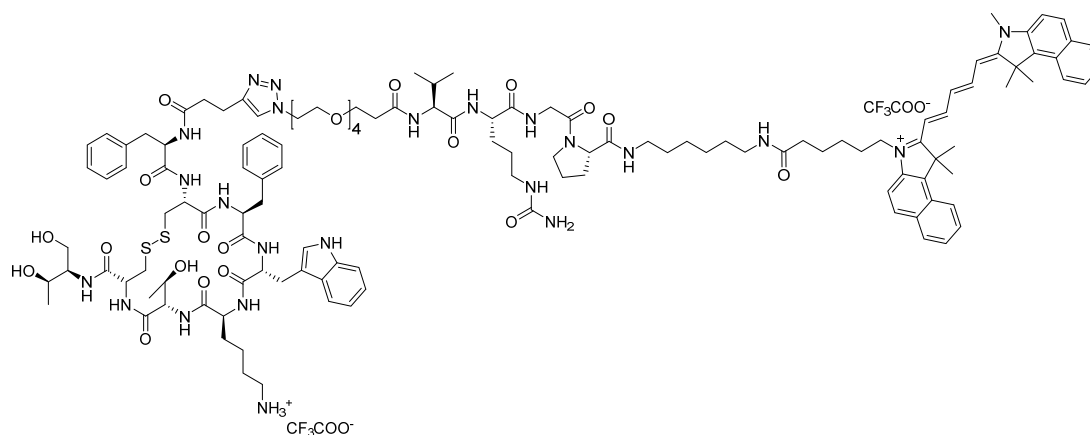


Cy5.5 (7.5 mg, 9.97 μmol, 1 eq), **5** (14 mg, 19.96 μmol, 2 eq), PyBOP (10.4 mg, 19.98 μmol, 2 eq) and HOBt·H₂O (3.4 mg; 22.2 μmol; 2.25 eq) were placed under argon atmosphere and dissolved with anhydrous DMF (0.5 mL). DIPEA (8.7 μL, 49.94 μmol, 5 eq) was added and the reaction mixture was stirred at RT for 4 h. Then, the solution was directly purified by RP-HPLC (method P3). Freeze-drying of fractions containing the product afforded **9** (14.4 mg, 98% yield) as blue powder.

HPLC-MS: *t_r* = 7.93 min, >99% purity (λ = 220 nm), *m/z* = 1364.91 (1364.81 [M]⁺); 682.99 (682.91 [M+H]²⁺)

HRMS (ESI-MS): *m/z* calculated for C₇₅H₁₀₇N₁₃O₁₁ [M+H]²⁺ 682.9101; found 682.9130

Synthesis of 10:



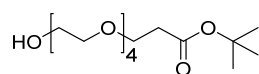
Azide **9** (4.5 mg, 3.05 μmol , 1 eq), alkyne **6** (4.1 mg, 3.38 μmol , 1.1 eq), $\text{CuSO}_4 \cdot 5\text{H}_2\text{O}$ (0.5 mg, 0.6 eq) and sodium ascorbate (0.24 mg, 0.4 eq) were placed under argon atmosphere and dissolved with a degassed solution of DMF/ H_2O (1:1, 0.5 mL). The solution was stirred for 24 h at 40 $^\circ\text{C}$ and was directly purified by RP-HPLC (method P3). Freeze-drying of desired fractions afforded **10** (6 mg, 73% yield) as blue powder.

HPLC-MS: $t_{\text{R}} = 6.99$ min, >99% purity ($\lambda = 220$ nm), $m/z = 1232.22$ (1232.14 $[\text{M}+\text{H}]^{2+}$); 821.82 (821.76 $[\text{M}+2\text{H}]^{3+}$); 616.62 (616.58 $[\text{M}+3\text{H}]^{4+}$)

HRMS (ESI-MS): m/z calculated for $\text{C}_{129}\text{H}_{178}\text{N}_{23}\text{O}_{22}\text{S}_2$ $[\text{M}+2\text{H}]^{3+}$ 821.7647; found 821.7670; calculated for $\text{C}_{129}\text{H}_{179}\text{N}_{23}\text{O}_{22}\text{S}_2$ $[\text{M}+3\text{H}]^{4+}$ 616.5754; found 616.5768

3) Synthesis of PEG spacer

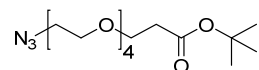
tert-Butyl-15-hydroxy-4,7,10,13-tetraoxapentadecanoate (**11**):



To a solution of tetraethyleneglycol (40.61 mL, 45.64 g, 235 mmol) in anhydrous THF (125 mL) a piece of sodium (1/4 cm) was added. After the sodium had reacted completely, *tert*-butylacrylate (11.98 mL, 10.57 g, 82.5 mmol) was added dropwise over 20 min and the resulting solution was stirred at RT overnight. The pH was adjusted to 7-8 with NaOH solution (1 N) and the solvents were removed in vacuum. The residue was dissolved in sat. NaCl solution (75 mL) and extracted with EtOAc (3 x 100 mL). The combined organic layers were dried over MgSO₄ and the solvent was removed under reduced pressure to obtain **11** (21.87 g, 82% yield) as colorless oil.

¹H-NMR (500 MHz, CDCl₃): δ (ppm) = 1.44 (s, 9H, C(CH₃)₃), 2.50 (t, J = 6.6 Hz, 2H, CH₂COO^tBu), 3.59-3.73 (m, 18H, OCH₂).

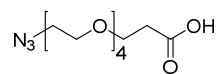
tert-Butyl 15-Azido-4,7,10,13-tetraoxapentadecanoate (**12**):



11 (1.50 g, 4.65 mmol, 1 eq) was dissolved in anhydrous THF (10 mL) and the resulting solution was cooled to 0°C. Methanesulfonyl chloride (0.54 mL, 6.98 mmol, 1.5 eq) and triethylamine (0.97 mL, 6.98 mmol, 1.5 eq) were added dropwise and the solution was stirred for 30 min at 0 °C and then overnight at RT. NaHCO₃ (0.27 g, 3.20 mmol, 0.7 eq) and NaN₃ (0.45 g, 6.98 mmol, 1.5 eq) were added with dist. water (10.5 mL) to the mixture and the resulting solution was stirred for 20 min at RT. THF was removed in vacuum and the remaining solution was stirred at 80 °C for 4 h. After cooling down, the mixture was extracted with DCM (3 x 30 mL), the combined organic layers were dried over MgSO₄ and the solvent was removed under reduced pressure. The crude was purified by column chromatography using PE/EtOAc (1:1) as eluent to obtain **12** (0.74 g; 46% yield) as colorless oil.

¹H-NMR (500 MHz, CDCl₃): δ (ppm) = 1.44 (s, 9H, C(CH₃)₃), 2.49 (t, 2H, J = 6.6 Hz, CH₂COO^tBu), 3.38 (t, 2H, J = 5.1 Hz, CH₂N₃), 3.59-3.68 (m, 14H), 3.70 (t, 2H, J = 6.6 Hz, CH₂CH₂COO^tBu).

15-Azido-4,7,10,13-tetraoxapentadecanoic acid (13):

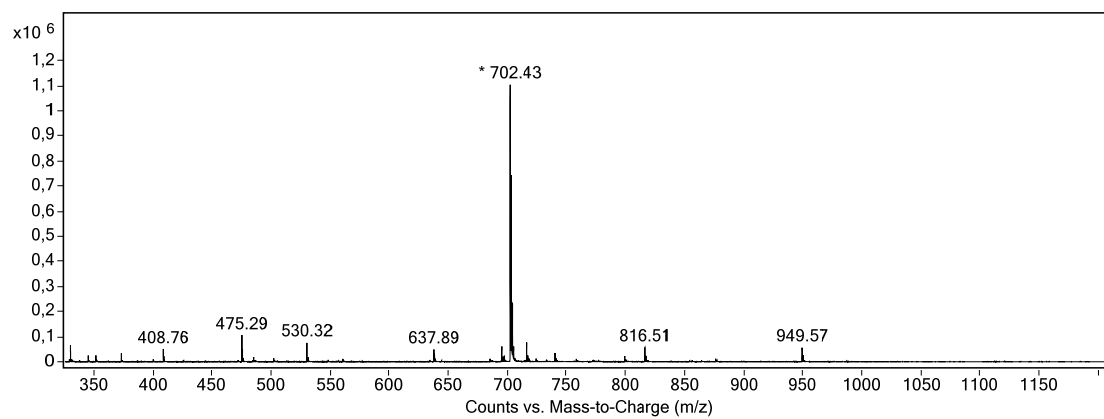
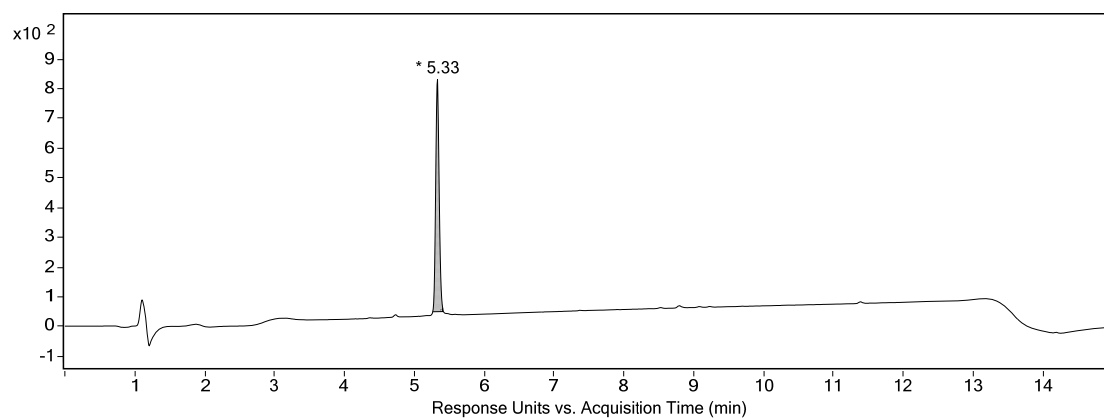


12 (0.22 g; 0.63 mmol) was dissolved in dry DCM (5 mL) and H₂O (0.25 mL). Then, TFA (5 mL) was added and the solution was stirred at RT for 1.5 h. The solvents were removed under reduced pressure and the product was coevaporated with diethyl ether (2 x 10 mL) to obtain **13** (0.18 g, 98% yield) as colorless oil.

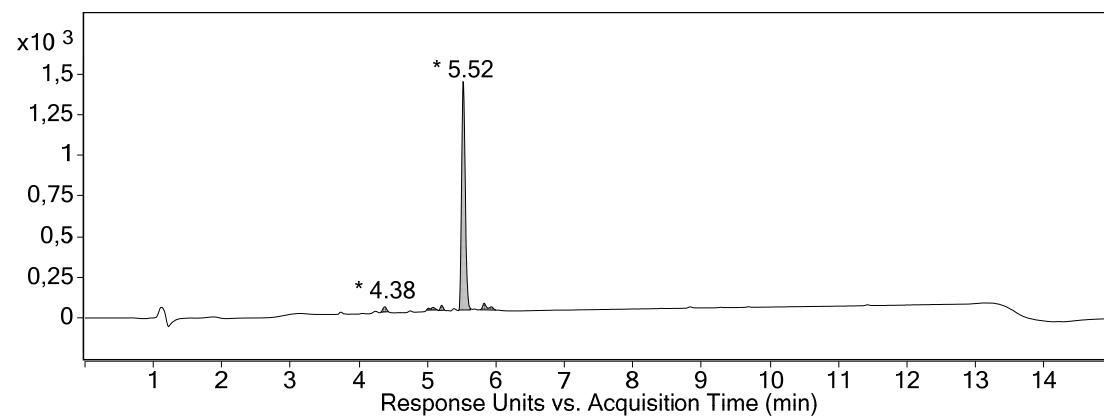
¹H-NMR (500 MHz, CDCl₃): δ (ppm) = 2.65 (t, 2H, J = 6.1 Hz, CH₂COOH), 3.40 (t, 2H, J = 5.0 Hz, CH₂N₃), 3.64-3.70 (m, 14H), 3.78 (t, 2H, J = 6.1 Hz, CH₂CH₂COOH).

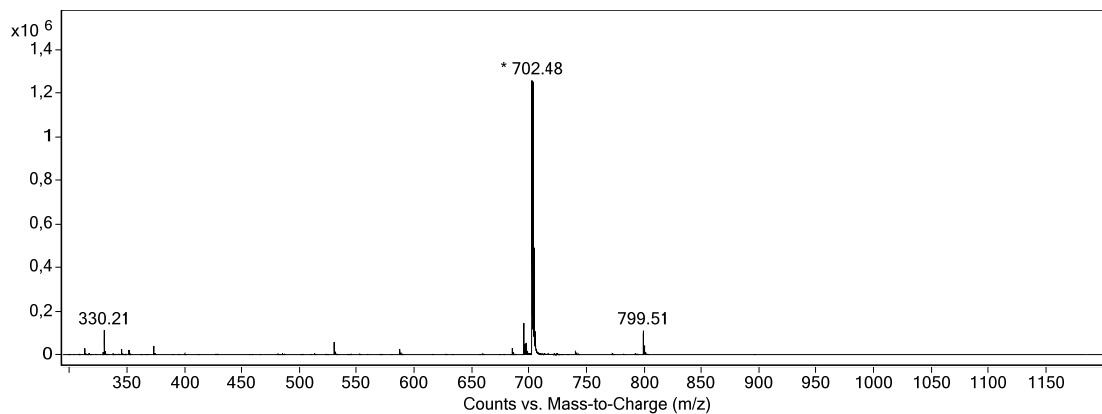
4) NMR, HPLC ($\lambda = 220$ nm) and mass spectra

1: HPLC-MS

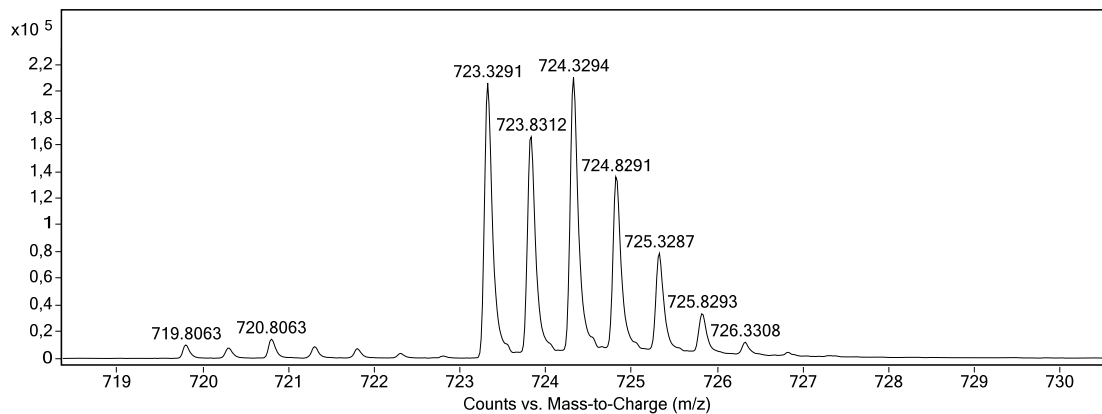
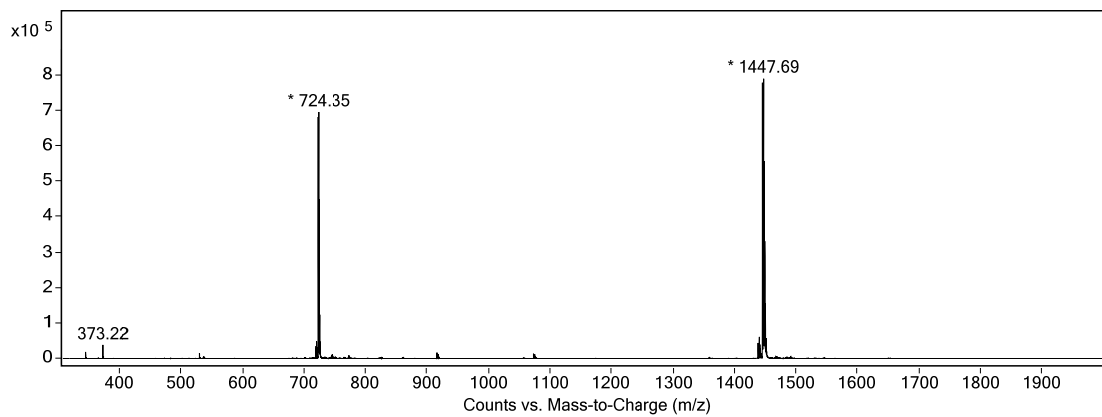
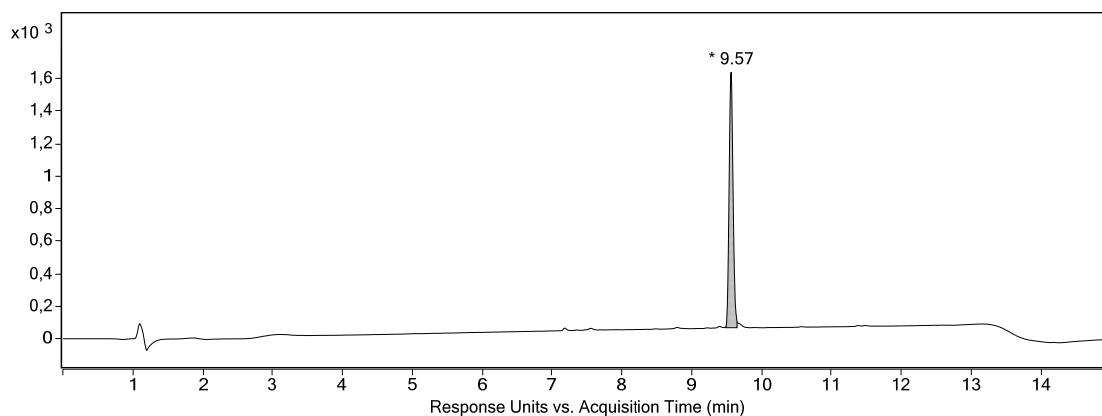


2: HPLC-MS

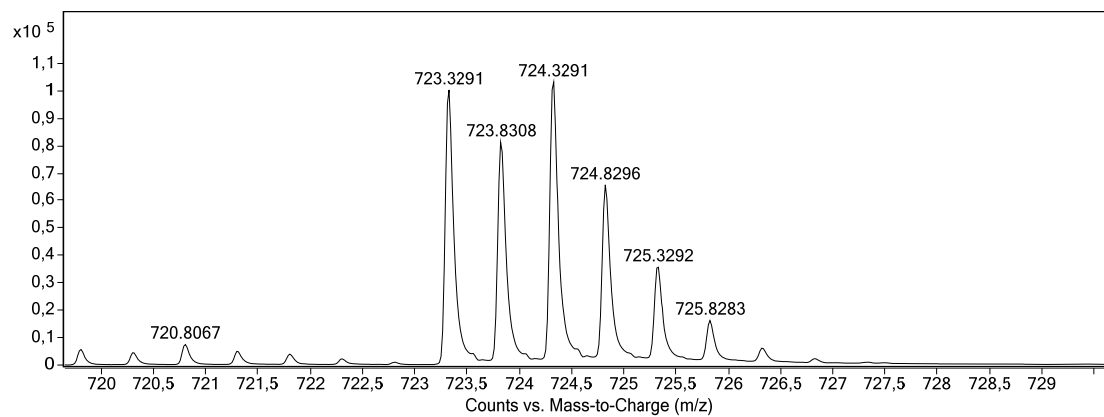
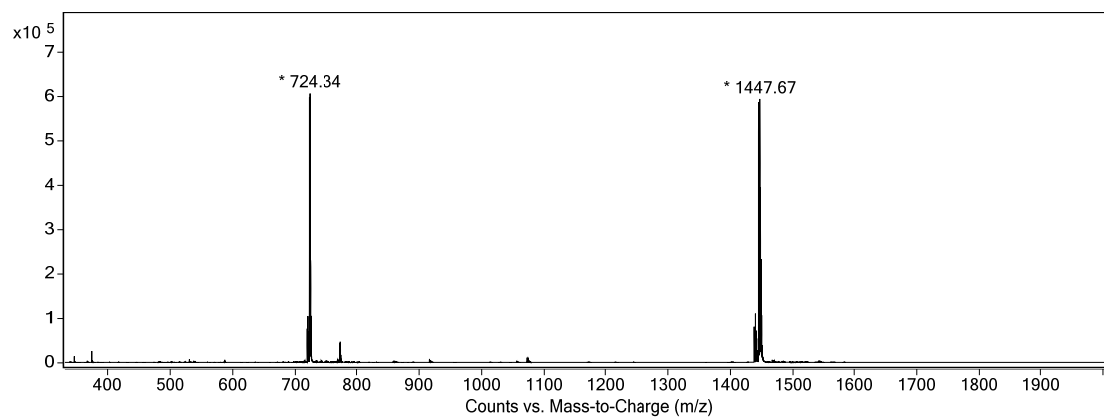
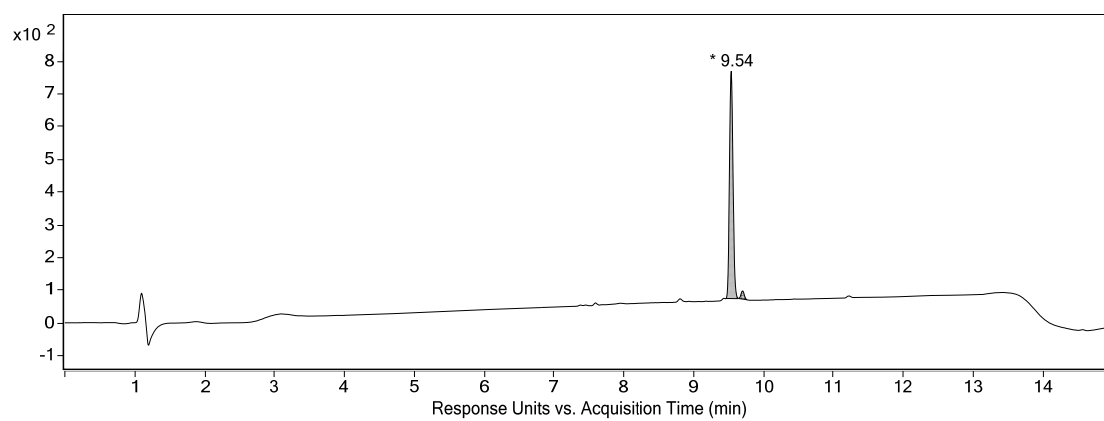




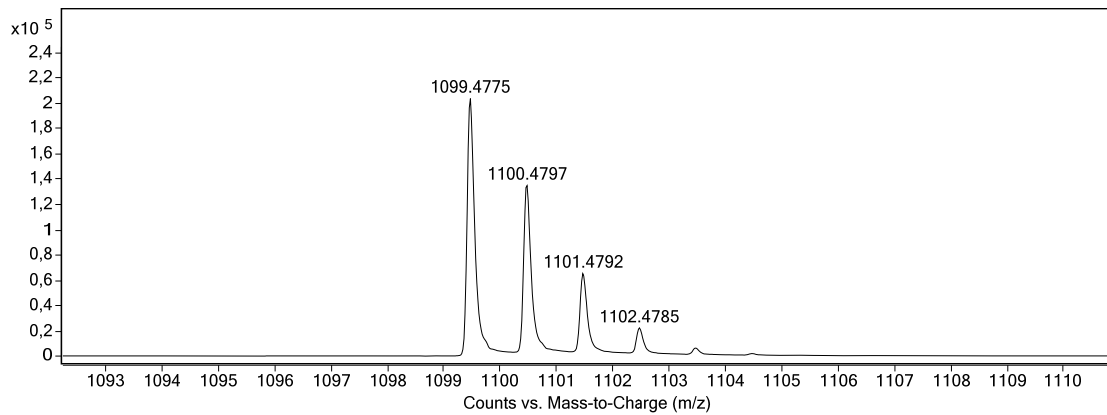
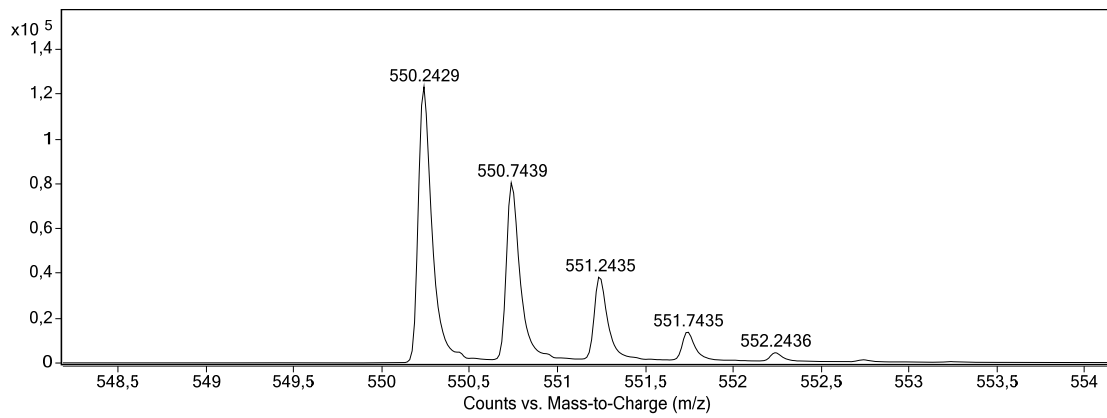
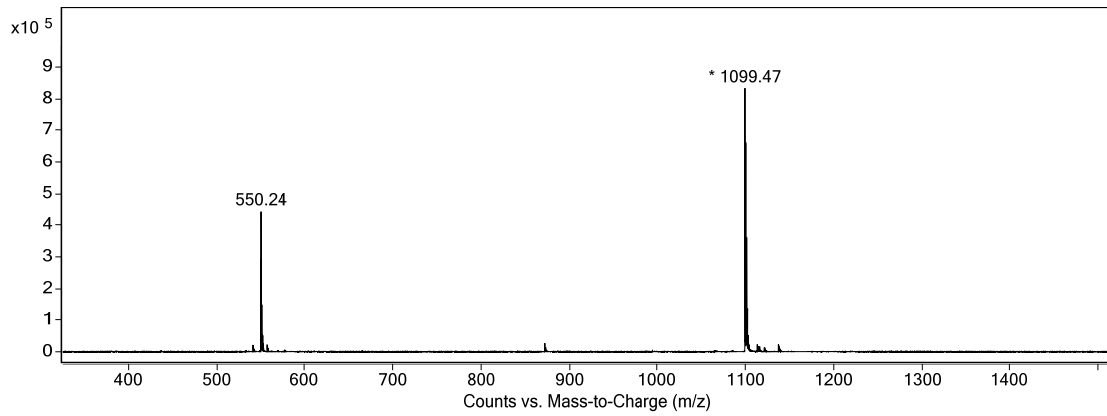
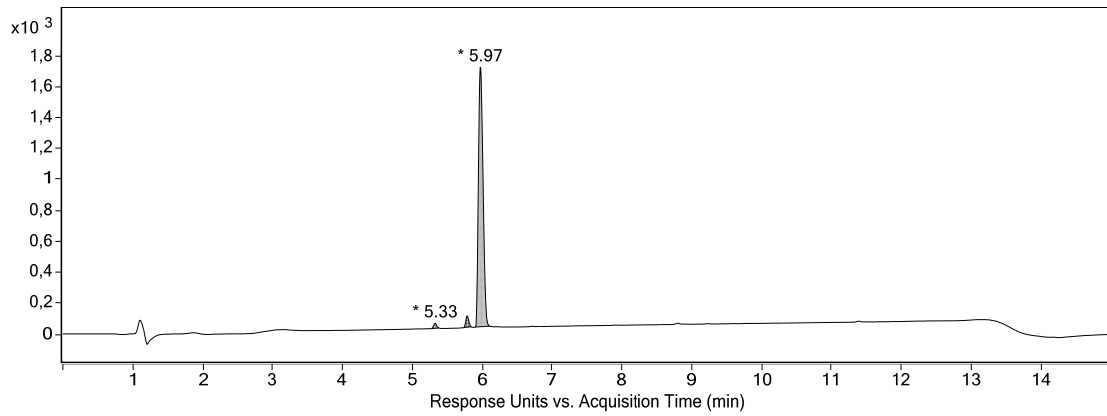
4: HPLC-MS and HRMS



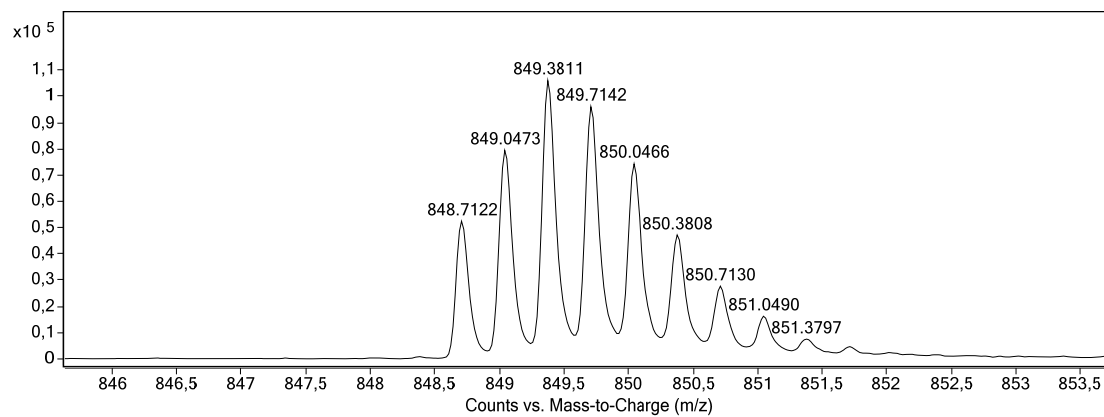
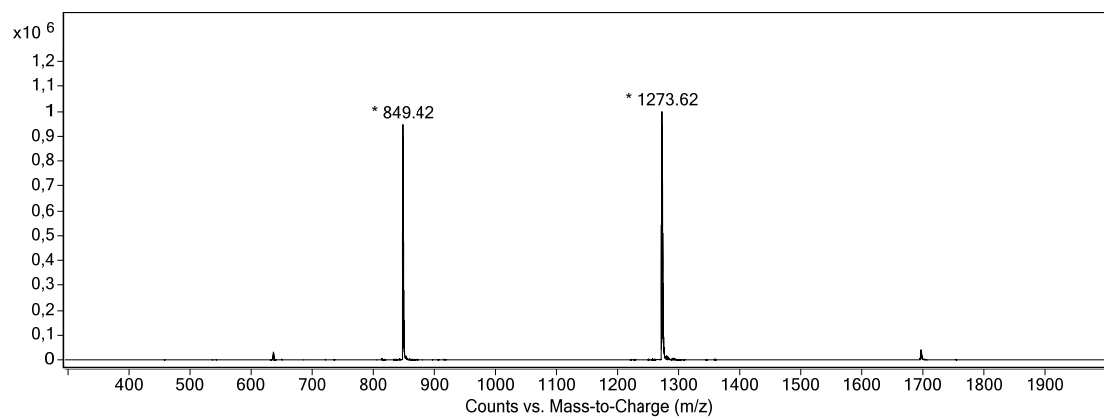
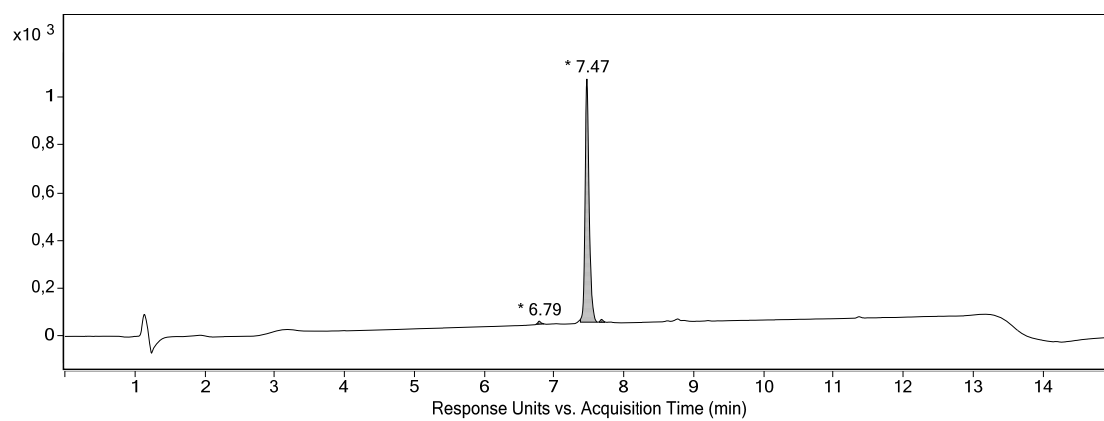
5: HPLC-MS and HRMS



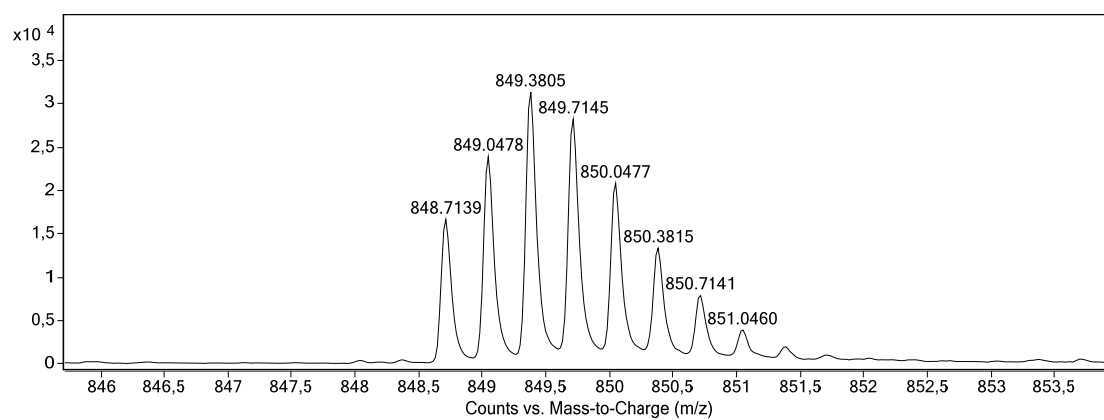
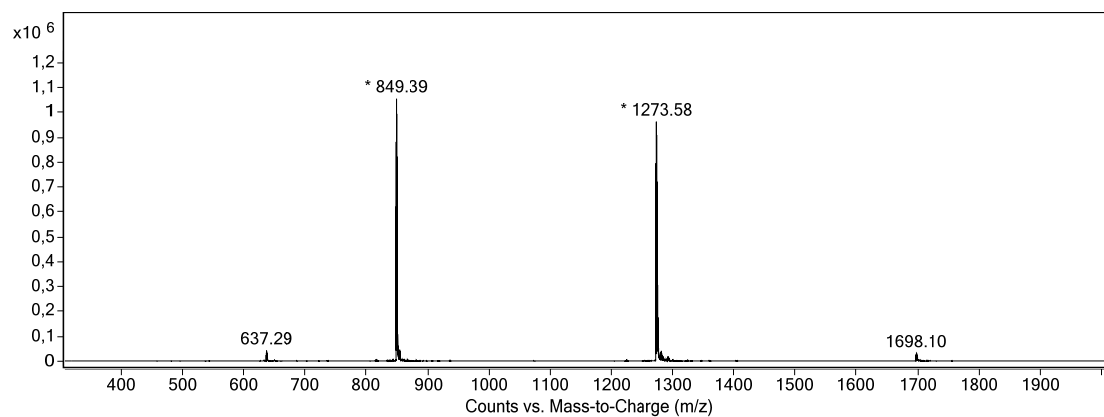
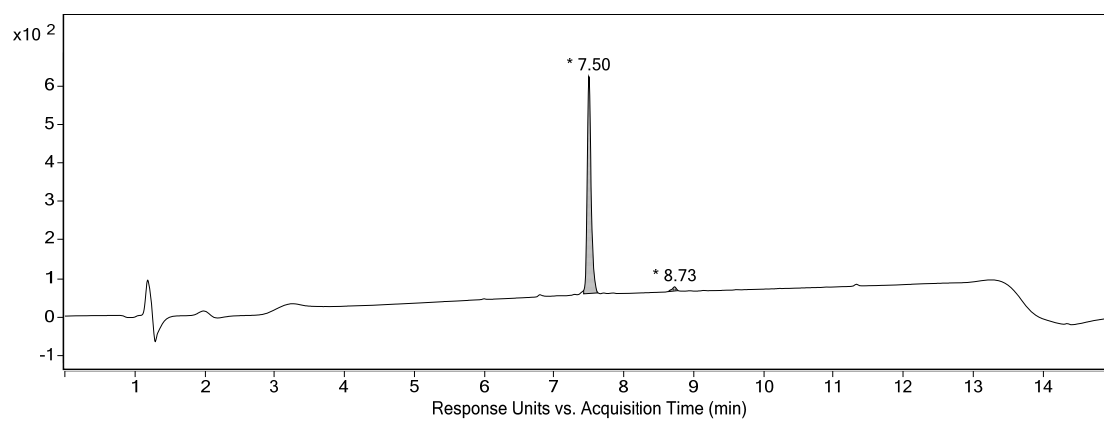
6: HPLC-MS and HRMS



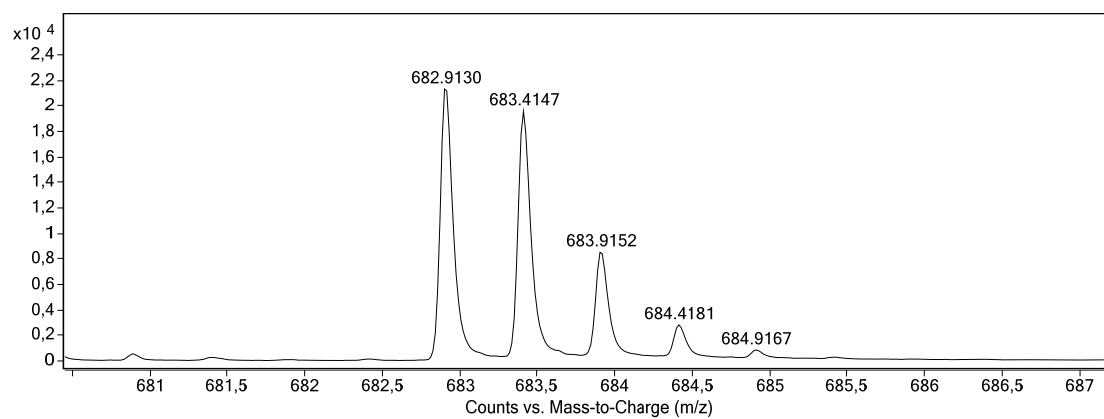
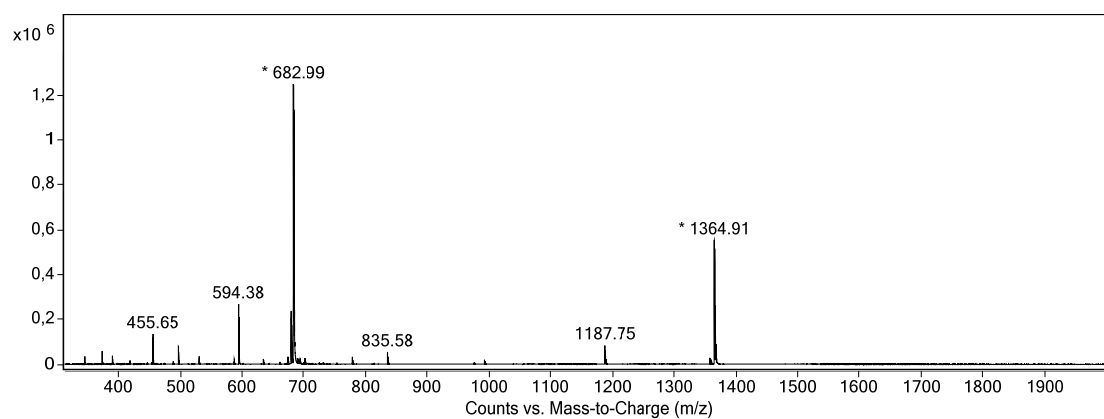
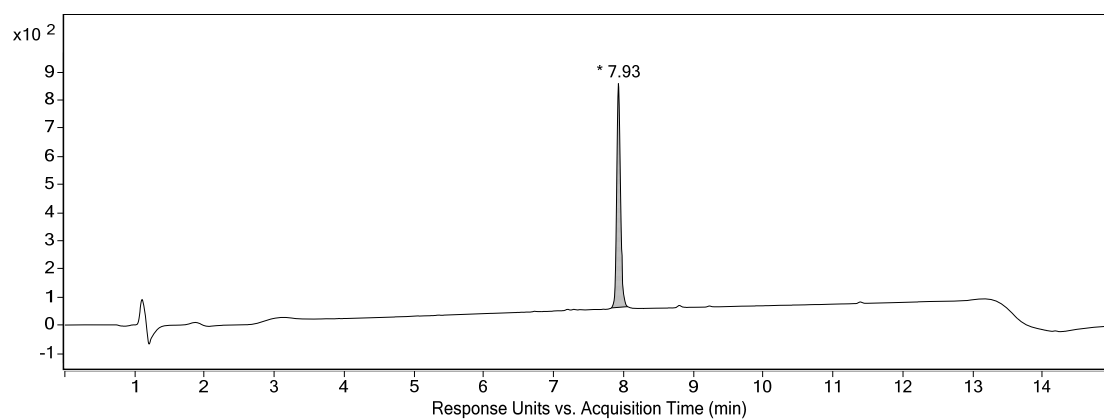
7: HPLC-MS and HRMS



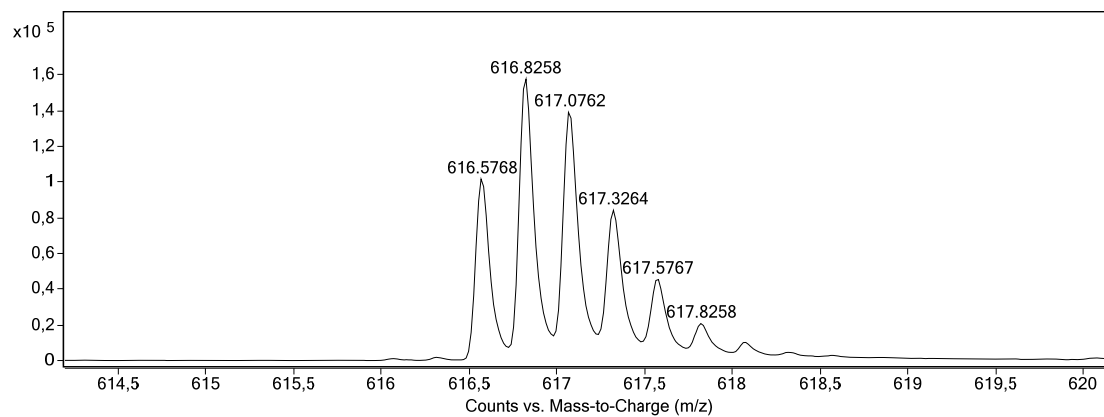
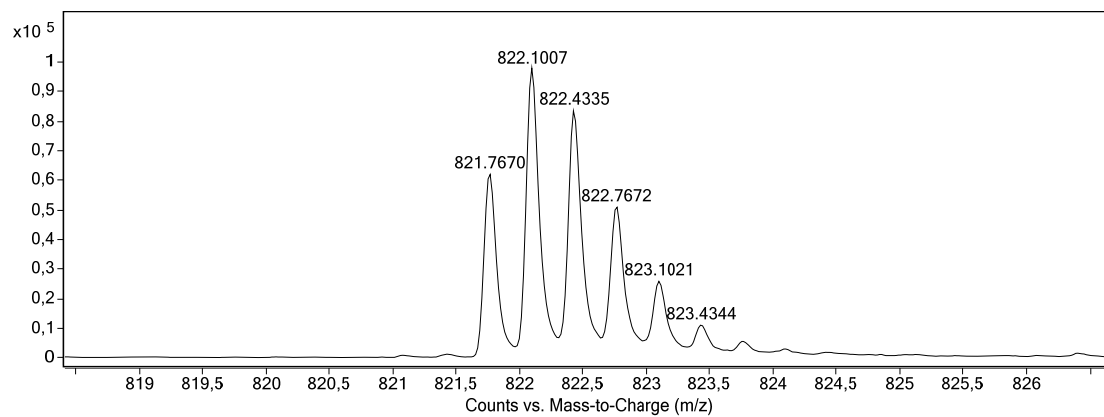
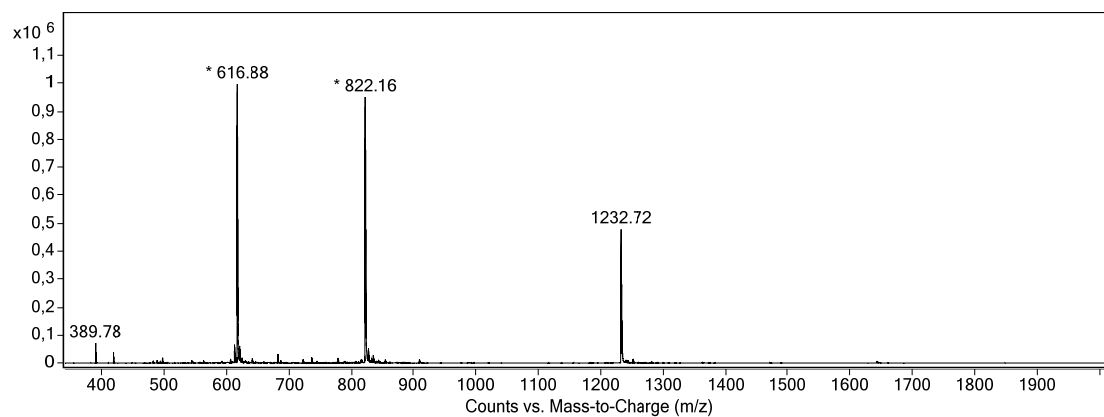
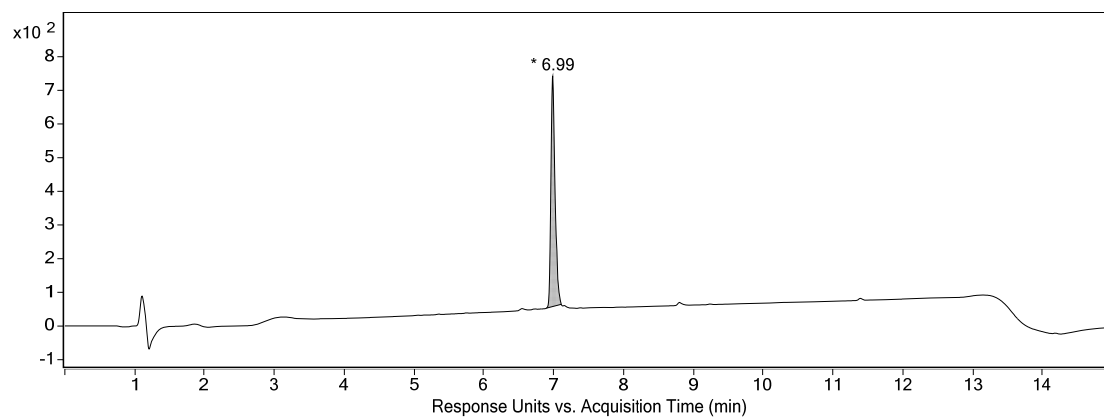
8: HPLC-MS and HRMS



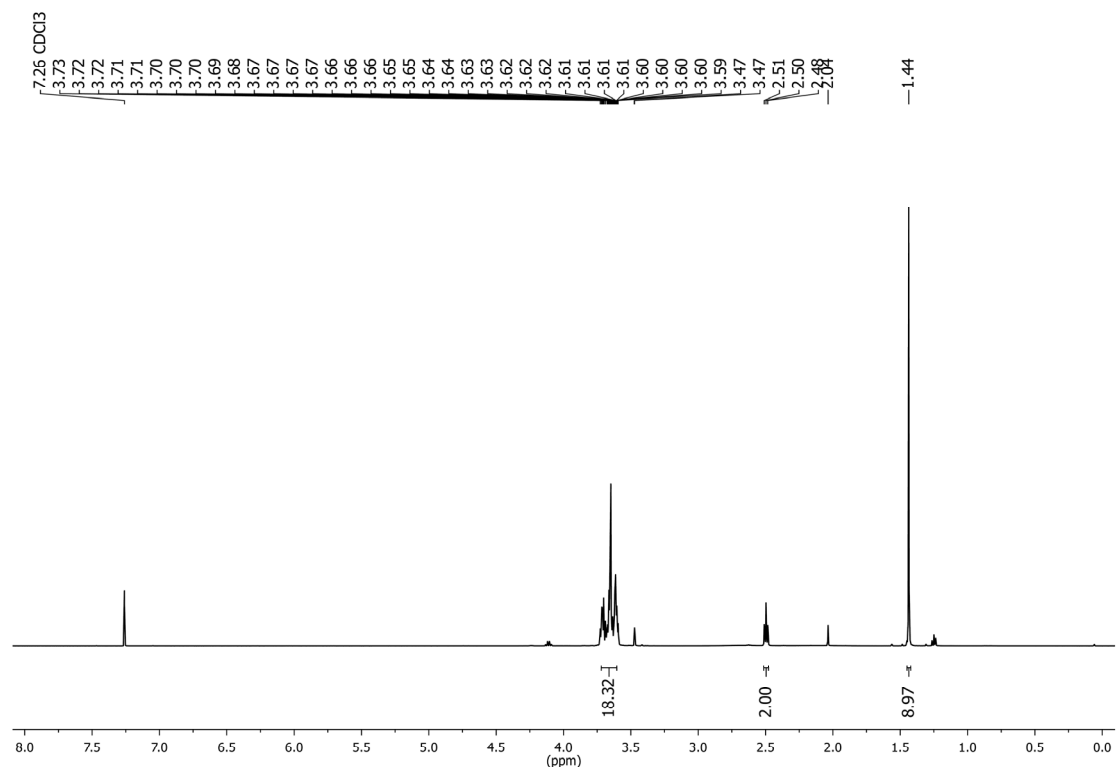
9: HPLC-MS and HRMS



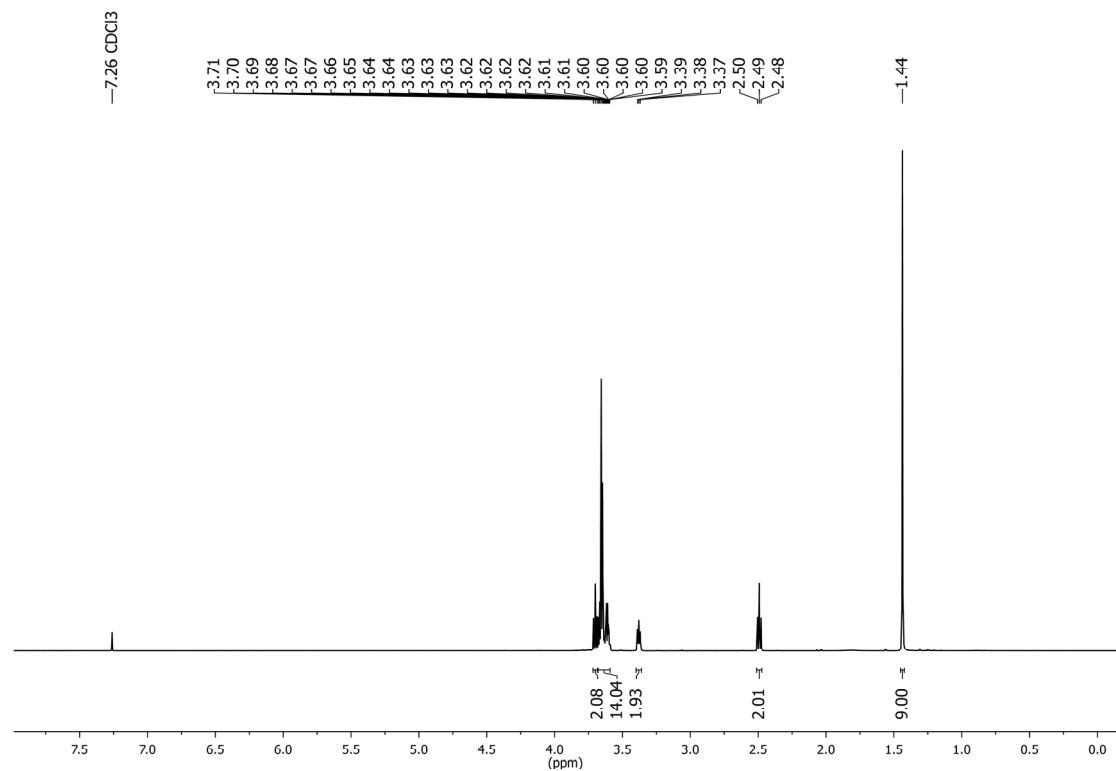
10: HPLC-MS and HRMS



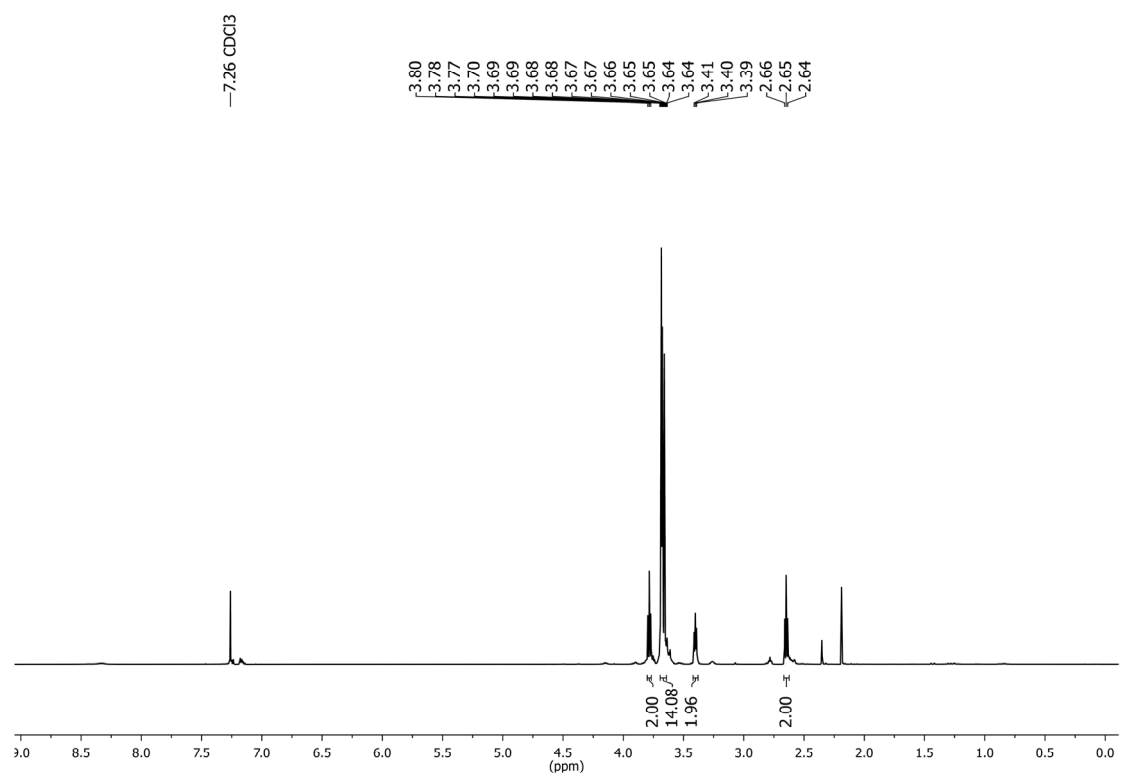
11: ¹H-NMR



12: ¹H-NMR



13: ¹H-NMR



5) Confocal microscopy

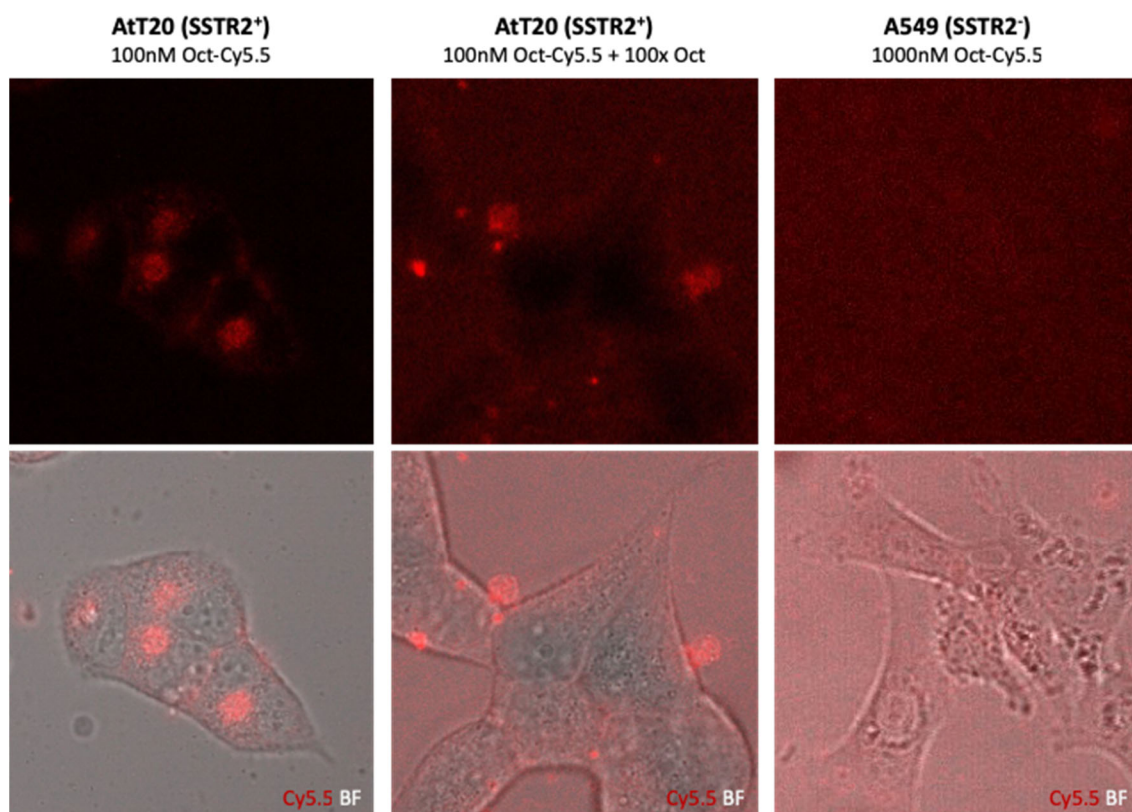


Figure S1. Confocal microscopy images from conjugate **10** in SSTR2 positive cell line AtT20 in absence (left) or 100-fold excess octreotide (middle), and in SSTR2 negative A549 cell line (right).

6) *In vivo* experiments

Animal experiments were approved by the Committee for Animal Experiments of the District of Southern Finland (ESAVI/6285/04.10.07/2014).

Implantation of tumors

For *in vivo* tumor targeting and antitumor efficacy experiments, three million AtT20/D16v-F2 murine pituitary tumor cells in 100 μ L PBS/Matrigel (v/v) were xenografted in the right flank of four-weeks-old female BALB/c nude mice (BALB/cAnNRj-Foxn1^{nu/nu}, Janvier Labs). The experiments started around 15 days after implantation, when the animals started to show physical signs of the hormone releasing tumor.

***In vivo* antitumor efficacy**

Animals bearing AtT20 tumors were randomized in three treatment groups ($n=9$) and injected intravenously with 5 mg/kg of conjugate **8** in 2% DMSO in water or a mix of unconjugated octreotide and cryptophycin in the respective molar concentration. Treatment was given once a week for a total of three weeks. Vehicle treatment was used as control. Mice were weighed, and the tumor sizes were monitored with an electronic caliper. Tumor volume was calculated using the ellipsoid formula $v = \pi/6 \cdot x \cdot y \cdot z$.

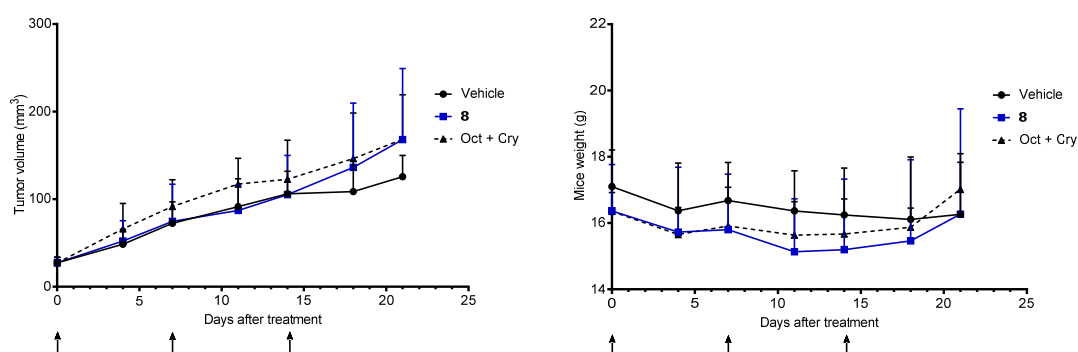


Figure S3. *In vivo* antitumor efficacy of conjugate **8** compared to vehicle and unconjugated mix of cryptophycin and octreotide (left), and body weight quantification during treatment (right).

